Development of Controllers Using FPGA for Fuel Cells in Standalone and Utility Applications

Kanhu Charan Bhuyan

Department of Electronics and Communication Engineering

National Institute of Technology

Rourkela-769008

August 2014

Development of Controllers Using FPGA for Fuel Cells in Standalone and Utility Applications

A Thesis submitted in partial fulfillment of the requirements for the degree of

Doctor of Philosophy

in

Electronics and Communication Engineering

By

Kanhu Charan Bhuyan

Roll: 510EC703

Under the Supervision of

Prof. Kamalakanta Mahapatra

National Institute of Technology

Rourkela-769008 (ODISHA)

August 2014

CERTIFICATE

This is to certify that the thesis entitled "**Development of Controllers using FPGA for Fuel Cells in Standalone and Utility Applications**", submitted to the National Institute of Technology, Rourkela by **Mr Kanhu Charan Bhuyan,** bearing Roll No. **510EC703** for the award of the degree of **Doctor of Philosophy** in Department of Electronics and Communication Engineering, is a bonafide record of research work carried out by him under my supervision.

The candidate has fulfilled all the prescribed requirements.

The thesis is based on candidate's own work, has not submitted elsewhere for the award of degree/diploma.

In my opinion, the thesis is in standard fulfilling all the requirements for the award of the degree of **Doctor of Philosophy** in Electronics and Communication Engineering.

Prof. Kamalakanta Mahapatra

Supervisor

Department of Electronics and Communication Engineering
National Institute of Technology, Rourkela, 769008
Odisha (INDIA)

Dedicated to

My Family

ACKNOWLEDGEMENTS

ABSTRACT

In the recent years, increase in consumption of energy, instability of crude oil price and global climate change has forced researchers to focus more on renewable energy sources. Though there are different renewable energy sources available (such as photovoltaic and wind energy), they have some major limitations. The potential techniques which can provide renewable energy are fuel cell technology which is better than other renewable sources of energy. Solid oxide fuel cell (SOFC) is more efficient, environmental friendly renewable energy source. This dissertation focuses on load/grid connected fuel cell power system (FCPS) which can be used as a backup power source for household and commercial units. This backup power source will be efficient and will provide energy at an affordable per unit cost.

Load/grid connected fuel cell power system mainly comprises of a fuel cell module, DC-DC converter and DC-AC inverter. This thesis primarily focuses on solid oxide fuel cell (SOFC) modelling, digital control of DC-DC converter and DC-AC inverter. Extensive simulation results are validated by experimental results.

Dynamic mathematical model of SOFC is developed to find out output voltage, efficiency, over potential loss and power density of fuel cell stack. The output voltage of fuel cell is fed to a DC-DC converter to step up the output voltage. Conventional Proportional-Integral (PI) controller and FPGA based PI controller is implemented and experimentally validated. The output voltage of DC-DC converter is fed to DC-AC inverter. Different pulse width modulation-voltage source inverter (PWM-VSI) control strategy (such as Hysteresis Current Controller (HCC), Adaptive-HCC, Fuzzy-HCC, Adaptive-Fuzzy-HCC, Triangular Carrier Current Controller (TCCC) and Triangular Periodical Current Controller (TPCC)) for DC-AC inverter are investigated and validated through extensive simulations using MATLAB/SIMULINK. This work also focuses on number of fuel cells required for application in real time and remedy strategies when one or few fuel cells are malfunctioning. When the required numbers of fuel cells are not available, DC-DC converter is used to step up the output voltage of fuel cell. When there is a malfunction in fuel cell or shortage of hydrogen then a battery is used to provide backup power.

The fuel cell power system based on shunt active power filter (APF) is designed for compensation of current harmonic and reactive power compensation in the AC power

distribution system. APF based fuel cell reduces the real power flow from grid side, which eventually reduces the power rating of inverter. The prototype model of single phase fuel cell power system with Hysteresis Current Control (HCC) technique is developed. FPGA (Field Programmable Gate Array) implementation of HCC is done using NI (National Instruments) cRIO-9014. FPGA implementation of three phase model of fuel cell power system is developed using Adaptive-fuzzy-HCC using Xilinx/System Generator.

Keywords: DC-DC Converter, DC-AC inverter, FPGA, NI cRIO-9014, PI Controller, PWM-VSI Controller, SOFC.

CONTENTS

LIST OF TABLES

LIST OF FIGURES

Figure	Title	Page No.

ABBREVIATION

AO	-	Analog Output
AI	-	Analog Input
AC	-	Alternating Current
AMP	-	Ampere
ASIC	-	Application Specific Integrated Circuits
AHCC	-	Adaptive Hysteresis Current Controller
BHEL	-	Bharat Heavy Electrical Limited
CAD	-	Computer Aided Design
CHP	-	Combined Heat and Power
CCM	-	Continuous Conduction Mode
CLB	-	Configurable Logic Block
CMOS	-	Complementary Metal Oxide Semiconductor
CRIO	-	CompactRIO
CSI	-	Current Source Inverter
DC	-	Direct Current
DMFC	-	Direct Methanol Fuel Cell
DCM	-	Discontinuous Conduction Mode
DGS	-	Distribution Generation System
DSP	-	Digital Signal Processing
DTC	-	Delhi Transport Corporation
DVR	-	Dynamic Voltage Restorer
EDA	-	Electronic Design Automation
FC	-	Fuel Cell

FCPS	-	Fuel Cell Power System
FLC	-	Fuzzy Logic Controller
FPGA	-	Field Programmable Gate Array
GE	-	General Electric
GND	-	Ground
HPS	-	Hybrid Power System
HB	-	Hysteresis Band
HCC	-	Hysteresis Current Controller
HDL	-	Hardware Description Language
HEV	-	Hybrid Electric Vehicles
IEEE	-	Institute of Electrical and Electronics Engineers
ISE	-	Integrated Software Environment
IGBT	-	Insulated Gate Bipolar Transistor
IOB	-	Input Output Blocks
LOM	-	Largest of Maximum
LPF	-	Low Pass Filter
LUT	-	Look Up Table
LABVIEW	-	Laboratory Virtual Instrumentation Engineering Workbench
MCFC	-	Molten Carbonate Fuel Cell
MOSFET	-	Metal Oxide Semiconductor Field Effect Transistor
MOM	-	Middle of Maximum
MNES	-	Ministry of Non-conventional Energy Source
MNRE	-	Ministry of New and Renewable Energy
NI	-	National Instruments
NL	-	Negative Large

NM	-	Negative Medium
NS	-	Negative Small
OE	-	Output Enable
OP-AMP	-	Operational Amplifier
PC	-	Personal Computer
PV	-	Photovoltaic
PL	-	Positive Large
PB	-	Positive Big
PS	-	Positive Small
PI	-	Proportional Integral
PID	-	Proportional Integral and Derivative
PCU	-	Power Conditioning Unit
PCS	-	Power Conversion System
PSS	-	Power System Simulation
PSM	-	Programmable Switch Matrix
PVS	-	Positive Very Small
PVB	-	Positive Very Big
PEMFC	-	Proton Exchange Membrane Fuel Cell
PAFC	-	Phosphoric Acid Fuel Cell
PLB	-	Programmable Logic block
PLL	-	Phase Locked Loop
PSpice	-	Simulated Program with Integrated Circuit Emphasis
PWM	-	Pulse Width Modulation
RIO	-	Reconfigurable Input/output
RTL	-	Resistor Transistor Logic

rms	-	root mean square
SOFC	-	Solid Oxide Fuel Cell
SOC	-	State of Charge
SMC	-	Sliding Mode Controller
SMPS	-	Switched Mode Power Supplies
SOM	-	Smallest of Maximum
TCCC	-	Triangular-Carrier Current Controller
THD	-	Total Harmonic distortion
TPCC	-	Triangular-Periodical Current Controller
TTL	-	Transistor-Transistor Logic
TERI	-	Tata Energy Research Institute
UAV	-	Unmanned Aerial Vehicles
UC	-	Ultra Capacitor
UGV	-	Unmanned Ground Vehicles
UTC	-	United Technologies Corporation
UPS	-	Uninterruptable Power Supply
VHDL	-	Very high speed integrated circuit Hardware Description Language
VLSI	-	Very Large Scale Integration
VSI	-	Voltage Source Inverter
VSC	-	Variable Structure Controller
ZE	-	Zero
ZVS	-	Zero Voltage Switching
ZCS	-	Zero Current Switching

LIST OF SYMBOLS

V_{fc} -   The stack voltage of the fuel cell

E_{fc} -   The reversible open circuit voltage

E -   Nernst instantaneous voltage

F -   Faraday's constant (C (kmol)$^{-1}$)

I_{fc} -   Fuel cell stack current (A)

I -   Current Density

m, n -   Constants

M -   Fluid molar mass

K -   Valve constant

B -   The slope of the Tafel line

K_{an} -   Anode valve constant (kmolkg)$^{1/2}$(atm s)$^{-1}$

K_{H_2} -   Hydrogen valve molar constant (kmol(atm s)$^{-1}$)

K_{O_2} -   Oxygen valve molar constant (kmol (atm s)$^{-1}$)

K_{H_2O} -   Water valve molar constant (kmol (atm s)$^{-1}$)

K_r -   Modeling constant (kmol (s A)$^{-1}$)

m_f -   Mass flow rate

M_{H_2} -   Molar mass of hydrogen (kg(kmol)$^{-1}$)

n_{H_2} -   Number of hydrogen moles in the anode channel (kmol)

N_0 -   Number of fuel cells

P_u -   Upstream Pressure

P_{H_2}	-	Hydrogen partial pressure (atm)
P_{H_2O}	-	Water partial pressure (atm)
P_{O_2}	-	Oxygen partial pressure (atm)
q_{O_2}	-	Input molar flow of hydrogen (kmol(s)$^{-1}$)
m_f, H_2^r	-	Hydrogen which reacts with oxygen
m_f, H_2^{in}	-	Hydrogen which enters anode
$q_{H_2}^{in}$	-	Hydrogen input flow (kmol(s)$^{-1}$)
$q_{H_2}^{out}$	-	Hydrogen output flow (kmol(s)$^{-1}$)
$q_{H_2}^r$	-	Hydrogen flow that reacts (kmol(s)$^{-1}$)
R	-	Universal gas constant ((1 atm) (kmol k)$^{-1}$)
r	-	Fuel cell internal resistance (Ω)
r_{H-O}	-	Hydrogen and oxygen flow ratio
T	-	Absolute temperature (K)
U_f	-	Utilisation factor
V_{an}	-	Volume of anode (m^3)
K_{an}	-	Anode valve constant
V_{FC}	-	DC output voltage of fuel cell system (V)
ζ_{H_2}	-	Hydrogen time constant (s)
ζ_{O_2}	-	Oxygen time constant (s)
ζ_{H_2O}	-	Water time constant (s)
V_{Conc}	-	Concentration voltage loss (V)
V_{act}	-	Activation voltage loss (V)

V_{Ohmic}	-	Ohmic voltage loss (V)
d	-	Duty ratio
V_0	-	Output voltage
T	-	Switching period
f_s	-	Switching frequency
S	-	Sliding surface
λ	-	Sliding co-efficient
V	-	Lyapunov function
T_k	-	Time duration of kth active state vector
T_{k+1}	-	Time duration of $(k+1)^{th}$ active state vector
T_s	-	Sampling period
ω	-	Angular frequency
f	-	Fundamental frequency
V_s or v_s	-	Supply voltage
I_s or i_s	-	Source current
I_L or i_L	-	Load current
I_{sm}	-	Peak value of the source current
V_{sm} or v_{sm}	-	Peak magnitude value of the source voltage
I_{sp}	-	Peak value of the extracted reference current
I_{max}	-	Magnitude of peak reference current
I_{rms}	-	rms line current
I_{sl}	-	Switching loss current

m_a	-	Modulation factor
m_f	-	Frequency modulation ratio of the PWM-VSI.
R_c	-	Interface resistor
L_c	-	Interface inductor
C_{dc}	-	DC-link capacitor
$V_{dc,ref}$	-	Reference of the DC-link capacitor voltage
V_{dc}	-	DC-link capacitor voltage
V_a	-	Inverter voltage for single-phase VSI
v_{sa}, v_{sb}, v_{sc}	-	Supply voltages a-phase, b-phase, c-phase
u_{sa}, u_{sb}, u_{sc}	-	Unit sine vector templates of a-phase, b-phase, c-phase
v_{ca}, v_{cb} and v_{cc}	-	Inverter voltages a-phase, b-phase, c-phase
i_{sa}, i_{sb}, i_{sc}	-	Source currents a-phase, b-phase, c-phase
$i_{sa}^*, i_{sb}^*, i_{sc}^*$	-	Reference currents a-phase, b-phase, c-phase
i_{la}, i_{lb}, i_{lc}	-	Load currents a-phase, b-phase, c-phase
S_a	-	Switching signals for single-phase VSI
S_a, S_b, S_c	-	Switching signals a-phase, b-phase, c-phase
$e(v)$	-	Error voltage
$T(s)$	-	Transfer function
K_P	-	Proportional gain

K_I	-	Integral gain
$e(n)$	-	Error signal
$ce(n)$	-	Change of error signal
$a-b-c$	-	Three-phase co-ordinate voltage/current signal
i_{dc}	-	DC-current component
v_{ref}	-	Reference voltage vector
L	-	Phase inductance
$i_{sa}+$	-	Rising current segment
$i_{sa}-$	-	Falling current segment
t_1 and t_2	-	Switching intervals of time t_1 and t_2
f_c	-	Modulation frequency
m	-	Slope of the reference current
Hz	-	Hertz
μF	-	Micro Farad
mH	-	milli Henry
kW	-	Kilo Watts
mV/div milli	-	Volt per division
Ω	-	Ohm
s	-	Time periods in seconds
%	-	Percentage

*C*hapter*-1*

1. INTRODUCTION

1.1   Introduction

There has been a sharp rise in consumption of energy worldwide since the last decade. Mostly generation of energy depends on fossil fuel which has a limited supply. Generation of power via conventional methods also causes irreversible damage to the environment. In many parts of the world there is a substantial gap between demand and supply of energy, which leads to the energy crisis scenario. The demand of electrical energy is increasing every day and is likely to rise by 75% in the year 2030 compared to today's demand [1], [2]. The government is spending a substantial amount of money to meet the ever increasing demand. So substantially energy crisis leads to economic crisis. To meet the demand of energy, mankind has been using renewable energy sources like wind power, solar power, biomass power from past few decades. Steady progress in market deregulation and new legislations in terms of environmental constraints and greenhouse gas emissions has created a significant opportunity for distributed generation. Rising public awareness for ecological protection and continuously increasing energy consumption, coupled with the shortage of power generation due to constraints imposed on new construction have further resulted in a steady rise in interest in renewable and clean power generation. The switch to renewable energy has been proved beneficial for both mankind and environment. So researchers are working towards new ways to generate energy from renewable sources. India is one of the first country to set up the

department of non-conventional energy sources way back in 1982 and ministry of non-conventional energy sources (MNES) in 1992. MNES was renamed as Ministry of new and renewable energy (MNRE) in 2006. According to ministry sources [3], till 30th Sep 2013, the grid connected power from different renewable energy sources is 29464.51 MW and off grid power from renewable energy sources in 921.3 MW. The major part of the renewable energy comes from wind power. Solar power comes a distant second. One drawback of wind and solar energy sources is their variability. Wind tends to blow intermittently and solar power is only available during the daytime. Ideally, excess renewable energy generated during times of plenty can be stored for use during periods when sufficient electricity is not available. But storing this energy is also a difficult task. Due to the practical limitation of wind and solar energy, chemical energy is widely used for generation of electricity. A fuel cell is a device which converts stored chemical energy (hydrogen, oxygen) to electrical energy. The conversion of the fuel to energy takes place via an electrochemical process which is non-polluting and efficient. One of the major advantages of a fuel cell system is that it can be placed at any site in a distribution system without geographic limitations to provide optimal benefit, and they are not intermittent in nature. Whereas for solar and wind energy generation proper geographical survey has to be carried out to find the best possible place for their installation. Fuel cells offer numerous advantages over conventional power plants to help them achieve that goal and widespread adoption, such as:

➢ High efficiency, even at part-load
➢ Few moving parts resulting in quiet operation, higher reliability, lower maintenance and longer operating life
➢ Fuel diversity
➢ Zero or low emission of greenhouse gases
➢ Combined Heat and Power (CHP) capability, without the need for additional systems (i.e., low temperature fuel cells can provide district heating while high temperature fuel cells can provide high-quality industrial steam)
➢ Flexible, modular structure
➢ Increased energy security by reducing reliance on large central power plants and oil imports

Some of the agencies involved in the research and development of fuel cells in India are Ministry of New and Renewable Energy Sources (MNES), Delhi Transport Corporation (DTC), Indian Railways, Indian Institute of Science and Central Glass & Ceramic

Research Institute, Tata Energy Research Institute (TERI), Bharat Heavy Electricals Ltd. (BHEL), and Reva Electric Car Company. Ministry of New and Renewable Energy Sources (MNES) has established programmes named chemical sources energy programme for research and development and National Hydrogen energy roadmap for fuel cell technology.

Fuel cell is widely used in space, military and vehicular applications. In space applications, fuel cell is used in launch vehicles, earth orbiting space craft, space shuttle, crew return vehicles, astronaut equipment, planetary, spacecraft, landers, rovers, and penetrators. The power sources used in a space mission has to meet some of the hardest performance requirements such as the power source should provide more power and it should also be compact in size and weight. The power source should operate in hard vacuum for 30,000 life cycles with a long active shelf life of 10 years. The power source should provide reliable power despite harsh environmental conditions including vibration, shock, and sub-zero temperature. Conventional power sources such as batteries are unable to meet these stringent requirements, so scientists have rested their faith on fuel cells. For the first time in August 21, 1962, PEM fuel cells were successfully used in Gemini space craft. Apollo space craft used alkaline fuel cells [4].

Fuel cells are widely used in military applications such as Unmanned Aerial Vehicles (UAV), Unmanned Ground Vehicles (UGV), solider portable power, warships, and submarines. Navy of German, Greek, South Korea, Italy and Poland have extensively used fuel cells in submarines.

Fuel cell is used to drive hybrid electric vehicles [5]. Designing a standalone fuel cell unit for hybrid electric vehicle (HEV) to meet all the steady state and transient demand will make the system bulky and costly. The standalone fuel cell unit can't recycle power in HEV so the energy dissipated during braking is wasted which increases the consumption of fuel. To reduce the cost of the fuel cell unit in HEV conventional batteries are used along with the fuel cell unit but the conventional battery has several limitations such as low power density, low cycle and calendar life and incapability to meet the requirement of transient load profile. So, batteries are replaced by ultra-capacitor (super capacitor). Ultra-capacitor has higher power density, high cycling capacity and provide clean and maintenance free operation. When used in parallel with fuel cell unit, ultra-capacitor provides sudden power required for acceleration in HEV. Ultra-capacitor module stores excess energy and helps in recycle of energy. Parallel

connection of fuel cell unit and ultra-capacitor unit provides an economical solution to meet the required power demand for transient and steady state load demand of an HEV [6], [7].

1.2   Shortcomings

Despite investment in fuel cell technology and a good amount of expertise among the academic community, India remains a relatively small market for fuel cells at present. The biggest challenges to fuel cell commercialisation remain affordability and the shortage of skills in manufacturing and maintaining fuel cells. Indian companies are procuring fuel cell stacks from manufacturers of North America and European Union and tailor the stacks to the customer requirements. However, with the potential for vast economies of scale and a history of technological advancing, the outlook for fuel cells is optimistic in the longer term. Most of the companies are working to develop fuel cell based application for energy backup, distributed generation and automobile.

1.3   Motivation of Research

Indian companies import fuel cell stack from North America and European Union and modify the stack to the requirement. In order to commercialize the fuel cell as an affordable medium of renewable energy sources, research has to be concentrated to develop fuel cell based low cost energy management system which will provide backup energy to household and commercial establishments at an affordable energy per unit cost. Digital control of DC/DC converter and DC/AC inverter plays a vital role in providing reliable supply to load/grid connected system. So, research has to be concentrated on state of art control techniques of the converter-inverter topology. Though there are several digital processors to implement the control law, the ideal processor has to be reliable, modular and low cost. The primary motivation of this thesis is to develop a modular, low cost digital control scheme for converter-inverter topology which will eventually lead to a fuel cell based energy management system, which provides backup energy to household and commercial units at a reasonable energy per unit cost.

1.4   Problem Formulation

Research is going on to develop load/grid connected fuel cell based energy management system. A household or commercial unit is connected by a grid for 24 hour power supply. When due to any unwanted circumstances, the grid ceases to function; the fuel cell units

need backup power for energy. Due to the advancement of technology, different renewable sources like photovoltaic (PV) and wind energy system are used as backup power units. But these systems have several drawbacks. Photovoltaic array based backup power operates in its peak only during day time. Efficiency of PV array is low and the energy per unit cost of PV array based backup power is considerably high. Wind energy based system is not suitable for every rural household. So fuel cell is emerging as an alternate medium for backup power supply.

Ideally fuel cell provides low output voltage and has to be stepped up by a power electronic converter for further processing. During any kind of unavoidable circumstances when fuel cell units are not working properly due to shortage of hydrogen then a battery can be used to get backup power. A fuel cell has an output voltage that depends on the number of cells connected in series or parallel. When there are sufficient numbers of fuel cell units available, then it provides sufficient output voltage and power electronic converter is not required. This thesis focuses on the above mentioned aspects. The converter output is fed to an inverter which converts DC to AC. Inverter control strategy also plays a vital role to provide backup power. So this thesis focuses to develop low cost digital control strategy for DC-DC converter and DC-AC inverter which will subsequently lead to design of load/grid connected fuel cell power system.

1.5   Literature Reviews

Limited fossil fuel and increasing environmental hazards have forced the scientists to work on renewable energy sources. One of the promising renewable energy sources is fuel cell where chemical energy is converted into electrical energy. Fuel cells are gaining much attention because of their light weight, compact size, low maintenance, low acoustic and chemical emission. They can serve as a source for electric power generation for stand-alone as well as grid tied applications. This section reviews relevant literature of fuel cell modelling, power conditioning circuits and the power quality aspect of fuel cell power system.

1.5.1   Modeling of Fuel Cell

To develop a fuel cell based power system, mathematical modelling of a fuel cell is an important aspect to gain insight about the fuel cell. Recently, significant amount of research is being conducted to develop an accurate mathematical model of fuel cell. Fuel

cell comes in three geometric configurations such as tubular, planar and monolithic. This section reviews some relevant modelling approach of different types of fuel cell.

Numerical modelling of different types and configurations of fuel cells are reviewed extensively in [8]. Electro-chemical model, micro and macro modelling of different fuel cell types are presented in this paper. Three dimensional time dependent numerical model of SOFC is reported in [9]. All the equations are written in a partial differential form, thus the model is independent of the cell geometry (planar, tubular, monolithic) and the modelling approach is time-dependent (i.e. 3D, 2D). In the literature [10], modelling of solid oxide fuel cell is carried out using lumped and distributed modelling approaches. The performance of this model is compared with a detailed distributed model and experimental results. One of the recent papers [11] presents the development of dynamic models for proton exchange membrane (PEM) fuel cells using electrical circuits. The models can also predict the temperature response of the fuel-cell stack and show the potential to be useful in external controller design applications for PEM fuel cells.

To develop a fuel cell power system, an accurate mathematical model of fuel cell along with power conditioning circuits is required. The modelling of fuel cell is non-linear in nature as depicted in the polarization curve (V-I curve) of fuel cell discussed in detail later in Chapter 2. As observed almost all fuel cell models along with power conditioning units only consider ohmic losses. However, it is also quite important to consider activation loss and concentration losses. While we develop models for the fuel cell along DC-DC and DC-AC converters we have taken into consideration of the activation loss and concentration losses. When these effects are considered, a better and more accurate model of the fuel cell evolves; hence along with power conditioning systems this system would provide a closer result compared to practical/real time situations.

1.5.2 DC-DC Converter for Fuel Cell System

This sub-section presents different control techniques of DC-DC converter using analog and digital domain. A boost converter is a power converter with output DC voltage which is greater than its input DC voltage. A boost converter steps up the output voltage; it stores energy by passing current(s) through an inductor and that energy is then delivered at intervals by a MOSFET regulated by PWM (Pulse Width Modulation) to a capacitor [12]. The charged capacitor will then supply a higher voltage at lower current to the load. Boost converter can be isolated or non-isolated type.

A zero-voltage switching (ZVS) three level DC/DC resonant converter for high-power operation is analysed at fixed and variable frequencies in [13] . The converter operates with wide input voltage variations without penalizing the efficiency. As a result, the converter is suitable for applications in which high efficiency and high power density are required. Experimental results for a 2.7 kW prototype verify the operation of the converter performance as designed. A new high efficiency transformer less DC/DC converter is proposed in [14] in which large step-up rations is achieved with low duty cycle. The design structure integrates a multiphase voltage multiplier that allows high static gain with low voltage stress in all the semiconductors used. The main advantages include, low voltage and current stresses, reduction of the turn-on and turn-off losses, low input voltage and current ripples, high efficiency and design modularity. An experimental result confirms the basic operation of the designed converter and theoretical analysis developed. A current-fed full bridge boost converter with zero current switching (ZCS) based on constant on-time for high voltage application is presented in [15]. The proposed converter utilizes the leakage inductance and the winding parasitic capacitance resonant tank to achieve zero current switching. In order to achieve zero current switching under wide load range, the turn-on time of the full bridge boost converter is kept constant and the output voltage is regulated via frequency modulation. With careful design of the circuit parameters, the proposed converter can be operated with ZCS under wide load range without the use of series connected diodes. A laboratory prototype implemented verifies the ZCS performance. In [16], the principle and electrical characteristics of the fuel cell has been discussed. They have proposed a DC-DC converter scheme to combine the fuel cell with storage system. They have used shifted pulse width modulation technique for the DC-DC converter fuel cell. State and transfer function model of the set made up of a proton exchange membrane (PEM) fuel cell and DC-DC converter is presented in [17]. The set is modelled as plant controlled by the converter duty cycle. This model describes the relationship between different electrical variables and is valid for any operating of fuel cell. The linearization technique is applied in order to obtain the entire system's transfer function. Digital control of DC-DC converter on fuel cell vehicles is developed in [18]. Based on the half bridge topology, the control circuit adopting DSP and the control method carried out. TMS320F2812, a highly integrated and high performance DSP is employed as the control core chip. This paper has described the hardware design and control methods. Finally it represents the control method of main DC-DC converter and inverter of Fuel Cell Vehicles.

Currently, there is a trend in which embedded control is applied to most power converters for various applications. As a result, control circuit size is significantly reducing as entire control circuit is configured into a single chip, system on chip (SOC) or FPGA. Therefore, some researchers have initiated research work in this area for making the control circuit simpler, effective and reconfigurable. In literature [19] the authors implemented a 1 kW power conditioner for fuel cell power system with lower ripples and faster dynamics. Poly-phase boost converter is used for power conditioning system which is controlled using current mode control technique. The DC-DC converter and inverter topology is controlled using digital controller implemented in DSP and FPGA. A detailed method of Hardware-in-the-Loop real-time simulation of switch-mode converters in FPGA is reported in [20]. A mathematical description of DC-DC boost converter model, its FPGA-based implementation and debugging results are presented. The results are compared with Simulink model and practical converter. The presented method of simulation can be used for verification of discrete control in designed converters and also as an educational platform. Digitally controlled DC-DC buck converter performed by FPGA circuitry is presented in [21]. All tasks, analog to digital conversion, control algorithm and pulse width modulation, were implemented in the FPGA. This approach enables high-speed dynamic response and programmability by the controller, without external passive components. In addition, the controller's structure can be easily changed without external components.

Fuel cell provides a low voltage (approx. 1.2 V DC) output at a reasonably high current. However, this does not suit many applications. Therefore, this voltage has to be stepped up using DC-DC converter. There are numerous DC-DC converter topologies available for this purpose. To provide a regulated DC voltage at the output a closed loop control is essential. Conventionally, the closed loop control is implemented in analog mode but there are certain limitations of analog mode control. In recent times, in most of the cases control law is implemented in digital domain.

Considering the above discussion, we agree that several topologies are available for dc-dc boost conversion. However, control laws are important as this would determine several performance metrics (ripple, settling time, response time) of the topology in general. Moreover, in the present dissertation our objective is to operate fuel cell based dc power system. Therefore, we do use the existing topologies, use suitable control structures that work well with the source. In our study we have used PI controller and

SMC controller. Furthermore, considering application perspective, it is also important to investigate implementation strategies. In our work, we have adopted digital domain; we have implemented PI controller and PWM control using FPGAs that provides flexibility for further modification through reconfigurable computing.

1.5.3   PWM-Current Control Technique for Fuel Cell Power System

DC-AC power converters are known as inverters. The function of an inverter is to change a DC input voltage to symmetric AC output voltage of desired magnitude and frequency. The output voltage of inverter could be fixed or variable frequency. The output waveforms of ideal inverters must be sinusoidal. However, the waveforms of practical inverters are non-sinusoidal and contain some harmonics. This section reviews different control techniques of DC-AC inverter using analog and digital domain.

A novel hierarchical control architecture for a hybrid distributed generation system that consists of battery and a Solid Oxide Fuel Cell is proposed in [22]. The overall aim is to optimize the power flow of this hybrid generation system for different modes of operation while taking into an account component and system constraints. An advanced fuzzy controller has been developed for optimal power splitting between battery and fuel cell. Simulation results of a test system illustrate improvement in the operation efficiency of hybrid system and the battery state of charge has been maintained at reasonable level. A single phase pulse width modulation (PWM) AC-DC power converter with the function power factor correction and active filter is proposed in [23] to reduce the harmonic currents flowing into the power system and to a nearly sinusoidal current with unit power factor. The circuit topology of the adopted three-level PWM AC/DC converter is based on a conventional two level full bridge rectifier and one AC power switch. No additional active filter is needed, since the converter adopted can simultaneously as a power factor corrector and an active filter. The advantages of the proposed three level converters, instead of a two-level converter, are in implementing a high voltage application using low voltage devices and reducing the voltage contents. A new grid connected inverter for fuel cells system is developed by [24]. It consists of a current-fed push-pull DC-DC converter and H-bridge inverter. A new dedicated voltage mode start-up procedure has been developed in order to limit the inrush current during start-up. The push-pull topology is selected in order to decrease the conduction losses in the switches due to the low fuel cell voltage. The inverter has shown to be reliable and to

exhibit high efficiency. In [25], a new high efficiency grid connected single phase converter for fuel cells. It consists of a two stage power conversion topology. The proposed converter consists of an isolated DC-DC converter cascaded with a single phase H-bridge inverter. The DC-DC converter is a current fed push-pull converter. The inverter is controlled as a standard single phase power factor controller with resistor emulation at the output. The converter is reliable and exhibits a high efficiency over a wide input power range. Experimental results verify that the inverter exhibits a high power factor and low current total harmonics distortion (THD). In [26], a fuel cell inverter system that employs a three-terminal push-pull DC-DC converter to steps up the fuel cell voltage (28 V) to ±200 V was designed and developed. Advantages of this design low cost, lower parts count, protection and diagnostic features that gives safety for the operator. It also provides flexibility and intelligence incorporated to suit varying system and control requirements.

A low cost fuel cell inverter is developed in [27]. This paper employs a three-terminal push-pull DC-DC converter to boost the fuel cell voltage (48 V) to ± 200 V DC. A four switch [insulated gate bipolar transistor (IGBT)] inverter is designed to produce 120 V/240 V, 60 Hz AC outputs. Experimental results have been presented to validate the design for linear and nonlinear loading conditions. Advantages of this design include lower parts counts, easy manufacturability, lower cost, protection and diagnostic features that provide safety and convenience for the operator. These papers [28] and [29] have developed a non-linear dynamic model of solid oxide fuel cell (SOFC). It can be used for dynamic and transient stability studies. The output voltage response of a stand-alone fuel cell plant to a step load changes, a fuel flow step change and a fast load variation. The proposed [30] power processing unit consists of the front-end DC-DC converter, the DC-AC inverter and the bidirectional DC-DC converter. Practical issues such as component rating calculation, high frequency transformer design, heat sink design, and protection are detailed aiming at the cost and efficiency targets. A low cost controller design is discussed along with current mode control, output voltage regulation with capacitor balancing and state of charge (SOC) control for battery management. A 10 kW hardware prototype was built and tested in the steady-state as well as in the transient-state. In [31], a new designed topology for fuel cell energy conversion is developed. A current-source sine wave voltage inverter is designed in the sense of voltage-clamping and soft-switching. This enables the use of a smaller inductor in the current source circuit and

compression of the voltage stress across switches about the two times of the DC bus voltage. Advantages include lower distortion, fast dynamic regulating speed and insensitivity to load variations, even under nonlinear load. An experimental and modelling of a proton exchange membrane (PEM) fuel cell is described in [32] . A small signal model of the electrochemical generator is developed. This model is the extrapolated in order to predict the high signal fuel cell behaviour. The frequency response to small current ripple is measured and modulated through an impedance spectroscopy. It is shown that a fuel cell stack offers possibilities to filter high frequency current harmonics by the intermediary of its double layer capacitor. Active and reactive power output of stand-alone fuel cell (proton exchange membrane fuel cell (PEMFC) is controlled in [33]. This analysis is based on an integrated dynamic model of the entire power plant including reformer. The paper [34] has suggested that fuel cell plant be designed to be capable of delivering ancillary services as well as power in order to facilitate their market entry. This paper narrates the initial fuel cell stack and power conditioning methodologies. SOFC stack models for power system simulation (PSS) have been proposed, as well as a model for the PCU of the plant. This paper also reported on modelling of the different fuel cell plant subsystems. In [35] , it has explained the fuel cell output voltage at the series of stacks is uncontrolled DC voltage that fluctuates with load variations. It is converted to controlled DC voltage by fuzzy logic control scheme that adjusts the duty ratio of the converter and also protects the fuel cell against sudden load changes and current reversal. Here, they have taken solid oxide fuel cell (SOFC) as a stand-alone power plant because of high output voltage and efficiency. A fuzzy logic based controller is designed for this purpose. The dynamic model of fuel cell and controllers for fuel cell based distributed generation systems (DGS) in stand-alone AC supply have developed in [36] . Dynamic model of fuel cell is considered. It has taken a unidirectional full-bridge DC to DC boost converter for the fuel cell and a bidirectional full-bridge DC-DC buck/boost for the battery. For three phase DC-AC inverter, a discrete-time state space model in the stationary *dq* reference frame is derived and two discrete time sliding mode controllers are designed. To demonstrate the proposed circuit model and control strategies, a simulation test bed using MATLAB/SIMULINK is developed. The paper [37] have used the fuel cell simulator designed and manufactured as electrical characteristics of fuel cell generation system uses a simple buck converter. Characteristics of voltage and current (V-I) curve for fuel cell is controlled by linear function. Fuel cell generation system performance, operation of full bridge DC-DC

converter and single phase DC-AC inverter are designed and manufactured for the fuel cell applications. The close agreement between the simulation and experimental results confirms the validity and usefulness of the proposed fuel cell simulator. In literature [38], fuel cell with DC-DC boost converter for 100W fuel cell power conditioning is discussed. Some topologies were tested and a boost converter was selected because of its best performance. This converter was made especially for a particular fuel cell application. Dynamic model of fuel cell is developed in [39]. This fuel cell is connected to DC-DC converter and electric motor. The focus of this paper is on controlling the power output delivered to an electric motor from a fuel cell through a DC-DC converter. It has not considered the control algorithms for input flows, temperature and other variables. They have taken PI (Proportional Integral) controller to control the duty ratio of DC-DC converter. Various power conversion systems (PCS) for hybrid power system with fuel cell and battery are explained in [40]. Theoretical explanation and informative and experimental results are given in this paper. The PCS plays an important role to deliver the generating power from fuel cells to various loads according demands. The PCS should be designed and operated with high efficiency, high performance and high reliability and especially low cost. The PCS consists of DC-DC converter, a bidirectional DC-DC converter and DC-AC inverter along with an energy storage unit. Proton exchange membrane fuel cell (PEMFC) model of fuel cell stack is developed in [41]. This model is used to predict the output voltage, efficiency and power of fuel cells as a function of the actual load current. Additionally this electrochemical model was tested on for the SR-12 Modular PEM Generator, a stack rated at 500 W, manufactured by Avista Laboratories, for the Ballard Mark V FC and for the BCS 500-W stack. The electrochemical model and fluid dynamic aspects of the chemical reactions inside the fuel cell stack is explained in [42]. It also explained the voltage losses due to ohmic, activation, and concentration losses are accounted for. It includes a fuel cell stack, a reformer model and DC-AC inverter model. Fuzzy logic control (FLC) scheme is used to control active and reactive power of PEM fuel cell system. The fuel flow is controlled simultaneously to control the active and reactive power. The paper [43] has investigated the proton exchange membrane fuel cell (PEM) as an alternative power sources. They have presented a circuit model for fuel cell and analysed the fuel cell power systems by using PSPICE. In literature [44] have developed a model of polymer electrolyte membrane fuel cells (PEM) for the purpose of constructing a non-linear control strategy for PEMFC by using exact linearization method. The fuel cell efficiency decreases as its

power output increases. In order for fuel cell system to obtain highly efficient operation with the same power generation, more cells and other auxiliaries such as a high-capacity compressor system etc. are required. They have connected fuel and DC-AC PWM inverter to the load. The paper [45] has developed a proton exchange fuel cell (PEM). They have constructed a DC-DC buck converter is used to step-down the PEMFC output voltage. The fuel cell and power converter have different dynamics. They must be suitably coordinated in order to satisfy the demanded load. A sliding mode control (SMC) scheme is proposed for DC-DC buck converter which guarantees a low and stable output voltage given transient response in the output voltage of the PEMFC. Finally, fuel cell model is combined with DC-AC inverter with pulse width modulation (PWM) technique used to generate switching signal of the inverter. A control strategy for hybrid power generation systems including fuel cell and photovoltaic as the main sources and battery energy storage as the auxiliary power source is proposed in [46]. The paper has described the dynamic models for the fuel cell, photovoltaic and battery bank and its power conditioning. It has developed the control strategy of power sources, DC-DC converter and DC-AC inverter to manage the power flow on the DC and AC sides. Non-linear control for fuel cell/battery/ultra-capacitor hybrid power sources (HPS) that improves the performance and durability of the fuel cell is proposed in [47]. The non-linear voltage control is analysed and designed by using systematic approach. The design goal is to stabilise the hybrid power sources output voltage at low voltage ripples. This paper describes the bi-buck topology as a power interface with inverter system. Generic dynamic model for a grid connected fuel cell plant is presented in [48] . The steady state power generation characteristics of the plant are derived and analysed. Two major loops for voltage and power control are incorporated. The paper presents an application of the proposed model to study of distributed generation for a utility that employs fuel cell and gas turbine plants. An FPGA based SPWM generator is presented in [49] , which is capable to operate at switching frequencies up to 1 MHz, thus it is capable to support the high switching frequency requirements of modern single-phase DC/AC power converters. An FPGA control of grid connected current controlled VSI is implemented in [50]. Various control functions and implementation methods are described. The practical viability of the system is evaluated in an experimental setup, where a VSI supplies 30 kW into the local grid at 400 V.

To get proper utility AC power supply from a fuel cell power system, DC-AC inverter plays a vital role. There are different control techniques of DC-AC inverter but the most widely used control technique is current mode control of inverter. The current mode control is an ideal choice because it is faster and easy to implement. In this work, we discuss several current control strategies; our primary purpose is to find out the best control law in the context of our application.

1.5.4   Shunt Active Power Filter for Fuel Cell Power System

The growth of consumer electronic devices has given rise to power quality issues. To solve the power quality issues additional power electronic circuits are installed. In a grid connected fuel cell system, the use of active power filter is mandatory to maintain the power quality. This section provides a literature review on modelling of fuel cell and power conditioning circuits.

Modelling, control and design analysis of a three-phase grid-interactive fuel cell system with active filter functions is designed in [51]. The main focus of this paper is to control the active power supplied by the fuel cell distributed generation system while compensating harmonics and reactive currents caused by the nonlinear loads using shunt active power filter. In literature [52], it presents a method for the performance improvement of a shunt active power filter (SAPF) using the indirect current control scheme. Compared to the conventional direct current control scheme, the indirect current control scheme gives better performance with a lower number of sensors. An implementation of a new control algorithm for a three-phase shunt active power filter to regulate load terminal voltage, eliminate harmonics, correct supply power-factor, and balance the nonlinear unbalanced loads is proposed in [53].

From the above discussion it is found that there is an increasing research interests in use of active power filters for improvement of power quality in a grid connected system.

In our present investigation; we demonstrate that it is possible to have a fuel cell based power system. Simultaneously, if desired, this also can act as an active power filter as fuel cell itself is a dc source and can act as a replacement for the capacitor/battery. In a normal situation, cost would be an issue; however as a supplementary source it could always be useful.

Generation of electricity from renewable energy source is one of the promising areas of research where researchers are working to develop distributed generation system to provide low cost electricity to mankind. Fuel cell is one of the alternative sources which can generate electricity from a chemical reaction. The major issue of fuel cell is cost, fuel and materials. The operation of fuel cell is primary area of research of material scientists and chemists. The electrical engineer tries to utilize the electricity generated by fuel cell in house hold applications. To develop a fuel cell power system accurate modelling of fuel cell and proper design of power conditioning circuits and controller are essential. Therefore, in this dissertation we have developed a prototype to demonstrate the practical scenario. Keeping in view of future expansion and alternate solution, FPGA based reconfigurable computing is adopted.

1.6   Objectives of the Thesis

A wide range of literature analysis has been carried out in perspective of this research. Based on the literature survey presented above, the main objective of our work is to simulate and experimentally validate a load/grid connected fuel cell power system. It is observed that there exists an opportunity to develop an efficient dynamic model of solid oxide fuel cell (SOFC) and study its performance when connected to load/grid.

- ➢ To develop a dynamic model of SOFC in MATLAB/SIMULINK.
- ➢ Development of SOFC model which includes the activation voltage loss, concentration voltage loss, and ohmic voltage losses and analysis of various dynamic responses such as stack voltage, stack current; stack power and efficiency.
- ➢ Design and development of DC–DC boost converter to step up the output voltage of fuel cell system to the desired voltage level. To test and verify performance of fuel cell with DC-DC converter with various control techniques like PI (Proportional Integral) controller, sliding mode controller (SMC) for output voltage variations of fuel cell. To validate control techniques through hardware set up and implement using FPGA implementations for reduction of control circuit size.
- ➢ To test the FCPS (Fuel Cell Power System) system for standalone/grid supply. The output of DC-DC converter is to be fed to an inverter which requires accurate gate pulses to operate. Control of PWM-VSI is required to generate gate pulses for the inverter. Different PWM-VSI current control schemes namely fixed

15

hysteresis current controller, adaptive hysteresis current controller, fuzzy hysteresis current controller, adaptive fuzzy hysteresis current controller, triangular-carrier current controller; triangular-periodical current controller are investigated which is required to improve the system performances.

➤ Design and development of shunt active power filter to improve the power quality using fuel cell system.

➤ Experimental validation of single phase fuel cell power system with suitable control scheme.

➤ To develop control schemes using FPGA that reduces circuit significantly also simplifies system development.

➤ FPGA based control structure for three phase fuel cell power system using suitable control scheme.

1.7   Scopes and Contributions

This thesis contributes towards developing a load/grid connected fuel cell based power system which is mainly used as backup power supply unit. The mathematical model of fuel cell system is developed and control schemes for the grid/load connected fuel cell power system have been investigated.

The main scopes of this works can be outlined as follows

➤ DC-DC converter is developed to step up the fuel cell output voltage to a required level. Digital control of DC-DC converter using Xilinx/Spartan-3E FPGA target device has been implemented.

➤ PWM VSI current control schemes are required to generate required gate pulses to the inverter with low switching losses. The following techniques are developed to generate the switching pulses for the inverter

- Fixed-HCC
- Adaptive-HCC
- Fuzzy-HCC
- Adaptive-fuzzy-HCC
- Triangular-carrier current controller
- Triangular-periodical current controller

➤ Fuel cell based shunt active power filter is developed to improve power quality and harmonic current compensation.

➢ Single phase fuel cell power system using hysteresis current control scheme is experimentally validated using NI-cRIO-9014 that includes FPGA.

➢ Three phase fuel cell power system using adaptive hysteresis current control scheme is experimentally validated using Xilinx/System Generator.

1.8 Organization of the Thesis

Chapter 1 introduces the need of renewable energy sources which can be used as backup power supply. The detailed literature review of fuel cell modelling, DC-DC converter, DC-AC inverter and active power filter for fuel cell is presented. The objective of the thesis and outline of the thesis is also presented.

Chapter 2 presents different types of fuel cell. This chapter narrates the principles of fuel cell operation, advantages and disadvantages of fuel cell. A detailed dynamic model for SOFC fuel cell is developed. It contains the mathematical modelling and electrical features of the fuel cell system. It also describes the different types of stack voltages i.e. i) Activation voltage loss, ii) Concentration voltage loss, and iii) Ohmic voltage loss. It includes the calculation of the partial pressure of hydrogen, oxygen and water.

Chapter 3 describes different control algorithms of DC-DC converters and the interconnection of fuel cell system with DC-DC converter. It explains the different types DC-DC converters and their working principles. PI controller, sliding mode controller, FPGA based PI controller have been developed for DC-DC converter. This chapter concludes development of prototype model of FPGA based controller.

Chapter 4 describes the various PWM-VSI current control techniques for load/grid connected fuel cell power system. The fixed-HCC, adaptive-HCC, adaptive-fuzzy-HCC, TPCC, and TCCC techniques are discussed that are used to generate the required switching signals of the PWM-inverter.

Chapter 5 investigates the performance of the fuel cell power system by employing different methods of PWM-VSI control techniques. Different control strategies (HCC, AHCC, Fuzzy-HCC, Adaptive-fuzzy-HCC, TPCC, and TCCC) for fuel cell power system are validated through extensive simulation using Matlab/Simpower system tools. The fuel cell power system is tested under linear load in steady-state conditions.

Chapter 6 presents an application of fuel cell based system for shunt active power filtering. It describes the shunt active power line conditioner topology, system

configuration, characteristics of harmonics as well as compensation principle. The active power line conditioner topology is developed with voltage source inverter that has a fuel cell as dc source.

Chapter 7 focuses on the hardware set-up and experimental verification of the single-phase fuel cell power system using fixed-HCC. DC-DC boost converter control is carried out using PI controller. PWM-VSI current controller (HCC) is designed and executed through NI-cRIO-9014. Three phase fuel cell power system using AHCC is experimentally validated using Xilinx/System Generator.

Chapter 8 General conclusions are derived from the thesis. This chapter also presents some future directions for research in the area of fuel cell power system connected to the load/grid.

$\mathcal{C}$*hapter*-2

2. DESCRIPTION OF FUEL CELL SYSTEMS

2.1   Introduction

The principle of the fuel cell was discovered by the German Scientist Christian Friendrich Schonbein in 1838. The first fuel cell was demonstrated in the year 1839 by Welsh Scientist and Barrister Sir William Robert Grove in the philosophical magazine and journal of science. In 1955, W. Thomas Grubb, a chemist working for the General Electric Company (GE), modified the original fuel cell design by using a sulphated polystyrene ion-exchange membrane as the electrolyte.

After three years, Leonard Niedrach devised a way of depositing platinum onto the membrane, which served as catalyst for the necessary hydrogen oxidation and oxygen reduction reactions. This is known as the "Grubb-Niedrach fuel cell". It was the first commercial use of fuel cell. In 1959, British engineer Francis Thomas Bacon developed a 5 kW stationary fuel cell. Later in 1959, Bacon and his colleagues showed a practical 5 kW unit capable of powering a welding machine. In the year 1960s, Pratt and Whitency licensed bacon's U.S. patents for use in the U.S Space program to supply electricity and drinking water. In the year 1991, the first hydrogen fuel cell based automobile was developed by Roger Billings.

United Technologies Corporation's (UTC) power was the first company to manufacture and commercialise a large, stationary fuel cell system for use as a co-generation power plant in hospitals, universities and large office buildings. The company has demonstrated

the first fuel cell capable of starting under freezing conditions with proton exchange membrane.

2.2   Principle of Fuel Cell

Fuel cell is a static device that converts the chemical energy of hydrogen and oxygen directly into electricity with by-product as water and heat. A simplified working fuel cell is shown in Fig.2.1 [41] . It consists of an electrolyte layer which is in contact with two electrodes, one fuelled with hydrogen fuel and the other with oxygen. The electrode fuelled with hydrogen acts as an anode electrode and the electrode fuelled with oxygen acts as cathode electrode. The fuel and oxidant are to be fed continuously to fuel cell. The electrolyte which acts like a membrane permits only the positive ions to flow from anode to cathode and acts as an insulator for electrons. The electron produced from the hydrogen fuel electrode after decomposition tries to get stable by going to cathode side which is accomplished by an external circuit and this way, electricity is generated. The reactions taking places in the fuel cell are described below:
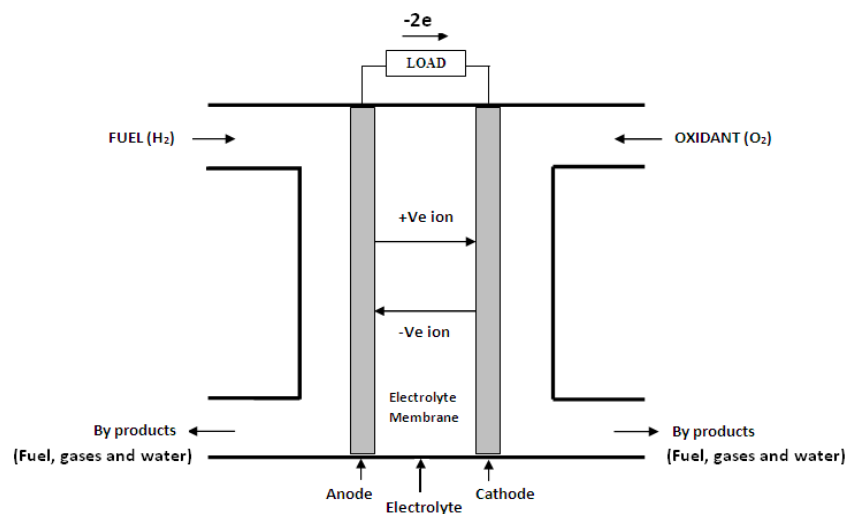
Fig.2.1 Basic working principle of fuel cell

Anode reaction:

$$H_2 \Rightarrow 2H^+ + 2e^-$$

(2.1)

Cathode reaction:

$$\frac{1}{2}O_2 + 2H^+ + 2e^- \Rightarrow H_2O$$

(2.2)

Overall reaction:

$$H_2 + \frac{1}{2}O_2 \Rightarrow H_2O$$

(2.3)
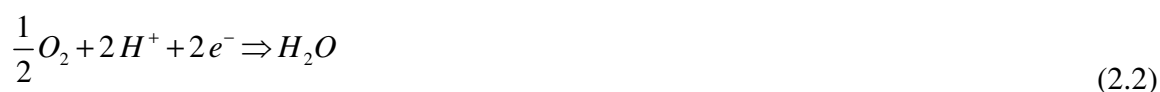
In a typical fuel cell, gaseous fuels and an oxidant (i.e. oxygen from air) are fed continuously to the anode (negative electrode) and the cathode (positive electrode) respectively and the electrochemical reactions take place at the electrodes to produce an electric current. A fuel cell, although having components and characteristics similar to those of a typical battery, differs in several aspects or features. The battery is an energy storage device and the maximum energy available is determined by the amount of chemical reactant stored within the battery itself. The battery will cease to produce electrical energy when the chemical reactants are consumed (i.e. discharged). In a secondary battery, the reactants are regenerated by recharging, which involves putting energy into the battery from an external source. The fuel cell, on the other hand, is an energy conversion device that theoretically has the capability of generating electrical energy as long as fuel and oxidant are supplied to the electrodes. In reality, degradation, primarily corrosion, or malfunction of components limits the practical operating life of fuel cells.

An ion species and its movement direction can be different, influencing the site of water production and removal. The ion can be either a positive or a negative ion, meaning that the ion carries either a positive or negative charge (deficit or surplus of electrons). The fuel flows past the surface of the anode or cathode opposite the electrolyte and generate electrical energy by electrochemical oxidation of fuel, (usually hydrogen) and the electrochemical reduction of the oxidant, (usually oxygen) [54]. In order to increase the rates of reactions, the electrode material should be catalytic as well as conductive, porous rather than solid. The catalytic function of electrodes is more important in fuel cells having lower temperature and less important in case of high temperature fuel cells because rate of ionization reaction increase with respect to the temperature of the fuel cells.

2.2.1   Advantages of Fuel Cell System

The major advantages of Fuel Cells are highlighted below:

➢ High energy conversion efficiency

➢ Modular design

➢ Fuel flexibility

➢ Cogeneration capability

➢ Rapid load response, relative to conventional power generation based prime movers

➢ Low environmental pollution and very low emissions

➢ Low noise

➢ High efficient power generation

➢ Reusability of exhaust heat

➢ Faster installation

2.2.2   Disadvantages of Fuel Cell System

The major disadvantages of Fuel Cells are highlighted below:

➢ High Cost of Market Entry

➢ Inadequate Infrastructure Support

➢ Production, Transportation, Distribution and Storage of hydrogen is difficult

2.2.3   Applications of Fuel Cell System

Fuel Cells have got wide applications which are indicated below:

➢ Stationary Power Sources

➢ Portable Power Sources

➢ Micro Power Sources

➢ Vehicles

➢ Distributed generation

➢ Automotive propulsion

➢ Space and other closed environmental electrical power supply

➢ Auxiliary power systems

➢ Derivative applications (portable units)

2.3 Different Types of Fuel Cell Technology

There are five main types of fuel cells currently that has been developed and/or distributed.(The kind of chemical reactions that take place in the cell, the kind of catalyst required, the temperature range in which the cell operates, the fuel required, and other factors.) There are several types of fuel cells currently under development, each with its own advantages, limitations, and potential applications [55], [56]. These include Phosphoric Acid Fuel Cells (PAFC), Molten Carbonate Fuel Cells (MCFC), Direct Methanol Fuel Cell (DMFC), Solid Oxide Fuel Cells (SOFC), and Proton Exchange Membrane Fuel Cells (PEMFC). Comparisons between these four fuel cells are outlined in Table 2.1.

Table 2.1 Comparisons of different types of fuel cells

	PAFC	MCFC	SOFC	PEMFC
Electrolyte	Phosphoric Acid	Molten Carbonate Salt	Ceramic	Polymer
Operating Temperature	190^OC	650^OC	1000^OC	80^OC
Fuels	Hydrogen Reformate	H_2/CO_2 Reformate	$H_2/CO_2/CH_4$ Reformate	H_2 Reformate
Reforming	External	External Internal	External Internal	External
Oxidant	O_2/Air	CO_2/O_2/Air	O_2/Air	O_2/Air
Efficiency	40-50%	50-60%	40-80%	40-50%

2.3.1 Phosphoric Acid Fuel Cell (PAFC)

Phosphoric Acid Fuel Cells (PAFC) are the most commercially developed type of fuel cell. PAFCs are being used in hospitals, nursing homes, hotels, office buildings, schools, utility power plants, and airport terminals. This type of fuel cell generates electricity at efficiency more than 40%, and if co-generated heat is used, the efficiency goes upto 85%. PAFCs have got both stationary and mobile applications. These cells have a wide

capacity range i.e. from 50 kW to 500 kW. Developers of PAFC are targeting commercial and light industrial applications in the 100-200 kW power range, for applications in generation of electrical energy and cogeneration processes. For such applications, PAFCs have demonstrated multiple favourable characteristics till date which are highlighted below:

- ➢ Packaged systems with extremely high reliability (some have operated in the field for > 9,000 hours of continuous service)
- ➢ Very low noise and vibration
- ➢ Negligible emissions

2.3.2   Molten Carbonate Fuel Cell (MCFC)

Molten Carbonate Fuel Cells (MCFC) promises high fuel to electricity efficiencies. These cells operate at about 650^0C/$1,200^0$F and can reform directly. It consists of two porous electrodes with good conductivity that is in contact with a molten carbonate cell. Due to its internal reforming capability, it separates the hydrogen from carbon monoxide fuel. The decomposition of hydrogen is taken through the water shift reaction to produce hydrogen. The major advantages of MCFC are higher efficiency as good as 50-60% and there is no need of metal catalyst and separate reformer due to its high operating temperature [57]. MCFCs are available in sizes ranging from 250 kW to 5 MW which are mainly static in nature. The high efficiency and high operating temperature of MCFC units makes it the most attractive power generation at base load, either in electric only or in cogeneration modes.

Potential applications for MCFCs include:

- ➢ Industrial
- ➢ Government facilities
- ➢ Universities

2.3.3   Proton Exchange Membrane Fuel Cell (PEMFC)

The PEM fuel cell uses a solid polymer electrolyte (Teflon-like membrane) to exchange the ions between two porous electrodes, which is an excellent conductor of protons and

an insulator for electrons. The chemical reactions those are involved in anode and cathodes are discussed in [58], [59].

Proton Exchange Membrane Fuel Cells (PEMFC) operate at relatively low temperatures (i.e., about 200 degrees Fahrenheit), have high power density, and can vary output quickly. PEMFCs range in size from sub-kW to 500 kW. Both stationary and vehicle applications are available.

PEMFC technology development has been driven in large part by the automotive sector, where the PEMFCs have a compelling advantage over other fuel cell technologies in terms of their size and startup time, as shown in Table 2.2 below.

Table 2.2 Comparison of size and start-up time of different fuel cells

Fuel Cell Technology	Peak Power Density (mW/cm^2)	Start-up Time (hours)
PAFC	~200	1-4
MCFC	~160	10+
SOFC(tubular)	150-200	5-10
SOFC(planar)	200-500	Unknown
PEMFC	~700	<0.1

PEM fuel cells are currently being developed for a broad range of applications including:

➢ Automotive

➢ Residential (<10 kW), both with and without cogeneration functionality

➢ Commercial (10 - 250 kW), both with and without cogeneration functionality

➢ Light industrial (250 kW and below), both with and without cogeneration functionality

➢ Portable power (several kW and small)

➢ Hospitals

2.3.4   Direct Methanol Fuel Cell (DMFC)

DMFC is the hybrid of PEMFC. DMFC still use the same polymer membrane used in the PEMFC, but the difference is that DMFC uses liquid methanol as fuel instead of

reformed hydrogen. During chemical reactions, the anode draws hydrogen by dissolving liquid methanol (CH_3OH) in water in order to eliminate the need of external reformer. At the cathode, the recombination of the positive ions and negative ions takes place, which are supplied from anode through external circuit and it is combined with oxidized air to produce water as a byproduct. The anode catalyst itself draws hydrogen from liquid methanol. The DMFC technology is relatively new compared to the rest of the types of fuel cell, but it does have potential. These fuel cells can be used for portable and micro power applications. The advantages of DMFC are that these are simple structure and good for low power/long period operations. However, those cells are having poor efficiency and are not suitable for high power and short term operations.

2.3.5   Solid Oxide Fuel Cell (SOFC)

The SOFC's are basically high temperature fuel cells. They use dense yttria stabilized zirconia, which is a solid ceramic materials as its electrolyte. Here, oxygen O^{2-} combines with hydrogen H^+ to generate water and heat. The SOFC produce electricity at a high operating temperature of about 1000 degree Celsius. The main advantages of the SOFC is that they are operated at high efficiency of 50-60% and a separate reformer is not required to extract hydrogen from the fuel due to its internal reforming capability.

Solid Oxide Fuel Cells (SOFC) can be scaled from kW-size units to MW-size units for large high-power applications, including industrial and large-scale central electricity generating stations. They can also be used in vehicles. Power generating efficiencies in SOFCs could reach upto 60% in normal operation and where the efficiency goes upto 80% in case of co-generation applications.

Solid oxide fuel cells are being considered for a wide variety of applications, especially in the 5-250 kW size range in the following areas:

➢ Residential cogeneration
➢ Small commercial buildings
➢ Industrial facilities

2.4   Features of Solid Oxide Fuel Cell (SOFC)

In this research SOFC has been considered for wide applications in general purposes. Each fuel cell has its own merits and demerits and field of applications. However, the

SOFC has been given due importance over other fuel cell because of the following main reasons:

➤ Suitable for stationary power applications with step load changes.

➤ Higher system efficiency and higher power density.

➤ Simpler design compared a fuel cell based on liquid electrolytes.

➤ Utilisation of the exhaust heat for co-generation application in industries.

➤ Internal reforming of natural gas reduces the cost considerably.

➤ Higher cell efficiency because of high temperature operation.

➤ Flexibility in fuel choices.

➤ Suitable for Distributed Generation (DG) application because of its high conversion efficiency.

➤ Integration flexibility with other power generating systems, such as automotive engines or gas turbines of various sizes.

2.5   Modeling of Solid Oxide Fuel Cell

2.5.1   Mathematical Model of Solid Oxide Fuel Cell

The following limitations are made in developing the mathematical model of fuel cell stack [60]:

➤ Fuel cell is fed with hydrogen and oxygen.

➤ The gases considered are ideal, that is, their chemical and physical properties are not co-related to the pressure.

➤ Nernst equation is applicable.

➤ Fuel cell temperature is stable all times.

➤ The pressure drop across the electrode channels is negligible.

➤ The ratio of pressure between the inside and outside of the electrode channels is sufficient to consider choked flow.

➤ Ohmic, activation, and concentration losses are considered.

2.5.2   Characterization of the Exhaust of the Channels in the Fuel Cell

The development of dynamic model of the fuel cell begins with choked flow equation [7], [34].

$$\frac{m_f}{P_u} = K\sqrt{M}$$

(2.4)

where,

m_f : mass flow rate (Kg/s)

P_u : upstream pressure

K : valve constant

M : Fluid molar mass

The utilisation factor (U_f) is defined as the ratio of amount of hydrogen that reacts with oxygen to the amount of hydrogen which enters the anode.

$$U_f = \frac{m_f H_2^r}{m_f H_2^{in}}$$

(2.5)

where,

U_f : Utilisation factor

$m_f H_2^r$: Hydrogen which reacts with oxygen

$m_f H_2^{in}$: Hydrogen which enters anode

The following equations can be obtained by considering the molar flow of any gas through valve to be proportional to its partial pressure inside the channel [34].

$$\frac{q_{H_2}}{P_{H_2}} = \frac{K_{an}}{\sqrt{M_{H_2}}} = K_{H_2}$$

(2.6)

$$\frac{q_{H_2O}}{P_{H_2O}} = \frac{K_{an}}{\sqrt{M_{H_2O}}} = K_{H_2O}$$

(2.7)

where,

q_{H_2} and q_{H_2O} : Molar flow rate of hydrogen and water through the anode valve respectively.

P_{H_2} and P_{H_2O} : Partial pressure of hydrogen and water in atm respectively.

K_{an} : anode valve constant.

M_{H_2} and M_{H_2O} : Molecular masses of hydrogen and water respectively.

K_{H_2} and K_{H_2O} : Valve molar constant for hydrogen and water respectively.

By substituting equations (2.5), (2.6), (2.7) in (2.4), the equation can be expressed as:

$$\frac{m_f}{P_{an}} = K_{an} \left[\left(1 - U_f\right) \sqrt{M_{H_2}} + U_f \sqrt{M_{H_2O}} \right]$$

(2.8)

2.5.3 Calculation of Partial Pressure of Hydrogen, Oxygen and Water

The ideal gas law is used to calculate the partial pressure of all the gases [34]. For hydrogen,

$$P_{H_2} V_{an} = n_{H_2} RT$$

(2.9)

where,

V_{an} : volume of the anode channel

n_{H_2} : hydrogen moles in the channel

R and T : universal gas constant and operating temperature of the fuel cell stack respectively.

From equation (2.9)

$$P_{H_2} = \frac{n_{H_2} RT}{V_{an}}$$

(2.10)

Taking the first derivative of equation (2.10)

$$\frac{d}{dt}\left(P_{H_2}\right) = \frac{d}{dt}\left(\frac{n_{H_2} RT}{V_{an}}\right)$$

(2.11)

$$= \frac{q_{H_2} RT}{V_{an}}$$

(2.12)

where, q_{H_2} is the time derivative of n_{H_2} and it represents the molar flow (kmol s^{-1}) of hydrogen. The hydrogen molar flow is further divided into three parts and their relationships can be expressed as follows [34], [33].

$$\frac{d}{dt}\left(P_{H_2}\right) = \frac{RT}{V_{an}}\left(q_{H_2}^{in} - q_{H_2}^{out} - q_{H_2}^{r}\right) \tag{2.13}$$

where,

$\qquad q_{H_2}^{in} \quad$ Molar flow rates of hydrogen in the channel

$\qquad q_{H_2}^{out} \quad$ Molar flow rate of hydrogen out of the channel

$\qquad q_{H_2}^{r} \quad$ Molar flow rate of hydrogen reacting in the channel

According to the electrochemical relationships, the quantity of hydrogen that reacts is given by [34], [61].

$$q_{H_2}^{r} = \frac{N_0 I_{fc}}{2F} = 2K_r I_{fc} \tag{2.14}$$

where,

$\qquad N_0$: number of cells connected in series in the stack

$\qquad I_{fc}$: fuel cell stack current

$\qquad F$: Faradays constant

$\qquad K_r$: modelling constant which is given as follows

$$K_r = \frac{N_0}{4F} \tag{2.15}$$

Substituting (2.14) in (2.13), the time derivative of hydrogen partial pressure can be expressed as

$$\frac{d}{dt}\left(P_{H_2}\right) = \frac{RT}{V_{an}}\left(q_{H_2}^{in} - q_{H_2}^{out} - 2K_r I_{fc}\right) \tag{2.16}$$

Replacing the output flow by (2.6) and taking the Laplace transform both sides followed by isolation of hydrogen partial pressure; it gives the expression for partial pressure of hydrogen as

$$P_{H_2} = \frac{\frac{1}{K_{H_2}}}{1 + \tau_{H_2} s} \left(q_{H_2}^{in} - 2K_r I_{fc} \right)$$

(2.17)

where, τ_{H_2} is the value of system pole associated with the hydrogen flow [34], expressed in seconds and given as:

$$\tau_{H_2} = \frac{V_{an}}{K_{H_2} RT}$$

(2.18)

In similar way, the partial pressure for the reactant, oxygen and product, water can be expressed as follows

$$P_{O_2} = \frac{\frac{1}{K_{O_2}}}{1 + \tau_{O_2} s} \left(q_{O_2}^{in} - K_r I_{fc} \right)$$

(2.19)

$$P_{H_2O} = \frac{\frac{1}{K_{H_2O}}}{1 + \tau_{H_2O} s} \left(2K_r I_{fc} \right)$$

(2.20)

where,

K_{O_2} and K_{H_2} : valve molar constant for oxygen and water block respectively.

2.6   Electrical Modeling of Fuel Cell System

The fuel cell voltage is usually very small, around 1.2 V. Due to their low output voltage it becomes necessary to stack many cells that need to be connected in cascaded series and parallel to increase its power capacity. Several sources contribute to irreversible losses in a practical fuel cell. The losses are called polarisation, over potential, or overvoltage, originate primarily from three sources:1) Activation polarisation 2) Ohmic polarisation 3) concentration polarisation.

The expression for stack output voltage V_{fc} of a fuel cell can be obtained applying Nernst's equation and also taking into account the voltage losses such as the ohmic, activation and mass transportation (concentration) losses as [34], [62], and [63].

$$V_{fc} = E_{fc} - V_{act} - V_{conc} - V_{ohmic}$$

(2.21)

where,

V_{fc}: the stack voltage of the fuel cell

31

E_{fc}: the reversible open circuit voltage (V)

V_{act}: the activation over voltage (V)

V_{conc}: the concentration over voltage (V)

V_{ohmic}: the ohmic voltage loss (V)

The value of the Nernst voltage equation (E_{fc}) is found from Nernst equation

$$E_{fc} = N_0 \left\{ E^0 + \frac{RT}{2F} \left(\ln \frac{P_{H_2} P_{O_2}^{0.5}}{P_{H_2O}} \right) \right\}$$

(2.22)

2.6.1 Activation Voltage Losses

The reason for this loss in SOFC is the sluggishness of chemical reaction that takes place on the surface of electrodes. A certain amount of voltage produced by fuel cell is lost in carrying the reaction forward that transfers the electrons to or from the electrode. Activation losses are estimated using Tafel equation [62]. This equation was derived by physical experimentation on various electrochemical reactions. The MATLAB simulated result of activation voltage loss for a fuel cell stack which is represented in Eq. (2.23) is shown in Fig. 2.2. It provides a relationship between the overvoltage at the surface of an electrode and the natural logarithm of the current density and can be used to calculate the activation voltage loss for the fuel cell [62], [63].

$$V_{act} = A \ln (i)$$

(2.23)

where

V_{act}: the activation voltage loss

A: the slope of Tafel line (Specific Constant for SOFC)

i: current density (current / electrode area)
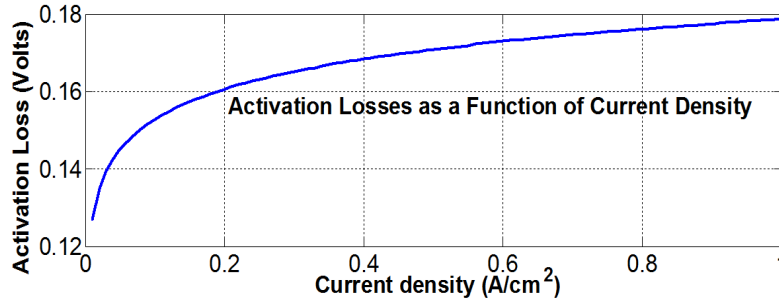
Fig. 2.2 Activation loss verses current density

2.6.2 Concentration Voltage Losses

These losses are also known as mass transport losses and are caused due to the reduction in concentration of reactants in the region of electrode as the fuel is consumed. The consumption of reactants at respective electrodes, i.e. hydrogen at the anode and oxygen at the cathode leads to a slight reduction in concentrations of the reactants [64]. Due to the reduction in concentrations, there is a drop in partial pressure of gases which will result in reduction of the electrode can produce. Unfortunately this loss cannot be calculated analytically with enough accuracy. Therefore, experimental results are used to estimate the loss. Following equation (2.24) has been developed on an experimental basis and is accepted as a good approximation of the mass transport losses.

$$V_{conc} = m \exp(ni)$$

(2.24)

where, m and n are constants.

2.6.3 Ohmic Voltage Losses

These losses in SOFCs are caused due to the resistance both to flow of electrons through the electrodes and to the migration of ions through the electrolyte. In addition, the fuel cell interconnects or bipolar plates also contribute to the ohmic losses [62]. The MATLAB simulated results of ohmic voltage loss of fuel cell stack are shown in Fig 2.3.

Ohmic loss is given as

$$V_{ohmic} = r I_{fc}$$

(2.25)

where, r is the internal resistance and I_{fc} is the fuel cell stack current.
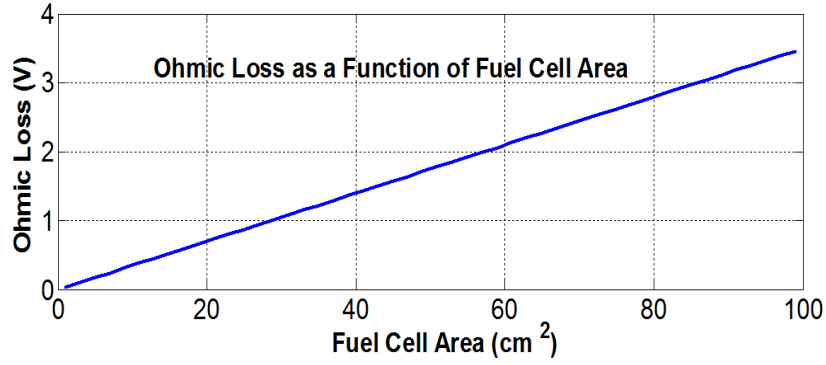
Fig 2.3 Ohmic loss verses fuel cell area

Ohmic losses can be minimised by reducing the internal resistance of the cell, which can be done in the following ways:

- Making electrolyte as thin as possible.
- Using electrodes with highest possible conductivity.
- Using appropriate materials for bipolar plates or cell interconnect.

2.6.4 Calculation of Stack Voltage

The output voltage of a single stack of fuel cell is represented as

$$V_{fc} = E_{fc} - V_{act} - V_{conc} - V_{ohmic} \tag{2.26}$$

Substituting the values of E_{fc}, V_{act}, V_{conc} and V_{ohmic} we get

$$V_{fc} = N_0 \left\{ E^0 + \frac{RT}{2F} \left(\ln \frac{P_{H_2} P_{O_2}^{0.5}}{P_{H_2O}} \right) \right\} - A\ln(i) - m(\exp(ni)) - rI_{fc} \tag{2.27}$$

The performance of a fuel cell can be expressed by the polarisation curve, which describes the cell voltage- current (V-I) characteristics of the fuel cell that are highly non-linear.

Some research paper, considers only the ohmic loss of fuel cell but here all the losses (ohmic loss, activation loss and concentration loss) are taken in to account. The detailed parameters of fuel cell are summarized in Table 5.1. The simulated result of cell voltage versus current density characteristic of a typical fuel cell system [65] is shown in Fig.2.4. It can be seen that a linear region exists because as the current density increases the voltage drops due to its ohmic nature. This region is called ohmic polarisation, it is

mainly due to internal resistance offered by various components. At low current level, the ohmic loss becomes less significant; the increase in output voltage is mainly due to activity of the chemical reactions. So this region is also called active polarisation. At very high current density the voltage fall down significantly because of the reduction of gas exchange efficiency, flooding of water in catalyst and this region is also called concentration polarisation.(Optimisation of fuel cell operating conditions, design of the power conditioning units, design of fuel cell stack systems, and design of controllers depend on such characteristics.)
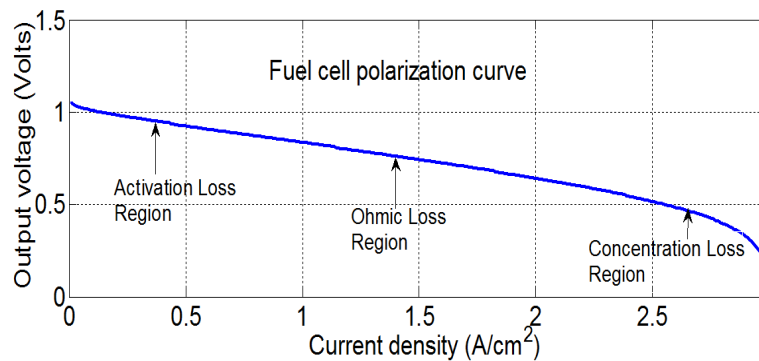
Fig.2.4 V-I Characteristic curve of single fuel cell

The MATLAB simulation results of power output verses current (P-I) characteristics of the fuel cell stack is shown in Fig.2.5. It is observed that the power output increases continuously with the increase in load current and attains its maximum value at certain load current. However after this value is attained, the power output falls rapidly due to the sudden increase in the ohmic and concentration (mass transportation) losses.
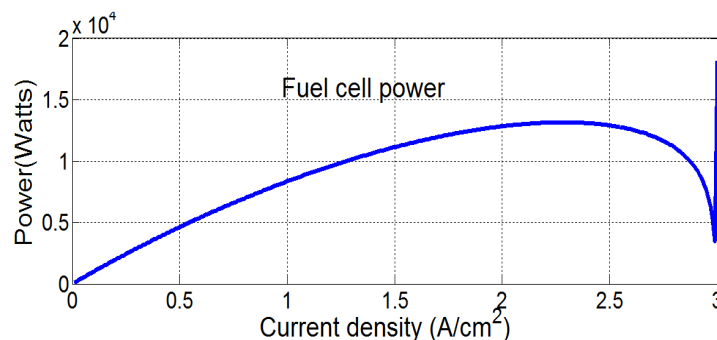
Fig.2.5 P-I characteristics of fuel cell

The simulation results of efficiency of fuel cell stack is shown in Fig.2.6. The efficiency of an actual fuel cell can be expressed in terms of the ratio of the operating cell voltage to the ideal cell voltage.

35
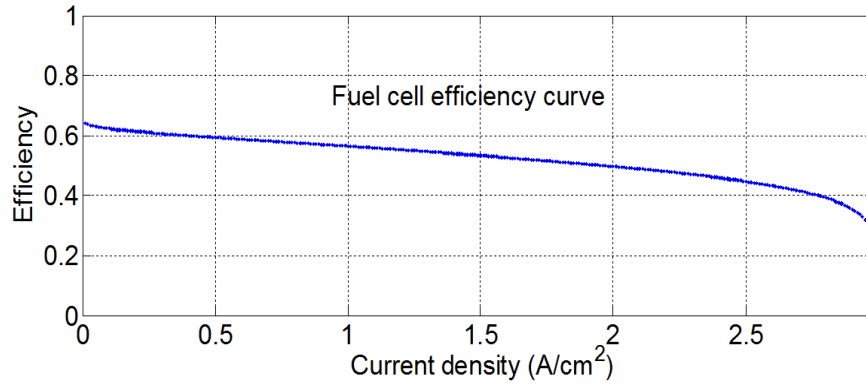
Fig.2.6 Efficiency-current characteristics of fuel cell

The actual cell voltage is less than the ideal cell voltage because of the losses associated with cell polarization and the iR loss, as discussed in the later section. The efficiency of the fuel cell can then be written in terms of the actual cell voltage,

$$\eta = U_f \frac{V_{fc}}{1.48} \tag{2.28}$$

where, U_f is the utilisation factor and V_{fc} fuel cell output voltage.

2.7   Summary

Fuel cells can convert an unusually high proportion of chemical energy in the form of fuel into DC electrical energy. It approaches the efficiency upto 60%, even without co-generation. The efficiency of fuel cell power plants is nearly twice as efficient as conventional power plants. The efficiency is not a function of the plant size for the fuel cell power plants. Fuel cells contribute significantly to the cleaner environment. The by-products so produced are primarily hot water and carbon dioxide which are very small amounts. It has robust and modular structure. Due to their modularity, fuel cells can be placed near the load centres which results in a potential savings in transmission network expansion. This chapter discusses the mathematical and electrical modelling of fuel cell and simulates the V-I, P-I characteristics and efficiency of fuel cell.

$\mathcal{C}$hapter-3

3. FUEL CELL WITH DC-DC CONVERTER

3.1   Introduction

Chapter 2 describes the mathematical model and electrical characteristics of SOFC. For a fuel cell power system connected to a load, DC-DC converter is required to step up or step down the output voltage of fuel cell. This chapter describes control strategy of DC-DC converter system. Both dynamic and static models of fuel cell system have been considered for analysis and simulation purposes.

Modern electronic systems require DC power supplies to regulate the output at a specified value, reduce AC voltage ripple on the DC output voltage and achieve multiple outputs that may differ in voltage and currents [66]. The fuel cell power supplies are expected to be high quality, light weight, reliable and efficient. The principle of operation of linear power regulators is based on a voltage or current divider, whereas the semiconductor switching devices are operated in their linear (active) region. At higher power levels, switching regulators are employed that controls the ON and OFF states of power electronic semiconductor switches. Due to the low power loss in both the states and there is no requirement of the power devices to operate in their active region, higher efficiency can be achieved. Also, due to the ability of the switches to operate at high frequency, the transformers and filters can be made smaller and lighter.

To have a more efficient conversion of power from the fuel cell stack to the load, it has been considered the application of DC-DC converters [16]. A DC-DC converter has the objective of converting the power from the fuel cell to usable form. DC-DC converters are largely used for switch-mode power supplies. The input to these converters is typically an unregulated DC voltage [67] which fluctuates due to the changes in the operating conditions. Switch mode DC-DC converters are used to convert the unregulated DC input into a regulated DC output at a desired voltage level. The average DC output voltage must be controlled to equal a desired level despite variations in the input voltage and output load. This is accomplished through the control of the ON and OFF times of the switches present in the converters.

One of the methods of controlling the output voltage is called Pulse Width Modulation (PWM). It employs switching at a constant frequency and adjusts the ON-time of the switch to control the output voltage. The duty-cycle defined as the ratio of the ON-time to the switching time period, is generated by comparing a signal-level control voltage with a repetitive waveform, typically a saw tooth. This control voltage signal is obtained by amplifying the error between the reference signal and the actual signal. The frequency of the repetitive waveform establishes the switching frequency, which is in the few kilohertz to a few hundred kilohertz range. Advantages of PWM switched converters include low component count, constant frequency operation, relatively simple control and is commercial available.

3.2   Power Switches Interface Methods

Different methods have been discussed extensively in the literature regarding the utilisation of the power generated by the Solid Oxide Fuel Cell (SOFC).It is obvious that the output power of fuel cell cannot be used directly to the load or to the grid. It needs to be conditioned before interfacing to the load or to the grid. So, the power conditioning unit (PCU) are employed which converts the power generated by fuel cell into a usable form. The components of PCU and the way they are connected constitute a number of topologies [7], [68]. The basic components of any of such topologies include

> ➢ Power source (SOFC)
> ➢ DC-DC Converter

Other additional components those may be used are as follows

> ➢ A support battery/PV array
>
> ➢ Boost/Buck converter
>
> ➢ L-C filters at input or output side
>
> ➢ Static switches

3.2.1 DC to DC Converters

Various types of design methodologies for the DC-DC converter have been suggested. Single stage converters do not provide isolation between the input and the output. The DC-DC converter either steps up or steps down the input voltage according to the converter used. The types of single stage DC-DC converters used are indicated as follows [69], [70].

> ➢ Boost Converter
>
> ➢ Synchronous Boost Converter
>
> ➢ Buck-Boost Converter
>
> ➢ Cuk Converter
>
> ➢ Fly–back Converter

The other types of DC/DC converters, that have a multistage operation, first convert the DC power to AC power and again back to DC. The AC signal can be easily boosted with help of a high frequency transformer incorporated in the design. This system offers electrical isolation between the input and output, as the transformer uses different grounds. This also facilitates continuous noise filtering from the primary side, resulting in reduction of electrical noise produced. The converter topologies under this scheme include

> ➢ Unidirectional full-bridge DC-DC power converter
>
> ➢ Push-pull DC-DC boost converter

Out of the above mentioned converters a few of them are described in brief for continuation purpose only. The fuel cell cannot suddenly respond to power demand during start-up or quick load changes due to its slow dynamics. As a result, a battery or flywheels deliver remaining power to the load for the transients [71].

3.2.1.1 Unidirectional/Bidirectional Full Bridge Converter

In this fuel cell, a low DC voltage output is used along with the unidirectional boost converter and other side bidirectional full-bridge DC-DC buck converter for battery. Furthermore, an isolated full-bridge DC-DC power converter is adopted to boost the low output DC voltage of the SOFC (Solid Oxide Fuel Cell) because its topology is suitable for high power application [72], [73], [74], and [75]. The circuit diagram of this topology is shown in Fig.3.1.
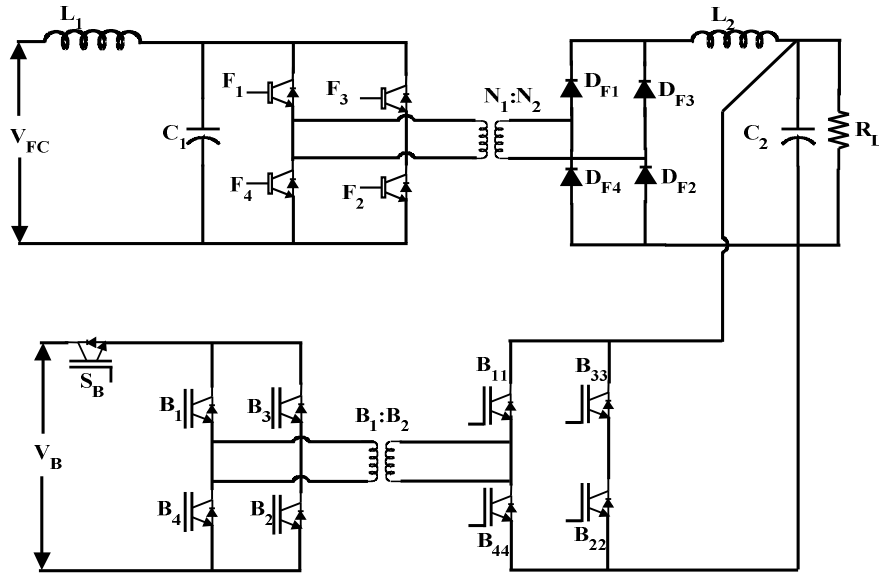
Fig.3.1 Unidirectional/ Bidirectional DC-DC power converter

The unidirectional power converter system consists of a fuel cell, an input filter, full bridge converter, a high frequency transformer, a bridge rectifier diode and an output filter [76], [77]. The bidirectional buck/boost power converter system for battery consists of battery, static switch, two full bridge power converters, and a high frequency transformer.

The unidirectional full bridge DC-DC boost converter allows in one direction power flow from the fuel cell to the load as reverse current can damage the fuel cell [78]. In addition, response of the power converter should be slow enough to meet slow dynamics response of the fuel cell. The bidirectional full-bridge DC-DC power converter permits power flow in both directions to facilitate discharging and recharging the battery [79]. Its response should be fast to compensate for the slow dynamics of the fuel cell during start-up or sudden load changes.

The main purpose of the battery is to provide the instantaneous power demand of the load till the fuel cell reaches its full operation state. During the charging state, the battery absorbs the energy over flow from the fuel cell. A full-bridge converter has advantages over other types of DC-DC converters [80], [81].

3.2.1.2 Push-Pull Converter

The DC-DC push-pull converter has simple construction in its gate drive and power circuits [69]. These are usually suggested for power supplies that are less than 1 kW with a low input voltage. The PWM DC-DC push-pull converter is shown in Fig.3.2. The switches S_1 and S_2 operate being shifted in phase by T/2 with the same duty ratio'd'. The duty ratio must be smaller than 0.5. When switch S_1 is ON, diode 'D_1' conducts and diode 'D_2' is OFF, the diode states are reversed when switch S_2 is ON and S_1 is OFF. When both controllable switches are OFF, the diodes are ON and share equally the filter inductor current [82]. The DC voltage transfer function of the push-pull converter is

$$V_O = \frac{2d}{n}$$

(3.1)

where, n = N_1/N_2.
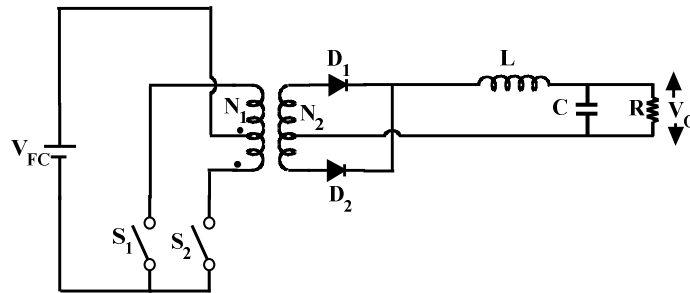
Fig.3.2 Unidirectional push-pull converter

3.2.1.3 Cuk Converter

It consists of DC input voltage source V_s, input inductor L_1, controllable switch S, energy transfer capacitor C_1 and diode D, filter inductor L_2, filter capacitor C, and load resistance R. Advantage of this topology is a continuous current at both the input and output of the converter [83]. Disadvantages of this converter are a high number of reactive components and high currents stresses on the switch, the diode and the capacitor C_1.

When the switch is ON, the diode is OFF and the capacitor C_1 is discharged by the inductor L_2 current. With the switch is in the OFF state, the diode conducts currents of the inductor L_1 and L_2, whereas the capacitor C_1 is charged by the inductor L_1 current. The circuit diagram is shown in Fig.3.3.
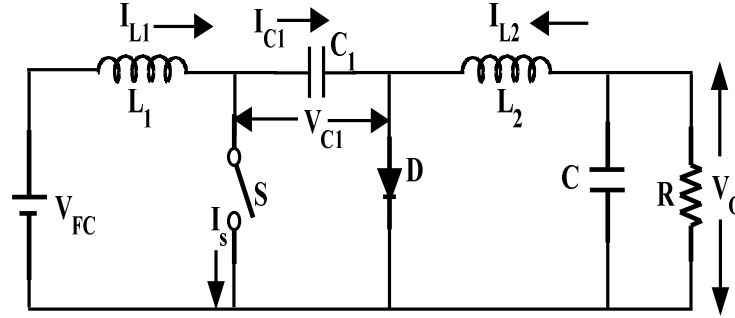
Fig.3.3 Cuk converter

To find the DC voltage transfer function of the converter, the principle is that the average current through a capacitor is zero for steady-state operation. Assuming inductors L_1 and L_2 are large enough to neglect their ripple current. Capacitor C_1 is in steady state if

$$I_{L_2}DT = I_{L_1}(1-D)T \tag{3.2}$$

For a lossless converter

$$P_S = V_S I_{L_1} = -\mathbf{V_O} I_{L_2} = P_O \tag{3.3}$$

By combining the equations (3.2) and (3.3), the DC voltage transfer function of the Cuk converter is

$$M_v = \frac{V_O}{V_S} = -\frac{D}{1-D} \tag{3.4}$$

This voltage transfer function is the similar as that for the buck-boost converter.

The boundaries between the CCM and DCM are determined

$$L_{b_1} = \frac{(1-D)R}{2Df} \tag{3.5}$$

and

$$L_{b_2} = \frac{(1-D)R}{2f} \tag{3.6}$$

The output part of the Cuk converter is identical to that of the buck converter. So, the expression for the filter capacitor C is

$$C_{\min} = \frac{(1-D)V_O}{8V_r L_2 f^2}$$

(3.7)

The peak-to-peak ripple voltage in the capacitor C_1 can be estimated as

$$V_{r1} = \frac{DV_O}{C_1 R_f}$$

(3.8)

A transformed version of the Cuk converter can be obtained by splitting capacitor C_1 and inserting a high frequency transformer between the split capacitors.

3.3 Design of Boost Converter (Step-Up)

A boost converter is a DC to DC power converter with an output voltage greater than its input voltage. It is a class of Switched-Mode Power Supply (SMPS) containing at least two semiconductor switches (a diode and a transistor) and at-least one energy storage element, a capacitor, inductor, or the two in combination [17], [84]. Filters are used to reduce the output voltage ripple. Fig.3.4 shows the circuit diagram of a boost converter.
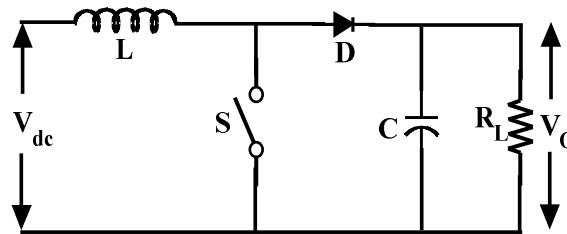
Fig.3.4 Boost converter circuit diagram

In the present investigation, the boost converter has been considered for providing a regulated DC output voltage at its terminals. DC-DC boost converter is the integral part of fuel cell power conditioning unit. The design of DC-DC boost converter and their controller plays important role to control power regulation particularly for DC common bus. The converter operates in the linear region operation of the fuel cell stack. Beyond the linear region, the fuel cell cannot be operated as electrolyte membrane of fuel cell may get damaged. The main advantages of the boost converter include higher efficiency and reduced number of components. The duty cycle has been varied at high switching frequency to convert the unregulated voltage into a regulated supply. The values of

inductor and capacitor have been chosen accurately to reduce the ripples. However , the large inductance tends to increase the startup time slightly while small inductance allows the coil current to ramp up to higher levels before switch turn OFF [69], [70]. The following assumptions have been made in the analysis:

➢ Steady state conditions exist.

➢ The switching period is *T*, and the duty ratio is *D*, so that the switch remains open for time *(1-D)T* and closed for time *DT*.

➢ The inductor current is continuous and always positive.

➢ The capacitor is very large and the output voltage is held constant at V_0.

➢ All components are ideal with no voltage drops across them.

i)   Analysis when switch is in closed condition

Fig.3.5 shows the equivalent circuit of the DC-DC boost converter during switch on time.
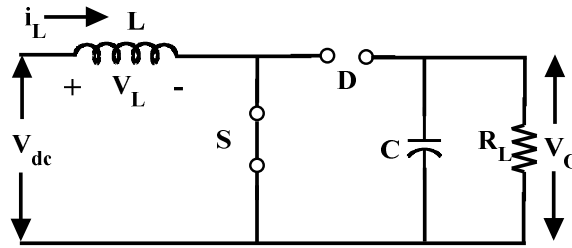
Fig.3.5 Equivalent circuit for DC-DC boost converter during switch ON time

During the time period *DT*, when the switch is closed, the inductor voltage can be written as

$$V_L = V_s = L\frac{di_L}{dt} \ or \ \frac{di_L}{dt} = \frac{V_s}{L}$$

(3.9)

The change in inductor current is given as

$$(\Delta i_L)_{Closed} = \frac{V_S DT}{L}$$

(3.10)

ii)   Analysis when switch is in open condition

When the switch is open for time period (1-D)*T, the equivalent circuit is shown in Fig.3.6.
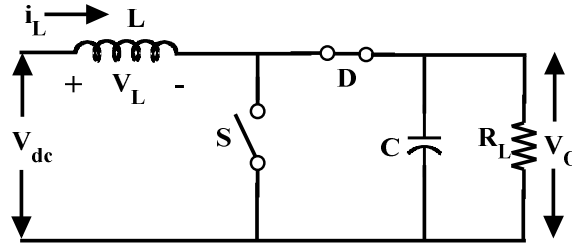
Fig.3.6 Equivalent circuit for DC-DC boost converter during switch OFF time

Assuming that the output voltage V_0 is a constant, the voltage across inductor is given as

$$V_L = V_S - V_O = L\frac{di_L}{dt} \quad or \quad \frac{di_L}{dt} = \frac{V_S - V_O}{L} \tag{3.11}$$

The change in inductor current while switch is open is given as

$$(\Delta i_L)_{Open} = \frac{(V_S - V_O)(1-D)T}{L} \tag{3.12}$$

The net change in inductor current must be zero, from equations (3.10) and (3.12)

$$(\Delta i_L)_{Closed} + (\Delta i_L)_{Open} = 0$$

$$V_O = \frac{V_S}{1-D} \tag{3.13}$$

The equation no. (3.13) gives the expression of the output voltage as a function of the duty cycle. The average current inductor is determined by considering that the power supplied by source must be same as power absorbed by the load.

$$P_O = \frac{V_O{}^2}{R_L} \tag{3.14}$$

and

$$V_S I_S = V_S I_L \tag{3.15}$$

Now from (3.13), (3.14) and (3.15), the inductor current is obtained as

$$I_L = \frac{V_S}{(1-D)^2 R_L} \tag{3.16}$$

where, R_L is the load resistance.

45

Maximum and minimum inductor currents are determined as

$$I_{max} = I_L + \frac{\Delta i_L}{2} = \frac{V_S}{(1-D)^2 R_L} + \frac{V_S DT}{2L}$$

(3.17)

$$I_{min} = I_L - \frac{\Delta i}{2} = \frac{V_S}{(1-D)^2 R_L} - \frac{V_S DT}{2L}$$

(3.18)

And the minimum value of inductance, obtained from the limiting value of the current to ensure continuity in conduction is given as

$$L_{min} = \frac{D(1-D)^2 R_L}{2 f_s}$$

(3.19)

where, f_s is the switching frequency in hertz.

A ripple in the output would exit whenever a capacitance is involved in the circuit. The voltage ripple due to the capacitor can be considered as

$$\frac{\Delta V_O}{V_O} = \frac{D}{R_L C f_s}$$

(3.20)

The size of reactive elements of boost converter can be determined from the rated voltage, voltage ripple and switching frequency of the converter based on the equations from (3.13) to (3.20) with voltage ripple < 0.1 % and switching frequency $fs = 10$ kHz .

Table 3.1 Simulation parameters of fuel cell with DC-DC converter

Parameters	Values
Voltage ripple	0.1%
Inductance: L	6 mH
Capacitance: C	1400 µF
Switching frequency : f_s	10 kHz
Desired DC output voltage	200 V
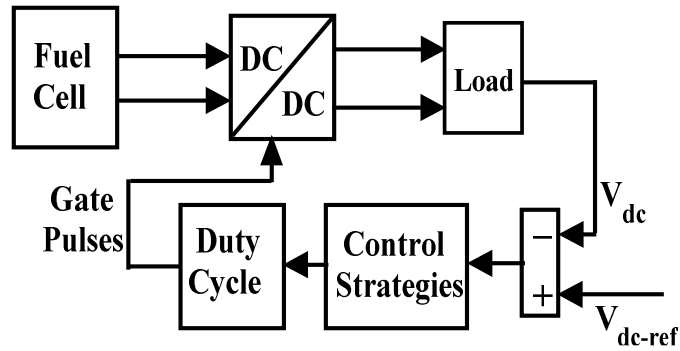
Fig.3.7 Control strategy for fuel cell with DC-DC converter

A block diagram for Simulink model of PI controlled DC-DC boost converter based on the designed parameters given in Table 3.1 is shown in Fig.3.7. The DC-DC converter is an integral part of fuel cell power conditioning unit. Hence , modeled PI boost converter has been used in SOFC based distributed generation system to maintain a constant voltage (200 V) output which is required as an input to inverter, irrespective of variation in the load and fuel cell terminal voltage. The PI controller reduces the steady-state error to zero. The process of sensing the control variable and measured quantities compared with reference signals are incorporated in Fig.3.7 [85]. The change in duty cycle for varying load is obtained by controlling PI parameter values suitably of voltage controller. The set parameters of PI controller are K_p and K_I are 0.001 and 0.15 respectively for the case considered.

3.4   Design of Buck Converter (Step-Down)

Basically, one unit of fuel cell provides a low DC voltage and high current. When N number of fuel cells are connected in series, the output voltage increases. So, buck converter is required to step down the output voltage to a desired level.

A buck converter is a step-down DC to DC converter. Its design is similar to the step-up boost converter, and like the boost converter it is a Switched-Mode Power Supply that uses two switches (a transistor and a diode), an inductor and a capacitor. It is shown in Fig.3.8.

The step-down DC–DC converter, commonly known as a buck converter consists of a DC input voltage source, controlled switch, diode, filter inductor, filter capacitor, and load resistance [86]. There are essentially two modes of operation the basis of inductor current. When inductor current is never zero for any period of time is called the

Continuous Conduction Mode (CCM), and other is Discontinuous Conduction Mode (DCM).
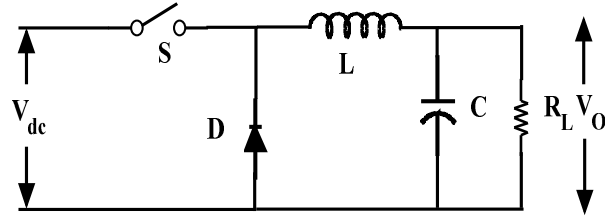
Fig.3.8 Buck converter circuit diagram

3.4.1 Working of Buck Converter

The circuit operates in two conditions; when the switch S is closed and other when it is open. The switch is operated by a switching pulse. When the switch is ON/closed; diode is reverse biased and conducts inductor current in forward direction [87]. During this period a positive voltage will appear across inductor and inductor current will increase gradually. Output voltage and current during this period will be

$$V_L = V_d - V_O$$

(3.21)

$$i_L = \frac{1}{L} \int V_L \, dt$$

(3.22)
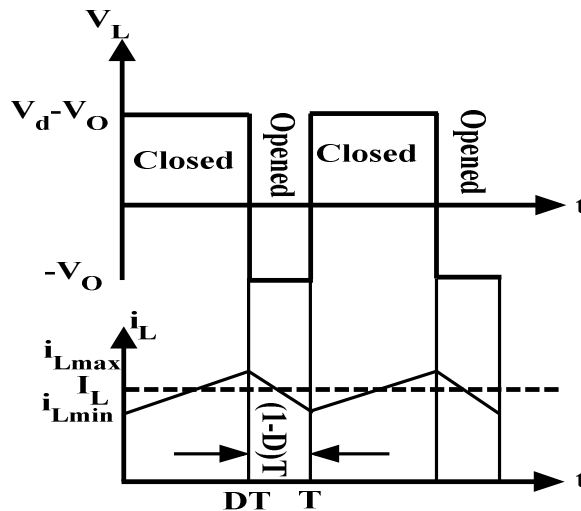
Fig.3.9 Inductor current of buck converter during ON and OFF periods

48

We can derive the change in inductor current as

$$V_L = V_d - V_O = L\frac{di}{dt}$$

(3.23)

$$\frac{di_L}{dt} = \frac{V_d - V_O}{L}$$

(3.24)

Assuming the ideal condition the inductor current will increase linearly as shown in Fig.3.9. So change in inductor current by time duration can be written as

$$\frac{di_L}{dt} = \frac{\Delta i_L}{\Delta t} = \frac{\Delta i_L}{DT}$$

(3.25)

From equation (3.24) and (3.25)

$$\Delta i_L = \frac{V_d - V_O}{L}.DT$$

(3.26)

Now when the switch will be open diode will be forward biased and will act as short circuited. Now the current flow will take place through diode. The stored inductor energy will give i_L continues to flow. The voltage across inductor will be

$$V_L = -V_O$$

(3.27)

$$V_L = -V_O = L\frac{di_L}{dt}$$

(3.28)

$$\frac{di_L}{dt} = \frac{-V_O}{L} = \frac{\Delta i_L}{\Delta t} = \frac{\Delta i_L}{(1-D)T}$$

(3.29)

$$\Delta i_L = \frac{-V_O}{L}.(1-D)T$$

(3.30)

For a steady state operation change in inductor current should be zero over a period. Therefore sum of the equation (3.26) and (3.30), it should be zero.

$$\frac{V_d - V_O}{L}(DT) + \left(\frac{-V_O}{L}\right)(1-D)T = 0$$

(3.31)

This reduces to

$$V_O = DV_d$$

(3.32)

From equation (3.32) plot will be
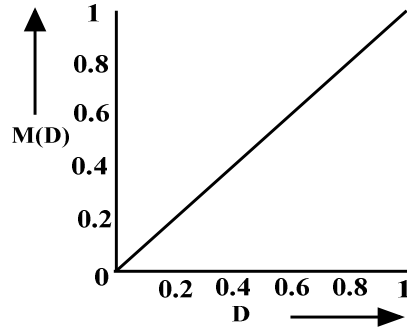
Fig.3.10 Plot of gain verses duty cycle

3.4.2   Analysis of Buck Converter

From equation (3.32), we can say that output voltage is depends on the duty cycle which can vary from zero to unity. So, it is called Step-down (Buck) converter. There are two mode of operation one is Continuous Current Mode (CCM) and the second is Discontinuous Current Mode (DCM). Buck converter to operate in CCM the parameters should be as given below:

Inductor value should

$$L > L_{min} = \frac{(1-D)}{2f} R \qquad (3.33)$$

Capacitor value is decided by the output voltage ripples desired

$$C = \frac{(1-D)}{8L f^2 r} \qquad (3.34)$$

$$r = \frac{\Delta V_O}{V_O} \qquad (3.35)$$

3.5   Fuel Cell Model with DC-DC Buck Converter

Assuming that the SOFC output voltage is to be used to charge a battery stack, the voltage is stepped-down to low voltage using a DC-DC buck converter with the topology shown in Fig.3.11 [88], [83].

50
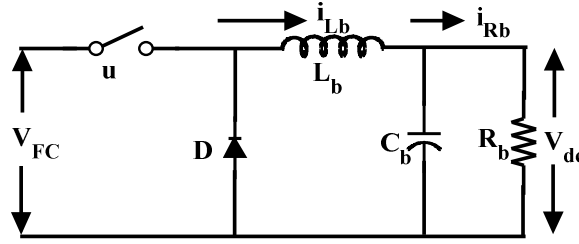
Fig.3.11 Topology of DC-DC buck converter

In constructing the simulink model of the converter, the inductor current i_{Lb} and capacitor voltage V_{dc} are selected as state variables. Furthermore, the input to the converter is set equal to the output voltage of the SOFC stack i.e. V_{FC}.

The voltage and current dynamics of the DC-DC buck converter

$$V_{FC} = V_L + V_{dc} = L_b \frac{di_{Lb}}{dt} + V_{dc}$$

(3.36)

$$\frac{di_{Lb}}{dt} = \frac{V_{FC}}{L_b} - \frac{V_{dc}}{L_b}$$

(3.37)

When switch is off state means 'u'=0

$$\frac{di_{Lb}}{dt} = -\frac{V_{dc}}{L_b}$$

(3.38)

Let the switch in DC-DC converter be closed for time 'u' and open for (1-u). Therefore, from (3.36) and (3.38), we will get that

$$\frac{di_{Lb}}{dt} = -\left(\frac{u}{L_b}\right)V_{dc} + \frac{u}{L_b}V_{FC} + -\left(\frac{1-u}{L_b}\right)V_{dc}$$

(3.39)

$$\frac{di_{Lb}}{dt} = \frac{u}{L_b}V_{FC} - \frac{1}{L_b}V_{dc}$$

(3.40)

By applying KCL

$$i_{Lb} = i_{Cb} + i_{Rb}$$

(3.41)

$$\frac{dV_{dc}}{dt} = \frac{i_{Lb}}{C_b} - \frac{V_{dc}}{R_b C_b}$$

(3.42)

$$\frac{dV_{dc}}{dt} = \frac{-1}{(1-u)C_b}i_{Lb} + \frac{u}{(1-u)R_bC_b}V_{dc}$$

(3.43)

From the above equation of (3.40) and (3.43), the state space model for the DC-DC buck converter is obtained as

$$\begin{bmatrix} \dot{i}_{Lb} \\ \dot{V}_{dc} \end{bmatrix} = \begin{bmatrix} 0 & \dfrac{-1}{L_b} \\ \dfrac{-1}{(1-u)C_b} & \dfrac{u}{(1-u)R_bC_b} \end{bmatrix} \begin{bmatrix} i_{Lb} \\ V_{dc} \end{bmatrix} + \begin{bmatrix} \dfrac{u}{L_b} \\ 0 \end{bmatrix} V_{FC}$$

(3.44)

3.6 Control Strategies

DC-DC converter is one of the primary power-conditioning systems in a fuel cell power system. To get the required output voltage from DC-DC converter, closed loop control is essential. There are different linear and non-linear control strategies for DC-DC converter. The main objective of the controller is to maintain the desired output voltage and compensate for any disturbances. The most widely used linear control strategy for DC-DC converter is voltage mode control using PI controller and one of the promising non-linear control strategy is Sliding Mode Control (SMC) strategy. The main advantage of sliding mode control is the robustness to unknown disturbances.

3.6.1 Sliding Mode Controller (SMC) Design Methodology

The sliding mode theory provides a method to design a controller for a system so that the controlled system is insensitive to parameter variations and external load disturbances [89]. The details of the Sliding Mode Control (SMC) method, equivalent control and application to converters can be found in the literature [90], [91]. The approach is realised by the use of a high speed switching control law which forces the trajectory of the system to move to a predetermined path in the state variable space called Sliding Surface and stays in that surface thereafter. Before the system reaches the switching surface, there is a control directed towards the switching surface that is called Reaching Mode. The regime of a control system in the sliding surface is called Sliding Mode. In sliding mode, a system's response remains insensitive to certain parameters variations and unknown disturbances.

One of the main features of this method is that one only needs to drive the error to a switching surface, after which the system is in sliding mode and robust against modelling uncertainties and disturbances [92]. A sliding mode controller is a Variable Structure Controller (VSC). Basically, a VSC includes several different continuous functions that maps plant state to a control surface, and the switching among different functions is determined by plant state that is represented by a switching function.

 If the following linear time invariant system state equation is given

$$\dot{x}(t) = Ax(t) + Bu(t)$$

(3.45)

which can be rewritten as

$$\dot{x}(t) = f(x,t,u)$$

(3.46)

where, x is the state vector of the system, u is the control input and f is the function vector. If the function vector f is discontinuous on a surface S(x) is called sliding surface in the sliding mode theory, then

$$f(x,t,u) = \begin{cases} f^+(x,t,u^+) \ if \ S > 0 \\ f^-(x,t,u^-) \ if \ S < 0 \end{cases}$$

(3.47)

The system is in sliding mode if its representative point moves on the sliding surface S(x). The sliding surface is also called as switching function because the control action switches depending on its sign on the two sides of the sliding surface. The sliding mode exists on the manifold S(x) = 0 if for the motion in subspace S with the origin is asymptotically stable with the finite of convergence.

$$\dot{S} = CAx + CBu$$

(3.48)

The equivalent control method was developed to drive the sliding mode equations in the manifold S(x) = 0. The solution $\dot{S} = 0$ is called equivalent control (u_{eq}).

$$u_{eq} = -(CB)^{-1}(CAx)$$

(3.49)

In sliding mode theory, the control problem is to find a control input u such that the state vector x tracks a desired trajectory x^* in the presence of uncertainties and external disturbance. The sliding surface may then be set to be of the form

$$S = x - x^*$$

<div align="right">(3.50)</div>

If the initial condition S (0) = 0 is not satisfied, then the tracking can only be achieved after a transient phase, called Reaching Mode.

Since the aim is to force the system states to the sliding surface [93], the adopted control strategy must guarantee the system trajectory move toward and stay on the sliding surface from any initial condition if the following conditions meet,

$$S\dot{S} \leq -\eta|S|$$

<div align="right">(3.51)</div>

where, η a positive constant that guarantees the system trajectories hit the sliding surface in the finite time. The required sliding mode controller achieving finite time convergence to the sliding surface is given by

$$u = \begin{cases} 1 \ for \ S > 0 \\ 0 \ for \ S < 0 \end{cases}$$

<div align="right">(3.52)</div>

3.6.2   Sliding Mode Controller (SMC) Design

The control problem is to provide the following condition

$$\lim_{t\to\infty} I_c(t) = I^*$$

<div align="right">(3.53)</div>

where, I^* is the reference input current. The controlled transient performance should be insensitive to parameter variation of the buck converter and external disturbances.

The state equation of the buck converter can be expressed in the following matrix form

$$\begin{bmatrix} \dot{i}_{Lb} \\ \dot{V}_{dc} \end{bmatrix} = \begin{bmatrix} 0 & \dfrac{-1}{L_b} \\ \dfrac{-1}{(1-u)C_b} & \dfrac{u}{(1-u)R_bC_b} \end{bmatrix} \begin{bmatrix} i_{Lb} \\ V_{dc} \end{bmatrix} + \begin{bmatrix} \dfrac{u}{L_b} \\ 0 \end{bmatrix} V_{FC}$$

<div align="right">(3.54)</div>

The entire control structure for sliding mode controller is shown in Fig.3.12.
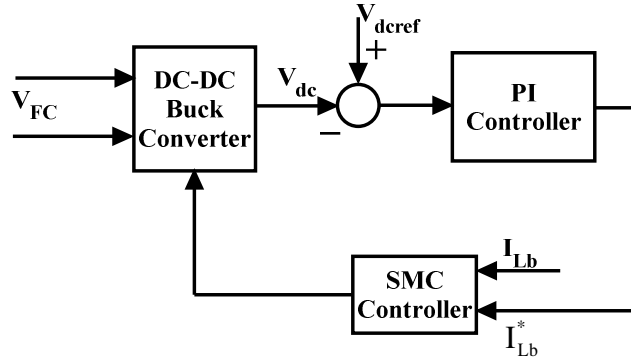
Fig.3.12 Control structure for sliding mode controller

A sliding surface with the desired dynamics of the corresponding sliding motion need to be determined for the sliding mode control [94]. The dynamic error of the system is

$$e(t) = i_{Lb} - i_{Lb}^*$$

(3.55)

Assuming the sliding line or sliding surface (S)

$$S = \dot{e} + \lambda e$$

(3.56)

where, λ is the sliding co-efficient.

Differentiating the equation (3.55), we can rewrite the equation as follows

$$\frac{de(t)}{dt} = \frac{d}{dt}\left(i_{Lb} - i_{Lb}^*\right)$$

(3.57)

By substituting the equation (3.40) in (3.57) equation, we can get

$$\dot{e} = -\frac{V_{dc}}{L_b} + \frac{u}{L_b}V_{FC} - \dot{i}_{Lb}^*$$

(3.58)

Again substituting the equation (3.58) in the equation (3.57), we can write the equation as follows

$$S = -\frac{V_{dc}}{L_b} + \frac{u}{L_b}V_{FC} - \dot{i}_{Lb}^* + \lambda e$$

(3.59)

When sliding mode exits then

$$S(x) = \dot{S}(x) = 0$$

(3.60)

Putting the equation (3.60) in (3.59), we can calculate the equivalent control component u_{eq}

$$u_{eq} = \frac{L_b}{V_{FC}} \left[\frac{V_{dc}}{L_b} + \ddot{i}_{Lb}^* - \lambda e \right] \tag{3.61}$$

The objective of sliding mode control is to force the system states to the sliding surface from any initial condition and remain on it. This is satisfied by the Lyapunov function of the form [95].

$$V = \frac{1}{2} S^2(x) \tag{3.62}$$

The control input 'u' have to be chosen so that the time derivative of 'V' must be negative definite i.e. $\dot{V} < 0$ *for* $S(x) \neq 0$ to ensure the stability of the system and to make the surface 'S' attractive.

$$\dot{V} = S\dot{S} < 0 = S \left[-\frac{\dot{V}_{dc}}{L_b} - \ddot{i}_{Lb}^* + \lambda e \right] \tag{3.63}$$

To enforce the convergence of the sliding surface, the control signal is defined as

$$u_S = \pm K \operatorname{sgn}(S) \tag{3.64}$$

where, K is chosen negative, and sgn (.) is sign function defined as

$$\operatorname{sgn}(S(x)) = \begin{cases} +1 \ if \ S(x) > 0 \\ -1 \ if \ S(x) < 0 \end{cases} \tag{3.65}$$

So, the total control law is

$$u_C = u_{eq} \pm u_S \tag{3.66}$$

The total control law can be rewritten by putting the equation (3.61) into (3.66)

$$u_C = \frac{L_b}{V_{FC}} \left[\frac{V_{dc}}{L_b} + \dot{i}_{Lb}^* - \lambda e \right] \pm K \operatorname{sgn}(S) \tag{3.67}$$

3.6.3   FPGA Controller

Conventionally, closed loop control of DC-DC converter is implemented using analog devices like op-amp or state of art PWM ICs. But the conventional analog mode control has some serious limitations like non-reconfigurable in nature, complex architecture and larger time for implementation. So scientists have shifted to digital domain to control the converter. With low cost digital computing device available in the market, digital control of DC-DC converter is one of the widely studied areas.

In digital control, the control algorithm is implemented in any of the digital computing device. The most widely used digital computing device is Field Programmable Gate Array (FPGA). This section implements voltage mode controller for DC-DC converter using FPGA. Voltage mode controller using PI controller is chosen because the control logic is simple and it's easy to implement. The PI and PWM controller when configured on Field Programmable Gate Arrays (FPGAs) improves the speed, accuracy, power, compactness, and cost effectiveness of the system. The block diagram of FPGA controller is shown in Fig.3.13.
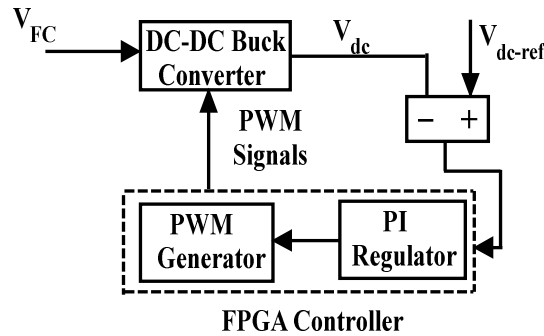
Fig.3.13 FPGA implementation of DC-DC buck converter with fuel cell

3.6.3.1 FPGA Implementation of PI Controller

The ideal continuous time PI controller can be expressed as [86].

$$y(t) = K_P e(t) + K_I \int e(t)dt \qquad (3.68)$$

where y(t) is the control output, K_P proportional constant, K_I is the integral constant and e(t) is the error between the reference V_{dcref} and V_{dc}. The s-domain expression of the corresponding PI controller can be written as:

$$Y(s) = \left[K_P + \frac{K_I}{s} \right] E(s)$$

(3.69)

Implementation equations (3.68) and (3.69) of PI controller in FPGA using VHDL needs to be written in discrete time form as FPGA is a digital device.

For this purpose, we used numerical method approach [96] that is trapezoidal method that approximates $\frac{1}{s}$ by

$$\frac{1}{s} = \frac{T}{2} \left(\frac{z+1}{z-1} \right)$$

(3.70)

where, T is the sample time. This discrete integral term can be written as:

$$y(n) = x(n) + K_I \frac{T}{2} u(n)$$

(3.71)

$$x(n+1) = y(n) + K_I \frac{T}{2} u(n)$$

(3.72)

where, y(n) is the output, u(n) is the error input and x(n) is the state. The complete discrete-time expression of PI controller is written as:

$$y(n) = y(n-1) + K_P u(n) + K_I \frac{T}{2} \left[u(n-1) + u(n) \right]$$

(3.73)

Fig.3.14 RTL Schematic of PI controller
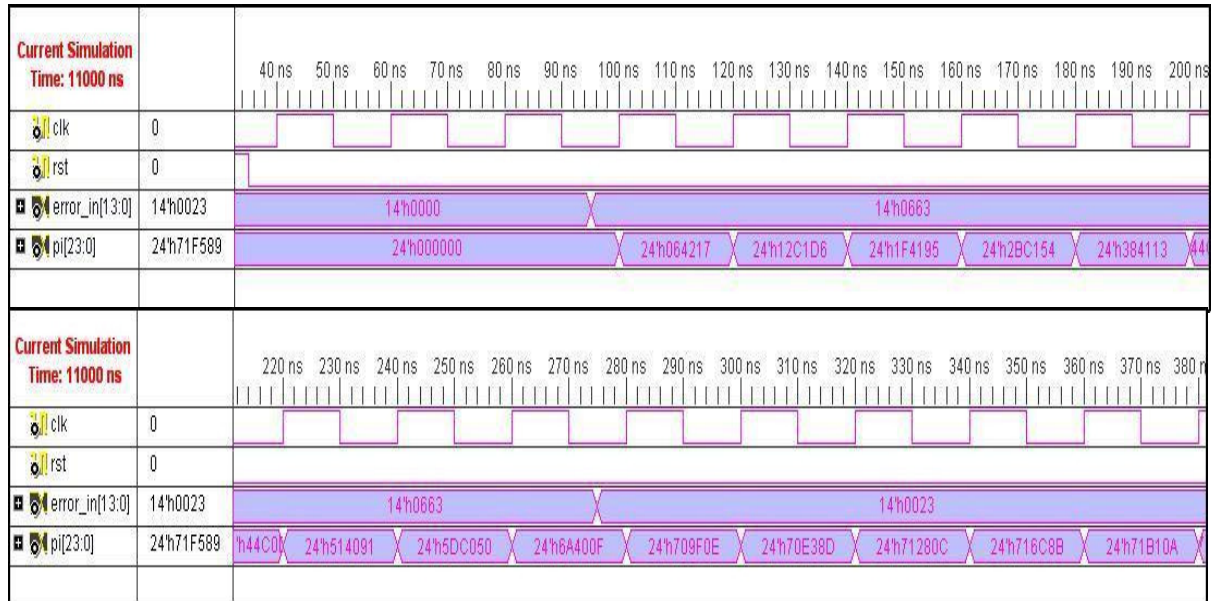
Fig.3.15 Test bench waveform of PI controller

Table 3.2 Design Summary of PI controller

Logic Utilization	Used	Available	Utilization
No. of slices	76	4656	1%
No. of slice flip flop	48	9312	0%
No. of 4 input LUTs	139	9312	1%
No. of boned IOBs	40	232	17%
No. of GCLKs	1	24	4%

3.6.4 PWM Technique

Switch-mode DC-DC converters utilize one or more switches to transform DC from one level to another. In a DC-DC converter with a given input voltage, the average output voltage is controlled by controlling duty cycle of the switch pulse. There are two methods for the generation of PWM, one by switching at a constant frequency and adjusting the on duration of the switch to control the average output voltage. The other method; where both the switching frequency and the on duration of the switch are varied. Variation in

59

the switching frequency makes it difficult to filter the ripple components in the input and the output waveforms of the converter [97], [98].
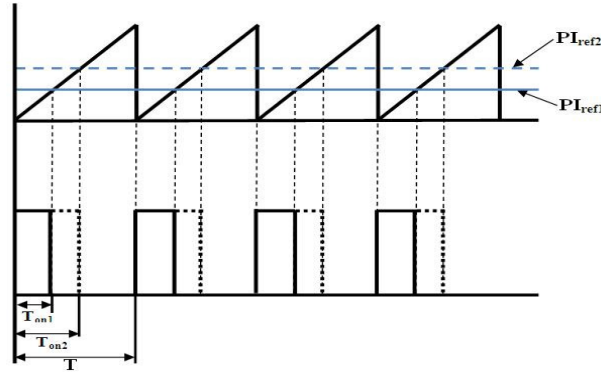
Fig.3.16 PWM duty cycle control structure

Here we adopt, a fixed frequency PWM technique is used. The working principle of this technique is shown in Fig.3.16. A repetitive signal which decides the frequency of PWM is compared with the PI output which acts as a reference signal. When PI output is more than the repetitive signal, then the PWM signal is high and vice-versa. When PI output changes, the ON period of the PWM signal changes as shown in Fig.3.16. Hence, we can control the buck converter output voltages.

3.6.4.1 FPGA Implementation of PWM Control

The PWM signal generation is done by comparing a stable reference signal which is here taken from a PI controller with a repetitive saw-tooth signal. A repetitive signal is generated by a counter, which counts from zero to maximum value and when it reaches the maximum count, the counter is reset to zero again. This process is repeated concurrently in a process block. The frequency of the PWM signal is decided by the frequency of this repetitive signal. The N-bit comparator is used, which compares the counter count and the reference signal input. When the reference input is higher than the repetitive signal the output of PWM signal is low, and when the reference input is lower than the repetitive signal the output of PWM signal is high. In this way, the PWM signal is generated which drives the power switch of the converter. In the SPARTAN-3E Xilinx board, a 14-bit ADC is available that gives a precision of 14 bit [99]. The error input is fed to this ADC which gives a 14-bit digital data. The K_I value used in our simulation model in MATLAB/SIMULINK is 500, this can be represented in 9 bit, after the addition and multiplication is done in the PI block; it will give a 24 bit output without any data

losses. So, a 24-bit counter and comparator are taken. The ADC which can give 14-bit data maximum at the rate of 1.5 MHz is quite sufficient for this type of application.
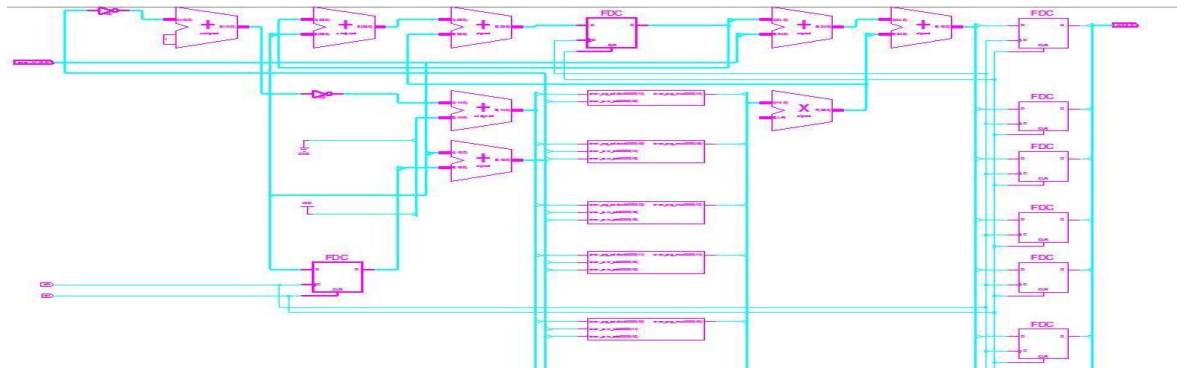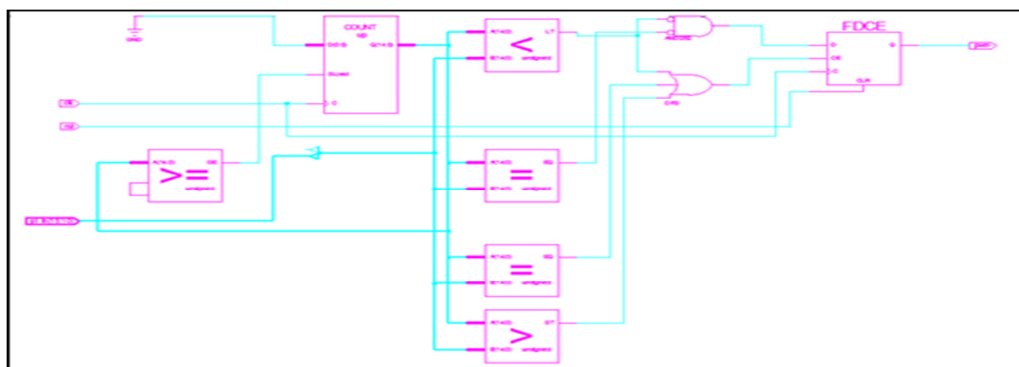

Fig.3.17 RTL schematic of PWM controller
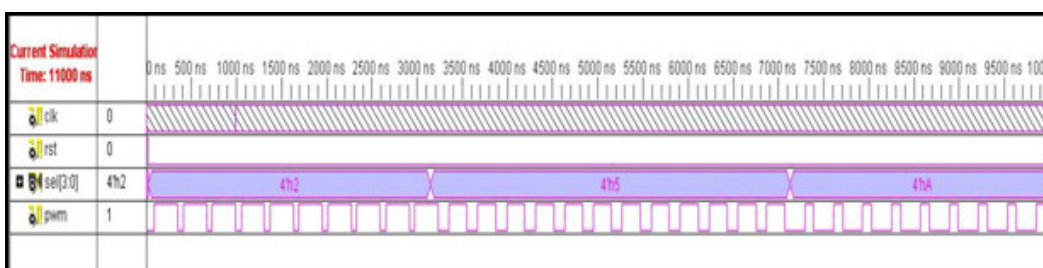
Fig.3.18 Test bench waveform of PWM controller

Table 3.3 Design summary of PWM controller

Logic Utilization	Used	Available	Utilization
No. of slice flip flops	16	9312	1%
No. of 4 input LUTs	26	9312	1%
No. of Occupied Slices	16	4656	1%
No. of slices containing only related logic	16	16	100%
Total no. of 4 input LUTs	27	9312	1%
No. of bonded IOBs	3	232	1%

3.7   Prototype Model of Controller

We have developed a prototype model of DC-DC buck converter. It is shown in Fig.3.19. The buck converter is designed with L = 8 mH; C = 100 uF, and load R = 20 ohms. The

duty cycle of the PWM signal with constant load is 50% as shown in Fig. 3.20. We have tested our prototype model with resistive load only. By changing the load, current varies which changes the voltage. For constant voltage, the duty cycle of the PWM switching pulse will change accordingly. We have tested the controller performance by decreasing the load, gradually the current requirement increases. From the V-I characteristics curve of SOFC model, a decrease in the output voltage with an increase in current density is shown. So, for a constant output voltage, the duty cycle will increase gradually which is shown in Fig. 3.21.

Voltage sensing is done by simple voltage dividing circuit which gives V_{dc}. This V_{dc} is subtracted from V_{dcref} using an op-amp subtractor circuit. This error signal e(t) = V_{dcref}-V_{dc} is fed to the FPGA based PI+PWM controller which is synthesized in XC3S500E development board. It is given to ADC (Analog to Digital conversion) module of XC3S500E board. LTC1407A-1 ADC converter IC has been used in this board which gives 14-bit digital output represented in 2's complement binary value. It has a precision of 14-bit. Maximum sampling rate which can be achieved is approximately 1.5 MHz Using PI modules, the error e(t) is minimised and PWM output is generated with its reference and output is taken from I/O pin F8 of XC3S500E board.

Using opto-coupler (HCPL817), PWM signal is interfaced with the DC-DC buck converter. The opto-coupler provides isolation between the FPGA board and the power circuit.
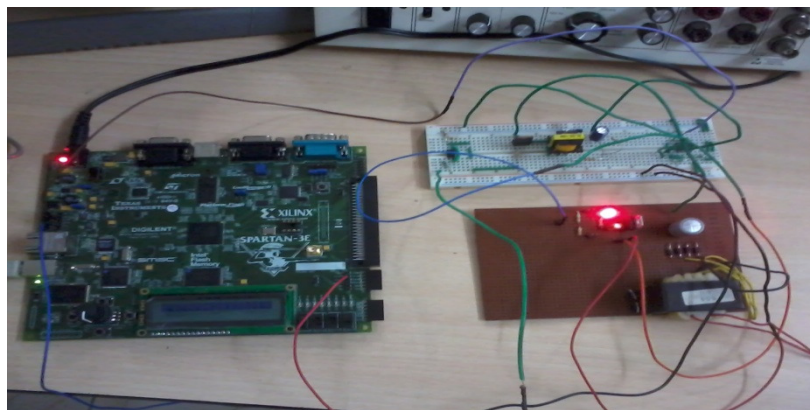
Fig.3.19 Prototype of buck converter with FPGA based PI & PWM controller
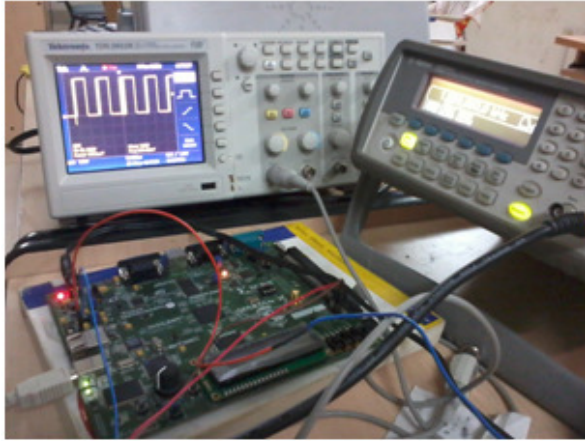
Fig. 3.20 PWM switching pulse with constant load
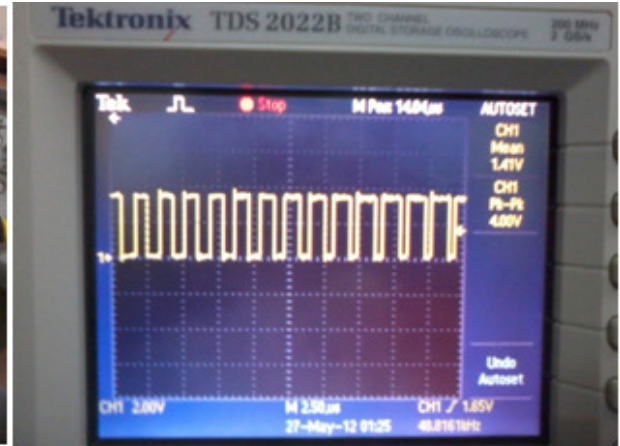
Fig. 3.21 Duty cycle change with the variation of load

3.8   Summary

This work proposes a comprehensive state space model for Fuel Cell Power System that comprises fuel cell, DC-DC buck converter and load. DC-DC converter is controlled using voltage mode PI control and sliding mode control. The voltage mode PI control scheme is implemented using FPGA. The use of FPGA simplifies the control circuit and adds flexibility to the system. DC-DC converter control for fuel cell power system is prototyped using XC3S500E development board containing a SPARTAN-3E Xilinx FPGA. The controller facilitates computing the pulse width and switches the MOSFET so that desired output voltage is obtained.

$$\mathcal{C}hapter\text{-}4$$

4. PWM-VSI CURRENT CONTROLLER FOR LOAD/GRID CONNECTED FUEL CELL

4.1   Introduction

Fuel cell generates DC output voltage which should be converted to AC by using DC-AC inverter. The inverter output is used for utility application as well as for distributed generation. This chapter, describes PWM-VSI current controller for load/grid connected fuel cell power system.

Inverters can be either voltage source inverter (VSI) or current source inverter (CSI). In VSI, DC source has negligible impedance and terminal voltage remains constant with load variations [100]. Some of the practical applications of inverter are documented in [101]. The voltage source inverter is more convenient because it is efficient, compact, economical and faster device in comparison to current source inverter. Here, inverter output voltage is dependent on the load impedance and thus terminal voltage can change substantially with changes in the load [102].

On the basis of the output waveform, inverters can be classified as square wave or pulse-width modulation (PWM) inverters. Square wave inverters produce a square wave AC voltage which is of constant magnitude. To get the sinusoidal waveform, LC filter circuit can be used at the output of the inverter [103].

Most of the current control techniques used in load/grid connected fuel cell power system is PWM-VSI control strategy. This thesis uses a VSI current controller technique within

the inverter. So, current control techniques should follow the below mentioned properties for efficient performance for load/grid connected fuel cell power system.

➢ Better utilization of the voltage source inverter.

➢ Low static and dynamic current-control errors (difference between the reference current and actual currents is less).

➢ Wide linear modulation range.

➢ Low amplitudes of lower order harmonics in output voltage to minimize the harmonics in output current.

➢ Lower switching losses in the power transistor (voltage source inverter) switches.

➢ Easy implementation and less computation time.

Fuel cell provides a DC output voltage whose magnitude is increased by a power electronic converter (Boost Converter). For utility and grid connected applications the output of boost converter is fed to DC-AC inverter. A DC-link capacitor is connected in the intermediate stage of DC-DC boost converter and DC-AC inverter. The DC-AC inverter is controlled by PWM-VSI technique. In this chapter, the following PWM-current control techniques are discussed and implemented for load/grid connected fuel cell power system.

➢ Fixed-HCC

♦ Two-level HCC

♦ Three-level HCC

➢ Adaptive-HCC

➢ Fuzzy-HCC

➢ Adaptive-fuzzy-HCC

➢ Triangular Carrier Current Controller (TCCC)

➢ Triangular Periodical Current Controller (TPCC)

4.2   Modeling of PWM-VSI

PWM-VSI can be used in both single phase and three phase mode. In this thesis, FCPS is developed that comprises either a single phase PWM-VSI or three-phase PWM-VSI depending on the system being considered. Single-phase system is implemented in both

simulation and hardware (Section 7.9 and 7.9.1), whereas we have only demonstrated extensive simulation for there-phase FCPS using three-phase PWM-VSI in Chapter 5.

4.2.1   Modeling of Single Phase PWM-VSI

The PWM-voltage source inverter has been modelled that comprises a single-phase AC-voltage applied through DC-link capacitor. An inverter is normally powered from a battery or any kind of dc source. In our investigation we have used fuel cell (DC power source); a DC-link capacitor is added after the buck/boost/buck-boost converter that follows fuel cell stack for maintaining DC voltage. In the analysis that follows in this thesis, we have shown a capacitor rather than a DC source. The single-phase voltages v_a on the input side can be expressed in terms of the DC-link capacitor voltage V_{dc} and switching functions states the ON/OFF status of the devices of each leg $S_a \, and \, S_b$ as [104]. Fig.4.1 shows the schematic of single-phase DC-AC voltage source inverter.
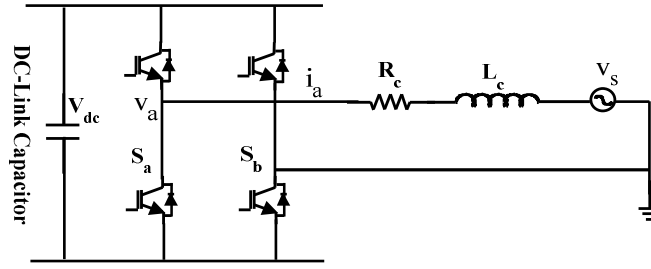
Fig.4.1 Single-phase DC-AC voltage source inverter

$$v_a = \left(S_a - S_b \right) V_{dc}$$

(4.1)

The single-phase currents i_a flowing through the filter impedance (R_c , L_c) are obtained by solving the following equations

$$\frac{di_a}{dt} = \dot{i}_a = \frac{1}{L_c} \left(v_s - v_a - R_c L_c \right)$$

(4.2)

The DC-link capacitor current can be obtained in terms of phase currents i_a and the switching status (1 for ON-state and 0 for OFF-state) of the devices S_a , S_b

$$I_{dc} = i_a S_a - i_a S_b$$

(4.3)

From this, the model equation of the DC-link capacitor voltage can be written as

66

$$\frac{dV_{dc}}{dt} = \dot{V}_{dc} = \frac{1}{C_{dc}}(i_a S_a - i_a S_b)$$

(4.4)

The DC-link capacitor voltage works as an energy storage element to supply real-power. In the steady state, the real power supplied by the source should be equal to the real-power demand of the load. Apart from this, a small power is needed to compensate the losses in the fuel cell power system.

4.2.2 Modeling of Three Phase PWM-VSI

The PWM-voltage source inverter has been modelled that comprises a three-phase AC-voltage applied through DC-link capacitor. The three-phase voltages v_{ca}, v_{cb} and v_{cc} on the input side can be expressed in terms of the DC-link capacitor voltage V_{dc} and switching functions states the ON/OFF status of the devices of each leg S_a, S_b and S_c as [105], [106]. Fig.4.2 shows the schematic of three-phase DC-AC voltage source inverter.
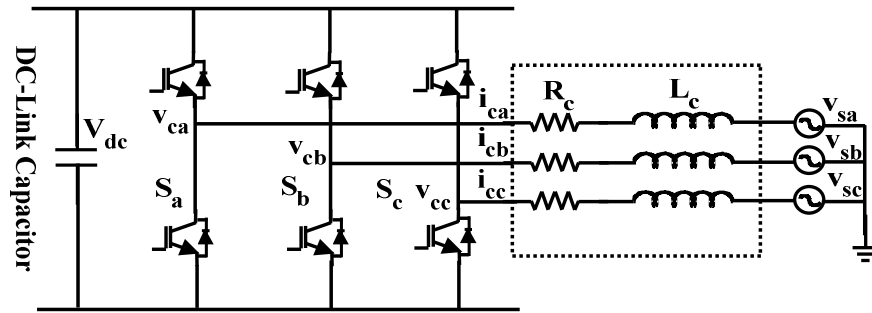
Fig.4.2 Three-phase DC-AC voltage source inverter

$$v_{ca} = \frac{V_{dc}}{3}(2S_a - S_b - S_c)$$

$$v_{cb} = \frac{V_{dc}}{3}(-S_a + 2S_b - S_c)$$

$$v_{cc} = \frac{V_{dc}}{3}(-S_a - S_b + 2S_c)$$

(4.5)

The three-phase currents i_{ca}, i_{cb} and i_{cc} flowing through the filter impedance (R_c, L_c) are obtained by solving the following equations

$$\frac{di_{ca}}{dt} = i_{ca}^{\cdot} = -(R_c/L_c)i_{ca} + (v_{sa} - v_{ca})/L_c$$

$$\frac{di_{cb}}{dt} = i_{cb}^{\cdot} = -(R_c/L_c)i_{cb} + (v_{sb} - v_{cb})/L_c \qquad (4.6)$$

$$\frac{di_{ca}}{dt} = i_{ca}^{\cdot} = -(R_c/L_c)i_{cc} + (v_{sc} - v_{cc})/L_c$$

The DC-link capacitor current can be obtained in terms of phase currents i_{ca}, i_{cb} and i_{cc} and the switching status (1 for ON-state and 0 for OFF-state) of the devices S_a, S_b and S_c

$$I_{dc} = i_{ca}S_a + i_{cb}S_b + i_{cc}S_c \qquad (4.7)$$

From this, the model equation of the DC-link capacitor voltage can be written as

$$\frac{dV_{dc}}{dt} = V_{dc}^{\cdot} = \frac{1}{C_{dc}}(i_{ca}S_a + i_{cb}S_b + i_{cc}S_c) \qquad (4.8)$$

The DC-link capacitor voltage serves as the energy storage element to supply real-power (to the inverter). In the steady state, the real power supplied by the source should be equal to the real-power demand of the load plus a small power to compensate the losses in the fuel cell power system.

4.3   Fixed-Hysteresis Current Controller

The conventional or fixed-hysteresis current control method for fuel cell power system can be carried out to generate the switching patterns of the inverter. Hysteresis current controller is widely used for single level and multilevel inverters. Researchers have implemented hysteresis current controller for multilevel inverter using programmable logic devices [107]. The hysteresis current controller can be classified as two-level and three-level hysteresis current controller.

In this thesis, we have developed a simulation model of fixed hysteresis current controller for single phase fuel cell power system and experimentally validated the simulated results. The block diagram of fixed hysteresis current controller for single phase fuel cell power system is shown in Fig.4.3.
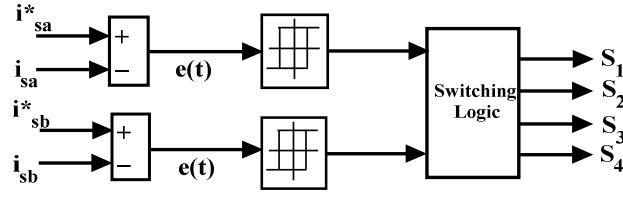
Fig.4.3 Block diagram of fixed HCC for single phase fuel cell power system

The current error $e(t)$ is the difference between the reference current (i_{sa}^{*}) and the actual current (i_{sa}). If the error current exceeds the upper limit of the hysteresis band, the upper switch of the inverter arm is turned OFF and the lower switch is turned ON.

4.3.1 Two-Level Hysteresis Current Controller

Conventional hysteresis current control operates the voltage source inverter by comparing the current error $e(t)$ against the fixed-hysteresis bands. This block diagram of the two-level hysteresis current controller is shown in Fig.4.4. The current error $e(t)$ is the difference between the reference current (i_{sa}^{*}) and the actual current (i_{sa}). If the error current exceeds the upper limit of the hysteresis band, the upper switch of the inverter arm is turned OFF and the lower switch is turned ON. As a result, the current starts decaying [108], [109]. Fig.4.5 shows the ON and OFF switching pulses to drive the fuel cell power system. If the error current crosses the lower limit of the band, the lower switch is turned OFF and the upper switch is turned ON. As a result, the current gets back into the hysteresis band. Hence, the actual current is forced to track the reference current within the hysteresis band.
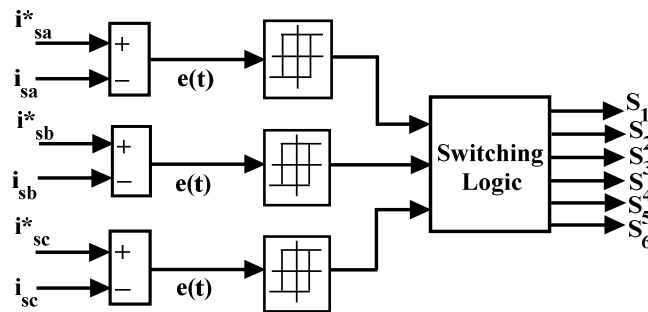
Fig.4.4 Block diagram of two-level HCC
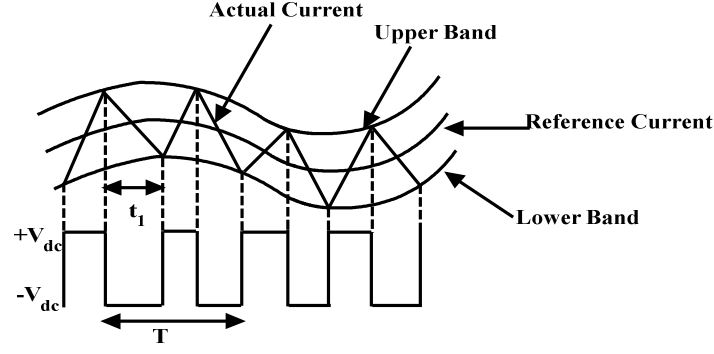
Fig.4.5 Two-level switching pattern

The phase-A switching performance is defined as

$$S = \begin{cases} OFF & if \ i_{sa}(t) > i_{sa}^*(t) + hb \\ ON & if \ i_{sa}(t) < i_{sa}^*(t) - hb \end{cases}$$

(4.9)

Similarly, the switching performance of phase-B and phase-C devices can be derived using hysteresis-bandwidth hb. Since the circuit is very simple, the two-level hysteresis controllers are widely used for fuel cell power system applications [110]. However, it does not use zero voltage from the inverter DC-side, only positive and negative DC supply voltages are used to generate the required switching pulses. It is well known that the harmonic performance of two-level modulation is inferior to three-level modulation. The two-level modulation generates significant sideband harmonics around the switching frequency. To overcome the problems, the three-level hysteresis modulation is implemented with three-level switching process. The three-level hysteresis current control approach provides superior performance on harmonic perspective.

4.3.2 Three-Level Hysteresis Current Controller

The implementation of three-level hysteresis controller are set as upper and lower band overlap boundaries and displacement of small offset current. Whenever the current error $e(t)$ (difference between the reference current (i_{sa}^*) and the actual current (i_{sa})) crosses an outer hysteresis boundary, the inverter output is set to an active positive or negative output to force a reversal of the current error. Similarly, whenever the current error reaches an inner hysteresis boundary, the inverter output is set to zero condition and the current error will be forced to reverse direction without reaching the next outer boundary. If the selection of zero output does not reverse the current trajectory, it will continue

through the inner hysteresis boundary to the next outer boundary, where an opposite polarity active inverter output will be controlled and the current will reverse in any direction [111]. The three-level HCC based switching process is shown in Fig.4.7. This block diagram of the three-level hysteresis current controller is shown in Fig.4.6. The current error is bounded between the upper-inner and lower-outer hysteresis boundaries for a positive inverter output. Similarly, the current error is bounded between the lower-inner and upper-outer hysteresis boundaries for a negative inverter output.
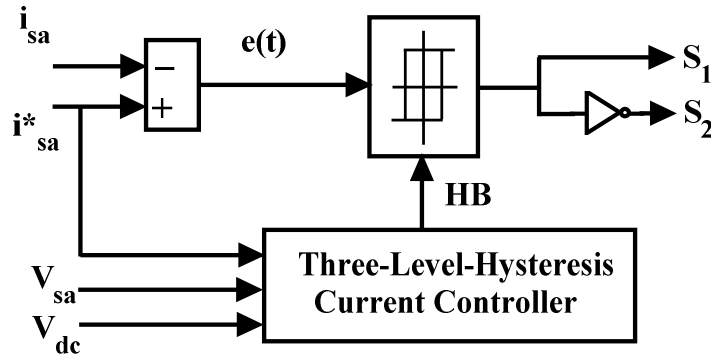
Fig.4.6 Block diagram of three-level HCC
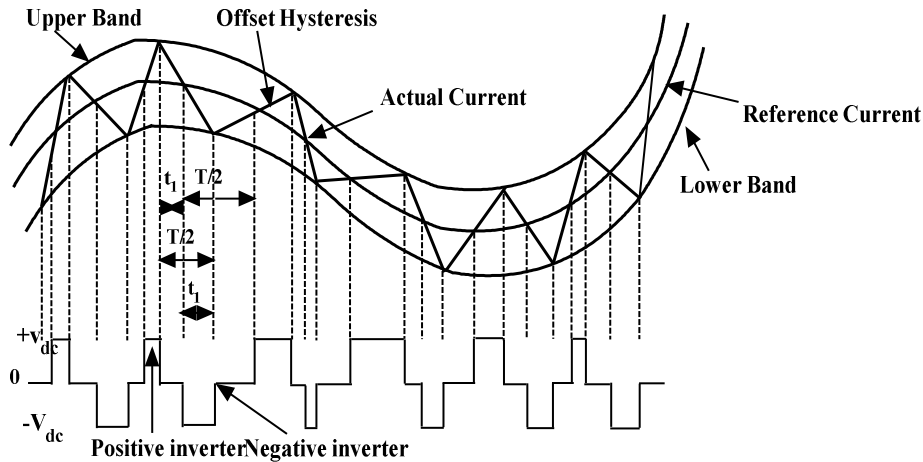
Fig.4.7 Switching patterns of the three-level HCC

A complete switching cycle of the two-level HCC goes from $0 \rightarrow t_1 \rightarrow T$; whereas the three-level HCC switching cycle goes from $0 \rightarrow t_1 \rightarrow T/2$. The switching process introduces a positive or negative DC-offset error in the average output current, depending on the polarity of the active output voltage. However, this error can be corrected by adding a compensation factor of half the hysteresis band offset magnitude to the phase

current reference. The polarity of this compensation factor is determined by the polarity of the most recent inverter active output. In other words, it is positive when positive inverter output is in use and vice-versa. The switching logic for A-phase switching operation of the inverter is given as [112]. The logical flow chart of three-level hysteresis current controller for phase 'A' is shown in Fig.4.8.

Fig.4.8 Flow chart of three-level HCC for phase 'A'

The advantages of fixed-HCC are simple design, unconditioned stability and accuracy. However, current control with a fixed hysteresis-band has the unsatisfactory feature of variable switching frequency. The slope of current waveform may vary widely and the peak amplitude of current waveform may exceed the hysteresis-band. Consequently, inverter switches will be operated at high switching frequency in order to track reference current. Adaptive-hysteresis current controller overcomes the fixed-HCC limitations [113]. This adaptive-HCC changes the bandwidth according to instantaneous current variation.

4.4   Adaptive-Hysteresis Current Controller

Fig.4.9 Block diagram of an adaptive-HCC
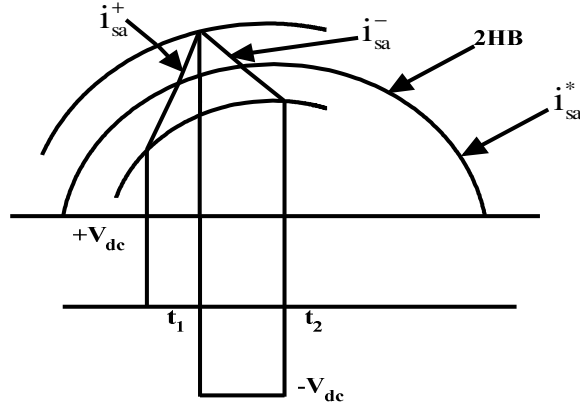
Fig.4.10 Single line switching function

Fig.4.9 shows the block diagram of adaptive-HCC based switching pulse generator for PWM-voltage source inverter. The adaptive-hysteresis band controller proposed by Bose [114] for the machine drive system is adopted here for fuel cell power system based on indirect current control theory. When the current error $e(t)$ (difference between the reference current (i_{sa}^{*}) and the actual current (i_{sa})) exceeds the upper limit of the adaptive-hysteresis band, the lower switch is turned ON. If the current error crosses the lower limit of the adaptive-hysteresis band, the upper switch is turned ON. Hence, the actual current is forced to track the reference current within the hysteresis-band. Fig.4.10 shows the single line switching representation of AC-side power flow of fuel cell power system. The following equations can be written for the switching interval t_1 and t_2 [115], [116].

$$\frac{di_{sa}^{+}}{dt} = \frac{1}{L}(V_{dc} - v_s)$$

(4.10)

$$\frac{di_{sa}^-}{dt} = -\frac{1}{L}(V_{dc} + v_s)$$

(4.11)

where, L = phase inductance, (i_{sa}^+) and (i_{sa}^-) are the respective rising and falling current segments.

From the geometry of Fig.4.10, the following equations can be written in the hysteresis-band curvature with respective switching intervals

$$\frac{di_{sa}^+}{dt} t_1 - \frac{di_{sa}^*}{dt} t_1 = 2HB$$

(4.12)

$$\frac{di_{sa}^-}{dt} t_2 - \frac{di_{sa}^*}{dt} t_2 = -2HB$$

(4.13)

$$t_1 + t_2 = T_C = \frac{1}{f_c}$$

(4.14)

where, t_1 and t_2 are the respective switching intervals, and f_c is the modulation frequency. Adding equation (4.12) and (4.13)

$$\frac{di_{sa}^+}{dt} t_1 + \frac{di_{sa}^-}{dt} t_2 - \frac{di_{sa}^*}{dt}(t_1 + t_2) = 0$$

(4.15)

Substituting $\dfrac{di_{sa}^+}{dt}$ and $\dfrac{di_{sa}^-}{dt}$ *values* in the equation (4.15)

$$\frac{(V_{dc} - v_s)}{L} t_1 - \frac{(V_{dc} + v_s)}{L} t_2 - \frac{di_{sa}^*}{dt}(t_1 + t_2) = 0$$

(4.16)

Simplify and substituting $(t_1 + t_2) = \dfrac{1}{f_c}$ in the equation (4.16)

$$\frac{V_{dc}}{L}(t_1 - t_2) - \frac{v_s}{L}(t_1 + t_2) - \frac{1}{f_c}\frac{di_{sa}^*}{dt} = 0$$

(4.17)

Simplify the equation (4.17)

$$(t_1 - t_2) = \frac{L}{V_{dc} f_c}\left(\frac{v_s}{L} + \frac{di_{sa}^*}{dt}\right)$$

(4.18)

Subtracting (4.13) from (4.12), we get

$$\frac{di_{sa}^+}{dt}t_1 - \frac{di_{sa}^-}{dt}t_2 - \frac{di_{sa}^*}{dt}(t_1 - t_2) = 4HB$$

(4.19)

Substituting $\frac{di_{sa}^+}{dt}$ and $\frac{di_{sa}^-}{dt}$ *values* in the equation (4.19)

$$\frac{(V_{dc} - v_s)}{L}t_1 + \frac{(V_{dc} + v_s)}{L}t_2 - \frac{di_{sa}^*}{dt}(t_1 - t_2) = 4HB$$

(4.20)

Simplify this equation (4.20)

$$\frac{V_{dc}}{L}(t_1 + t_2) - \frac{v_s}{L}(t_1 - t_2) - \frac{di_{sa}^*}{dt}(t_1 - t_2) = 4HB$$

(4.21)

Further simplify and substituting $(t_1 + t_2) = \dfrac{1}{f_c}$ in the equation (4.21)

$$\frac{V_{dc}}{f_c L} - (t_1 - t_2)\left(\frac{v_s}{L} + \frac{di_{sa}^*}{dt}\right) = 4HB$$

(4.22)

Here substituting $(t_1 - t_2)$ value in the equation (4.22)

$$\frac{V_{dc}}{f_c L} - \frac{L}{V_{dc} f_c}\left(\frac{v_s}{L} + \frac{di_{sa}^*}{dt}\right)^2 = 4HB$$

(4.23)

Simplify this equation (4.23)

$$HB = \frac{1}{4}\left[\frac{V_{dc}}{f_c L} - \frac{L}{V_{dc} f_c}\left(\frac{v_s}{L} + \frac{di_{sa}^*}{dt}\right)^2\right]$$

(4.24)

Further simplify the equation (4.24)

$$HB = \frac{0.25 V_{dc}}{f_c L}\left[1 - \frac{L^2}{V_{dc}^2}\left(\frac{v_s}{L} + m\right)^2\right]$$

(4.25)

Here, v_s is the supply voltage, V_{dc} is the DC-link capacitor voltage, L is the coupling

inductor, and $m = \dfrac{di_{sa}^*}{dt}$ is the slope of the reference current signals. The hysteresis band

HB can be modulated at different points of fundamental frequency to control the switching pulses of the inverter. The calculated hysteresis bandwidth *HB* is applied to the switching operation of HCC. The switching operation is created by S-functions in MATLAB and is adopted in the Simulink model to produce gate control-switching pulses to drive the inverter.
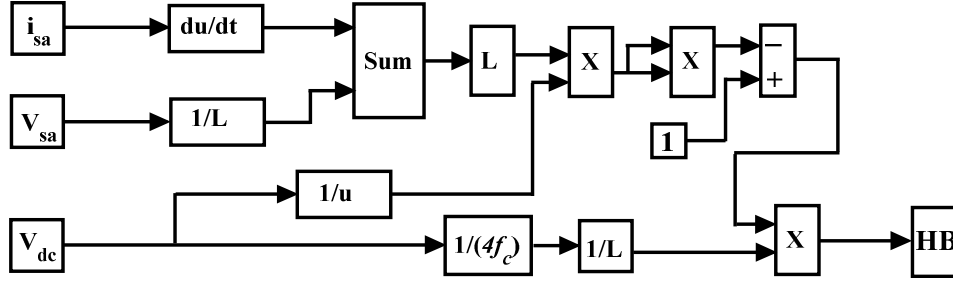
Fig.4.11 Block diagram of an adaptive-hysteresis bandwidth calculation

The block diagram of the adaptive-hysteresis bandwidth calculation is shown in Fig.4.11. This adaptive-HCC ensures more switching power losses due to high frequency, which is solved by the adaptive-fuzzy-HCC. The Adaptive-Fuzzy-HCC calculates the hysteresis bandwidth effectively with the help of fuzzy logic and reduces the switching power losses.

4.5 Adaptive-Fuzzy Hysteresis Current Controller

To improve the fuel cell inverter performance without precise knowledge of the fuel cell power system parameters (Interface inductor and DC-link capacitor voltage), the hysteresis band value can be implemented with a fuzzy logic controller [115] [117]. The block diagram of adaptive-fuzzy-HCC is shown in Fig.4.12. The adaptive-fuzzy-hysteresis bandwidth is modulated as a function of slope reference current and supply voltage. The slope of the reference current di_{sa}^{*}/dt and supply voltage v_S are used as inputs for fuzzy processing as shown in Fig.4.13. The adaptive-fuzzy hysteresis band *HB* is the output of the fuzzy controller.
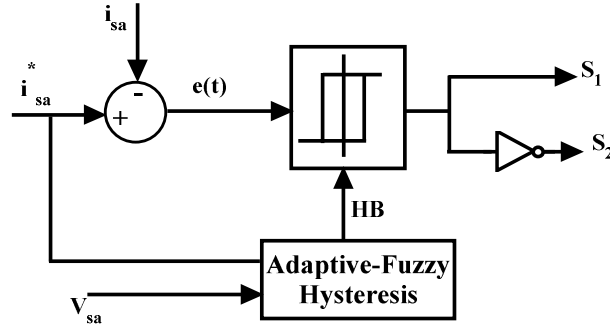
Fig.4.12 Block diagram of Adaptive-Fuzzy-HCC
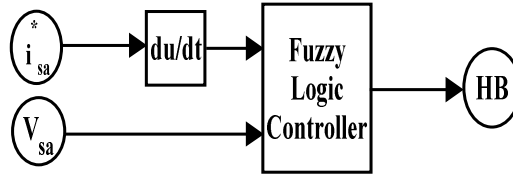
Fig.4.13 Fuzzy processing

The fuzzy logic is characterized by

➢ Five-fuzzy sets (NB, NM, ZE, PM and PB) for each input (slope of the reference current di^*_{sa}/dt and supply voltage v_S) and output variable (Positive Very Small (PVS), Positive Small (PS), Positive Medium (PM), Positive Big (PB) and Positive Very Big (PVB)) of adaptive-fuzzy hysteresis band HB as shown in Fig.4.14.

➢ Triangular membership function is used.

➢ Mamdani-type min-operator.

➢ Defuzzification using the centroid method.
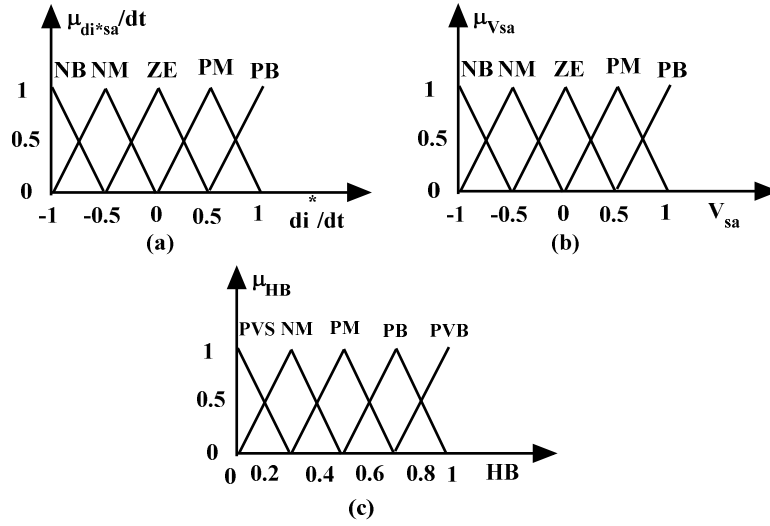
Fig.4.14 Membership functions for the input and variables di_{sa}/dt, v_{sa} and HB

The fuzzy logic rules are stored as linguistic variables required by rule evaluator. The 25-rules are used in this adaptive-fuzzy-hysteresis current controller that is given in Table 4.1.

Table 4.1 Fuzzy logic rules

HB		di^*_{sa}/dt				
		NB	NM	ZE	PM	PB
V_{sa}	NB	PB	PM	PM	PM	PB
	NM	PB	PM	PS	PM	PB
	ZE	PVB	PM	PVS	PM	PVB
	PM	PB	PM	PS	PM	PB
	PB	PB	PM	PM	PM	PB

The output of fuzzy logic controller *HB* (hysteresis bandwidth) is modulated at different points of the fundamental frequency cycle to control the switching pulses of the voltage source inverter. For symmetrical operation of all three-phases, the hysteresis bandwidth *HB* is denoted as HB_a, HB_b and HB_c of the same value, but having 120^0 phase difference. The Adaptive-Fuzzy HCC based hysteresis bandwidth *HB* should maintain

the modulation frequency f_c as quasi constant. This controller reduces the switching power losses and improves the PWM-VSI performances for fuel cell inverter significantly.

4.6   Triangular-Carrier Current Controller

The triangular-carrier current controller is one of the familiar methods to generate gate control switching pulses of the fuel cell power system. The PWM based TCCC is utilized independently for each phase. It directly generates the VSI-switching pulses of the three (A, B, C) phase system [118] . In case of A-phase, the actual source current is represented as i_{sa} and reference current is represented as i_{sa}^*. Similarly, B-phase and C-phase currents are represented as i_{sb} and i_{sb}^* and i_{sc} and i_{sc}^* respectively. Fig.4.15 shows the block diagram of the A-phase followed triangular-carrier current controller.
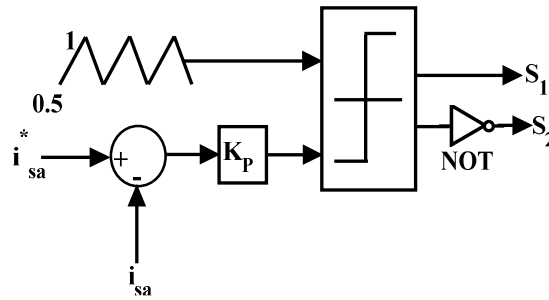
Fig.4.15 Block diagram of triangular-carrier current controller

To determine the switching transitions through the error current $e(t)$ (reference current i_{sa}^* compared with the actual source current i_{sa}) is amplified with proportional gain. The output error signal is compared with triangular carrier signal to generate the required switching pulses. In A-phase, if the current error signal is greater than the triangular carrier signal, the upper inverter switch is ON. However, if the current error signal is smaller than the triangular signal, the lower inverter switch is ON. Similarly, the switching performance of phase-B devices can be derived by comparing with triangular signals. Thus the switching frequency of the power transistor is equal to the frequency of the triangular carrier signal. The triangular-carrier controller provides best harmonic distortion and the current ripple lower than the other methods. However, this controller with proportional gain introduced for overshoot problems and it has lower bandwidth.

4.7 Triangular Periodical Current Controller

The triangular-periodical current controller is used to generate the switching pulses of the PWM-voltage source inverter. This technique switches the power transistor of the inverter during the transitions of a fixed clock frequency [119].
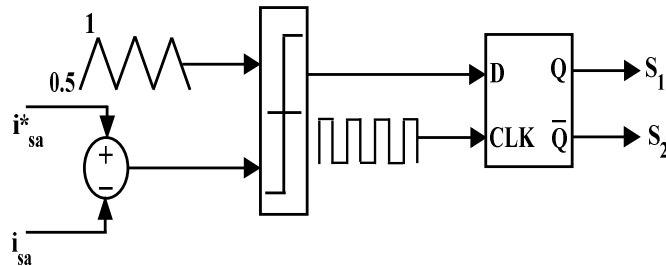
Fig.4.16 Block diagram of triangular-periodical current controller

The triangular-periodical current controller is utilized independently for each (A, B, C) phase of the inverter. Fig.4.16 shows the block diagram of the triangular-periodical current controller. The reference current i_{sa}^* is directly compared with the actual current i_{sa} to determine the error signal. The error current is compared with the triangular carrier signal and the output is connected to D-Latch. The D-Latch maintain at a regular interval Ts synchronized with the clock of frequency equal to $1/Ts$. Thus the switching frequency of the power transistor is equal to the clock frequency. The merit of this technique is that the minimum time between switching transitions which will limit to the period of the sampling clock. However, the actual switching frequency is not clearly defined and it has fixed bandwidth.

4.8 Summary

The PWM-current control techniques are used to generate the required PWM signals for voltage source inverter. The fixed-HCC, adaptive-HCC and adaptive-fuzzy-HCC, triangular-carrier current controller, triangular-periodical current controller, techniques are discussed.

The fixed-HCC is simple in design, unconditioned in stability and easy to implement. However, this control scheme exhibits several unsatisfactory features such as the uneven switching frequency where the switching frequency varies within a particular band limit. Adaptive-HCC overcomes these limitations. The adaptive-HCC changes the bandwidth according to instantaneous current variation. However, the adaptive-HCC is having more

switching power losses due to high frequency switching. These problems can be solved by the adaptive-fuzzy-HCC.

The adaptive-fuzzy-HCC method calculates the bandwidth using the fuzzy logic controller without precise knowledge of the fuel cell power system parameters. The adaptive-fuzzy-HCC method has reduced the switching power losses and improves the performance of the fuel cell power system compared to other techniques.

The TCCC technique is very simple to implement; only a fixed amplitude and frequency triangular-carrier signal is compared with the error current (difference between reference current and actual current). The TPCC uses a triangular-carrier signal comparator and a D flip-flop per phase. However, the TCCC, TPCC are claiming more switching power losses due to fixed frequency performance.

*C*hapter-5

5. SIMULATION RESULTS AND ANALYSIS

5.1 Introduction

A fuel cell power system is considered as a backup power source for residential and industrial loads. Reformer model of fuel cell power system is developed by [120]. Fuel cell provides a low DC voltage which has to be converted to AC for different standalone and grid application. For conversion of DC to AC, a DC-AC inverter is used. The DC-AC inverter requires accurate gate pulses which are generated by different control configurations of PWM-VSI already presented in previous chapter. Some of the well-known control configuration of PWM-VSI current controller is summarized in Chapter 4.

The main objective of this chapter is to simulate fuel cell based power system in different possible configurations. The fuel cell power system consists of fuel cell, battery, DC-DC converter, DC-AC inverter, load and grid.

5.2 Configuration of Load/Grid Connected Fuel Cell Power System

Certain critical loads need uninterrupted/continuous power. It is also desirable to provide continuous supply to residential/commercial/industrial loads, which is provided by a grid. When due to any unavoidable circumstances (like thunderstorm, cyclone, grid maintenance), the grid is not able to provide 24 hour supply to the load, a backup power is necessary. There are many renewable energy sources which provide an efficient backup power, but fuel cell based backup power is considered more reliable than others because of its numerous advantages discussed in Chapter 2. A synchronization mechanism helps to switch from one power supply to other.

When fuel cell is connected as a backup power supply, there can be different real life scenario like non-availability of required number of fuel cells, malfunction of fuel cell which will hamper the supply of backup power. Considering the above mentioned situation, this thesis considers three different investigations where fuel cell acts as a backup power supply. When there is less number of fuel cells available then the DC output voltage is also low, so a DC-DC boost converter is used to increase the output DC voltage level. This configuration is summarized in section 5.3. When there is no grid supply and a malfunctioned fuel cell then a battery is connected to provide backup power supply. This configuration is described in section 5.4. Another configuration is when there is sufficient number of fuel cells then the fuel cell output is no longer required to be stepped up and can be directly fed to the inverter through DC-link capacitor. This configuration is summarized in section 5.5.

5.3   Load/Grid Connected to Fuel Cell Power System with DC-DC Converter

This section gives a detailed description of a load/grid connected fuel cell power system where the fuel cell system works only as a backup power source. An ideal output voltage of a single fuel cell is 1.2 V DC which has to be stepped up to an appropriate level with the help of a DC-DC boost converter. The boost converter is controlled by a PI controller that is described in Chapter 3. For utility/grid supply the output DC voltage of fuel cell has to be fed to an inverter. A DC-link capacitor is connected in parallel to the DC bus side. The main objective of DC-link capacitor is to supress the ripple produced by switching current and voltage in DC-DC converter. The other primary motive of the DC-link capacitor is that it decouples the DC power source from the AC power source by charging and discharging the difference of two currents. The inverter requires PWM signals to operate. To provide accurate switching pulses to the inverter, four basic components are necessary namely, controller, unit sine vector, reference current generator. The reference current extraction process is obtained through unit current vector and magnitude analyser. The magnitude analyser is used to estimate the required amplitude of load current. The maximum value of load current is multiplied with the unit current templates to generate the required reference current. The reference current is compared with actual current (from output of LC filter) to generate the PWM signals using fixed-HCC/adaptive-HCC techniques which is fed to the inverter gate. The inverter is connected with an LC filter which supresses the ripple of inverter output voltage. The

inverter side is connected to the grid side by an interfacing inductance. Subsequently, the grid is connected to the load.

The performance of different controller based fuel cell power system is evaluated through Matlab/Simpower tools. Fig.5.1 shows the block diagram of the three-phase fuel cell power system.
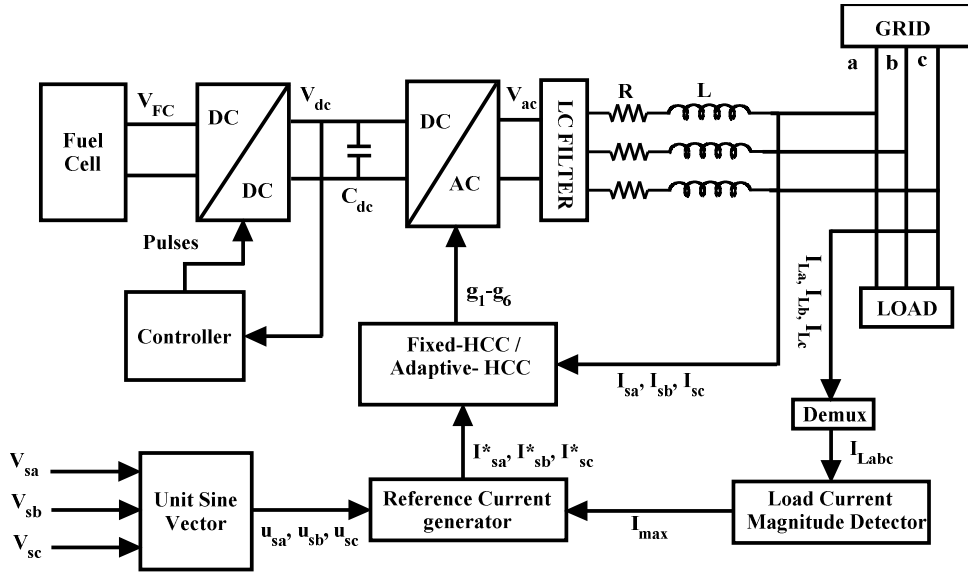
Fig.5.1 Block diagram of fuel cell power system

To achieve the unit sine vector templates, the instantaneous supply voltages are sensed and given as

$$V_{sa} = V_m \sin(\omega t)$$
$$V_{sb} = V_m \sin(\omega t - 120^0)$$
$$V_{sc} = V_m \sin(\omega t + 120^0)$$

(5.1)

where, V_m - peak value of the source voltage

$\quad\quad \omega = 2\pi f$ - fundamental angular frequency

To generate the unit sine vector templates, three phase supply currents are considered. The unit sine vector templates are derived as [121].

$$u_{sa} = \frac{V_{sa}}{V_m} = \sin(\omega t)$$

$$u_{sb} = \frac{V_{sb}}{V_m} = \sin(\omega t - 120^0)$$

$$u_{sc} = \frac{V_{sc}}{V_m} = \sin(\omega t + 120^0)$$

(5.2)

The magnitude analyser estimates the peak current I_{max}. This peak current multiplies with an output of unit sine vector to generate the required reference current.

$$i_{sa}^* = I_{max} \, u_{sa} = I_{max} \, \sin(\omega t)$$

$$i_{sb}^* = I_{max} \, u_{sb} = I_{max} \, \sin(\omega t - 120^0)$$

$$i_{sc}^* = I_{max} \, u_{sc} = I_{max} \, \sin(\omega t + 120^0)$$

(5.3)

By comparing the reference current with the actual current to generate the voltage source inverter (VSI) switching pulses using PWM current controller.

The detailed parameter of the fuel cell power system is summarized below. In Table 5.1 shows the fuel cell parameters.

Table 5.1 Parameters of Solid Oxide Fuel Cell (SOFC)

Absolute Temperature (T)	1273^0 K
Faraday's Constant (F)	96487 C/(mol)
Universal Gas Constant (R)	8314 J/(k mol K)
Standard Reversible cell potential (E_o)	1.2 V
Number of cells in stack (N_0)	380
Constant , $K_r = \frac{N_o}{(4F)}$	0.996×10^{-6} k mol/ (s A)
Maximum fuel utilization	0.9
Minimum fuel utilization	0.7
Optimum fuel utilization	0.85

Valve molar constant for hydrogen (K_{H_2})	8.43×10^{-4} k mol/ (s atm)
Valve molar constant for oxygen (K_{O_2})	2.81×10^{-4} k mol /(s atm)
Valve molar constant for water (K_{H_2O})	2.52×10^{-3} k mol /(s atm)
Response time for hydrogen flow (ζ_{H_2})	26.1 s
Response time for oxygen flow (ζ_{O_2})	2.91 s
Response time water flow (ζ_{H_2O})	78.3 s
Ohmic loss (r)	0.126 Ω
Ratio of hydrogen to oxygen (r_{H-O})	1.145

The detailed parameter of the DC-DC Boost converter is summarized Table 5.2.

Table 5.2 Parameters in DC-DC boost converter

Inductance (L)	2 mH
Capacitance (C)	1400 μF
Equivalent Load (R)	5 Ω
Switching Frequency (f_s)	7 kHz
Proportional Gain (K_p)	0.15
Integral gain (K_I)	0.005

The detailed parameter of the DC-AC inverter is summarized Table 5.3.

Table 5.3 System parameters (For Matlab/Simulink Simulation)

Parameters	Values
Supply voltage/frequency	440 V / 50 Hz
Interface Inductor ($R_c\ L_c$)	1 Ω ,1.5 mH

DC-Link capacitance (C_{DC})	2200 µF
Reference voltage (V_{dc_ref})	500 V
Voltage source inverter	6 IGBTs/diodes

In the above model, fixed-HCC and adaptive-HCC techniques are used for PWM-VSI controller. The switching losses are increased in the fixed-HCC due to high frequency operation. These techniques add high frequency ripples in the generated current. The current controller performance is improved by using the adaptive-HCC technique. This adaptive-HCC changes bandwidth according to instantaneous current variation. Fig.5.2 illustrates the switching patterns of fixed-HCC and adaptive-HCC PWM-current controllers.
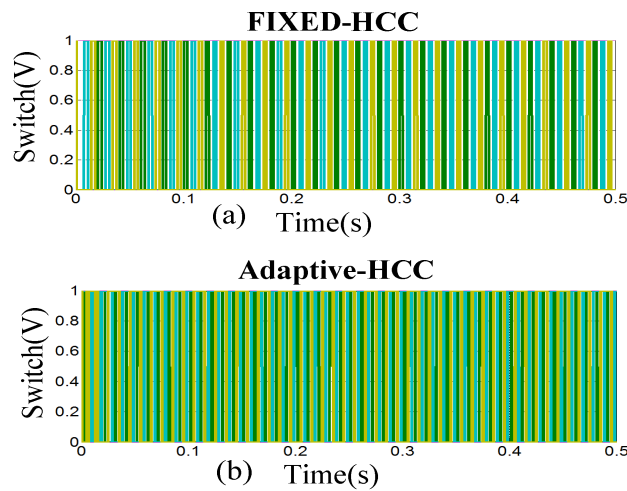
Fig.5.2 Switching patterns of Fixed-HCC, and Adaptive-HCC techniques

5.3.1 Simulation Results of Fuel Cell Power System using HCC and AHCC

The load current magnitude detector and unit sine vector with HCC and AHCC PWM-current controller is simulated under balanced load conditions. The simulated results indicated in Fig.5.3 and Fig.5.5 is obtained using fixed-HCC and adaptive-HCC technique respectively. The fixed-HCC or adaptive-HCC is used to generate the switching pulses to drive the fuel cell power system. In this simulation, 380 numbers of fuel cells are considered and these fuel cells are connected in series. The fuel cells provide an output voltage of 456 V DC, but due to the major losses like ohmic losses and minor losses like concentration losses and activation losses there is a loss of some

voltage (around 56 V). So the fuel cell voltage comes down around 400 V DC. The fuel cell output voltage is shown in Fig.5.3 (a). To step up the fuel cell voltage upto 500 V, a DC-DC boost converter is used. The specification of boost converter is shown in Table 5.2. The output of boost converter is fed to DC-AC inverter through a DC-link capacitor. The boost converter output is shown in Fig.5.3 (b). The inverter output is passed through LC filter to suppress the ripples. The LC filter is unable to suppress all the ripples of inverter output current. Fig.5.3 (c) shows the inverter output current. Here some amount of ripples is present due to grid side interfacing inductance and LC filter. The interfacing inductance is also useful for isolation between inverter side and load/grid side. Fig.5.3 (d) shows the output voltage of inverter after filter. When a major breakdown of grid occurs, the inverter output voltage is fed to load. Harmonics of the line current is measured for this particular controller and it is observed that the THD is 4.24%.

The simulation of adaptive-HCC PWM current controller is simulated in MATLAB/ SIMULINK. Fig.5.5 (a) shows the fuel cell output voltage. The DC-DC boost converter output voltage is shown in Fig.5.5 (b). This boost converter is used to increase the fuel cell output (400 V DC) upto 500 V DC regulated voltage. The boost converter output is fed to the DC-AC inverter through DC-link capacitor. The inverter output is injected to LC filter to eliminate the ripples. The LC filter only suppresses the ripples of the inverter output voltage. But some amount of ripples are present in the inverter output current because the presence of interfacing inductance between inverter and load/grid. Fig.5.5 (c) shows the output current of inverter. The inverter output voltage after filter is sinusoidal in nature and it is shown in Fig.5.5 (d). The output voltage is fed to the load when the power failure occurs in the grid. Harmonics of the line current is measured for this particular controller and it is observed that the THD is 4.20%.

Fig.5.3 Simulation waveform of (a) Fuel cell output voltage, (b) DC-DC Boost converter output voltage, (c) Inverter output current, and (d) Inverter output voltage (Fixed-HCC)
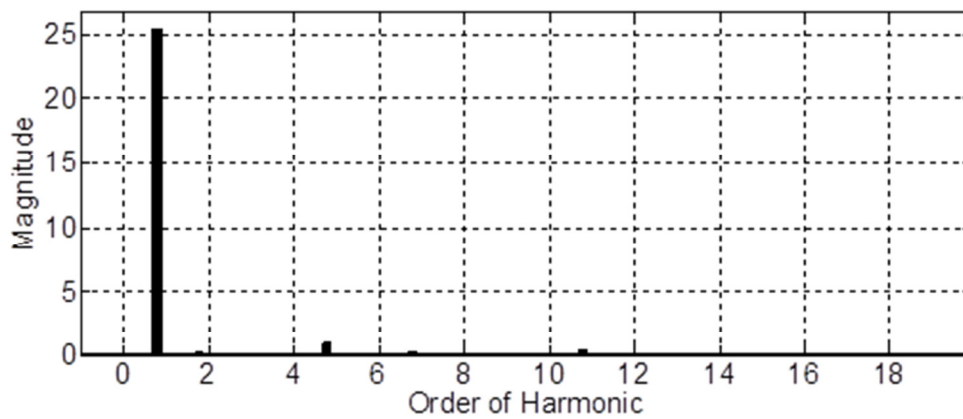
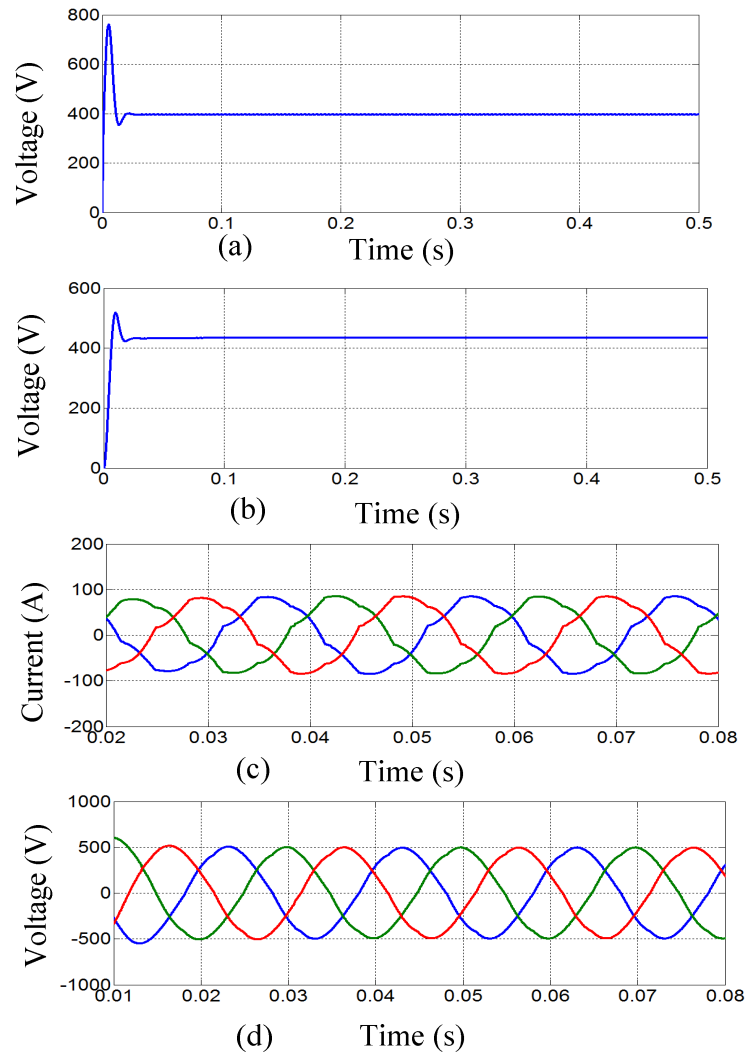*Fig. 5.4 Measured harmonics of Fixed-HCC*

89

Fig.5.5 Simulation waveform of (a) Fuel cell output voltage, (b) DC-DC Boost converter output voltage, (c) Inverter output current, and (d) Inverter output voltage (A-HCC)

Fig. 5.6 Measured harmonics of A-HCC

5.4 Load/Grid Connected Fuel Cell Power System with Battery

In some realistic situations, when there is low supply of hydrogen (H_2) or any kind of malfunction of fuel cell unit then fuel cell power source can't work as a backup supply. In this situation, a battery is used to resume the supply to the load. A switch is connected in parallel with the fuel cell unit. When fuel cell is not working then the battery is activated through the switch but under normal condition when fuel cell is working properly, the switch is off. Fig.5.7 shows the block diagram of load/grid connected fuel cell power system with battery.
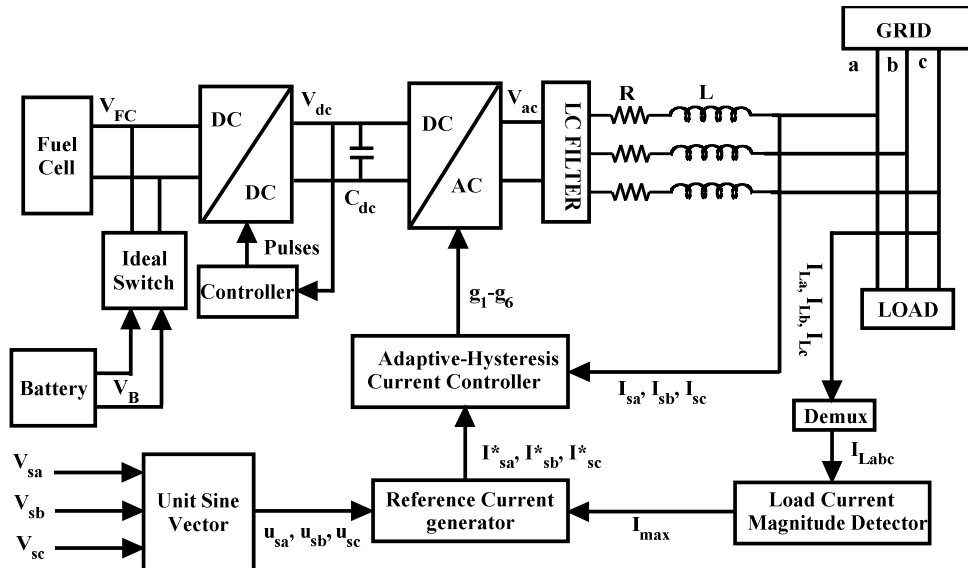
Fig.5.7 Block diagram of fuel cell power system with battery

In this configuration, adaptive hysteresis current controller (A-HCC) is used to generate accurate gate signals to drive the inverter. The load current magnitude detector (Three-

phase spectrum analyser) is used to estimate the maximum amplitude of load current $(I_{\max})$. The maximum value of load current is multiplied with the unit current templates to generate the required reference current. The reference current is compared with actual current (from output of LC filter) to generate the PWM signals using Adaptive-HCC techniques which is fed to the inverter gate.

5.4.1 Simulation Results of Fuel Cell Power System with Battery Using AHCC Controller

The simulation of adaptive-HCC PWM-VSI current controller is simulated in MATLAB/ SIMULINK. Fig.5.8 (a) shows the fuel cell output voltage. The output voltage of battery which is connected in parallel with fuel cell is shown in Fig.5.8 (b). The battery output voltage is fed to the DC-DC boost converter when the shortage of fuel input (H_2) to the fuel or permanent damage occurs in the fuel cell. The DC-DC boost converter output voltage is shown in Fig.5.8 (c). This boost converter is used to increase the fuel cell or battery output (400 V DC) upto approximately 500 V DC regulated voltage. The boost converter output is fed to the DC-AC inverter through DC-link capacitor. The inverter output is injected to LC filter to eliminate the ripples. The LC filter only suppresses the ripples of the inverter output voltage. But some amount of ripples are present in the inverter output current because the presence of interfacing inductance between inverter and load/grid. Fig.5.8 (d) shows the output current of inverter. The inverter output voltage after filter is shown in Fig.5.8 (e) which is fed to the load when the power failure occurs in the grid. Harmonics of the line current is measured for this particular controller and it is observed that the THD is 4.20%.
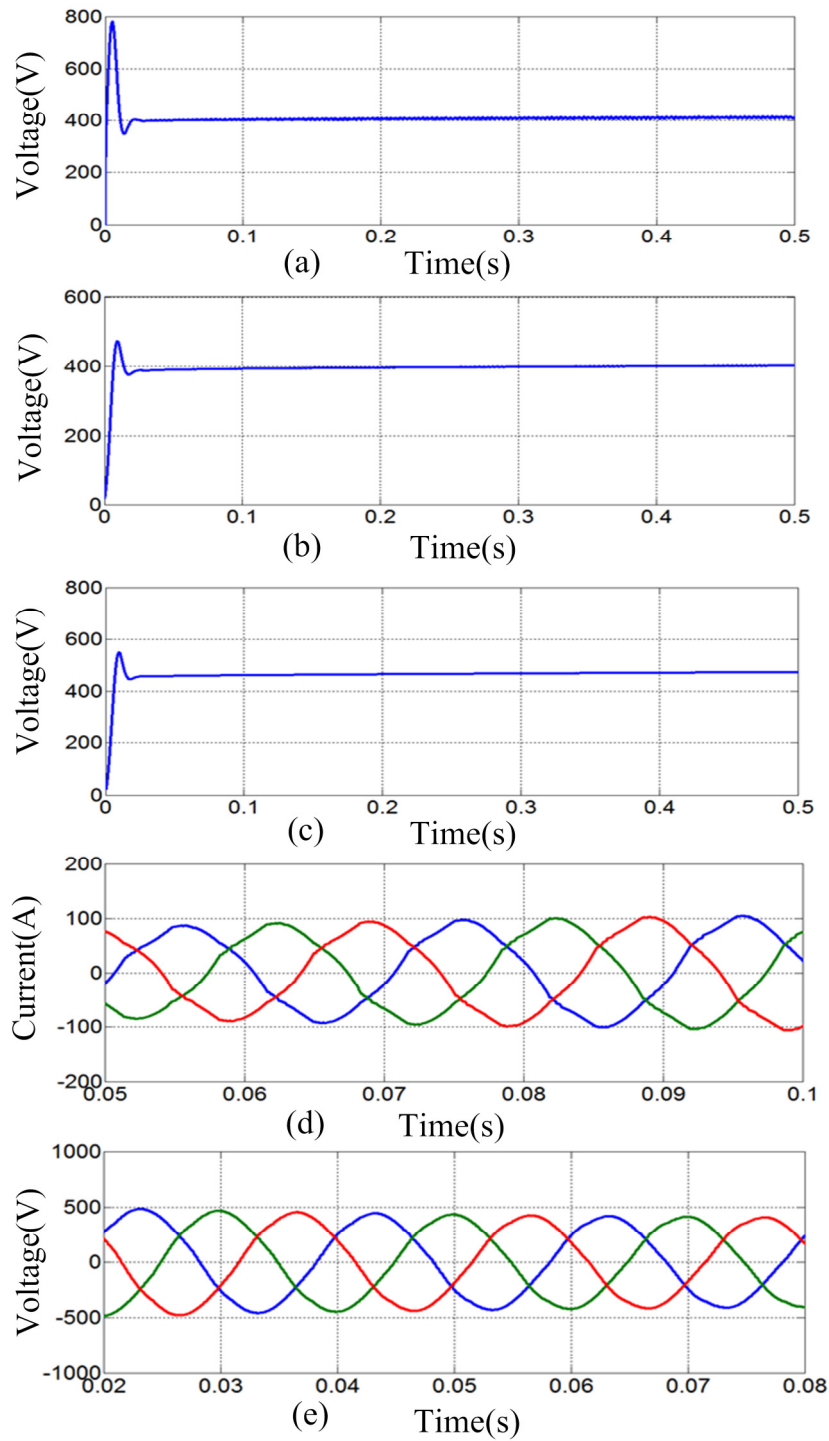
Fig.5.8 Simulation waveform of (a) Fuel cell output voltage, (b) Battery output voltage, (c) DC-DC Boost converter output voltage, (d) Inverter output current and (e) Inverter output voltage (AHCC)
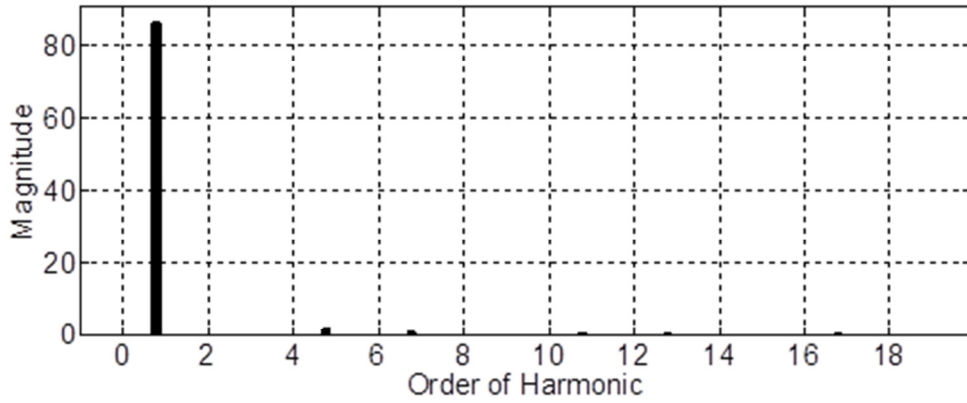
Fig. 5.9 Measured harmonics of A-HCC
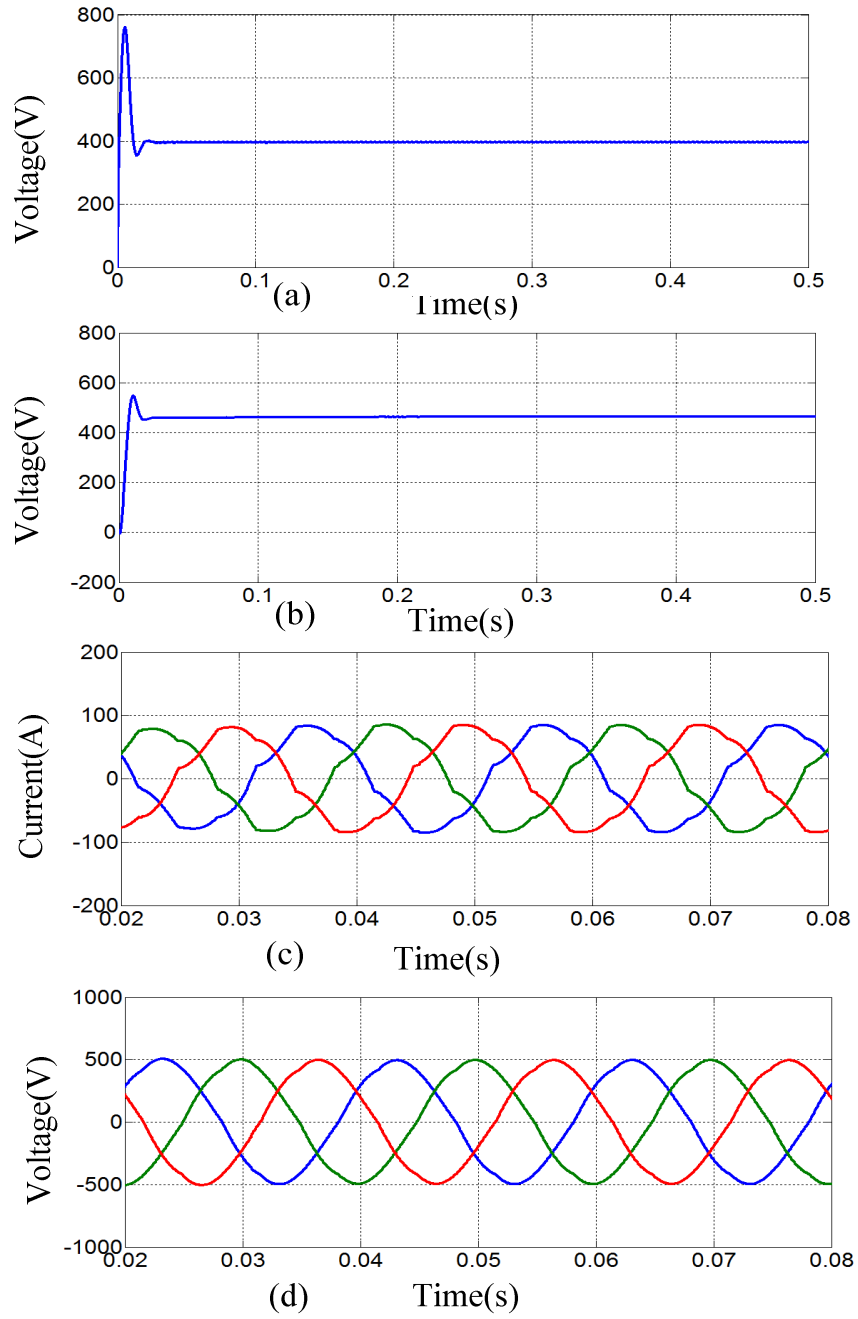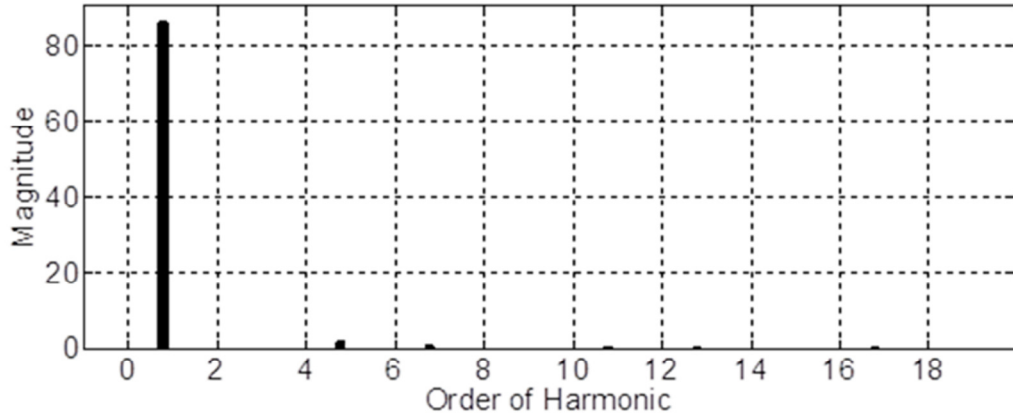
5.5 Load/Grid Connected Fuel Cell Power System without DC-DC Converter

When there is sufficient number of fuel cell units, the output voltage is 500 V. In this particular case, there is no need of a boost converter to increase the DC level of the output voltage. So in this configuration, boost converter is not required. There are some advantages of exclusion of boost converter such as, boost converter is an additional hardware circuit and it needs a control algorithm to operate. When boost converter is not included, the hardware complexity and cost of the hardware is reduced. Fig.5.10 shows the block diagram of load/grid connected fuel cell power system.
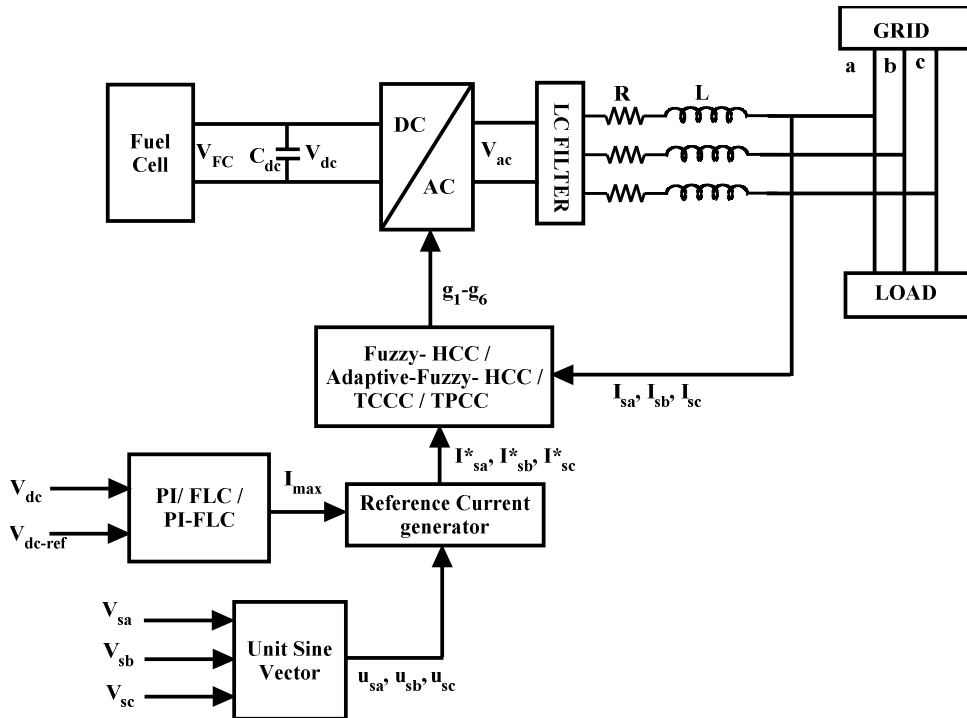
Fig.5.10 Block diagram of fuel cell power system without DC-DC converter

In this configuration, the reference current extraction process is developed from unit current vector along with a controller. The controller is used to estimate the maximum amplitude of supply current using DC-link capacitor voltage of fuel cell power system. The maximum value generated by the controller is multiplied by unit current vector templates to generate the required reference current. The reference current is compared with the actual current to generate the PWM signals using fuzzy-HCC/adaptive-fuzzy-HCC/TCCC and TPCC techniques which is fed to the gate of the inverter. Different controller topologies such as PI, fuzzy logic controller (FLC) and PI-fuzzy logic controller (PI-FLC) are used to generate the maximum current from DC-link capacitor voltage. Section 5.5.1 and 5.5.3 are describing the working principles of PI and fuzzy logic controller.
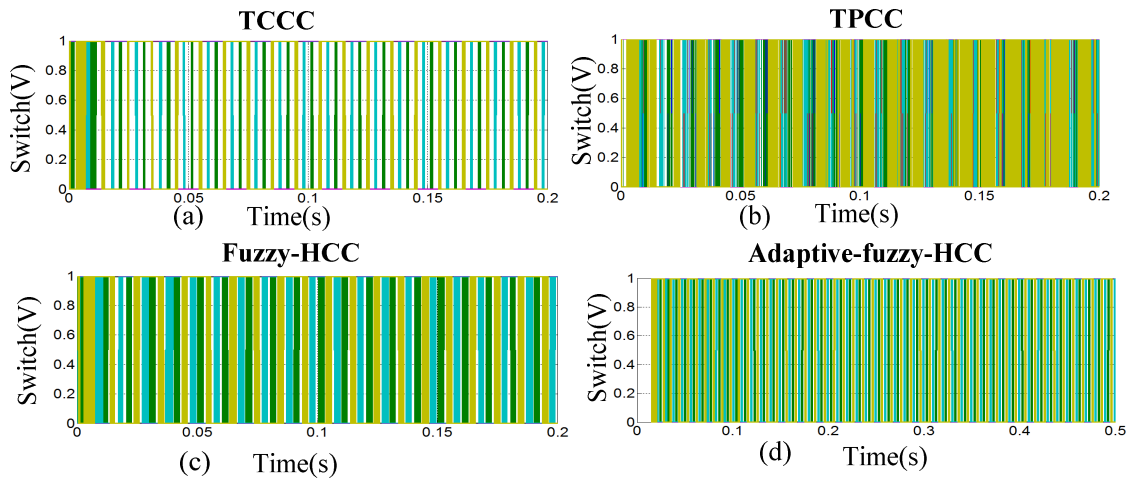
Fig.5.11 Switching patterns of (a) TCCC, (b) TPCC, (c) Fuzzy-HCC, (d) Fuzzy-Adaptive-HCC techniques

In the above model fuzzy-HCC, adaptive-fuzzy-HCC, TCCC and TPCC techniques are used for PWM-VSI controller. The switching patterns of these techniques are shown in Fig.5.11.

5.5.1   PI Controller

The PI-controller is used to determine the reference current to control the DC-link capacitor voltage. The output of PI-controller is treated as the peak value of the estimated source current. Fig.5.12 shows the block diagram of PI-controller to determine the reference currents. The DC-link capacitor voltage is sensed and compared with DC

95

reference voltage. The voltage error (e (v) = $V_{dc\text{-}ref} - V_{dc}$) at the sampling instant is fed as input to the PI-controller.
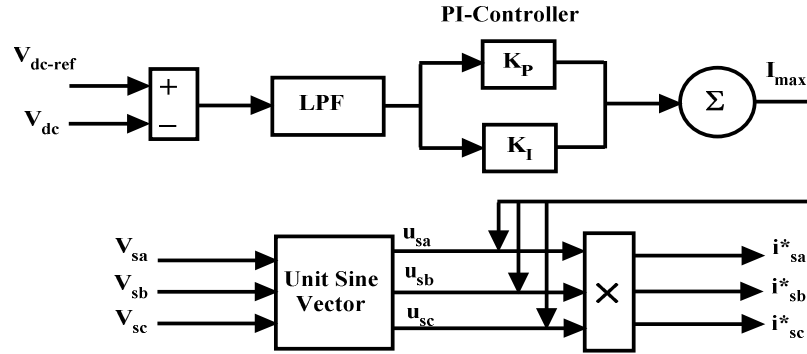
Fig.5.12 Block diagram of the PI-controller

Low Pass Filter (LPF) is introduced to filter out the ripples present in the capacitor voltage. The transfer function of PI-controller is defined as

$$T(S) = \frac{u(s)}{e(s)} = K_P + \frac{K_I}{s}$$

(5.4)

where, K_P and K_I are the proportional and integral constants. These parameters are determined by heuristic method. The values of K_P and K_I are 0.3 and 9 respectively. The proportional gain reduces the transient behaviour of the system and integral gain reduces the steady-state error.

5.5.2 Simulation Results of Fuel Cell Power System using PI Controller with TPCC and TCCC Controller

PI controller with various PWM-current controllers for fuel cell power system is simulated under balanced load side conditions. The simulation in Fig.5.13 and Fig.5.15 are focused on PI with triangular periodical carrier controller (TPCC) and triangular carrier current controller (TCCC) technique respectively.

In this simulation, 380 numbers of fuel cells are considered and these fuel cells are connected in series to make the fuel cell output voltage 400 V DC. The fuel cell output voltage is shown in Fig.5.13 (a). The output voltage of DC-link capacitor is fed to DC-AC inverter. The output of DC-link capacitor voltage is shown in Fig.5.13 (b). The inverter output voltage is fed to LC filter to supress the ripples. The LC filter is unable to supress all the ripples of inverter output current. Fig.5.13 (c) shows the inverter output

current. Here some amount of ripples is present due to grid side interfacing inductance and LC filter. The interfacing inductance is also useful for isolation between inverter side and load/grid side. Fig.5.13 (d) shows the output voltage of inverter after filter. When a major breakdown of grid occurs, the inverter output voltage is fed to load. Harmonics of the line current is measured for this particular controller and it is observed that the THD is 4.38%.

Fig.5.13 Simulation waveform of (a) Fuel cell output voltage, (b) DC-link capacitor voltage, (c) Inverter output current, and (d) Inverter output voltage (TPCC)

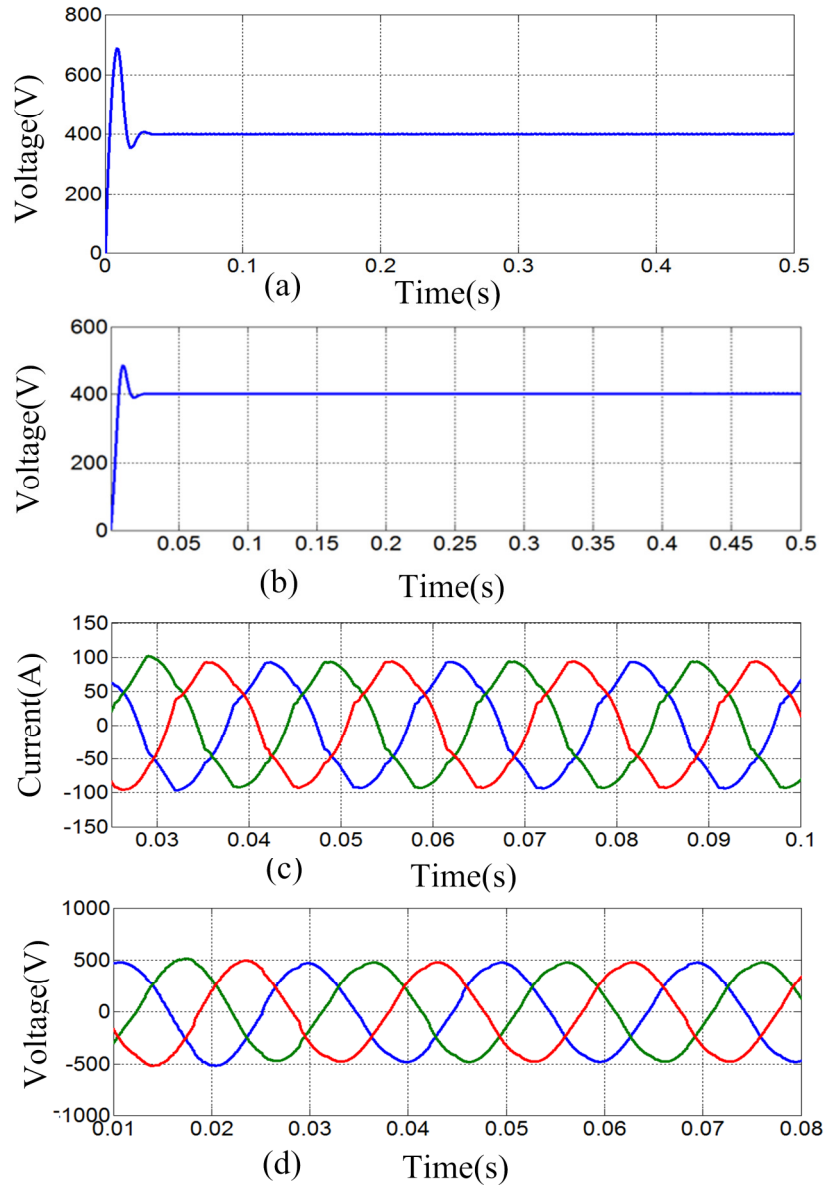*Fig. 5.14 Measured harmonics of TPCC*

Fig.5.15 Simulation waveform of (a) Fuel cell output voltage, (b) DC-link capacitor voltage, (c) Inverter output current, and (d) Inverter output voltage (TCCC)
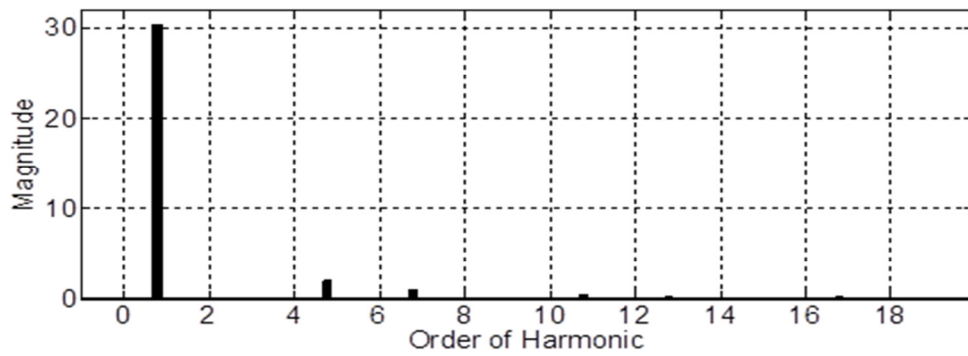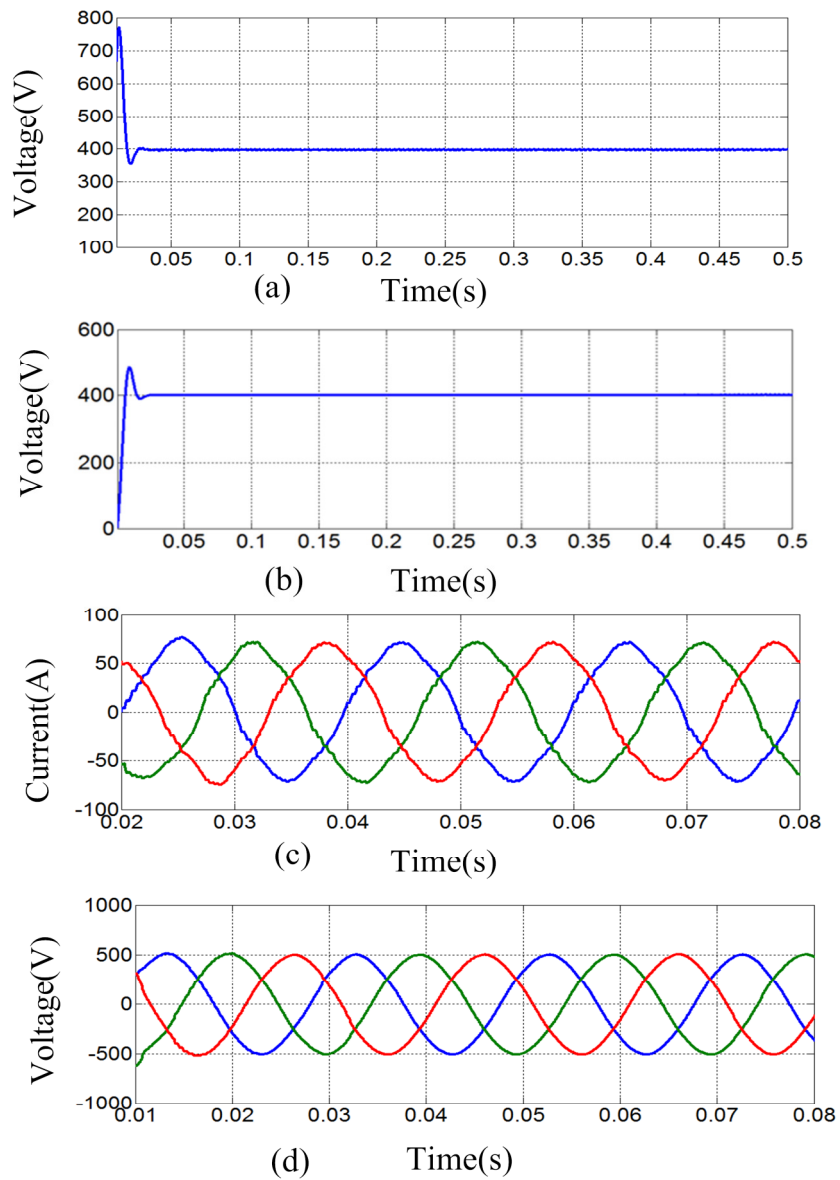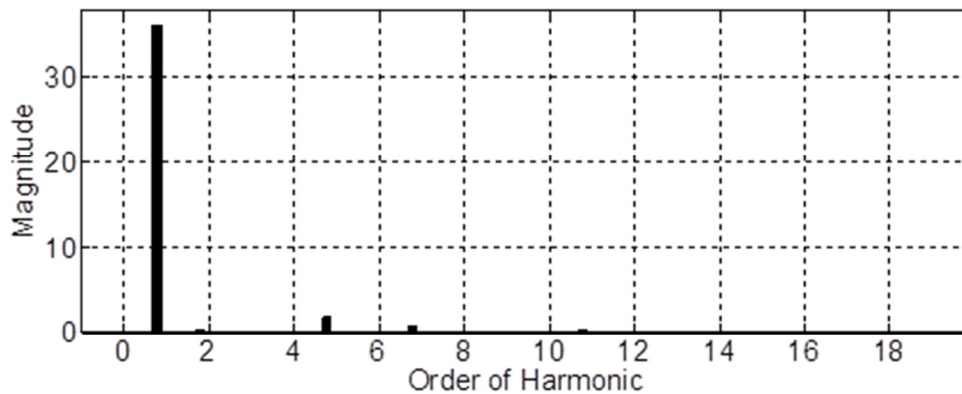
Fig. 5.16 Measured harmonics of TCCC

The fuel cell output voltage 400 V DC is shown in Fig.5.15 (a). The DC-link capacitor voltage output is shown in Fig.5.15 (b). The output voltage of fuel cell is fed to DC-AC inverter through DC-link capacitor. The inverter output voltage is fed to LC filter to supress the ripples but the LC filter is unable to supress all the ripples of inverter output current. Fig.5.15 (c) shows the inverter output current. The output voltage of inverter is fed to the grid. Fig.5.15 (d) shows the output voltage of inverter after filter. The TPCC/ TCCC is used to generate the PWM signals to drive the fuel cell power system. Harmonics of the line current is measured for this particular controller and it is observed that the THD is 4.44%.

5.5.3   Fuzzy Logic Controller: A General Overview

Conventional PI controller requires a mathematical model of the system, which is difficult to obtain under parametric variations, non-linearity and load disturbances. Another drawback of the conventional controller is that the proportional, integral and derivative gains are chosen by different tuning methods or by trial and error method. Recently a lot of research has been going on to improve the performance of conventional controller by utilizing fuzzy logic [122]. In this improved controller architecture, the general structure of conventional controller is retained and fuzzy logic is used to provide intelligence to the operation of controller.

Fuzzy logic focuses on linguistic variable in natural language and aims to provide foundations for approximate reasoning with imprecise proposition. Fuzzy set theory has provided a mathematical strength to capture the uncertainties associated with human cognitive process [122].

The functional architecture of a closed loop system with fuzzy logic controller is shown in Fig.5.17. Fuzzy logic controller comprises of three main units such as fuzzification unit, fuzzy inference system and defuzzification unit. Fuzzy inference system comprises of an inference mechanism and a rule base. There are two well-known fuzzy inference mechanisms namely MAMDANI and Takagi-Sugeno-Kang (TSK). The main difference between MAMDANI inference and TSK inference is that the consequent of MAMDANI inference are fuzzy proposition whereas the consequent of TSK inference are crisp proposition.
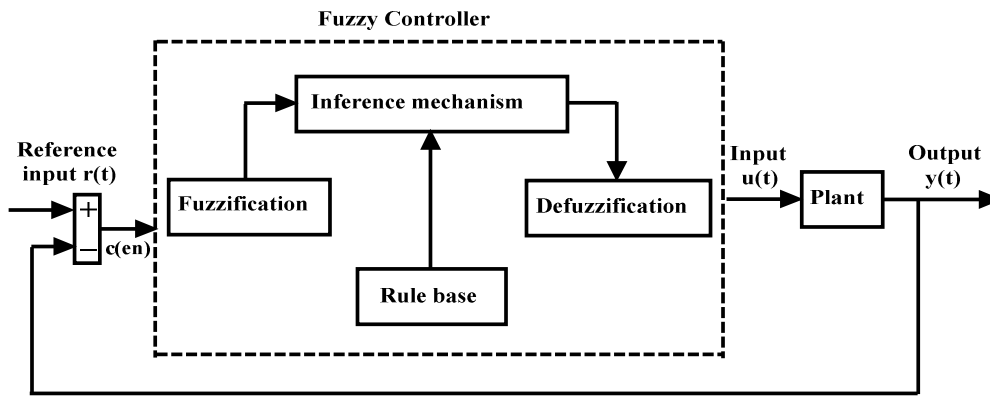
Fig.5.17 Schematic diagram of fuzzy logic controller

Fuzzy logic provides an inference morphology that enables approximate human reasoning capabilities to be applied to knowledge based systems. Fuzzy IF-THEN rules are expressed as

IF {premise$_1$} THEN {consequent$_1$}

IF {premise$_1$} AND {premise$_2$} THEN {consequent}

A typical rule, with 2 input variables (x_1 and x_2) and 1 output variable (y) for MAMDANI fuzzy inference system is

IF x_1 is A_1 AND x_2 is A_2 THEN y is B_1

A typical rule of TSK fuzzy inference system is

IF x_1 is A_1 AND x_2 is A_2 THEN $y = f(x_1, x_2)$

Defuzzification is a mapping form from a space of fuzzy control actions defined by fuzzy sets on an output universe of discourse, in to non-fuzzy (crisp) control action. There are

many approaches of defuzzification but center of area (COA) defuzzification is most popular.

5.5.4 Fuzzy Logic Controller

To get the reference current from DC-link capacitor voltage fuzzy logic controller is used [123]. The block diagram of fuzzy logic controller is shown in Fig.5.18.
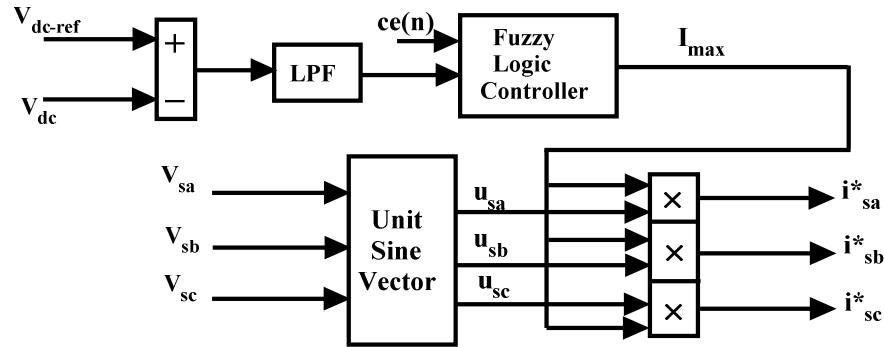
Fig.5.18 Block diagram of fuzzy logic controller

Here the input variables of fuzzy logic controller are error ($e(n)$) and change in error $ce(n)$.

where, $e(n) = V_{dc-ref} - V_{dc}$ and $ce(n) = \dfrac{d}{dt}(ce(n))$.

The output variable of fuzzy logic controller is absolute value of peak reference current I_{max}.

Fig.5.19 shows the possible assignment of fuzzy membership function for $e(n)$, Fig.5.20 shows the possible assignment of fuzzy membership function for $ce(n)$ and Fig.5.21 shows the possible assignment of fuzzy membership function for I_{max}.
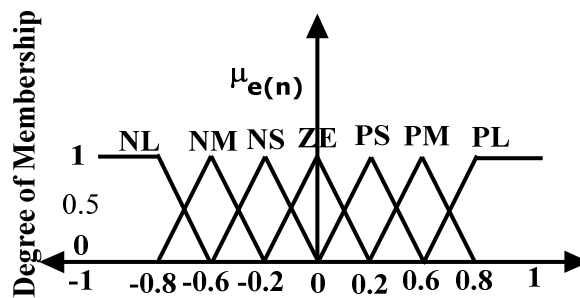
Fig.5.19 Input variables "e(n)" of FLC
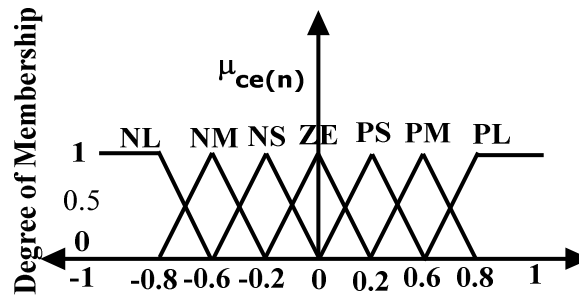
Fig.5.20 Input variables " ce(n)" of FLC
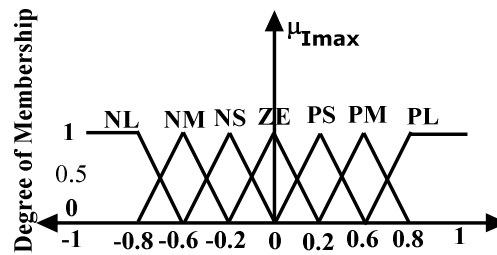
Fig.5.21 Output variable "I_{max}" of FLC

The membership functions are labelled as Negative Large (NL), Negative Medium (NM), Negative Small (NS), Zero (ZE), Positive Small (PS), Positive Medium (PM), Positive Large (PL).

After the assignment of membership functions for input and output variables, fuzzy IF-THEN rule base is created. In this problem, MAMDANI fuzzy inference system is considered and the rule matrix is shown in Table 5.4.

Table 5.4 Rule matrix for MAMDANI fuzzy inference

I_{max}		Error e(n)						
		NL	NM	NS	ZE	PS	PM	PL
Change in error ce(n)	NL	NL	NL	NL	NL	NM	NS	ZE
	NM	NL	NL	NL	NM	NS	ZE	PS
	NS	NL	NL	NM	NS	ZE	PS	PM
	ZE	NL	NM	NS	ZE	PS	PM	PL
	PS	NM	NS	ZE	PS	PM	PL	PL
	PM	NS	ZE	PS	PM	PL	PL	PL
	PL	ZE	PS	PM	PL	PL	PL	PL

The rule matrix can be interpreted as

IF e(n) is NL AND ce(n) is NL THEN I$_{max}$ is NL

The rule matrix provides a fuzzified value of I_{max} as output which has to be converted in to crisp value for actual implementation. The process of conversion from fuzzified value to crisp value is known as de-fuzzification. Here centre of area de-fuzzification method is used, which can be represented by

$$COA = \frac{\int_{X_{min}}^{X_{max}} f(x).x\,dx}{\int_{X_{min}}^{X_{max}} f(x)\,dx}$$

(5.5)

The output of the fuzzy controller estimates the magnitude of peak reference current I_{max}. This estimated magnitude of peak-current multiplied with an output of unit sine vector determines the reference currents.

5.5.5 Simulation Results for fuel Cell Power System using Fuzzy Logic Controller with Fixed-HCC and Adaptive-HCC

Fuzzy logic controller with fixed-HCC/adaptive-HCC are simulated and investigated under balanced load side conditions. The fuzzy-HCC/adaptive-fuzzy-HCC are used to generate the switching pulses to drive the fuel cell power system. The simulation of fuzzy-HCC and adaptive-fuzzy-HCC are shown in Fig.5.22 and Fig.5.24 respectively. For this simulation, 380 numbers of fuel cells are considered and these fuel cells are connected in series to make the fuel cell output voltage 400 V DC. The fuel cell output voltage is shown in Fig.5.22 (a). The output voltage of fuel cell is fed to DC-AC inverter through a DC-link capacitor. The DC-link capacitor output voltage is shown in Fig.5.22 (b). The inverter output voltage is fed to LC filter to supress the ripples. The LC filter is unable to supress all the ripples of inverter output current. Fig.5.22 (c) shows the inverter output current. Here some amount of ripples is present due to grid side interfacing inductance and LC filter. The interfacing inductance is also useful for isolation between inverter side and load/grid side. Fig.5.22 (d) shows the output voltage of inverter after filter. When a major breakdown of grid occurs, the inverter output voltage is fed to load.

103

Harmonics of the line current is measured for this particular controller and it is observed that the THD is 3.98%.
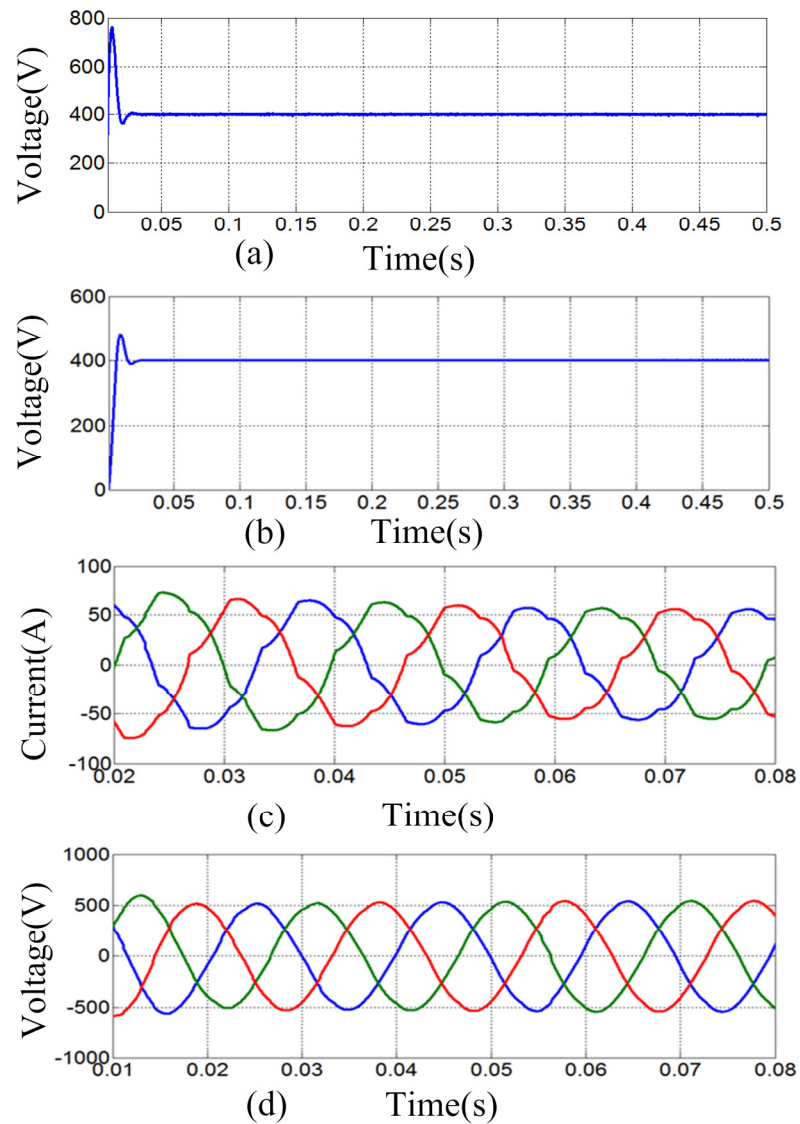
Fig.5.22 Simulation waveform of (a) Fuel cell output voltage, (b) DC-link capacitor voltage, (c) Inverter output current, and (d) Inverter output voltage (Fuzzy-HCC)
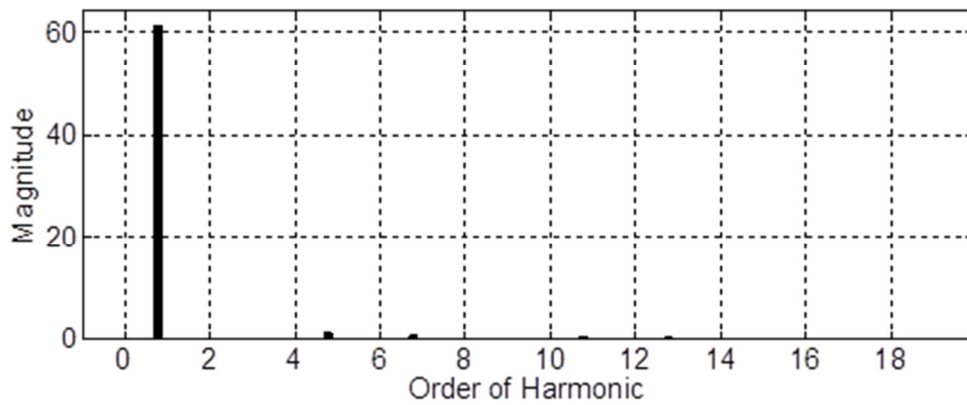
Fig. 5.23 Measured harmonics of Fuzzy-HCC
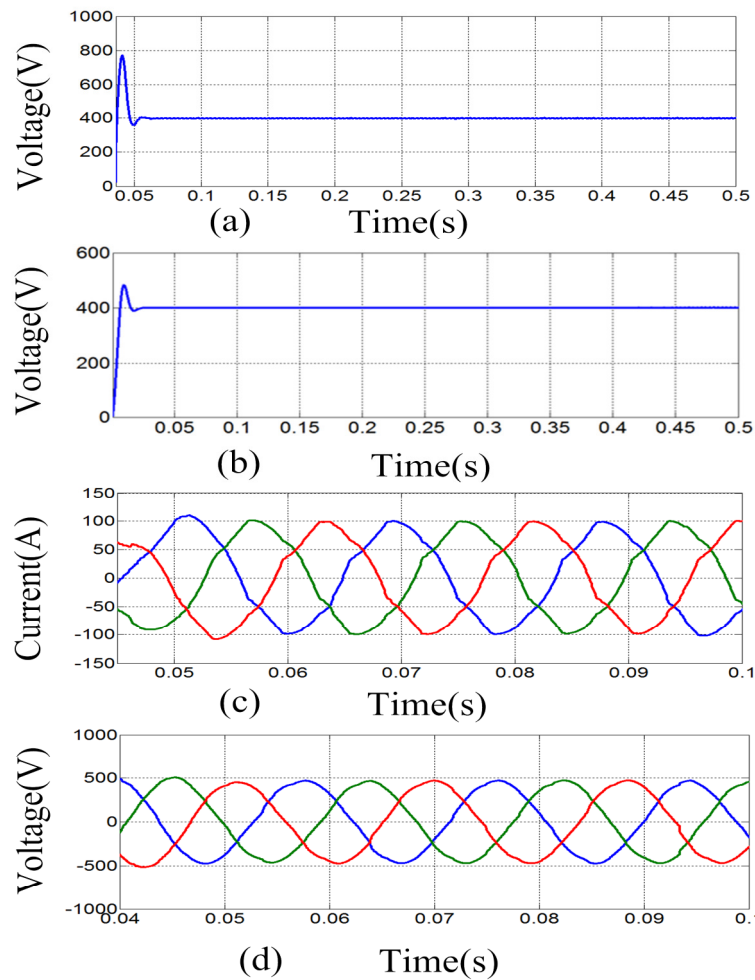
Fig.5.24 Simulation waveform of (a) Fuel cell output voltage, (b) DC-link capacitor voltage, (c) Inverter output current, and (d) Inverter output voltage (Fuzzy-Adaptive-HCC)

105
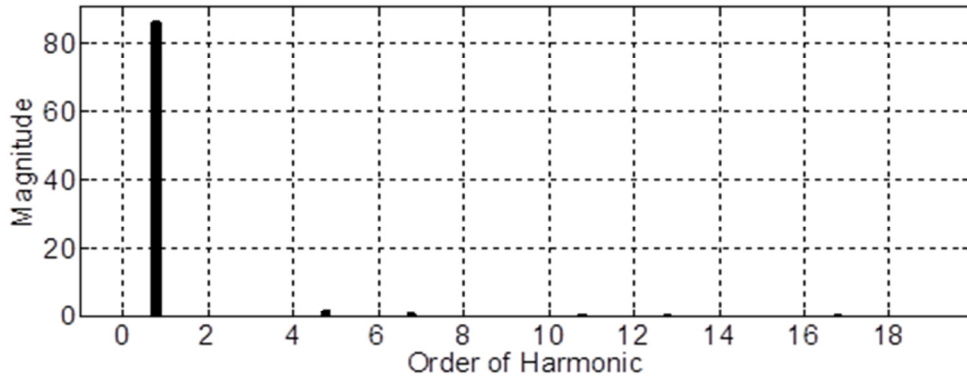
Fig. 5.25 Measured harmonics of Fuzzy-adaptive-HCC

Fig.5.24 is obtained using adaptive-fuzzy-HCC controller to generate the switching signals for fuel cell power system. Fig.5.24 (a) shows the fuel cell output voltage. The DC-link capacitor output voltage is shown in Fig.5.24 (b). This voltage output is fed to the DC-AC inverter. The inverter output is given as input to LC filter to eliminate the ripples. The LC filter only suppresses the ripples of the inverter output voltage. But some amount of ripples are present in the inverter output current because the presence of interfacing inductance between inverter and load/grid. Fig.5.24 (c) shows the output current of inverter. The inverter output voltage after filter is shown in Fig.5.24 (d) which is fed to the load when the power failure occurs in the grid. Harmonics of the line current is measured for this particular controller and it is observed that the THD is 3.82%.

5.5.6 PI-Fuzzy Logic Controller

In section 5.5 a fuzzy logic controller is implemented to calculate I_{max}. In this section the general architecture of PI controller is retained and fuzzy logic controller is used to improve the controller architecture to calculate I_{max}. This architecture is known as PI-Fuzzy Logic Controller (PI-FLC).
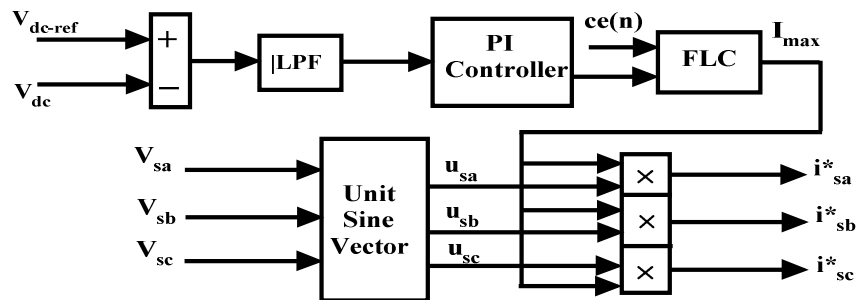
Fig.5.26 Block diagram of the PI with fuzzy logic controller

106

Here the input variables of fuzzy logic controller are error ($e(n)$) and integral of error ($ce(n)$)

where, $e(n) = V_{dc-ref} - V_{dc}$ and $ce(n) = \int e(n)$.

The output variable of fuzzy logic controller is incremental value of peak reference current I_{max} .

Fig.5.27 shows the possible assignment of fuzzy membership function for $e(n)$, Fig.5.28 shows the possible assignment of fuzzy membership function for $ce(n)$ and Fig.5.29 shows the possible assignment of fuzzy membership function for I_{max} .
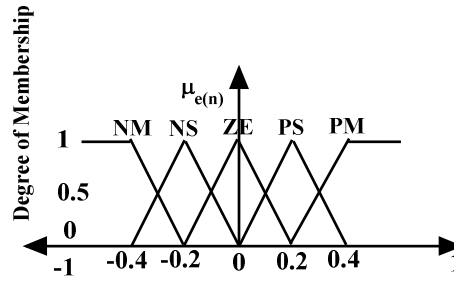
Fig.5.27 Input variables "e(n)" of PI-FLC
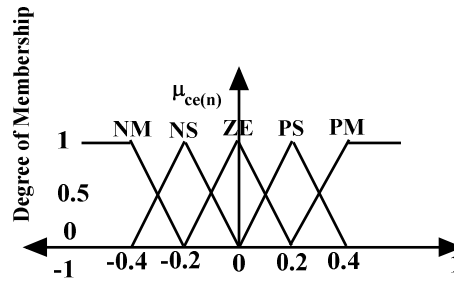
Fig.5.28 Input variables "ce(n)" of PI-FLC
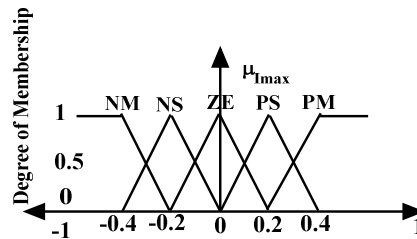
Fig.5.29 Output variable "I_{max}" of PI-FLC

The membership functions are labelled as Negative Medium (NM), Negative Small (NS), Zero (ZE), Positive Small (PS), and Positive Medium (PM).

After the assignment of membership functions for input and output variables, fuzzy IF-THEN rule base is created. In this problem, MAMDANI fuzzy inference system is considered and the rule matrix is shown in Table 5.5.

Table 5.5 Rule matrix for PI-FLC using MAMDANI fuzzy inference

I_{max}		Error e(n)				
		NM	NS	ZE	PS	PM
Change in error ce(n)	NM	NM	NM	NM	NS	ZE
	NS	NM	NM	NS	ZE	PS
	ZE	NM	NS	ZE	PS	PM
	PS	NS	ZE	PS	PS	PM
	PM	ZE	PS	PM	PM	PM

The rule matrix can be interpreted as

IF e(n) is NM AND ce(n) is NM THEN I$_{max}$ is NM

The rule matrix provides a fuzzified value of I_{max} as output which has to be converted in to crisp value for actual implementation. The process of conversion from fuzzified value to crisp value is known as de-fuzzification. Here centre of area de-fuzzification method is used, which can be represented by

$$COA = \frac{\int_{X_{min}}^{X_{max}} f(x).xdx}{\int_{X_{min}}^{X_{max}} f(x)dx}$$

(5.6)

This estimated magnitude of peak-current multiplied with an output of unit sine vector determines the reference currents. The reference currents are compared with actual source currents to generate the switching pulses using PWM-VSI current controller.

5.5.7 Simulation Results of Fuel Cell Power System using PI-Fuzzy Controller with Fixed-HCC and Adaptive-HCC

PI-Fuzzy logic controller with various PWM-current control techniques are simulated and investigated under balanced load side conditions. The simulation in Fig.5.30 is obtained using PI-FLC with fixed HCC. For this simulation, 380 numbers of fuel cells are considered and these fuel cells are connected in series to make the fuel cell output voltage 400 V DC. The fuel cell output voltage is shown in Fig.5.30 (a).The DC-link capacitor output voltage (400 V DC). The output of DC-link capacitor voltage is fed to DC-AC inverter. The DC-link capacitor output is shown in Fig.5.30 (b). The inverter output voltage is fed to LC filter to supress the ripples. The LC filter is unable to supress all the ripples of inverter output current. Fig.5.30 (c) shows the inverter output current. Here some amount of ripples is present due to grid side interfacing inductance and LC filter. The interfacing inductance is also useful for isolation between inverter side and load/grid side. Fig.5.30 (d) shows the output voltage of inverter after filter. When a major breakdown of grid occurs, the inverter output voltage is fed to load. Harmonics of the line current is measured for this particular controller and it is observed that the THD is 3.45%.
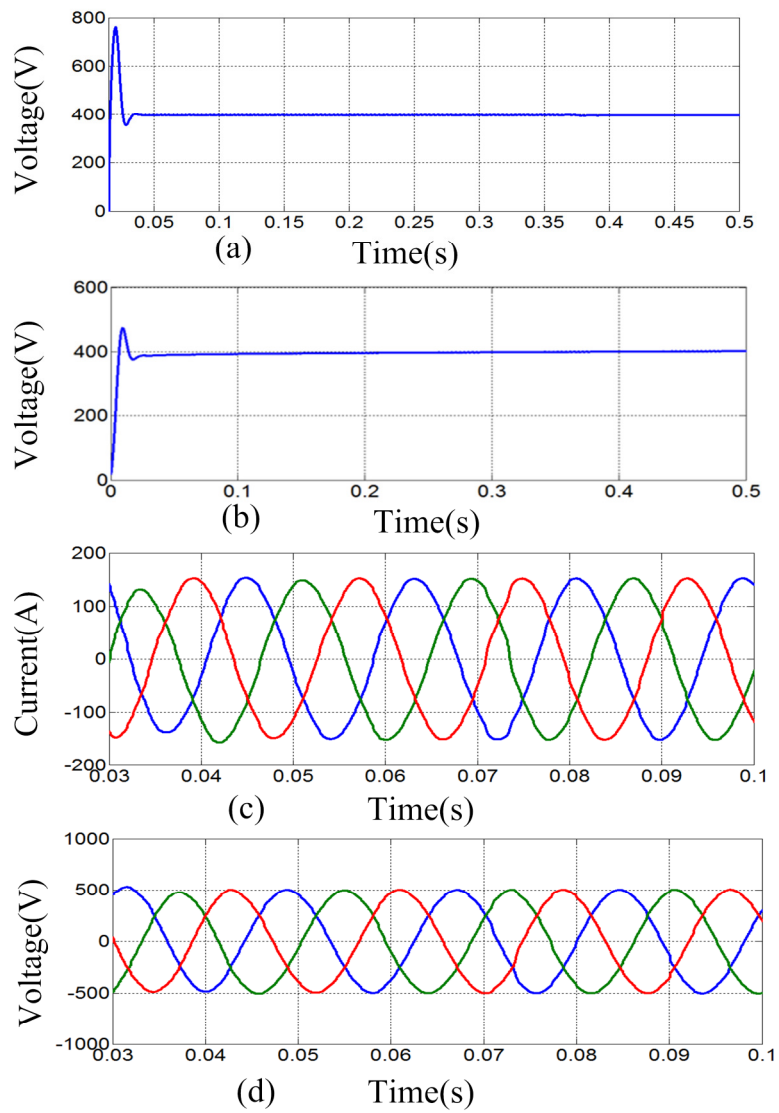
Fig.5.30 Simulation waveform of (a) Fuel cell output voltage, (b) DC-link capacitor voltage, (c) Inverter output current, and (d) Inverter output voltage (PI-Fuzzy-HCC)
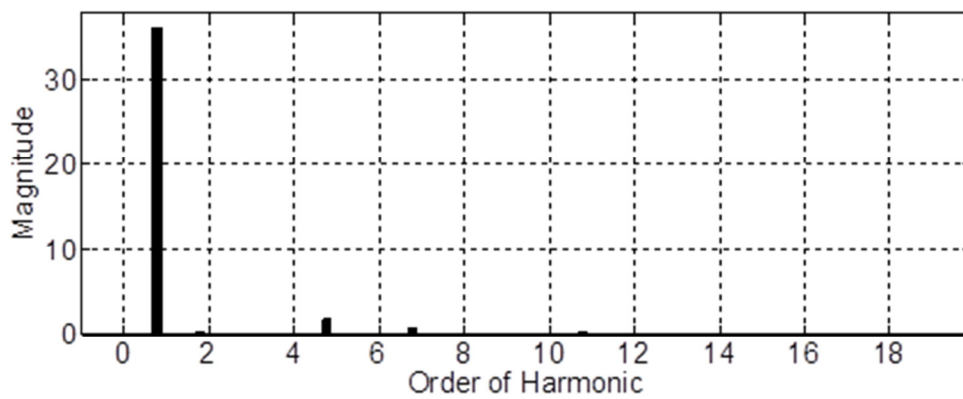
Fig. 5.31 Measured harmonics of PI-Fuzzy-HCC

110

The simulation in Fig.5.32 is obtained using PI-FLC with fuzzy-adaptive-HCC to generate the PWM signals to drive the fuel cell power system.
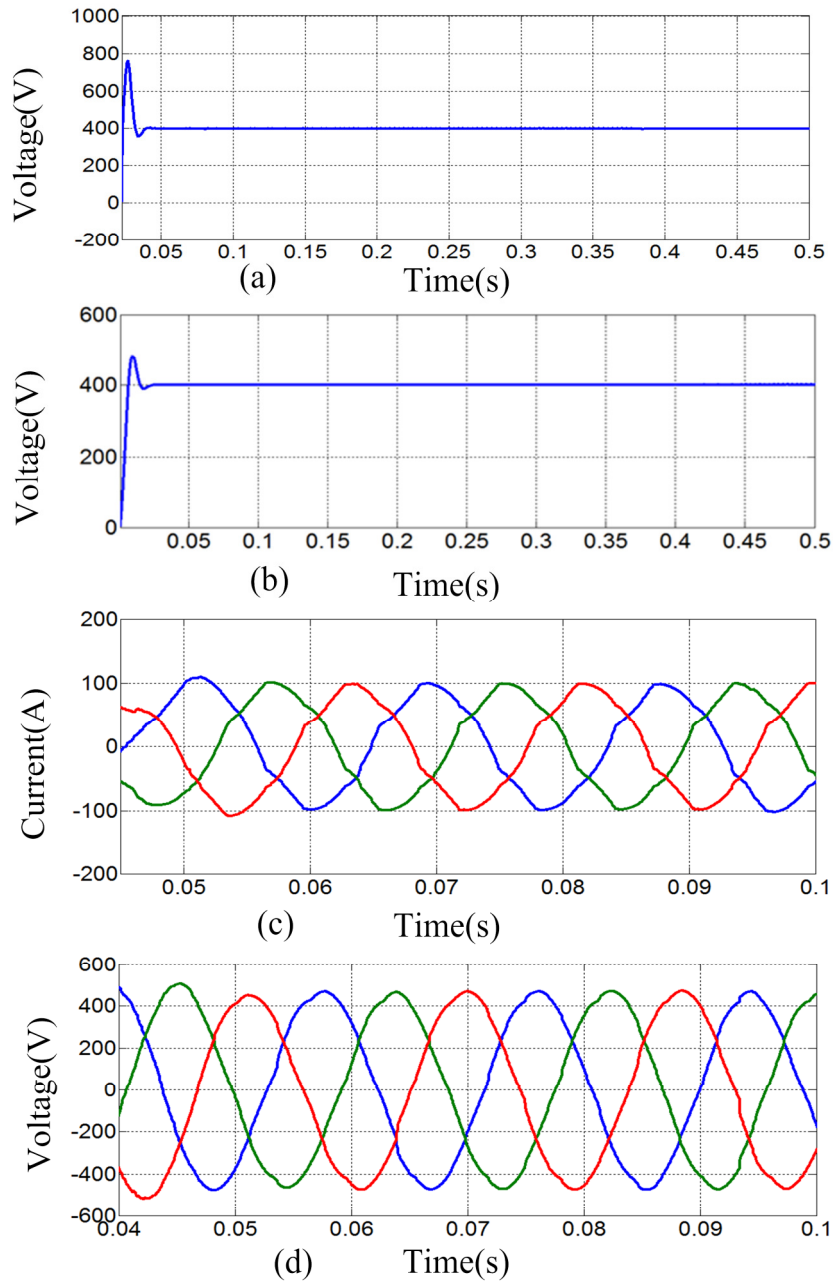
Fig.5.32 Simulation waveform of (a) Fuel cell output voltage, (b) DC-link capacitor voltage, (c) Inverter output current, and (d) Inverter output voltage (PI-Adaptive-Fuzzy-HCC)

111
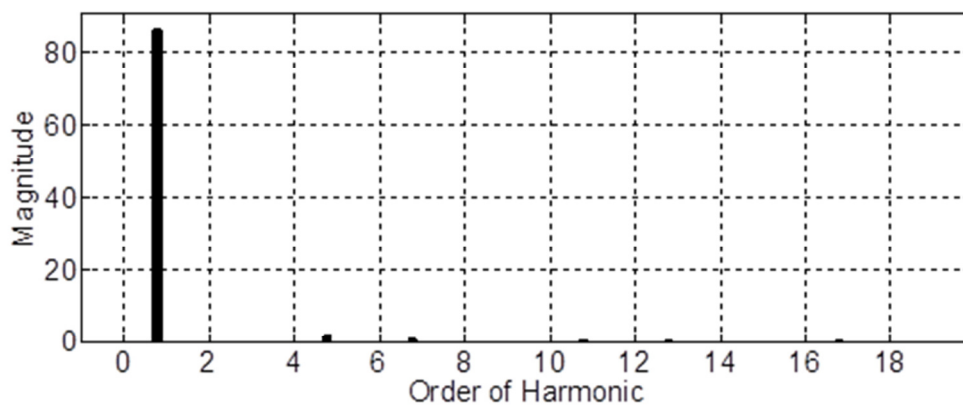
Fig. 5.33 Measured harmonics of PI-Adaptive-Fuzzy-HCC

Fig.5.32 (a) shows the fuel cell output voltage. The DC-link capacitor output voltage is shown in Fig.5.32 (b). The DC-link capacitor output voltage is fed to the DC-AC inverter. The inverter output is given as input to LC filter to eliminate the ripples. The LC filter only suppresses the ripples of the inverter output voltage. But some amount of ripples are present in the inverter output current because the presence of interfacing inductance between inverter and load/grid. Fig.5.32 (c) shows the output current of inverter. The inverter output voltage after filter is shown in Fig.5.32 (d) which is fed to the load when the power failure occurs in the grid. Harmonics of the line current is measured for this particular controller and it is observed that the THD is 3.15% which is acceptable in terms of IEEE standard.

Harmonic distortion of line current is measured using different control strategy. The comparisons of THD of line current are summarized in Table 5.6.

Table 5.6 Measured THD under various PWM-VSI techniques

PWM VSI Techniques	PI Controller	Fuzzy Controller	PI-Fuzzy Controller
TCCC	4.44 %	-	-
TPCC	4.38 %	-	-
Fixed HCC	4.24 %	3.98 %	3.45 %
Fuzzy HCC	4.20 %	3.95 %	3.40 %
Adaptive HCC	4.18 %	3.82 %	3.35 %
Adaptive Fuzzy HCC	4.11 %	3.71 %	3.15 %

From the above table, it is seen that if adaptive-fuzzy-HCC is used, the harmonic distortion is around 3.15% which is the lowest among all the controllers.

5.6   Summary

This chapter investigates different control configurations of PWM-VSI for DC-AC inverter used in fuel cell power system. This chapter also gives emphasis upon two different real life situations like lack of sufficient number of fuel cells and shortage of fuel. In first case, DC-DC boost converter is used to step-up the fuel cell voltage to a required level. The stepped up voltage is fed to the DC-AC inverter. Fixed-HCC and adaptive HCC PWM-VSI control strategy is used to acquire the required gate pulses of inverter. In second case, DC-DC boost converter is used to step up the fuel cell voltage which is eventually fed to a DC-AC inverter. Adaptive-HCC PWM-VSI control is used to generate required gate pulses for the inverter. In this configuration, a battery is connected in parallel to the fuel cell stack as a backup unit.

When sufficient fuel and sufficient number of fuel cells are available, the PWM-VSI control of DC-AC inverter is performed with the help of fuzzy-hysteresis, adaptive-hysteresis, TPCC and TCCC. Adaptive-hysteresis changes the bandwidth according to the instantaneous current variations, whereas adaptive-fuzzy-hysteresis is used to compensate the uncertainty in the hysteresis band.

Chapter-6

6. SHUNT ACTIVE POWER FILTER FOR SOLID OXIDE FUEL CELL

6.1   Introduction

This chapter presents the control and design analysis of a three-phase load/grid interactive fuel cell power system (FCPS) with active power filters. It also presents shunt active power line conditioner topology with fuel cell power system. The fuel cell based shunt active power filter (APF) is designed for current harmonic compensations and reactive power compensation in the AC power distribution system. It is used in low power (<100 kVA), medium power (100 kVA-10 MVA) and high power (>10 MVA) applications. It consists of power circuit and the control unit.

The developed fuel cell model is connected to the DC-side of the voltage source inverter for interfacing with the grid. The inverter normally injects the power generated from the fuel cell to the grid as and when required and also can act as active power filter to compensate load current harmonics and load reactive power demand if desired.

The design of fuel cell based shunt active power line conditioner comprises of power transistor, DC- link capacitor, interface inductor parameters and control unit [124]. The control unit is implemented through the reference current extraction method and the PWM-current control technique. In recent years, the digital controllers for APLC are implemented using Microprocessor/DSP/FPGA for real time operations [125], [126].

Shunt active power filter is controlled using PI controller [127] and fuzzy logic controller [128].

6.2   APLC Techniques for Fuel Cell

The fuel cell based shunt active power stage is a bi-directional current converter that consists of switching network and a filter component. Each of the switches in the switching network is IGBTs with anti-parallel diodes to allow current flow in both directions. The APLC is developed with PWM based current source inverter or voltage source inverter. The current source inverter behaves as non-sinusoidal current source to compensate the harmonic current which is generated by the non-linear load. The voltage source inverter is more convenient because it is efficient, compact, economical and faster device in comparison to current source inverter.

The output of the inverter is connected to the utility/grid through an interfacing inductor for compensating the harmonic current. The fuel cell interactive shunt APF can inject fuel cell power into distribution line to support reactive power compensation and filter harmonic currents caused by nonlinear load. It is connected in parallel with nonlinear loads to compensate the harmonic currents. The APF injects a compensating current (in opposite phase) identical with the harmonic current to compensate the harmonic current. Therefore, the net current drawn from the distribution network at the point of common coupling (PCC) will be a sinusoidal current of only fundamental frequency.

6.2.1   Shunt APLC Configurations

The active power line conditioner system can be classified as

- ➤ Single-phase system
- ➤ Three-phase system
    - ＋ Three-phase three-wire system
    - ＋ Three-phase four-wire system

6.2.1.1 Single-Phase System

Harmonics present in single-phase system is eliminated by using active power line conditioner. The widespread use of computers, printers and electronic equipment, in offices and household appliances create harmonic related problems in distributed power system and it can be solved by single-phase active power line conditioner [129]. The

single-phase fuel cell based shunt APLC is implemented using voltage source inverter. It consists of two-leg, four-switching power transistor with a DC-link capacitor. The schematic diagram is shown in Fig.6.1. The inverter is connected in parallel with loads to PCC through interface inductor. The single-phase fuel cell based shunt APLC compensates current harmonics by injecting equal and opposite harmonic compensation current. As a result, the compensated current becomes sinusoidal and it is in phase with the voltage.
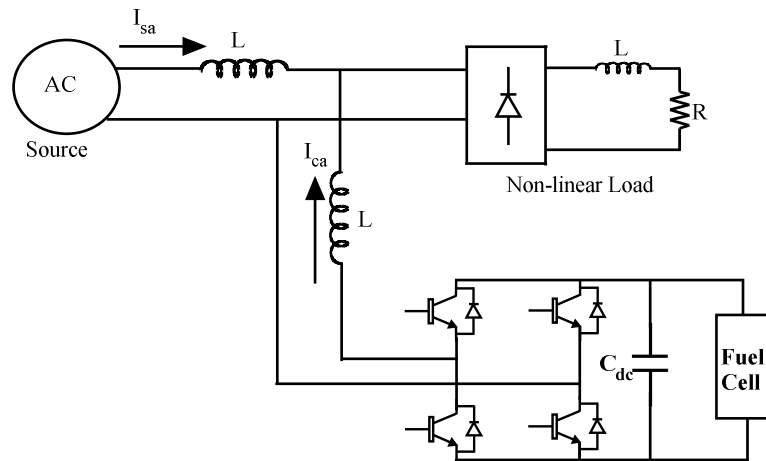
Fig.6.1 Single-phase shunt active power line conditioner system

6.2.1.2 Three-Phase Three-Wire System

Fig.6.2 shows the two-level PWM-voltage source inverter which includes three-phase, three-wire fuel cell based shunt active power line conditioner system. The PWM-VSI consists of six-power transistors with DC-link capacitor. It is connected with the PCC through interface inductor. The interface inductor suppresses the higher order harmonic components caused by the switching operation of the power transistors. Reduction of current harmonics present in the distribution line is achieved by injecting equal and opposite amount of compensating current at the PCC [129] , [70].
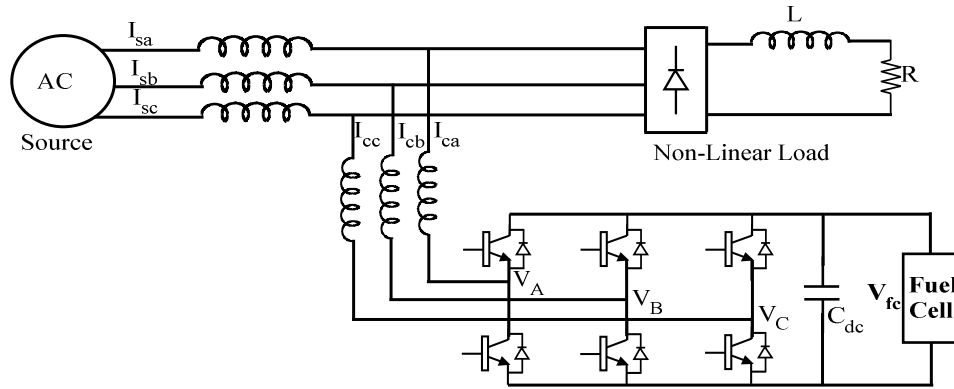
Fig.6.2 Three-phase three-wire shunt active power line conditioner system

6.2.2 Principle of Fuel Cell Based Shunt APLC System

The basic principle of active power line conditioner was proposed during 1970s. However, the actual design of active power line conditioner was proposed by Gyugyi and Strycula in 1976 [130]. The fuel cell based shunt APLC often refers to the compensation in the current harmonics and reactive-power. Fig.6.3 shows the schematic diagram of the fuel cell based shunt active power line conditioner. The shunt active power line conditioner compensates current harmonics by injecting equal-and-opposite harmonic components. This principle is applicable to any type of non-linear load that creates harmonics.

A shunt active power filter is connected in parallel with the non-linear load to detect its reactive power and harmonic current to the system for compensating current. The shunt active power filter consists of an inductance L_c and a resistance R_c per phase on the AC-side of three-phase IGBT bridge current controlled voltage source inverter (CC-VSI) with a DC-link capacitor C_{dc} [131], [132].
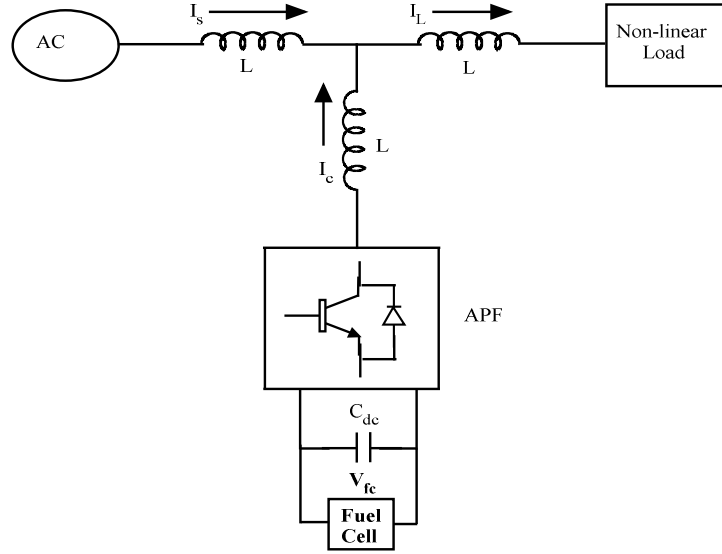
Fig.6.3 Schematic diagram of shunt APLC system

6.2.2.1 Characteristics of Harmonics

Harmonic distortion is observed in both the voltage and current waveform. Most of the current distortion is generated by electronic loads or non-linear loads. These non-linear loads might be single phase or three-phase. The electronic loads generate positive and negative sequence as well as zero sequence harmonic currents. The Fourier series represents an effective way to study and analyse the harmonic distortion [133].

$$f(t) = a_0 + \sum_{h=1}^{\infty} [a_h \cos(h\omega t) + b_h \sin(h\omega t)]$$

$$= a_0 + \sum_{h=1}^{\infty} c_h \sin(h\omega t) + \psi_h \qquad (6.1)$$

where,

$f(t)$ - periodic function of frequency f

$\omega = 2\pi f$ - angular frequency period

$T = 1/f = 2\pi/\omega$ - time period

c_h - h^{th} harmonic of amplitude

hf - harmonic frequency and ψ_h - phase

The Fourier series coefficients are given by

$$a_0 = \frac{1}{T} \int_0^T f(t)\, dt = \frac{1}{2\pi} \int_0^{2\pi} f(t)\, dx, \quad where\ x = \omega t \qquad (6.2)$$

$$a_h = \frac{2}{T} \int_0^T f(t)\cos(h\omega t)dt = \frac{1}{\pi} \int_0^{2\pi} f(t)\cos(hx)dx \qquad (6.3)$$

$$b_h = \frac{2}{T} \int_0^T f(t)\sin(h\omega t)dt = \frac{1}{\pi} \int_0^{2\pi} f(t)\sin(hx)dx \qquad (6.4)$$

$$c_h = \sqrt{a_h^2 + b_h^2} \qquad and \qquad \psi_h = \tan^{-1}\left(\frac{a_h}{b_h}\right) \qquad (6.5)$$

The distorted periodic current or voltage waveform expanded into a Fourier series is expressed as follows

$$I(t) = \sum_{h=1}^{\infty} I_h \cos(h\omega t + \varphi_h) \qquad (6.6)$$

$$V(t) = \sum_{h=1}^{\infty} V_h \cos(h\omega t + \theta_h) \qquad (6.7)$$

where,

I_h - h^{th} harmonic peak current, ϕ_h is the hth harmonic current phase

V_h - h^{th} harmonic peak voltage, θ_h is the hth harmonic voltage phase

ω - angular frequency $\omega = 2\pi f$, f is the fundamental frequency

6.2.2.2 Characteristics of Harmonic Compensation

From the grid, the instantaneous supply voltage V_s is written as

$$V_s(t) = V_{sm} \sin \omega t \qquad (6.8)$$

The instantaneous source current I_s is represented as

$$I_s(t) = I_L(t) - I_c(t) \tag{6.9}$$

The non-linear load current I_L comprises the fundamental and the harmonic current components, which is represented as [134].

$$I_L(t) = \sum_{h=1}^{\infty} I_h \sin(n\omega t + \Phi_h)$$
$$= I_1 \sin(\omega t + \Phi_1) + \left(\sum_{h=2}^{\infty} I_h \sin(n\omega t + \Phi_h) \right) \tag{6.10}$$

In equation (6.10), there are three terms

$$I_L(t) = \underbrace{I_1 \sin(\omega t)}_{active} + \underbrace{I_1 \cos(\omega t)}_{reactive} + \sum_{n=2}^{\infty} \underbrace{I_h \sin(n\omega t + \Phi_h)}_{harmonics} \tag{6.11}$$

The instantaneous load power is computed from the supply voltage and load current. The load power calculation is given as

$$P_L(t) = I_L(t) * V_s(t)$$
$$= \left[V_{sm} I_1 \sin^2 \omega t * \cos \varphi_1 \right] + \left[V_{sm} I_1 \sin \omega t * \cos \omega t * \sin \varphi_1 \right] +$$
$$\left[V_{sm} \sin \omega t * \left(\sum_{h=2}^{\infty} I_h \sin(n\omega t + \Phi_h) \right) \right] \tag{6.12}$$
$$= P_f(t) + P_r(t) + P_h(t)$$

From the above equation, the load power has fundamental or active power $P_f(t)$, reactive power $P_r(t)$ and harmonic power $P_h(t)$.

The real (fundamental) power is extracted from the total load power and it is given as

$$P_f(t) = V_{sm} I_1 \sin^2(\omega t) * \cos \varphi_1 = V_s(t) * I_s(t) \tag{6.13}$$

If the active power line conditioner provides the total reactive and harmonic power, the source current $I_s(t)$ will be in phase with the supply voltage and should be sinusoidal.

The source currents after compensation can be expressed as

$$I_s(t) = P_f(t)/V_s(t) = I_1 \cos\varphi_1 \sin(\omega t) = I_{sm} \sin(\omega t) \tag{6.14}$$

where, $I_{sm} = I_1 \cos\varphi_1 \sin(\omega t)$ - peak value of the source current

There are also some switching losses in the voltage source inverter, and hence the utility must supply small overhead for the capacitor leakage and inverter switching losses in addition to the real power of the load. The total peak current supplied by the source is

$$I_{sp} = I_{sm} + I_{sl} \tag{6.15}$$

where,

$I_{sp} = I_1 \cos\varphi_1 + I_{sl}$ peak value of the extracted reference current,

I_{sl} - switching loss current.

If the active power line conditioner provides the total reactive and harmonic power; then $I_s(t)$ will be in phase with supply voltage and close to sinusoidal waveform. In this case, the active power line conditioner must provide the following compensation current

$$I_c(t) = I_L(t) - I_s(t) \tag{6.16}$$

Hence, for accurate and instantaneous compensation of reactive and harmonic currents, it is necessary to estimate the fundamental component of the load current.

6.3   Synchronous Reference Frame Theory

The conventional and modified-synchronous reference frame (SRF) based shunt active power line conditioner system is modelled and evaluated through MATLAB/ Simpower tools. The model consists of three-phase voltage source inverter and connected through the interface inductor in parallel with rectifier load as shown in Fig.6.4.
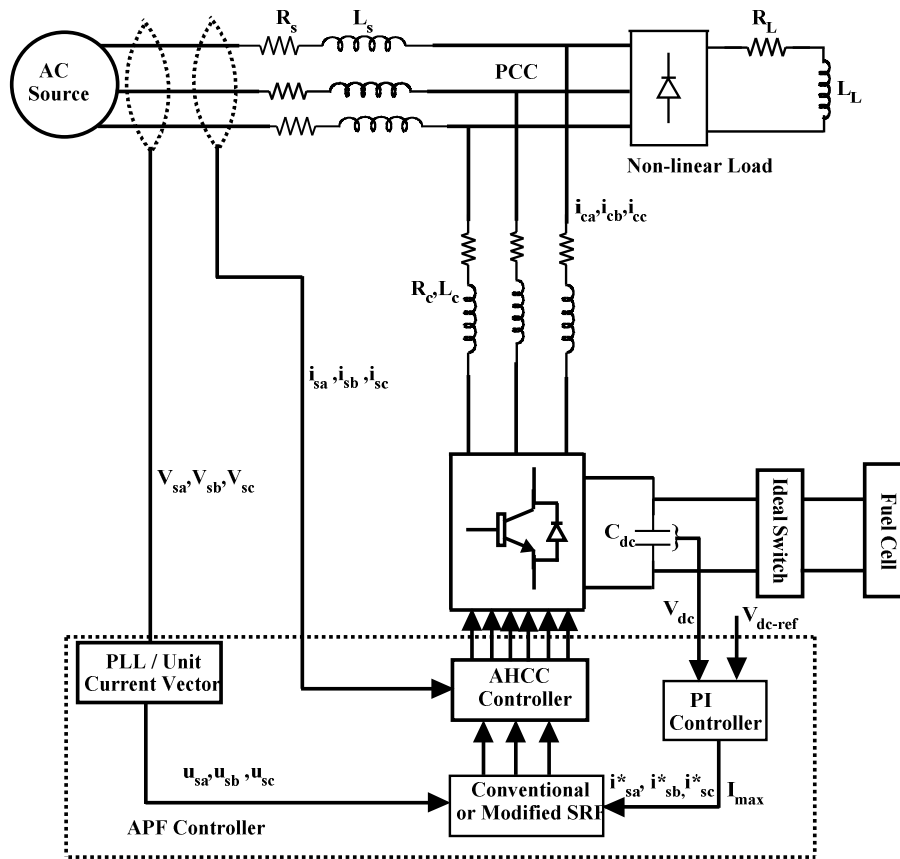
Fig.6.4 Complete schematic diagram of shunt active power filter for fuel cell

The APLC controller uses the conventional/modified-SRF with PWM-VSI current control techniques. The conventional or modified-SRF is used to extract the required reference currents from the distorted load currents. The reference currents are compared with actual currents to generate the switching pulses using PWM-VSI current controller (Adaptive-HCC techniques) to drive the active power line conditioner. The APLC provides the essential compensating current to compensate current harmonics and reactive-power in the connected system.

The time domain based synchronous reference frame theory is utilized to extract the reference current from the distorted line current. The SRF control strategy operates in steady-state as well as in dynamic-state to control the active power line conditioner in real-time application. Another important characteristic of SRF theory is the simplicity of the calculations, which involves only algebraic calculation [135]. There are two-types of SRF control methods derived; (i) conventional-SRF and (ii) modified-SRF.

6.3.1 Conventional-SRF

The basic structure of SRF method consists of PLL-circuit for vector orientation and PI-controller for DC-link capacitor voltage regulator. Fig.6.5 shows the block diagram of the conventional-SRF method. The three-phase load currents i_{la}, i_{lb}, i_{lc} in stationary coordinates are converted into the two-phase direct axis (d) and quadratic axis (q) rotating coordinates currents $i_d - i_q$ as

$$\begin{bmatrix} i_d \\ i_q \end{bmatrix} = \frac{2}{3} \begin{bmatrix} \sin\theta & \sin\left(\theta - \frac{2\pi}{3}\right) & \sin\left(\theta + \frac{2\pi}{3}\right) \\ \cos\theta & \cos\left(\theta - \frac{2\pi}{3}\right) & \cos\left(\theta + \frac{2\pi}{3}\right) \end{bmatrix} \begin{bmatrix} i_{la} \\ i_{lb} \\ i_{lc} \end{bmatrix} \tag{6.17}$$

The reference frame is rotating synchronously with fundamental currents. Therefore, time variant currents with fundamental frequencies are constant after transformation. Thus, currents are separating simultaneously (to DC and AC components). The d-axis current components are used for harmonic eliminations and q axis current components are used for reactive-power compensations. The $d - q$ transformation output signals depend on the load current and the performance of the phase locked loop [136].
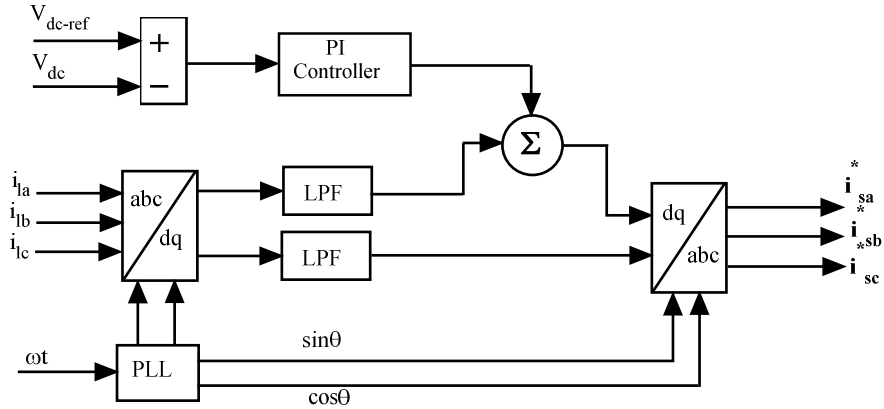
Fig.6.5 Block diagram of the conventional-SRF method

The PLL-circuit is providing the vectorized fundamental frequency ($\sin\theta$ and $\cos\theta$) for synchronization. The $i_d - i_q$ currents are passed through a low pass filter to filter the higher order harmonic components and permit fundamental frequency components. The PI-controller is used to eliminate the steady state error of the DC-component and maintains the DC-capacitance voltage of the inverter. The proportional and integral gains

123

determine the dynamic response and settling time of the DC-bus capacitor voltage respectively [137]. The desired reference current ($a-b-c$ stationary frame) is calculated from $i_d - i_q$ rotating frame using inverse transformation,

$$\begin{bmatrix} i_{sa}^* \\ i_{sb}^* \\ i_{sc}^* \end{bmatrix} = \begin{bmatrix} \sin\theta & \cos\theta \\ \sin\left(\theta - \frac{2\pi}{3}\right) & \cos\left(\theta - \frac{2\pi}{3}\right) \\ \sin\left(\theta + \frac{2\pi}{3}\right) & \cos\left(\theta + \frac{2\pi}{3}\right) \end{bmatrix} \begin{bmatrix} i_d \\ i_q \end{bmatrix} \tag{6.18}$$

The extracted reference current is compared with actual currents and hence generates the required switching pulses for the inverter using PWM-VSI current controller. However, the conventional-SRF control strategy requires a PLL-circuit based on the supply voltage. But the design of a high performance PLL-circuit is difficult, when various non-idealities like multiple zero crossing are occurring in the supply voltage. A simple and efficient method is used to calculate the unit vector, which is incorporated with the modified- SRF method.

6.3.2 Modified-SRF

The block diagram of modified-SRF structure is shown in Fig.6.6. The modified-SRF method consist of simplified unit vector generation for vector orientation, DC-link capacitor voltage regulator and stationary-rotating synchronous frames to extract the reference current.
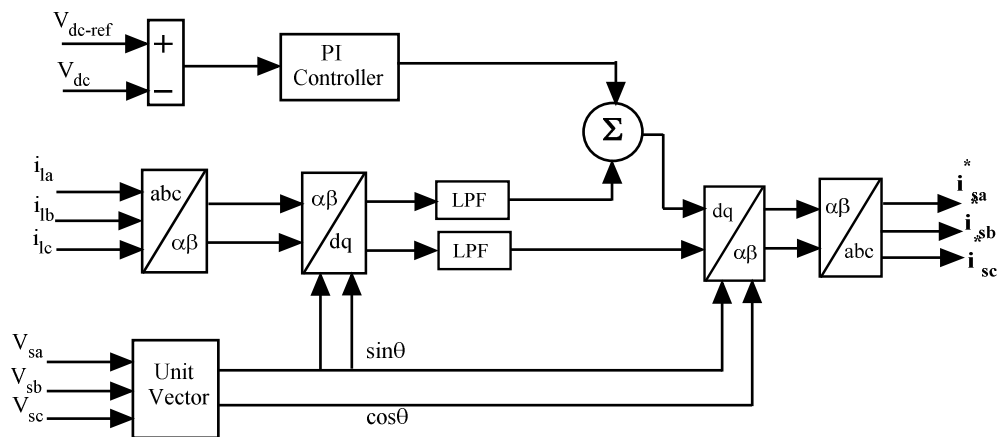

Fig.6.6 Block diagram of the modified - SRF method

6.3.2.1 Unit Vector Generation

To generate the unit sine vector templates, the instantaneous supply voltages are sensed and given as

$$V_{sa} = V_{sm} \sin(\omega t)$$
$$V_{sb} = V_{sm} \sin\left(\omega t - 120°\right) \qquad (6.19)$$
$$V_{sc} = V_{sm} \sin\left(\omega t + 120°\right)$$

where,

V_{sm} - peak value of the source voltage,

$\omega = 2\pi f$ - fundamental angular frequency.

The simple and efficient unit vector generator is used for vector orientation. Fig.6.7 shows the block diagram of a unit vector generation method. To generate the synchronization vector the instantaneous supply voltages are sensed and computed. The instantaneous three-phase source voltages are transformed into the two-phase stationary $\alpha - \beta$ voltages using Clarke transformation given in equation (6.20).

$$\begin{bmatrix} v_\alpha \\ v_\beta \end{bmatrix} = \sqrt{\frac{2}{3}} \begin{bmatrix} 1 & \dfrac{-1}{2} & \dfrac{-1}{2} \\ 0 & \dfrac{\sqrt{3}}{2} & \dfrac{-\sqrt{3}}{2} \end{bmatrix} \begin{bmatrix} v_{sa} \\ v_{sb} \\ v_{sc} \end{bmatrix} \qquad (6.20)$$

Similarly, the instantaneous space vector current(s) is transformed into the $\alpha - \beta$ coordinate current(s) by Clarke transformation that is given as

$$\begin{bmatrix} i_\alpha \\ i_\beta \end{bmatrix} = \sqrt{\frac{2}{3}} \begin{bmatrix} 1 & \dfrac{-1}{2} & \dfrac{-1}{2} \\ 0 & \dfrac{\sqrt{3}}{2} & \dfrac{-\sqrt{3}}{2} \end{bmatrix} \begin{bmatrix} i_{sa} \\ i_{sb} \\ i_{sc} \end{bmatrix} \qquad (6.21)$$

The orthogonal coordinates of voltage v_α and current i_α on α-axis, and v_β *and* i_β on β-axis respectively.

Transforming equation (6.19) to $\alpha - \beta$ plane using equation (6.20) and simplifying,

$$v_{s\alpha} = \frac{3}{2} v_m \sin(\omega t)$$

$$v_{s\beta} = -\frac{3}{2} v_m \cos(\omega t)$$

(6.22)

The $\alpha - \beta$ voltages are filtered using first order digital low pass filter whose frequency is ω (at fundamental frequency). After filtering, the percentage of hth order harmonics of the sensed supply voltage are reduced by a factor of $\sqrt{2/(h^2+1)}$. It cancels the higher order harmonics, notches and high frequency noise. The estimated magnitude of the space vector generated is as follows [138].

$$\vec{V} = \overrightarrow{V_{\alpha\beta}} = v_{s\alpha} + j v_{s\beta} = \sqrt{(v_{s\alpha}{}^2 + v_{s\beta}{}^2)}$$

(6.23)

From the derivation in equation (6.23), it is evident that the unit vectors can be generated by transforming the supply voltage to $\alpha - \beta$ plane and dividing the $\alpha - \beta$ components by the magnitude of the space vector. Hence, the unit vector generation is defined as

$$\cos\theta = \frac{v_\alpha}{\sqrt{(v_{s\alpha}{}^2 + v_{s\beta}{}^2)}} = \frac{(3/2) v_m \sin(\omega t)}{(3/2) v_m} = \sin(\omega t)$$

$$\sin\theta = \frac{v_\beta}{\sqrt{(v_{s\alpha}{}^2 + v_{s\beta}{}^2)}} = \frac{-(3/2) v_m \cos(\omega t)}{(3/2) v_m} = -\cos(\omega t)$$

(6.24)

This unit vector generation method results in elimination of supply harmonics, high frequency noise and notches in the distribution of supply voltages.
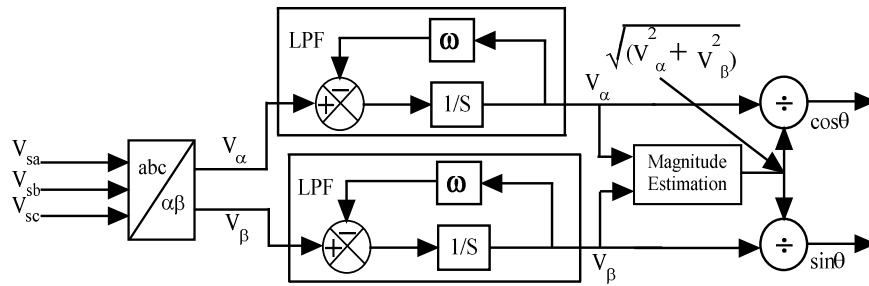
Fig.6.7 Block diagram of the unit vector generation

6.3.3   Case-1 Conventional-SRF

Given figures in below shows the adaptive hysteresis current controller (AHCC) techniques under diode-rectifier load with the steady-state condition. The DC-link capacitor voltage is shown in Fig.6.8. Fig.6.9 shows the source current before compensation. It indicates the source current contains fundamental and harmonic current components. To compensate harmonic current components, the APLC supplies the compensating current as shown in Fig.6.10. Consequently, the harmonic current compensation is achieved by injecting equal but opposite harmonic components. Fig.6.11 shows the source current after compensation. It indicates the source current after the compensation becomes sinusoidal.
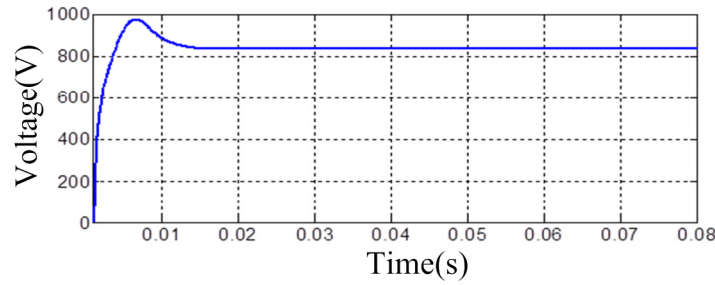
Fig.6.8 DC-link capacitor voltage
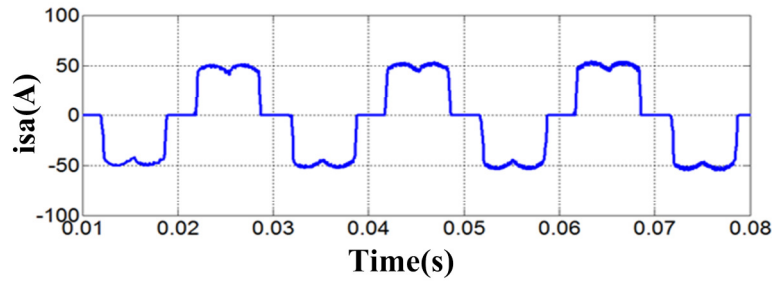
Fig.6.9 Source current before compensation
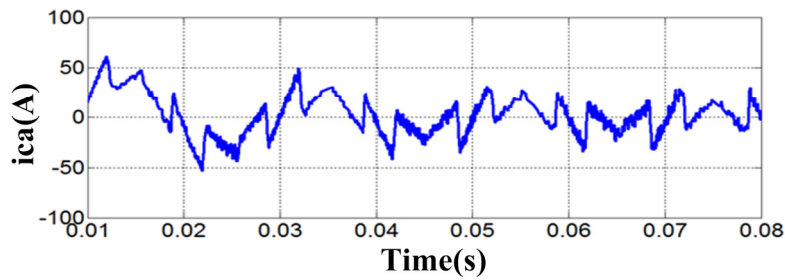
Fig.6.10 Compensation current
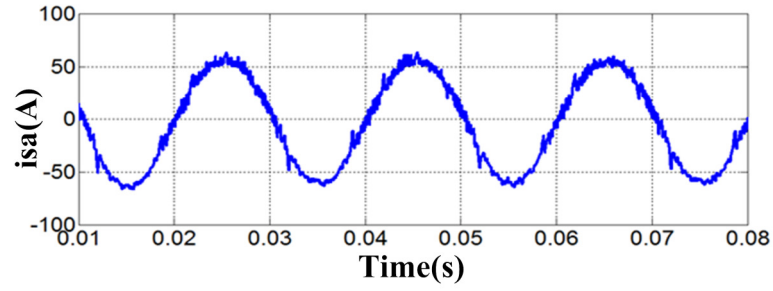
Fig.6.11 Source current after compensation

6.3.4   Case-2 Modified-SRF

Mentioned figures in below are obtained using modified-SRF with adaptive-HCC (AHCC) based shunt APLC system under steady-state. Fig.6.12 shows the instantaneous supply voltages and indicates the three-phase voltages are balanced. Fig.6.13 shows the source currents before compensation that contains fundamental and harmonic components due to thyristor-rectifier load.
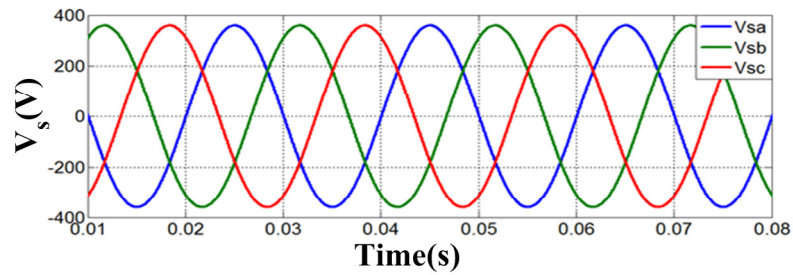
Fig.6.12 Supply voltages
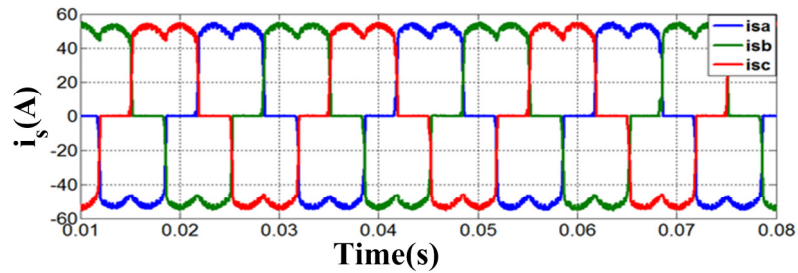
Fig.6.13 Source current before compensation
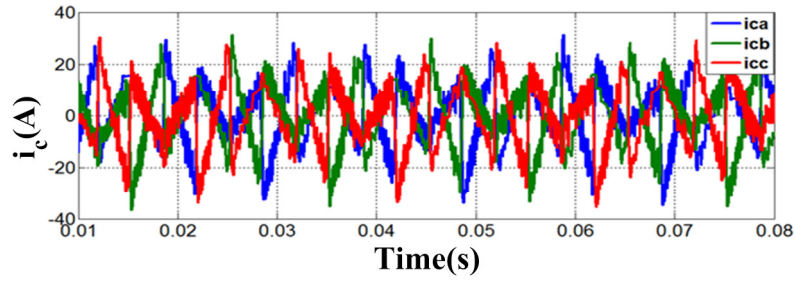
Fig.6.14 Compensation current
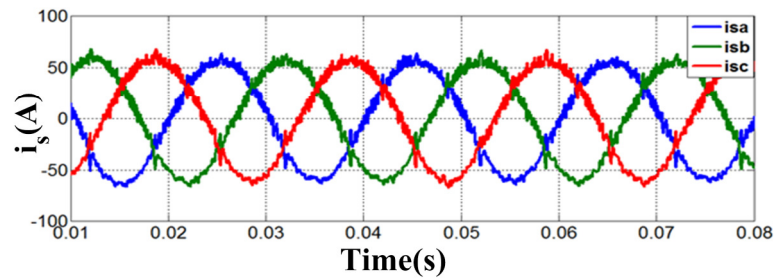
Fig.6.15 Source current after compensation

The APLC provides the necessary compensating currents as shown in Fig.6.14; it compensates harmonic current components by injecting equal and opposite harmonic components. The APLC operates as current source injecting the harmonic current components generated by the load but phase shifted by 180^0. As a result, components of harmonic currents in the load currents are cancelled by the effect of the APLC. Fig.6.15 shows the source currents after compensation and indicates the source currents after compensation are sinusoidal and in-phase with the supply voltages.

(a)

(b)

(c)

(d)
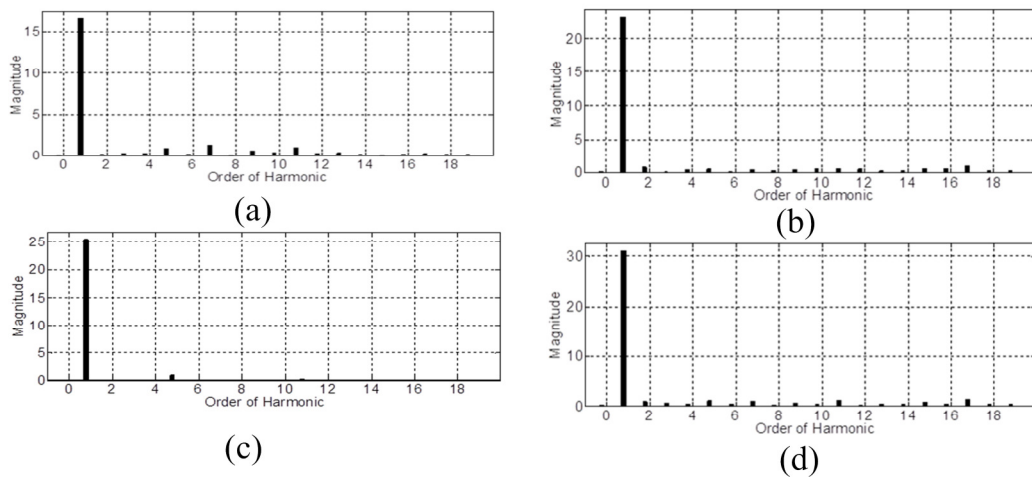
Fig. 6.16 Comparative study of THD of different techniques

(a) SRF without APLC, (b) SRF with APLC, (c) Modified SRF without APLC, (d) Modified SRF with APLC

Fig. 6.16 shows the comparative analysis of THD of different techniques. Without APLC the THD of line currents (with diode load) is 26.66%. When SRF with AHCC based APLC technique is used to compensate the harmonics the THD is reduced to 3.92% and when Modified SRF with AHCC based APLC technique is used, the THD of line current is measured as 3.74% which is better in accordance with the IEEE-519 standards. The detailed comparative analysis of active power, reactive power, THD is summarized in Table 6.1.

Table 6.1 Comparative study between SRF and Modified SRF with AHCC (Diode load)

AHCC		
Controller	**Without APLC**	**With APLC**
SRF	P = 8.99 kW Q = 239 VAR THD = 26.66%	P = 9.22 kW
		Q = 104 VAR
		THD = 3.92%
Modified SRF		P = 9.32 kW
		Q = 102 VAR
		THD = 3.74%

The simulated results indicate that the conventional and modified SRF with AHCC technique based APLC supresses the reactive power and improves the power quality. From the above discussion it is observed that modified SRF with AHCC technique based APLC is superior than SRF with AHCC technique based APLC in terms of THD, active and reactive power.

6.4   Summary

This chapter presents the modelling and control of fuel cell with shunt active power filter. It presents the analysis of grid connection of fuel cell in conjunction with shunt active power filter under condition of varying load demand. The entire model of fuel cell with shunt active power filter is developed in MATLAB/SIMULINK. The simulation results shows that the voltage source inverter injects active power at the point of common coupling (PCC) and compensates load reactive power. It maintains a sinusoidal current from/to grid. A common inverter is utilised to inject power generated to the grid and improve the power quality at point of common coupling. The simulation results give the better performance of SAPF for change in non-linear loads by using shunt active power filter. Any standard method available in the literature can be utilized for extracting fundamental component; however we have restricted our discussion to SRF and modified SRF methods only. The simulated results indicate conventional and modified SRF with AHCC technique based APLC supresses the reactive power and improves the power quality.

Chapter-7

7. EXPERIMENTAL RESULTS AND ANALYSIS

7.1 Introduction

This chapter confers about the hardware set-up and experimental verification of single phase fuel cell power system (FCPS). The objective of the hardware set-up is to demonstrate the working of load connected single phase fuel cell power system. The performance of the load connected FCPS depends on (i) reference current generation technique and ii) PWM-VSI current controller. Different PWM current control methods are available to generate the switching pulses to the inverter. Out of different PWM current control methods, Hysteresis current controller (HCC) is used for experimental validation of FCPS performance.

7.2 Description of Hardware Modules

The block diagram of the FCPS (Fuel Cell Power System) experimental set up is shown in Fig.7.1. The single phase power quantities (voltages and currents) are converted to low voltage signals using Hall Effect voltage and current transducers. Hall Effect sensor voltage and current output used by control algorithm, which generates the VSI (voltage source inverter) switching pulses. These pulses are passed through blanking circuit to include a dead time in order to prevent the short circuit of the DC-link capacitor through switches in the same VSI leg. The blanking circuit output pulses are given to the VSI

through opto-isolator circuit to isolate the high power network and the signal conditional circuits. The major components of the experimental set-up are given as follows:

➢ Fuel Cell Emulator

➢ Voltage Source Inverter

➢ Transducer Circuit (Voltage and current transducer)

➢ Synchronisation Circuit

➢ Peak Detector Circuit

➢ HCC Technique for VSI in Fuel Cell Power System

➢ Blanking Circuit

➢ Opto-isolation Circuit

➢ Power Supply Modules

The design details and entire hardware development of above mentioned circuits are represented in the following subsections.
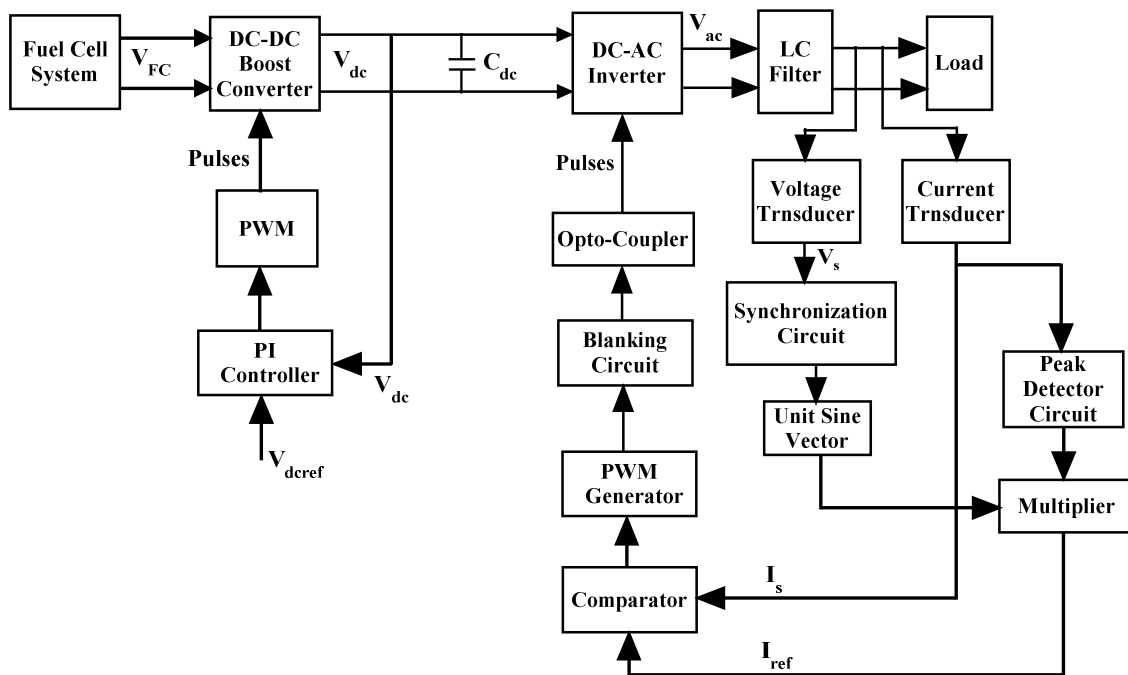
Fig.7.1 Block diagram representation of experimental set-up for fuel cell power system
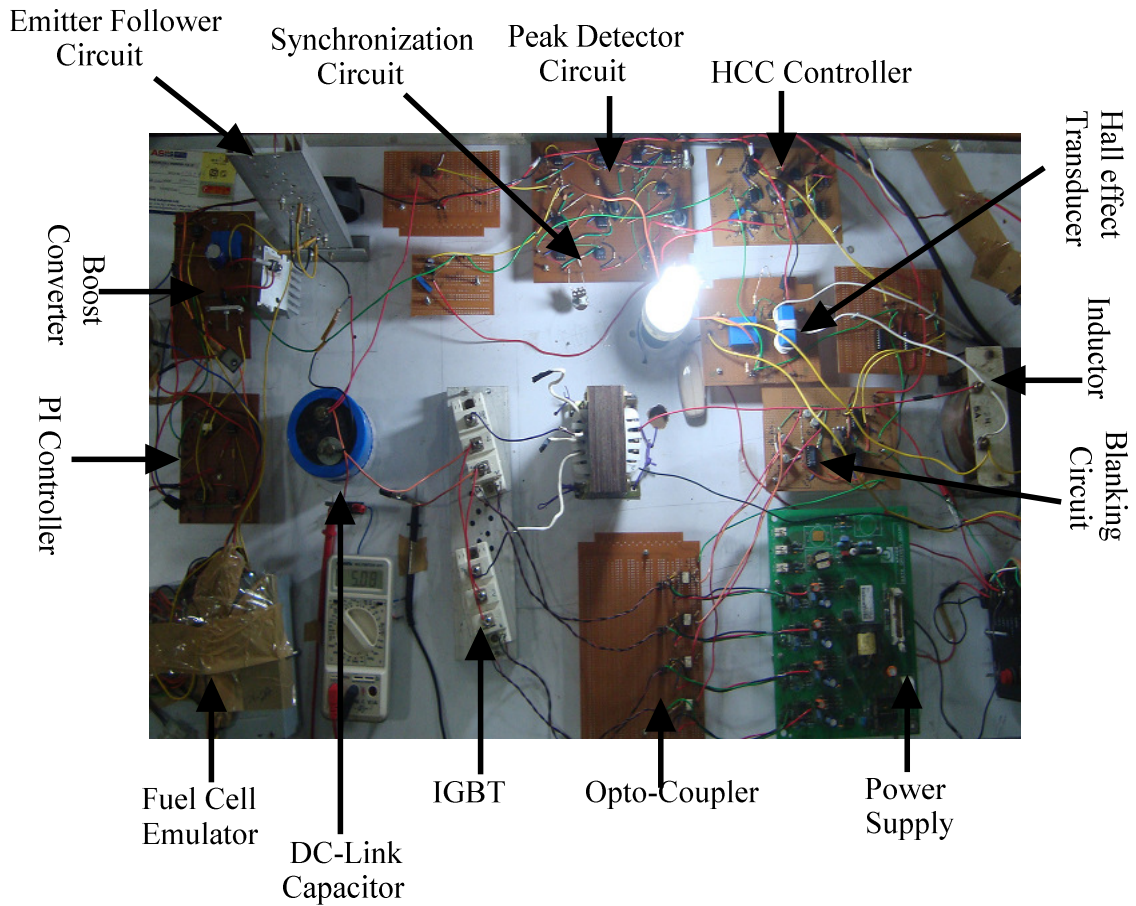
Fig.7.2 Photograph of complete hardware setup for fuel cell power system

7.2.1   Fuel Cell Emulator
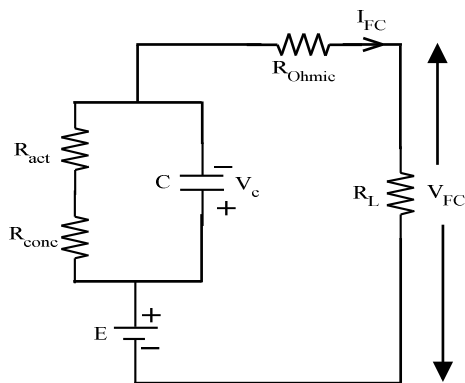
Fig.7.3 Fuel cell emulator equivalent circuit

The fuel cell emulator is used in place of actual fuel cell. The circuit diagram of fuel cell emulator is shown in Fig.7.3. The emulator replicates the solid oxide fuel cell and open circuit voltage (E) is generated using variable DC power supply. The fuel cell emulator also represents losses of actual fuel cell like ohmic, concentration over potential and

134

activation over potential. The value of emulator parameters like activation resistance (R_{act}) and concentration resistance (R_{conc}) is taken as 33 Ω each. The capacitor (C) is designed by using the two electrolyte capacitor (4700 µF) connected in parallel. The resistance (R_{Ohmic}) is assumed to be equal to the internal resistance of the multiple DC power supply.

The output of fuel cell voltage V_{FC} is given by:

$$V_{FC} = N_{cell}\, E_{cell} = E - V_{act} - V_{conc} - V_{ohmic}$$

(7.1)

where, V_{FC} is the fuel cell output voltage; E is the open circuit voltage, V_{act}, V_{conc}, and V_{ohmic} are the activation, concentration and ohmic over potential of the fuel cell respectively. The detailed descriptions of all the voltage losses are given in Chapter-2.

Relationship between the voltage and current in the fuel cell can be modelled [139], [140] as

$$V_{FC} = E - AT \ln\left(\frac{I_{FC}}{I_o}\right) - BT \ln\left(\frac{I_L - I_{FC}}{I_L}\right) - I_{FC} R_{ohmic}$$

(7.2)

Where, I_{FC} is the fuel cell output current, I_0 is the exchange current, I_L is the limiting current, R_{ohmic} is the ohmic resistance of the fuel cell and A,B are activation and concentration co-efficient respectively. Furthermore E, A, and B are dependent on the operating temperature of the fuel cell whereas the ohmic resistance (R_{ohmic}) of the fuel cell depends on its own characteristics. The photograph of the fuel cell emulator is shown in Fig.7.4.
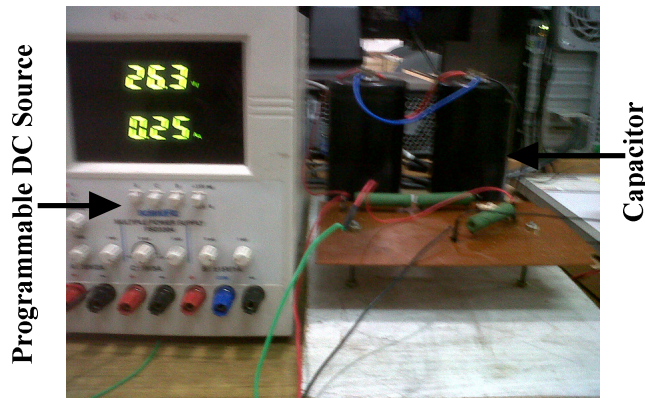
Fig.7.4 Photograph of fuel cell emulator

135

7.2.2   Voltage Source Inverter

The voltage source inverter generates required voltage and current as dictated by the load with the help of control circuit. A typical VSI consists of suitably connected power electronic switches (IGBT, MOSFET, GTO-based thyristor etc.) with anti-parallel diodes and DC voltage sources. The VSI is chosen based on the application. The design of interface inductance (L_f), DC-link capacitors (C_{dc}) is important issue and described in [141]. Fig.7.5 shows the circuit diagram of VSI with single phase bridge configuration.
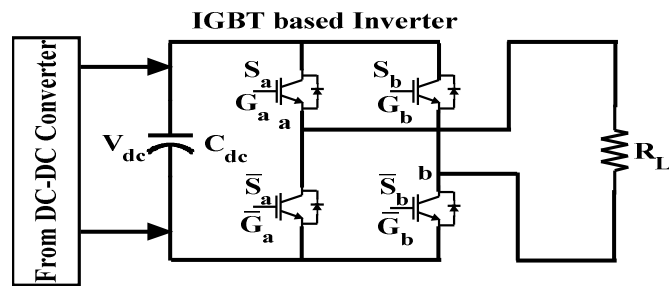
Fig.7.5 Single phase power circuit of the voltage source inverter

7.2.3   Transducer Circuit

The power quantities are sensed and transformed to low voltage signals using the Hall Effect voltage and current transducers. The Hall Effect transducer also provides isolation between the power network and signal conditioning circuits. The Hall Effect voltage sensor LEM LV 25-P and current sensor LEM LA 55-P are used in this work to convert the power level voltage (154 V) and current quantities to low-level analog signals in the ±2 V peak to peak range.

7.2.3.1   Design of Voltage Transducer Circuit

The circuit diagram of the Hall Effect voltage transducer is shown in Fig.7.6.
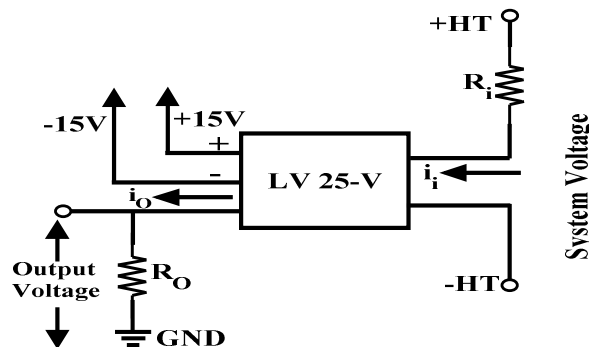
Fig.7.6 Schematic of the Hall Effect voltage transducer circuit

136

In this present experimental set-up, the power voltage is scaled down from the ±154 V range to the ±2 V range. The input resistance R_i is selected such that the output resistance falls in the range of 100-350 Ω as specified by the data sheet of the transducer [142]. For V_i = 154 V and R_i = 43 kΩ, the input current I_i is calculated as:

$$I_i = \frac{V_i}{R_i} = \frac{154}{43} = 3.58 \ mA$$

(7.3)

The conversion ratio (CR_v) for this Hall Effect transducer is 2500:1000. So, the output current is I_0 is found as

$$I_o = I_i(CR_v) = 3.58 \times 2.5 = 8.95 \ mA$$

(7.4)

The output measuring resistance is calculated so as to obtain 2 V at the output corresponding to an input of 154 V. Then, we get

$$R_{vo} = \frac{V_o}{I_o} = \frac{2}{8.95 \times 10^{-3}} = 223 \ \Omega$$

(7.5)

Voltage Transducer   Current Transducer
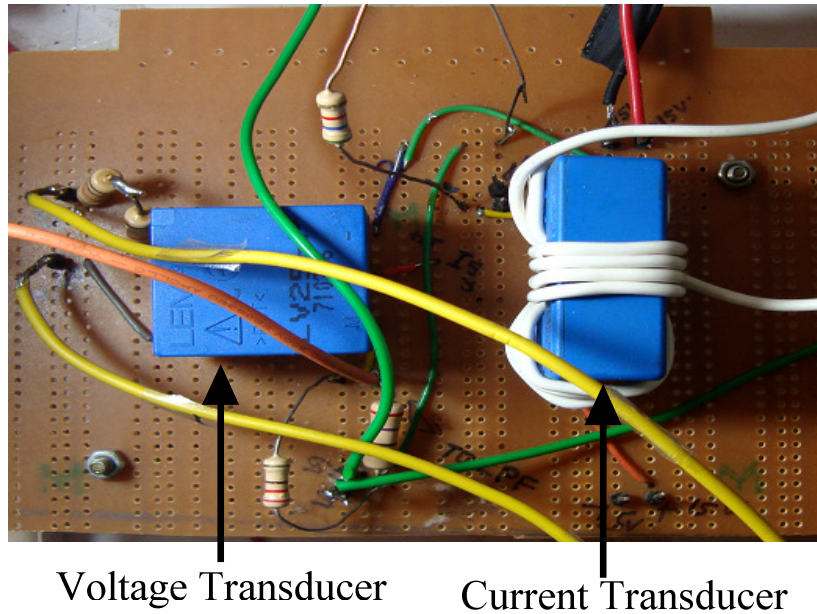
Fig.7.7 Photograph of voltage sensor and current sensor

7.2.3.2 Design of Current Transducer Circuit

The circuit diagram for the Hall Effect current transducer is shown in Fig.7.8. Here a current of ±10 A in the power network is converted to voltage signal of ±2 V. The number of primary turns (N_P) on current transducer (as shown in Fig.7.8) is chosen such

that the output resistance falls in the range of 15-160 Ω as specified by the data sheet of the current transducer [143]. The conversion ratio (CR_i) for this Hall Effect transducer is 1:1000. For $N_P = 9$ and the primary current $I_i = 10$ A, the output current is obtained as follows:

$$I_o = \frac{N_p I_i}{CR_i}$$ (7.6)

$$I_o = \frac{9 \times 10}{1000} = 0.09 \ A$$ (7.7)

The output resistance is adjusted to obtain 2 V at output, corresponding to an input of 10 A. So, we get

$$R_{vo} = \frac{V_o}{I_o} = \frac{2}{0.09} = 22\Omega$$ (7.8)
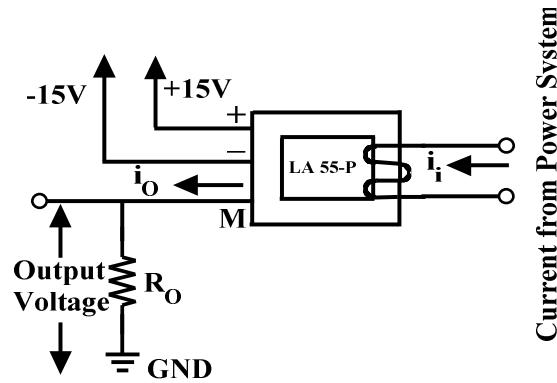
Fig.7.8 Schematic of the Hall Effect current transducer circuit

7.3   Synchronizing Circuit

The peak detector circuit will get current and voltage values from Hall Effect transducers. As, grid consists of many disturbances like harmonics, voltage fluctuations. To eliminate such disturbances we used synchronisation circuit that can extract the fundamental signal from the grid. This is achieved by OP-AMP (TL081)-based circuit [144] shown in Fig.7.12. It is the combination of a low-pass filter and a phase detector. A second order low-pass Butter-worth filter is designed for a cut-off frequency of 50 Hz. The phase shift introduced by the low-pass filter is corrected using the phase corrector by adjusting the control resistance R_c. The signal is passed through the unit sine vector circuit to generate the pulse having amplitude is 1 V shown in Fig.7.9. The output of unit

sine vector is multiplied with peak detector circuit output to give the reference current shown in Fig.7.10. The comparison between reference current and source current is shown in Fig.7.11.
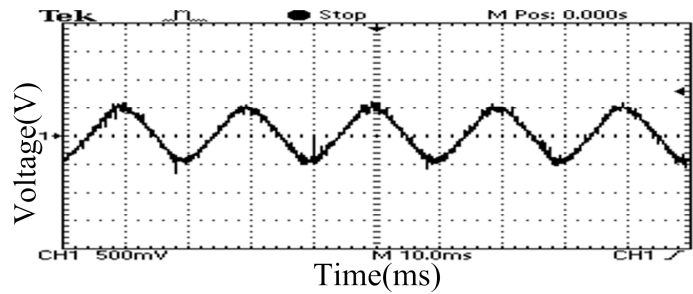
Fig.7.9 Unit sine vector
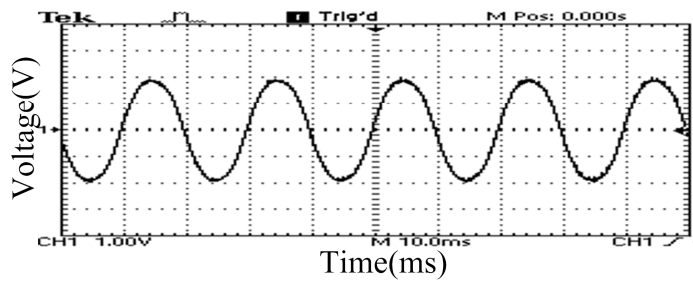
Fig.7.10 Reference current
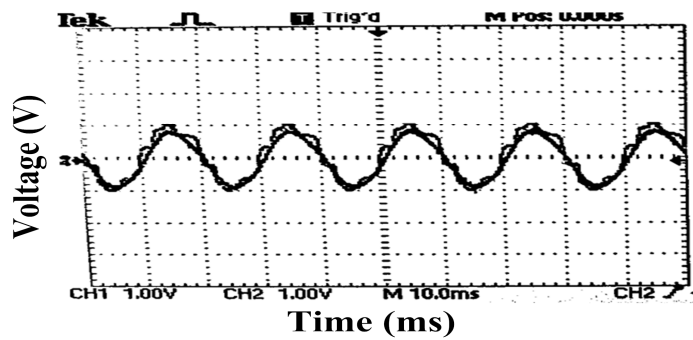
Fig.7.11 Comparison between reference and source current
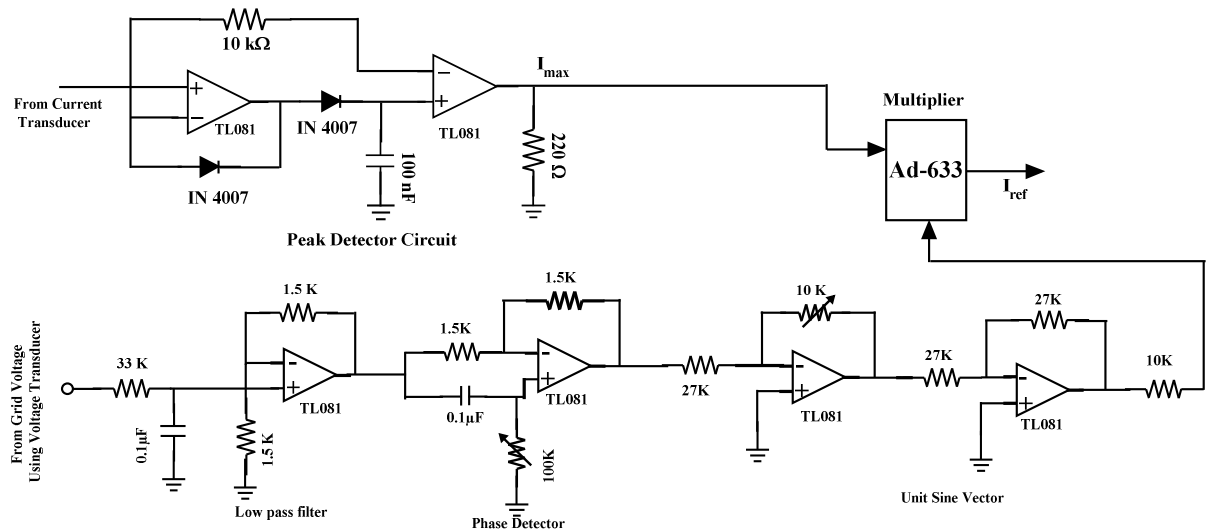
Fig.7.12 Diagram of synchronization circuit

7.4 Peak Detector Circuit

The peak current detector circuit is shown in Fig.7.13. The peak current is obtained through current transducer by using peak detector circuit. The output of the peak detector circuit is used to derive the reference for the source current. The reference current waveform for the source is obtained through multiplication of peak detector output (K) with sin(ωt). The source voltage is first stepped down using a Hall Effect transducer and is than scaled down to obtained sin(ωt) signal using scale changer. Therefore we get a signal sin(ωt). This signal is multiplied using AD-633 with peak detector output. So that reference is generated.
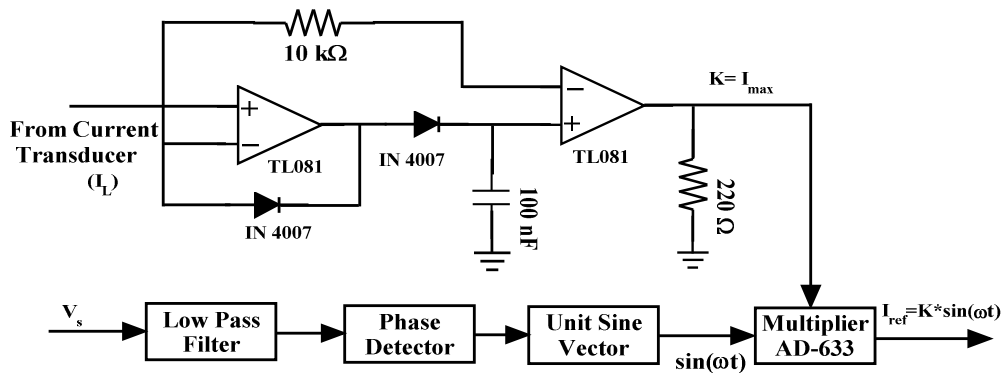
Fig.7.13 Peak detector circuit

140

7.5   HCC Technique for VSI in Fuel Cell Power System

The HCC technique is used to generate the control signal. The circuit is shown in Fig.7.15. The purpose of this circuit is to modulate the current in PWM-VSI. The task of the controller is computing the current error and to generate switching signals for the inverter so as to regulate the error within the hysteresis band. The blanking circuit uses this signal to generate switching signals for all four switches. It is ensured that the outgoing switches are turned off first. The incoming switches are then turned on. Therefore, a change from 0 to 1 in the 7400 output is delayed by 3 µs where as a change from 1 to 0 in the 74F74 output is passed immediately. This is achieved via monostable multivibrator SN74123 and AND gate 7408. It is to be noted that this 3 µs delay is sufficient to ensure that IGBTs are turned off. This is a mandatory requirement in PWM-VSI. Otherwise two switches in the same leg will be turned on resulting shorting of the DC voltage.
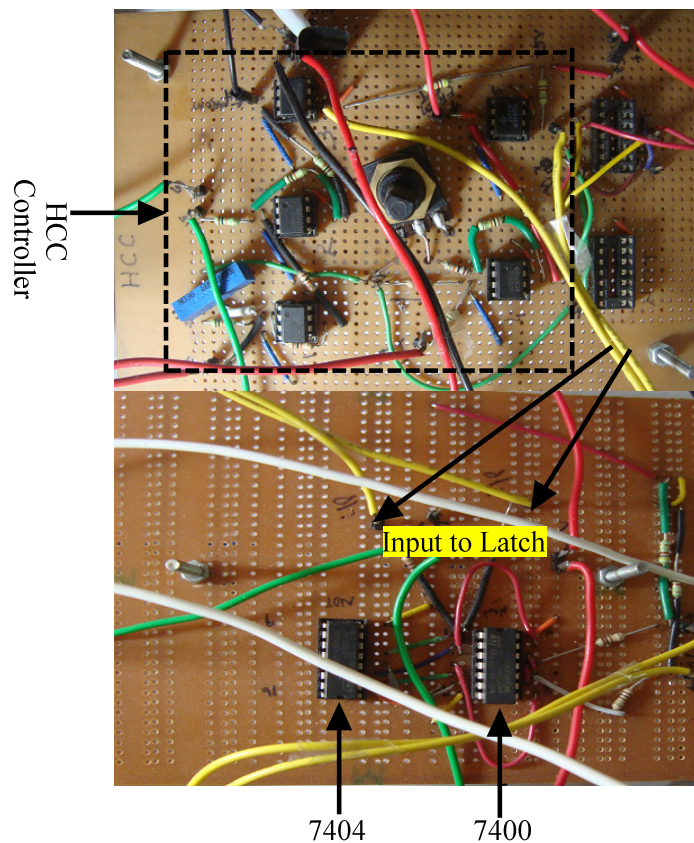
Fig.7.14 Photograph of Hysteresis Current Controller (HCC) circuit
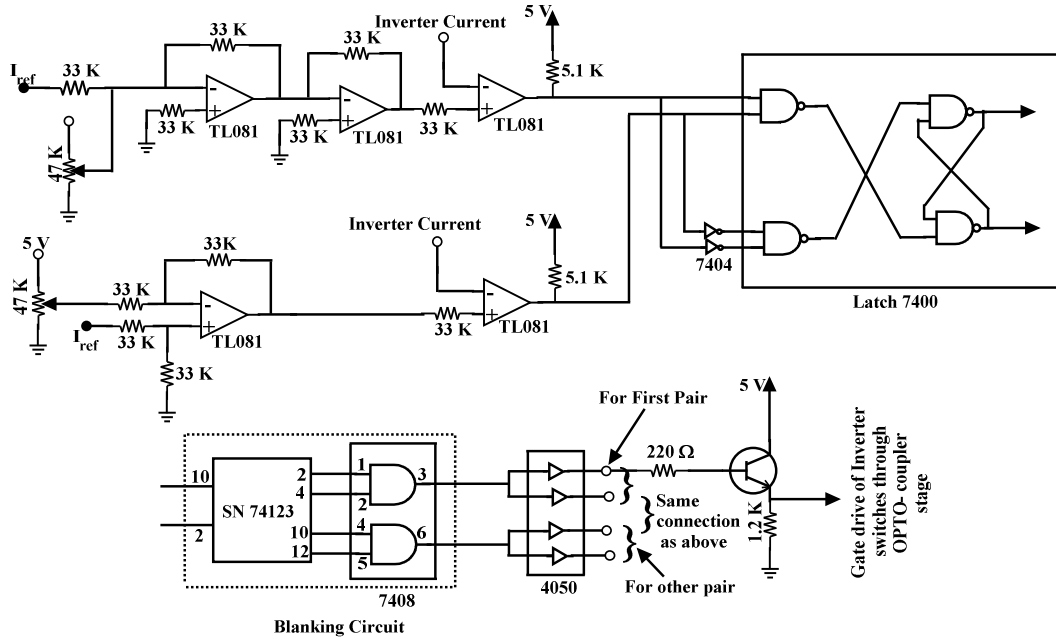
Fig.7.15 Hysteresis Current Controller (HCC) circuit

The reference current that is to be tracked is obtained from the controller circuit. Op-Amp based adder and subtraction circuit generate upper and lower hysteresis band. A Hall-Effect current sensor is used for the measurement of actual source current. This signal is then compared with the reference source already generated. Based on the error signal a particular switch pair is fired and the other pair is turned OFF. It may be noted that when there is no need for changing the status of the switches the RS latch holds the old status. The photograph of hysteresis current controller is shown in Fig.7.14.

7.6   Blanking Circuit

The hysteresis current controller generates the switching pulses for the VSI. These pulses are not directly given to the IGBT switches in order to prevent the short circuit of the DC-link capacitor during the turning ON and OFF of both the switches in the same leg. So, a dead time is provided between the turning ON and OFF of the switches in the same leg. The blanking circuit is shown in Fig.7.16 used for this purpose. Its inputs are the switching pulses S_a and $\bar{S}_a$ generated from the hysteresis current controller (HCC) circuit. The integrated circuit 74SN123 has two identical units of mono-stable multivibrator and the detailed circuit diagram for single identical channel of the blanking circuit is shown in Fig.7.18. This unit generates a shot pulse $S_a\overline{shot}$ with duration of t_d. The gate signal G_a is generated by ANDing $S_{a\,\overline{shot}}$ and $\bar{S}_{a\,\overline{shot}}$ using IC7408 and passing

142

this signal through a buffer (CD4050) and a transistor (CL100). Similarly, the complementary gate signal $\bar{G}_a$ can be obtained. The blanking output of first and second channel and third and fourth channel is shown in Fig.7.17. It presents the inclusion of the dead band in the gate signal G_a and $\bar{G}_a$.
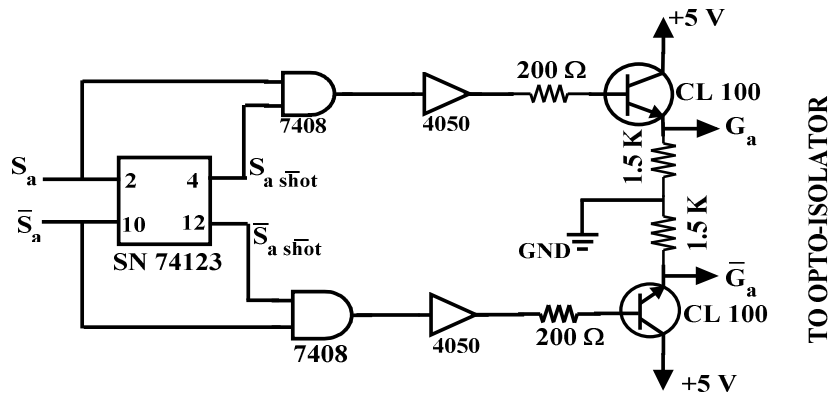
Fig.7.16 Schematic diagram of blanking circuit
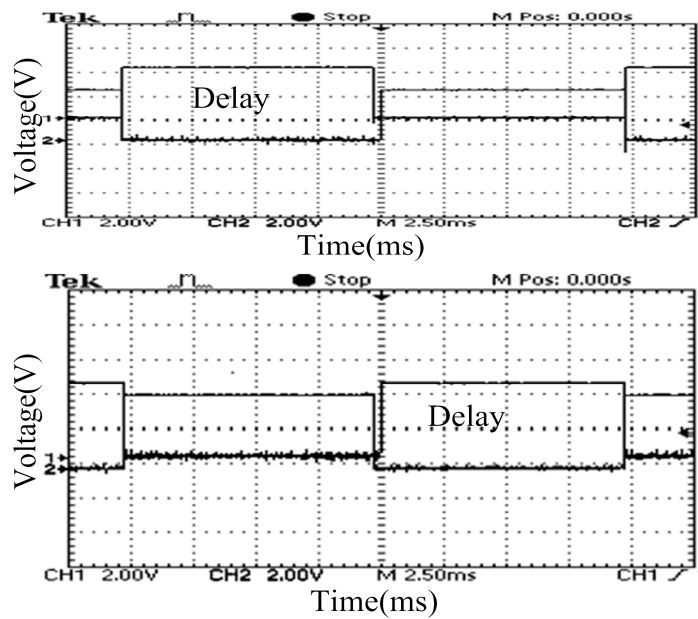
Fig.7.17 Delay waveform of blanking circuit
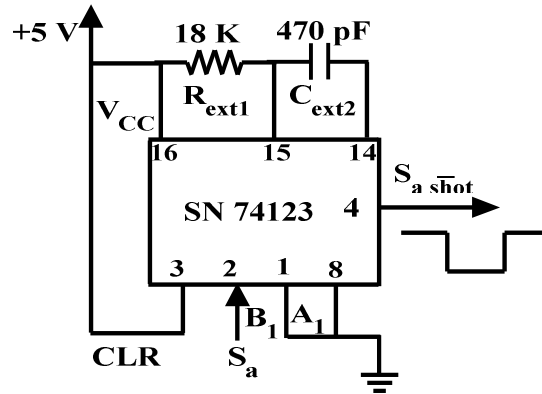
Fig.7.18 Monostable multivibrator circuit connection diagram

7.6.1 Design of the External Resistance and Capacitor

The expression for finding the delay duration (t_d) of the mono-stable multi-vibrator output pulse width in nanoseconds from the data sheet is given as [145].

$$t_d = 6 + 0.05\,C_{ext} + 0.45\,R_{ext}C_{ext} + 11.6\,R_{ext}$$

(7.9)

where, R_{ext} and C_{ext} are the external resistance and capacitance in kΩ and pF respectively. In this work, the values of external resistance and capacitance are R_{ext} = 18 kΩ and C_{ext} = 470 pF respectively.
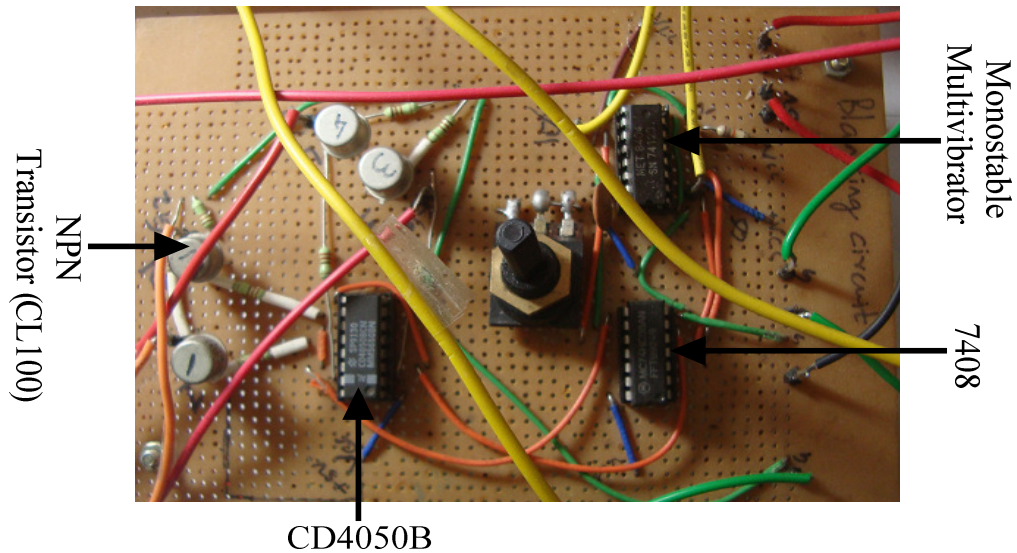
Fig.7.19 Photograph of blanking circuit

7.7   Optoisolation Circuit

The pulse width modulation (PWM) signals available from the blanking circuit cannot be directly applied to gates of the IGBT switches which are a part of the high-power network. So, high speed opto-couplers (TLP-250) with isolated DC power supplies are used for providing isolation between the logic control circuit and the power network. The internal and external circuit details of the opto-coupler are shown in Fig.7.20.
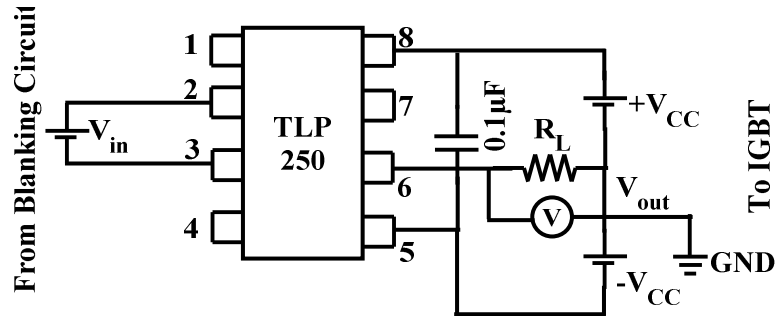
Fig.7.20 An Opto-coupler circuit

7.8   Power Supply Modules

Experimental setup requires regulated variable DC power supplies. To make the experimental setup more reliable and flexible, separate transformers and power supplies are used to power the individual module.

To generate a ±15 V bipolar DC regulated supply, a 230/18-0-18 V centre tapped step-down transformer of 500 mA rating is used is shown in Fig.7.21. A full bridge rectifier diode rectifier (D_1-D_4, using IN 4007) is used to convert AC to DC. Two identical electrolyte capacitors (C_{dc}) of value 2200 µF are used to smoothen the output voltage. A local ground (gnd) is created by connecting the centre tap of the transformer and mid-point of the capacitors. The unregulated DC voltage is taken as input to the voltage regulator ICs, 7815 and 7915, to produce regulated DC output voltages of +15 V and -15 V, respectively. The +5 V supply can be generated using a fixed voltage regulator IC 7805.
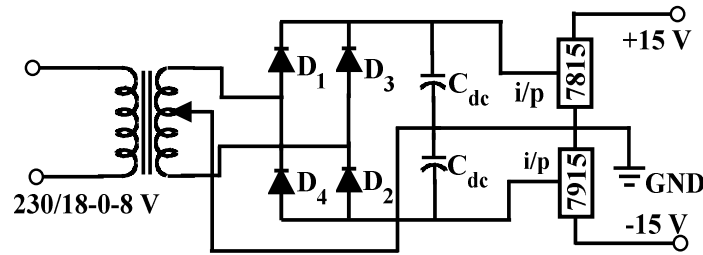
Fig.7.21 DC regulated power supply

7.9   Simulation Results

The block diagram of single phase fuel cell power system is shown Fig.7.22.
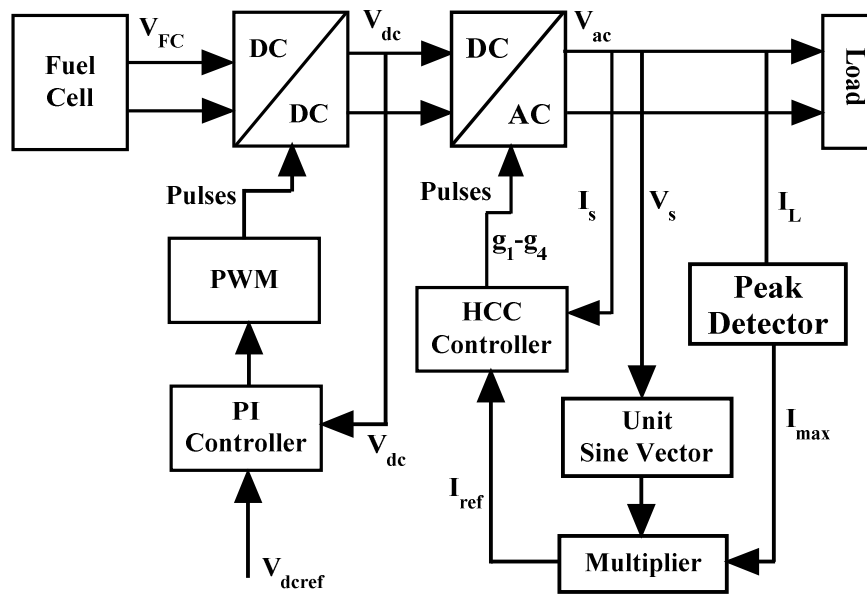
Fig.7.22 Block diagram of single phase fuel cell power system

For simulation of the above system, following parameters are considered.

1. Supply voltage   230 V

2. Frequency   50 Hz

3. Interfacing inductance   1.8 mH

4. Capacitance   2200 μF

The waveform of the instantaneous single-phase balance supply voltage is shown in Fig.7.23 (a) and source current in Fig.7.23 (b).The simulation waveform of single phase inverter output is shown in Fig.7.23 (c) .

146
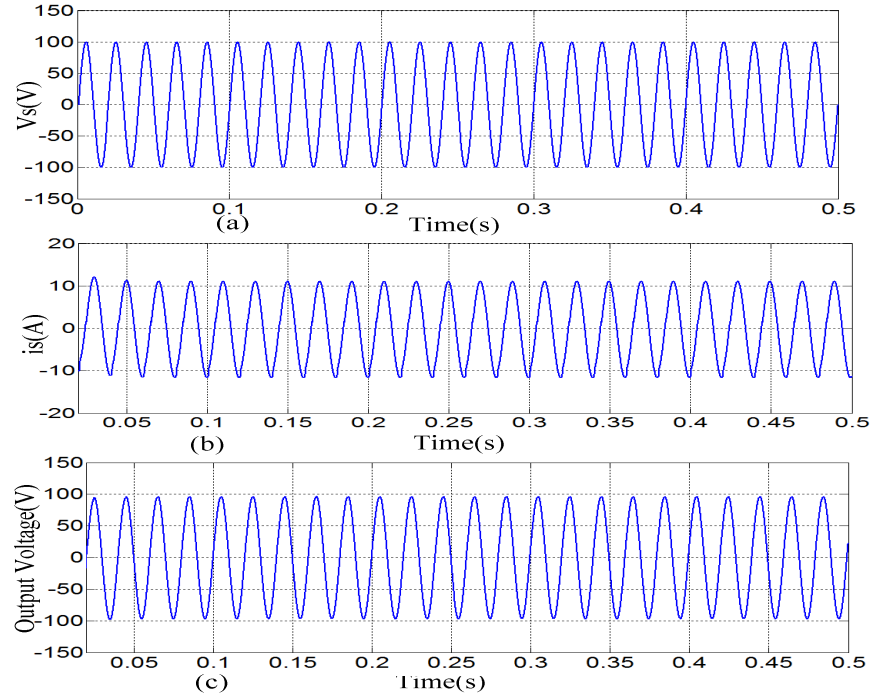
Fig.7.23 Simulation wave forms of (a) Supply voltages, (b) Source currents, and (c) Inverter output voltages

The hysteresis current controller (HCC), as discussed in section 7.5 is simulated for single phase fuel cell. For the experimental verification of HCC is described in section 7.9.1 with identical parameters.

7.9.1   Experimental Results

The prototype model of fuel cell power system consists of four-IGBT-SKM75GB063D, DC-link capacitor 6800 µF and an inductor (5 mH). The single phase supply voltages, load currents and DC voltage signals are sensed and computed, which are main inputs of the controller. Fig.7.22 shows the schematic diagram of the fuel cell power system using hysteresis current controller technique. The HCC technique is used to generate the switching pulses of the voltage source inverter. The required switching pulses are provided to the IGBT inverter via compactRIO through the gate driver circuits. The performance of the fuel cell power system has been experimented under the linear load. Initially, voltage source inverter acts as rectifier to charge the DC-link capacitor voltage through pre-charger circuit. When the DC voltage is equal to the supply voltage that is considered as a floating mode, the inverter will be in the ON-state.

Fig.7.24 shows the experimental wave form of single-phase supply voltages of the fuel cell power system. These wave forms indicate that the supply voltages (Vs = 150 V) are almost sinusoidal. The inverter output waveform before filter is shown in Fig.7.25. Fig.7.26 shows the source currents of fuel cell power system. The direct current control HCC technique is employed for generating gate control switching pulses to drive the fuel cell power system. The DC-link capacitor voltage is shown in Fig.7.27.
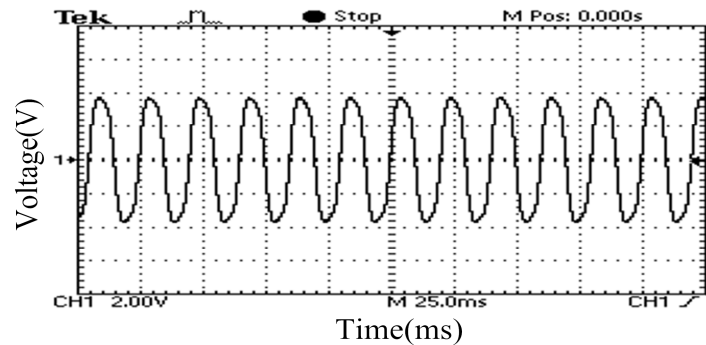
Fig.7.24 Waveforms of supply voltages
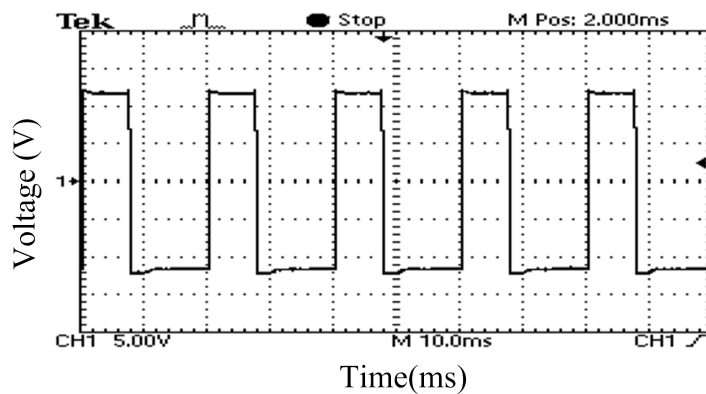
Fig.7.25 Inverter output before filter
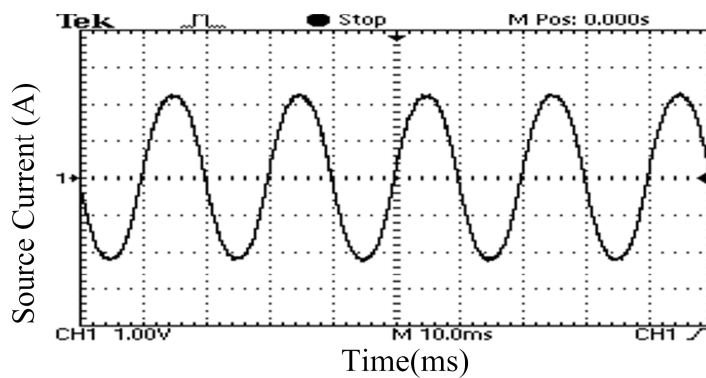
Fig.7.26 Source current

148
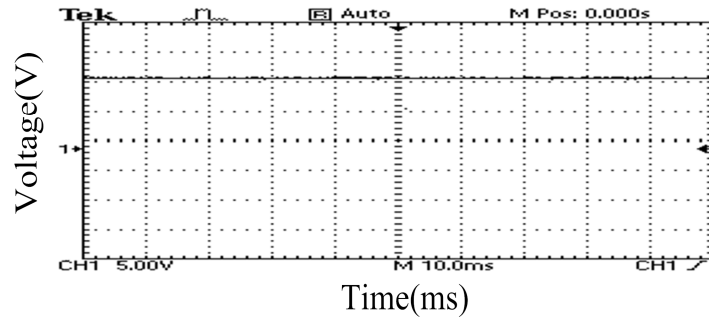
Fig.7.27 DC-link capacitor voltage

7.10   Field Programmable Gate Array

Field Programmable Gate Array (FPGA) is an integrated circuit which can be re-configured by a designer according to design specification. The FPGA configuration is generally specified using a Hardware Description Language (HDL). The advantages of FPGA over Application Specific Integrated Circuit (ASIC) are

➢ ASICs are designed for a specific application using CAD tools. Developing an ASIC takes more time and is expensive.

➢ It is not possible to correct the errors of ASIC after fabrications.

➢ FPGA can be re-configured according to design specification.

➢ The design and prototype time of FPGA is less as compared to ASIC.

FPGA contains programmable logic components called logic blocks and a hierarchy of reconfigurable interconnects that allow the blocks to be weird together. Logic blocks can be configured to perform complex combinational and sequential functions. In most FPGAs, the logic blocks also include memory elements which can be flip-flop or more complete blocks of memory.

7.10.1 Structure of Field Programmable Gate Array

FPGA architecture consists of an array block, called configurable logic block (CLB), input/output pads and routing channels of same width.

Configurable logic Block (CLB):
CLB is the basic component of FPGA and it is used to implement a user specific combinational and sequential logic. A CLB contains a cluster of basic logic element (BLEs) connected through a local routing network. Each BLE contains a 4 input look up

149

table (LUT-4) and a Flip-Flop [146]. Modern FPGAs contain typically 4 to 10 BLEs in a single cluster.
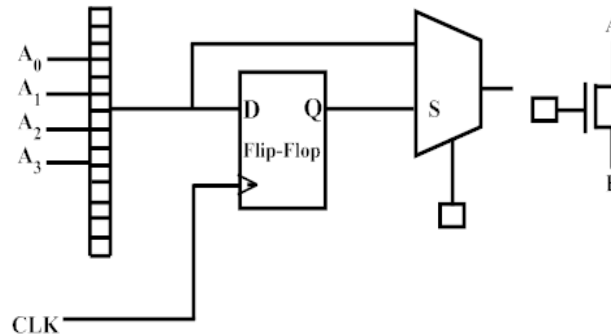
Fig.7.28 Configurable logic block (CLB)

Fig.7.28 shows the basic schematic of CLB.

*Interconnects***:**

The interconnection resources allow the implementation of an entire digital system by connecting various individual circuits (subsystems) that have been implemented on different CLBs in an FPGA. The interconnect resources in a typical FPGA can be classified as

(1) *General Purpose Interconnects:* Signal between CLBs and input output blocks can be routed through switch matrices as they travel along the horizontal and vertical interconnect lines.

(2) *Direct Interconnects*: Adjacent CLBs are interconnected directly.

(3) *Long Lines*: Long lines provide for high fan out, low-skew distribution of signals that must travel relatively long distances. They span the entire length or width of the interconnect area.

FPGA interconnects are normally un-segmented (each wiring segment spans only one logic block before it terminates in a switch box). A switch box is a switching matrix that contains programmable interconnections to all the wiring segments that terminate inside it. By turning on some of the programmable switches within a switch box, longer paths can be constructed.

IOB:

Input/output blocks provide an interface between the FPGA and the real world signal. Fig.7.29 shows a simplified IOB. Each IOB can be used as an input and output depending on the state of the output enable (OE). IOBs are bi-directional and they act as output when OE is high and input when OE is low. The OE bit can be programmed statically or set to the output of a CLB. IOBs contain D-Flip-Flops for latching the input and output signals.
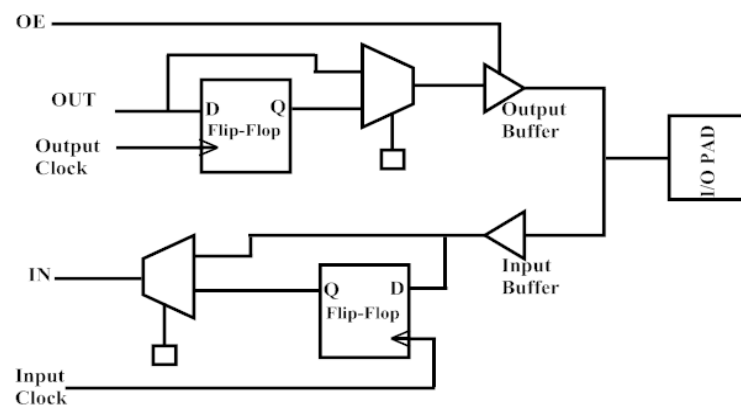
Fig.7.29 Input/output block

FPGA has a distributed configuration memory. The memory locations are distributed over the chip and need to be loaded to configure the FPGA. Special I/O pins that are not configurable by the user are used to load the program to the memory.

7.10.2 Programming of Field Programmable Gate Array

Synthesis tools provided by FPGA vendor, translate the HDL (Hardware Description Language) code into bit stream, which is downloaded to the configuration memory of the FPGA. But recent trends also offer the possibility to use high level languages like C, C++ and System C. Further, there are library based solutions which are optimized for a specific device.

Hardware description language: HDL is the most common approach to program an FPGA. There are two major languages, VHDL and Verilog. VHDL was developed in the 1980s by the Department of Defence. It is essentially as subset of ADA with extensions for describing hardware. Verilog was originally C like programming language to model hardware and later it became an IEEE standard like VHDL.

***High level language*:** System C, Handel-C and even generic C++ can be used for FPGA programming. Tools are available from various vendors like Celoxica, Synopsys, which supports high-level languages. MATLAB with Accelchip plug-in generates bit-stream for specific target boards from Xilinx and Altera.

***Library-based solutions*:** FPGA manufacturer Xilinx and Altera offer parameterized macros to generate code for common blocks such as arithmetic functions or specialized memories. The output of the macros is HDL code that can be included in the developers' synthesis process. This reduces the development time.

Graphical tool based design: MATLAB/Xilinx and LABVIEW are providing high level logical blocks for designing high performance digital controller. These tools provide automatic synthesis and translate the code in to bit stream which is implemented to the configuration memory of the FPGA board.

The major function of a real time control system is to sense the measurement signals with the help of transducer from the physical world and give it to the controller to compute necessary control signals. The control signal is sent to the physical world to perform necessary control action. For a distributed control, input and output are sensed remotely from physical world with the help of remote I/O modules and the data is sent to real time controller via a TCP/IP connection. The real time controller computes the control law and sends the control signal via TCP/IP to the physical world. Though FPGA is widely used for digital control applications, it is not used for distribute control applications because the lack of TCP/IP connectivity.

National Instruments compactRIO is an ideal hardware which can perform distributed control applications. It includes a computer controller running the LABVIEW real-time operating system, and an FPGA that interfaces with the real-time computer to control various modules installed in the chassis. The chassis communicates with a host computer via TCP/IP. The detailed description of structure and functionality of cRIO-9014 is given in section 7.11.

7.11   CompactRIO-9014

National Instruments (NI) compactRIO is a small rugged industrial data acquisition and control system powered by Reconfigurable Input-Output (RIO). NI compactRIO incorporates a real-time processor and reconfigurable FPGA for reliable stand-alone

embedded or distributed applications. CompactRIO systems are developed using LABVIEW, the LABVIEW Real-Time (RT) Module and the LABVIEW FPGA Module [147] . CompactRIO comprises of following modules:

➢ 4 or 8-slots reconfigurable chassis

➢ Power supply

➢ Real time embedded processor

➢ Swappable industrial I/O modules

Block diagram of programmable controller is shown in Fig.7.30.
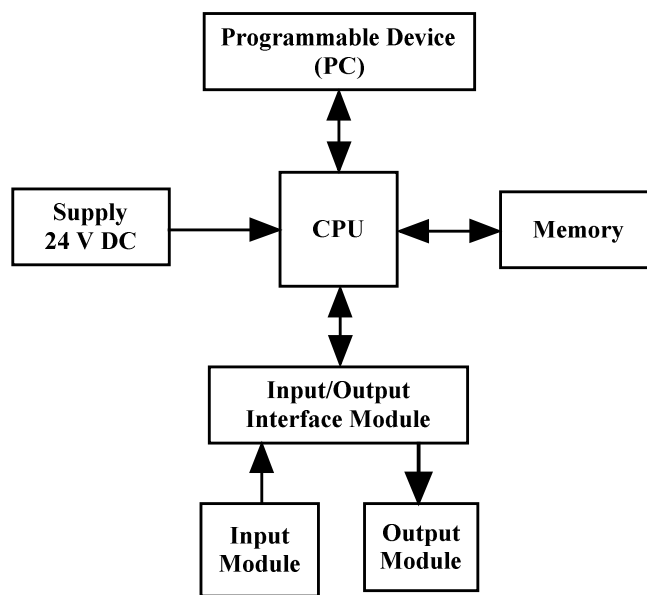
Fig.7.30 Block diagram of programmable controller

7.11.1 Reconfigurable Chassis

The reconfigurable chassis, as shown in Fig.7.31, is the heart of NI compactRIO embedded systems. The reconfigurable chassis features the same rugged metal construction that characterizes the entire compactRIO platform.
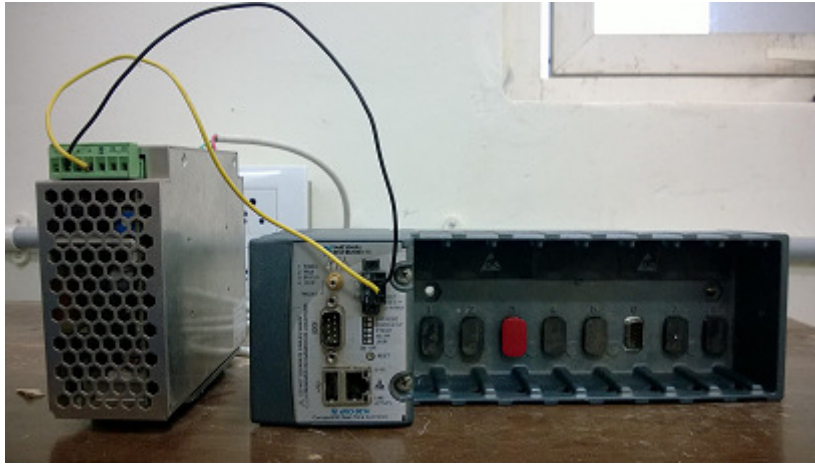
Fig.7.31 The reconfigurable chassis

7.11.2 Power Supply

CompactRIO-9014 consists of a power supply module which provides DC output of (24 V, 5 A) to the real time embedded processor and input output modules.

7.11.3 Real Time Embedded Processor

CompactRIO combines a low-power consumption real-time embedded processor with a high-performance RIO FPGA chip. A local peripheral control interface (PCI) bus connection provides a high-performance interface between the RIO FPGA and the real-time processor. The cRIO core has built-in data transfer mechanisms to pass data to the embedded processor for real-time analysis, post-processing, data logging, or communication to a networked host computer. The RIO FPGA chip is connected to the I/O modules in a star topology, for direct access to each module. Fig.7.32 depicts a cRIO real-time processor.

Fig.7.32 Real time processor

7.11.4 Input/output Modules

Each compactRIO I/O module contains built-in signal conditioning and screw terminal, BNC or D-Sub connectors. By integrating the connector junction box into the modules, the compactRIO system significantly reduces the space requirements and cost of field wiring. A variety of I/O types are available including ±10 V simultaneously sampling analog inputs/outputs, 24 V industrial digital I/O with up to 1 A current drive. Because the modules contain built-in signal conditioning for extended voltage ranges or industrial signal types [147]. Such an I/O module is shown in Fig.7.33.

Fig.7.33 An I/O module

NI 9201: An 8-channel Analog Input Module

NI 9201 has ten detachable screw-terminal connectors. Each channel has an AI terminal for analog input, COM, the common terminal or pin, is internally connected to the isolated ground reference of the module [148].

Some of the main features of NI 9201 are listed below

- ➢ 8 analog inputs, ±10 V input range
- ➢ 500 kS/s aggregate sampling rate
- ➢ 12-bit resolution, single-ended inputs, screw terminal or D-Sub connectors
- ➢ Hot-swappable operation; overvoltage protection; isolation
- ➢ - 40 to 70 °C operating range

NI 9263: A 4-channel Analog Voltage Output Module

NI 9263 has four analog output channels and each channel has an analog output terminal, AO. NI 9263 also has common terminals, COM, that is internally connected to the isolated ground reference of the module [149].

Some of its characteristics are mentioned below:

- ➢ 4 simultaneously updated analog outputs, 100 kS/s
- ➢ 16-bit resolution
- ➢ Hot-swappable operation
- ➢ - 40 to 70 °C operating range

In this thesis, hysteresis current controller (HCC) and adaptive-fuzzy-HCC (AFHCC) is developed using cRIO-9014 and Xilinx System Generator respectively. Section 7.12 discusses HCC design using cRIO-9014 and section 7.13 presents AFHCC design using Xilinx System Generator. Earlier in Chapter 3 we have demonstrated the use of FPGA for PWM and PI controllers. Use of FPGA reduces the circuit size to a great extent besides providing flexibility for modification and further development.

7.12   Hysteresis Current Control using cRIO

In section 7.5 analog design of HCC is discussed. An analog design of controller has some serious limitations. One of the major limitations of analog design of controller is that the structure and control law is fixed in nature. The other limitation is that the analog

design has complex circuit connections; it takes time for design and prototyping which adds to the cost of the system. Because of the advancement of digital technology, now day's different digital controllers are used for digital control of power electronics and drives applications. Digital controller provides flexibility in design and it takes less time for design and prototyping.

In recent time, Field Programmable Gate Array (FPGA) is emerging as one of the front runners in programmable logic component based devices. FPGA is a matrix of configurable logic blocks (CLBs) which are interconnected and it is re-programmable. FPGA can design specific hardware architecture, according to the control objective. This approach reduces the execution time.

In this experimental set up, single phase load connected fuel cell power system is developed. CompactRIO-9014 is used to implement HCC which provides accurate pulse width modulation signals to drive the DC/AC inverter. Fig.7.34 shows the schematic diagram of fuel cell power system using cRIO-9014 and Fig.7.35 shows the experimental setup of fuel cell power system using cRIO-9014.
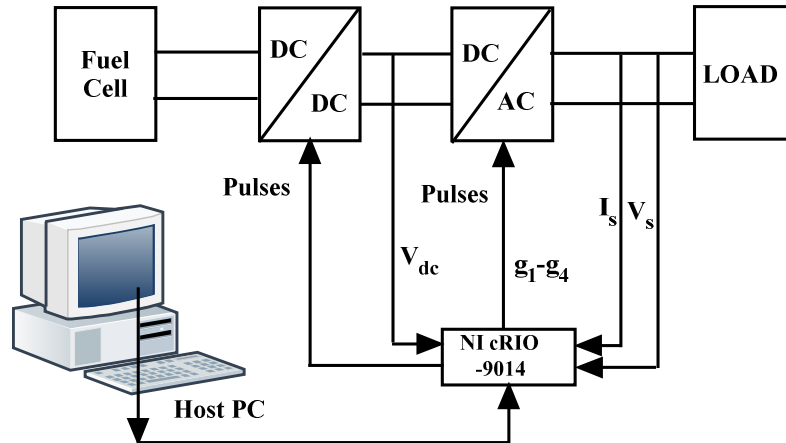
Fig.7.34 Schematic diagram for fuel cell power system
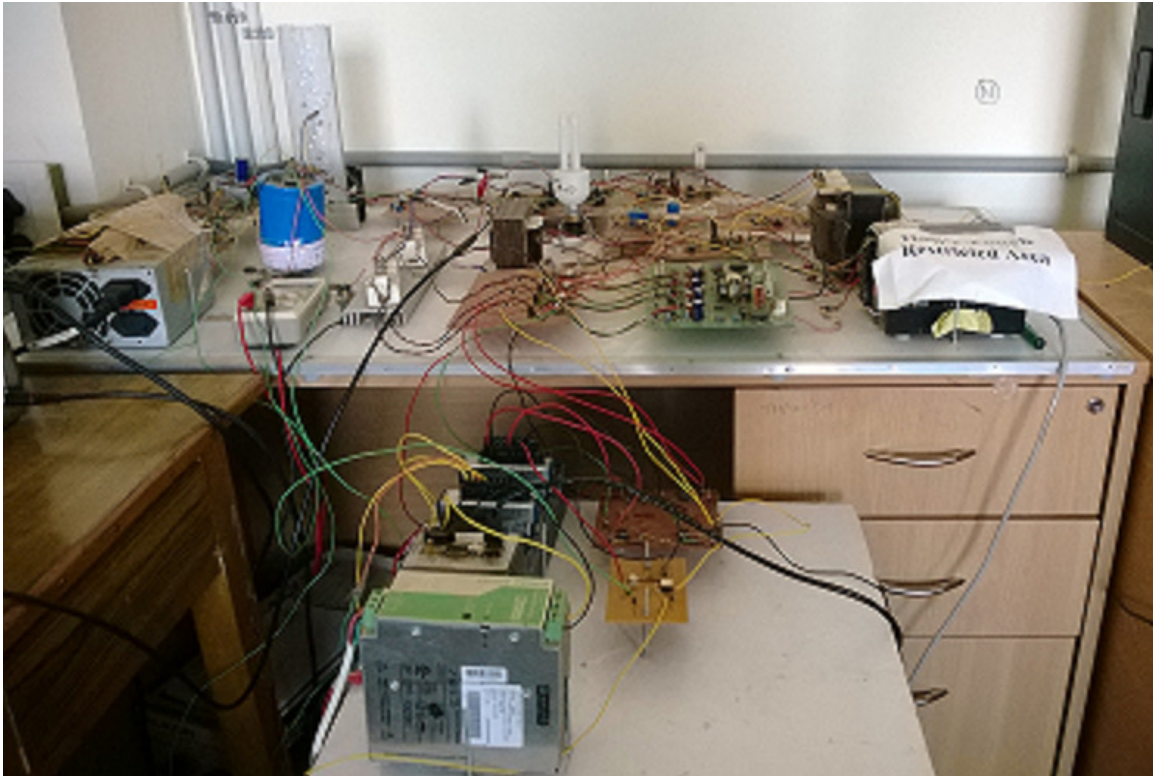
Fig.7.35 Experimental set-up for fuel cell power system

The compactRIO embedded system features a 200 MHz processor that executes the LABVIEW Real-Time applications. The controller features a 10/100 Mb/s Ethernet port, a real-time clock and watchdog timers. The cRIO-9014 is provided 9 V to 35 V DC, 20 W supply input.

CompactRIO starts a LABVIEW Real-Time Module executable when powered on. The executable contains the LABVIEW FPGA Module code. The LABVIEW Real-Time Module executable waits for an incoming TCP/IP connection from the host in order to pass control messages. The cRIO establishes a second TCP/IP connection for transferring data back to the host when the host initiates an acquisition. The USER1 LED remains lit until the acquisition finishes or an error occurs after establishing a connection with a host system.
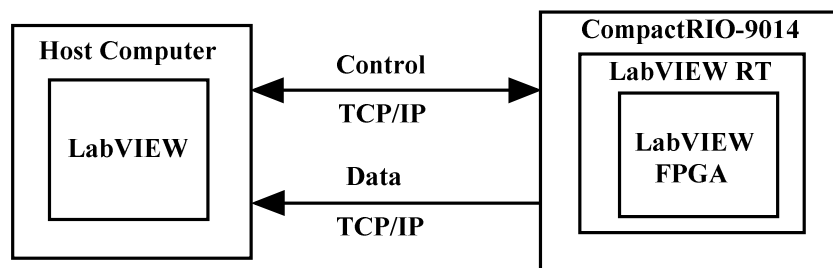
Fig.7.36 CompactRIO interfacing with host computer

158

This section describes the design and implementation of HCC using cRIO-9014. Fig.7.36 shows the block diagram of control architecture. Table 7.1 describes the cRIO modules used in this experiment.

Table 7.1 CompactRIO module descriptions

Slot	Module type	Description
	NI cRIO-9014	Real-Time Controller with 128 MB DRAM, 2 GB Storage
3	NI 9201	8-channel Analog Input Module
6	NI 9263	4-Channel, 100 kS/s, 16-bit, ±10 V, Analog Output Module

Fig.7.37 shows the experimental waveform of output voltage of a single-phase fuel cell power system. This output waveform indicates that the supply voltages are almost sinusoidal of frequency 50 Hz. Fig.7.38 shows the dead band waveform of hysteresis current controller. The delay time between two different pulses is 3 µs. The direct current control HCC technique is designed in cRIO for generating gate control switching signals to drive the fuel cell power system. The inverter output voltage waveform is shown in Fig.7.39. The PI controller is also designed in cRIO to control the DC-link capacitor voltage. The DC-link capacitor voltage is shown in Fig.7.40.
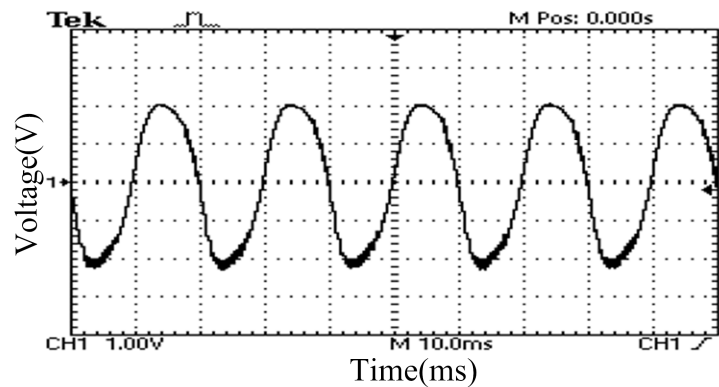
Fig.7.37 Waveforms of supply voltages
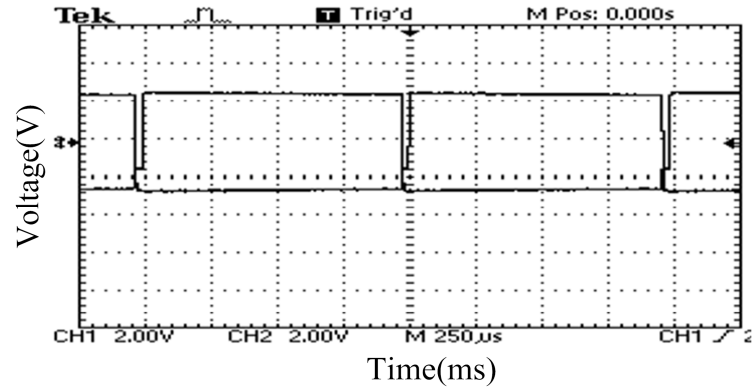
Fig.7.38 Delay waveform of blanking circuit
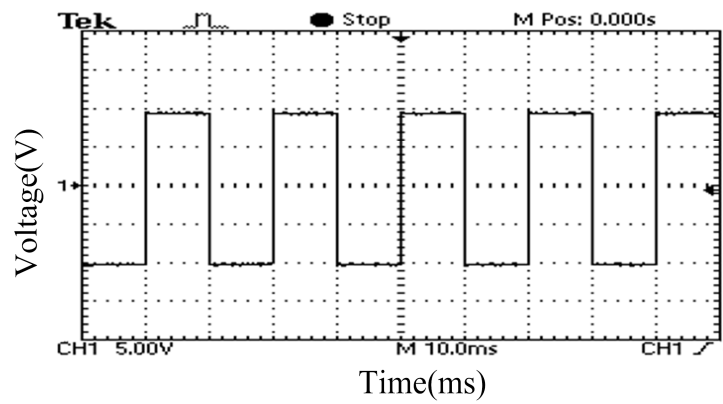
Fig.7.39 Inverter output before filter
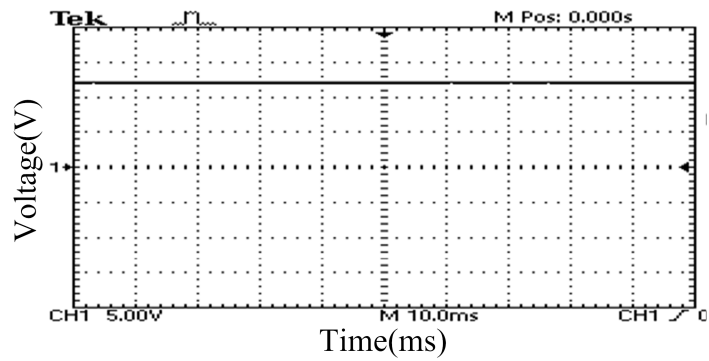
Fig.7.40 DC-link capacitor voltage
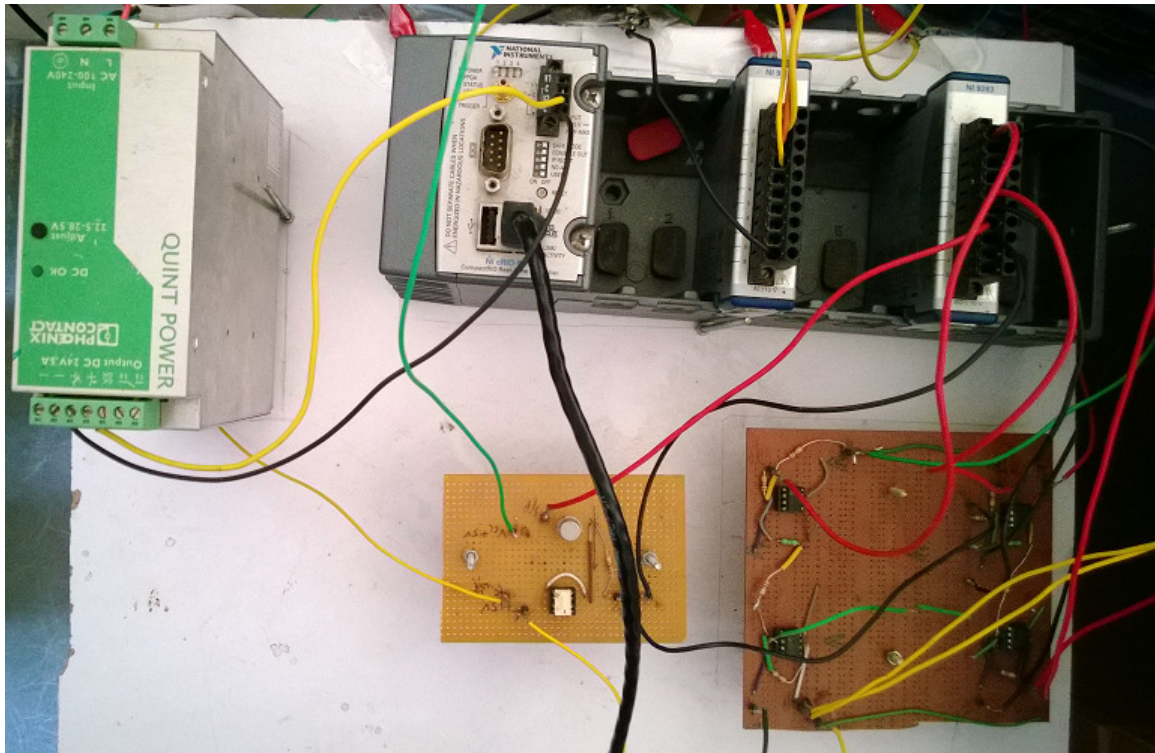
Fig. 7.41 CompactRIO as controller

Fig.7.42 Front panel of Hysteresis Current Controller (HCC) parameters

We have designed the hysteresis current controller (HCC) in LABVIEW platform. The design parameters of the HCC controller are shown in Fig.7.42.
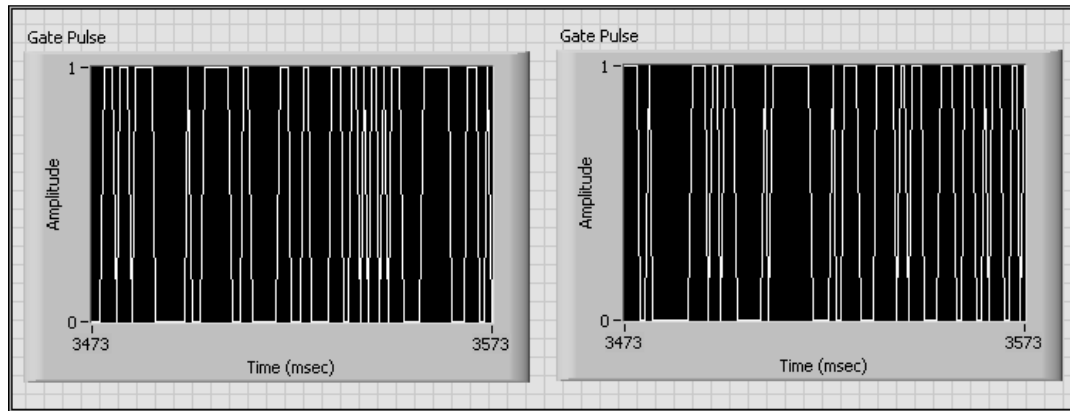
Fig.7.43 Switching patterns of Hysteresis Current Controller (HCC) technique

The front panel of the HCC technique is shown in Fig.7.43. The direct current control HCC technique is designed in LABVIEW for generating gate switching signals to drive the fuel cell power system.

The PI controller for DC-link capacitor voltage of front panel is shown in Fig.7.44. The proportional and integral gain is chosen 1 and 1.66797 respectively.
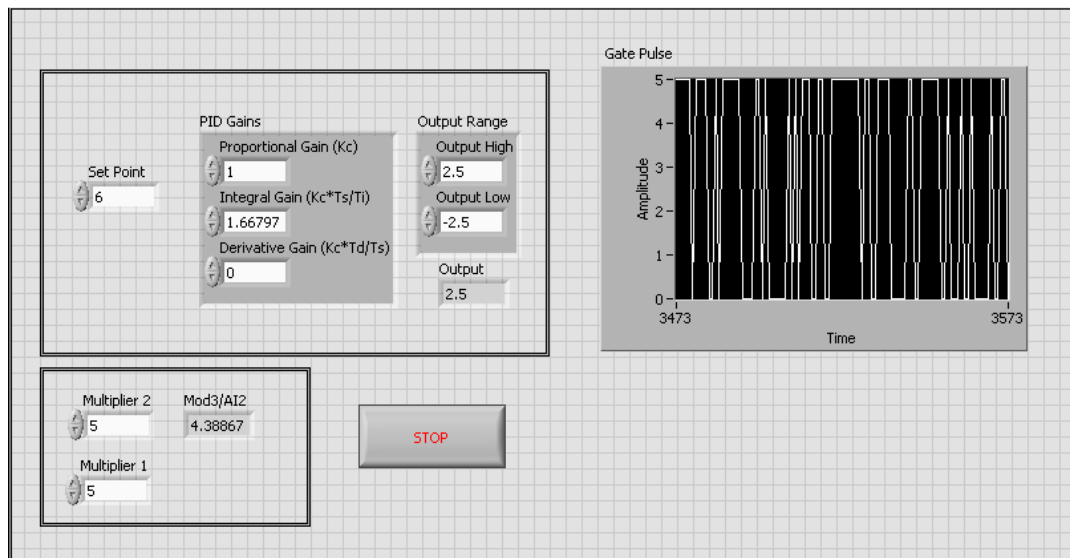
Fig.7.44 PI controller parameters with PWM signals for boost converter

7.13   Xilinx System Generator (FPGA) Controller Design

MATLAB/SIMULINK software package provides a powerful high level modelling environment for people who are involved in system modelling and simulations. Xilinx System Generator Tool developed MATLAB/SIMULINK package is widely used for

162

algorithm development and verification purposes in Digital Signal Processing (DSP) and Field Programmable Gate Arrays (FPGAs). System Generator Tool allows an abstraction level algorithm development while keeping the traditional block sets. At the same time automatically translating designs into hardware implementations that are faithful, synthesizable and efficient.

The three-phase PWM DC-AC inverter is driven by voltage source inverter (VSI) is analysed by using a MATLAB/SIMULINK model. The control signals for the VSI in the related model are generated by Xilinx FPGA chip. MATLAB/SIMULINK package plug-in with Xilinx System Generator Tool provides facility to generate bit stream for target board. Control algorithm developed using Xilinx System Generator Tool can be conveniently used with traditional Simulink block sets can be translated to the VHDL. The bit-stream can be generated using synthesis tools.

The performance of the FPGA controller based fuel cell power system is verified through System Generator/Xilinx platform. The Xilinx/System Generator is a tool that allows high-level tool for designing high-performance systems to implement on FPGA processor. A close interconnection with the MATLAB/SIMULINK software makes the implementation of complex hardware designs an easy task. All of the down-stream FPGA implementation steps including synthesis and place and route are automatically performed to generate an FPGA programming file. To design and dump on FPGA using the Simulink/Xilinx simulation model, the Gateway In and Gateway Out define the boundary of the FPGA. Fig.7.45 shows the block diagram of the AHCC Controller design using Xilinx blockset/Matlab. The following steps are carried out to design the FPGA controller:

Gateway-In: The adaptive-fuzzy-HCC technique is designed using the Simulink/Xilinx Blockset. The three-phase supply voltages, source currents and the DC-link capacitor voltage are sensed, which are the inputs of the controller. These sensed signals are sent through the Xilinx gateway-in, which converts integer, double and fixed-point to Xilinx fixed-point.

Gateway-Out: The adaptive-fuzzy-HCC generates switching pulses as a fixed point that converts into Simulink fixed point through Gateway-out. The entire controller is computed and design using Xilinx block-set for FPGA implementation.

System Generator*:* Once the controller design is completed, the hardware implementation file is generated using System Generator token properties editor. One option is to select HDL Netlist which allows the FPGA implementation steps of RTL synthesis and place and route to be performed interactively using tool specific user interfaces. Alternatively, you can select Bit-stream as the Compilation target and System Generator will automatically perform all implementations. The generated VHDL code is implemented in the FPGA kit. The FPGA processor provides the switching pulses to drive the voltage source inverter through proper interfacing circuits (protection circuits and gate driver circuits).
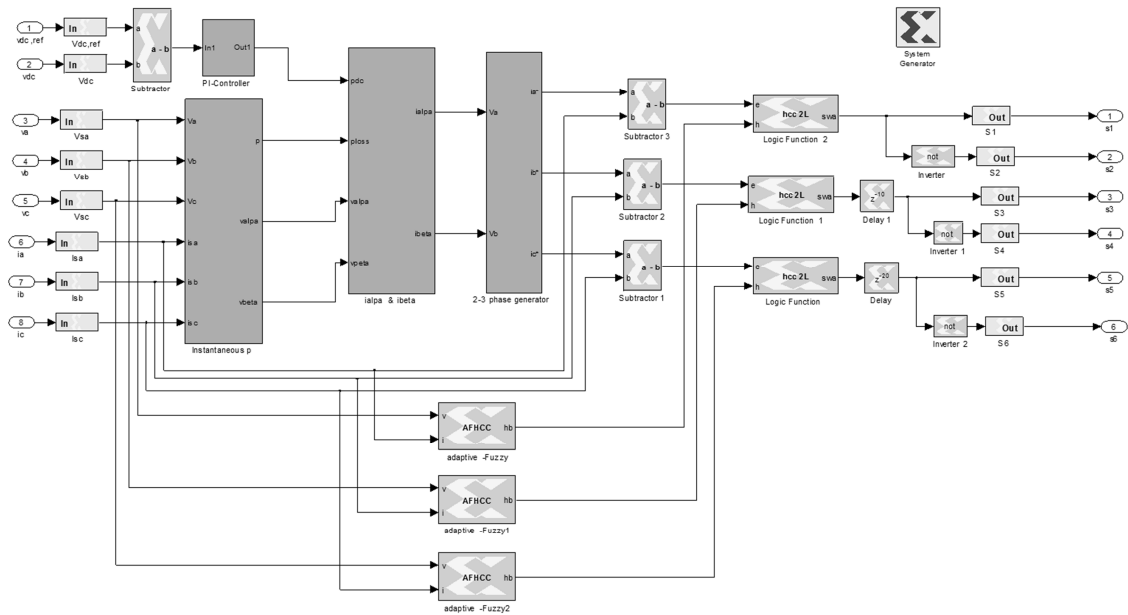
Fig.7.45 Controller design using Xilinx blockset/Matlab

Adaptive-Fuzzy-HCC: The 10-bit reference currents are compared with the 10-bit digitized actual currents $(i_{sa}, i_{sb} \, and \, i_{sc})$ to generate switching pulses using the adaptive-fuzzy-HCC. The adaptive-fuzzy-hysteresis bandwidth can be modulated as a function of slope reference di_{sa}^{*} / dt current and supply voltage v_s which are used as inputs for fuzzy processing. The adaptive-fuzzy hysteresis band HB is the output of the fuzzy controller. This fuzzy logic controller is programmed in the S-function code and can be made as an adaptive-fuzzy block using the Mcode block. Similarly, the variable HCC is created by S-functions in MATLAB to produce gate control-pulses to drive the VSI.

7.13.1 FPGA Implementation

The digital controller is tested and implemented in FPGA hardware by using the following two methods; i) Hardware co-simulation and ii) Xilinx ISE-iMPACT.

7.13.1.1 Hardware Co-Simulation

The system generator allows for hardware co-simulation interfaces that make it possible to integrate an FPGA processor directly into MATLAB/SIMULINK simulation. The system generator is a system level modelling tool that facilities digital hardware design and provides high-level abstractions that are automatically compiled into an FPGA board. This tool provides access to underlying FPGA resources through lower level abstractions, allowing the user to implement highly efficient designs. Programming an FPGA board using the system generator the following steps are followed

- Design the suitable control method using Xilinx block-set as a Simulink model. The Xilinx block-set allows constructing bit-accuracy and cycle-accurate models of an FPGA circuit.
- The code generator has "hardware co-simulation" compilation targets (HDL Netlist target) that automatically create a bit-stream file.
- After creating the bit-stream, the system generator automatically integrates an FPGA hardware platform configured with this bit-stream back into Simulink as a run time block.

The digital control method is simulated with hardware co-simulation; results for the compiled digital control part are executed and implemented in the FPGA target device. This performs the compiled part to be tested in actual hardware and can speed up simulation dramatically.

7.13.1.2 Xilinx ISE-iMPACT

The VHDL program code is generated by the system generator after the verification and simulation of the controller design. The VHDL program is synthesized using Xilinx-ISE 10.1 software. The ISE^{TM} (Integrated Software Environment) based FPGA design flow comprises the following steps:

- Design Entry
- Design Synthesis
- Design Implementation

➢ Design Verification

➢ Xilinx® device programming.

The Xilinx device programming uses iMPACT to create a BIT file for debugging and downloads it into the target device XILINX/ SPARTAN-3E FPGA.

Once the program is configured to FPGA kit, it acts as adaptive-fuzzy-HCC based FPGA controller and generates gate control switching pulses. These pulses are connected to opto-isolator circuit for preventing the ground sharing between the FPGA-processor and power converter. The output of the opto-isolator is connected through the driver circuit to each switching device for controlling the fuel cell power system.

7.13.2 Results and Analysis

The input signals $(i_{sa}, i_{sb}, i_{sc}, v_{dc}, v_{sa}, v_{sb}, v_{sc})$ are converted to fixed point for digital-design. The required switching pulses $(s_1, s_2, s_3, s_4, s_5, s_6)$ are generated from the digitized adaptive-fuzzy-HCC technique. The entire control algorithm is designed using Xilinx-block set and VHDL code is generated using system generator. The VHDL code is tested and compiled in the Xilinx-ISE 10.1 project navigator. The HDL code of analysis, synthesis and RTL schematic view is executed as shown in Fig.7.46.
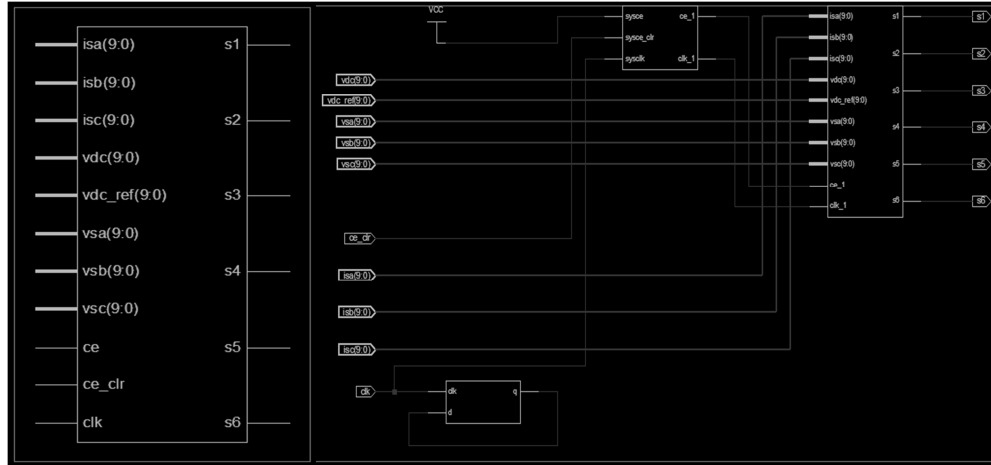
Fig.7.46 View of the RTL schematic

The three-phase supply voltages $(v_{sa}, v_{sb} \, and \, v_{sc})$, source currents $(i_{sa}, i_{sb} \, and \, i_{sc})$ and the DC-link capacitor voltage (V_{dc}) are sensed, which are the main inputs of the digital controller. These sensed analog signals are converted to fixed-point using Xilinx gateway in. Fig.7.47 shows the input signals, which are converted to fixed point for digital-design.
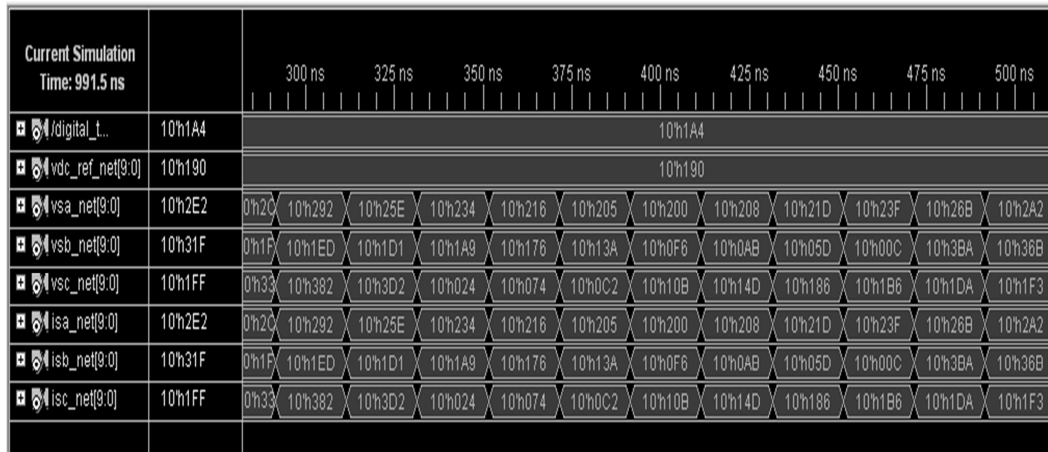
Fig.7.47 VHDL simulation result (input signals)

The six-channel gate control switching pulses are generated using adaptive-fuzzy-HCC. The VHDL program is generated by the system generator using Simulink platform. Fig.7.48 shows, six-gate switching pulses and clock signals to drive the fuel cell power system inverter.
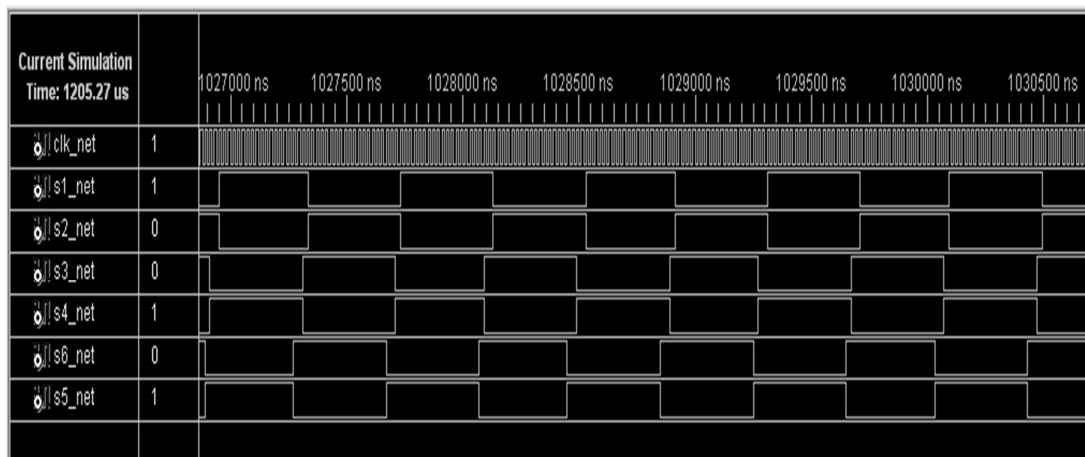
Fig.7.48 Six-channel gate driver switching pulses using VHDL code

The MATLAB/SIMULINK based system generator provides the interface with Xilinx-Spartan-3E board in Xilinx-iMPACT interface through USB cable. The USB cable is able to program the FPGA with 12-MHz speed. The compilation target automatically creates a bit-stream file and dumps it to FPGA board. This system clock frequency is set at 50 MHz at pin location C9 of the internal FPGA board. Fig.7.49 shows the photograph of Xilinx/Spatran-3E FPGA implementation using Xilinx ISE tool. The proposed controller design is simulated and compilation portion is tested successfully through the FPGA kit in real time environment.
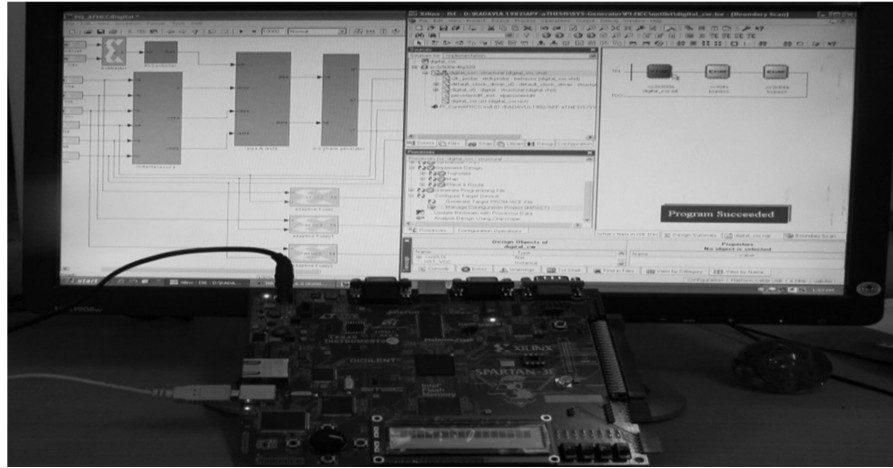
Fig.7.49 Photograph of Xilinx/Spatran-3E FPGA implementation

Remarks: The adaptive-fuzzy-HCC control algorithm is designed and implemented in the FPGA-kit using Xilinx ISE. The controller is modeled using the Xilinx Blockset and tested through the MATLAB/SIMULINK environment. The Matlab/Xilinx tool leads in high-level logical blocks for designing high-performance digital systems. From the Simulink, VHDL code is generated for this particular controller using System Generator. The VHDL code is verified and synthesized in the Xilinx ISE 10.1 Platform. After synthesizing the code, the programming bit file is generated and configured on the target FPGA device. The FPGA provides the switching pulses to drive the PWM-voltage source inverter through gate driver circuits.

7.14   Summary

The following conclusions can be drawn out of this chapter: -

➢ The single-phase fuel cell system with HCC controller is experimentally validated.

➢ Hardware setup with hysteresis current controller is demonstrated. The result obtained from the experimental set up is presented.

➢ HCC technique reduces the switching power loses without compromising on performance.

➢ HCC technique for single phase fuel cell power system is implemented using National Instruments compactRIO-9014 and results are presented.

➢ FPGA based Adaptive-Fuzzy-HCC (AFHCC) controller for three-phase fuel cell power system is designed and experimentally validated and results are presented.

Chapter-8

8. CONCLUSIONS AND FUTURE WORK

8.1 Conclusions

The main objective of thesis is to develop a load/grid connected fuel cell power system which can be used for backup power supply. Digital control scheme of DC-DC converter and DC-AC inverter has been developed and the extensive simulation results are validated through experimental setup.

The general conclusions are drawn from the thesis

➢ **Fuel Cell Modelling:** Mathematical modelling of solid oxide fuel cell (SOFC) is developed which considers different types of losses. Electrical characteristics (output voltage, efficiency, and power density and voltage losses) of SOFC are simulated through MATLAB.

➢ **FPGA Control of DC-DC Converter:** A DC-DC boost converter is developed to step up the output DC voltage of SOFC. Conventional PI controller and Sliding Mode Control (SMC) scheme has been designed for DC-DC converter. Conventionally the control circuit of DC-DC converter is implemented using analog components but due to the non-re-configurability nature of the analog control, it is not reliable in nature. So the control circuit of power converter is implemented using FPGA. FPGA is an ideal choice of digital computing device

because it's modular in nature and can be re-configured in real time. FPGA implementation of PI controller is designed and experimentally validated.

➢ **PWM-VSI Control Schemes:** The fuel cell power system is implemented with PWM-current controlled voltage source inverter. Different control schemes (TCCC, TPCC and Fixed-HCC, Fuzzy-HCC, Adaptive-HCC and Adaptive-Fuzzy-HCC) of PWM-VSI are summarized.

➢ **Fuel Cell as Back-up Power Unit:** As fuel cell provides backup power, there can be numerous real life scenarios such as non-availability of required number of fuel cell units, malfunction of fuel cell etc. This thesis considers the above mentioned scenarios. When the required numbers of fuel cells are not available, DC-DC converter is used to step up the output voltage of fuel cell. When there is a malfunction in fuel cell or shortage of hydrogen then a battery is used to provide backup power. The fuel cell power system is simulated through MATLAB/SIMULINK with different conditions.

In a first case, the DC-AC inverter is controlled using fixed-HCC and adaptive HCC. When there is any kind of malfunction of fuel cell then battery is connected to provide backup power supply. In this case, adaptive hysteresis controller is used for DC-AC inverter. When there is sufficient number of fuel cells is available then DC-AC inverter is controlled using fuzzy-HCC, Adaptive-fuzzy HCC, TCCC and TPCC.

The harmonics of line currents are analysed and it's found that Adaptive-fuzzy-HCC technique reduces the switching losses and improves the fuel cell power system performance in comparisons with the TCCC, TPCC, fixed-HCC and the Adaptive-HCC. The measured total harmonic distortion of the source currents is in the compliance with IEEE 519 and IEC 61000-3 harmonic standards.

➢ **Fuel Cell Based Shunt APF:** The fuel cell power system based on shunt active power filter (APF) is designed for compensation of current harmonic and reactive power compensation in the AC power distribution system. APF based fuel cell reduces the real power flow from grid side, which eventually reduces the power rating of inverter.

➢ **Experimental Validation:** The prototype model of single phase fuel cell power system with hysteresis current control (HCC) technique is developed. FPGA implementation of HCC is done using NI-cRIO-9014. Three phase model of fuel

170

cell power system is developed using adaptive-HCC using Xilinx/System Generator. The adaptive-HCC PWM-VSI control algorithm is designed and implemented in the FPGA-kit using Xilinx ISE. First, the controller is modeled using Xilinx Blockset. From the Simulink, VHDL code is generated for this particular controller using System Generator. The VHDL code is verified and synthesized in the Xilinx ISE 10.1. After synthesising the code, the programming bit file is generated and configured on the target device. The FPGA provides the switching pulses to drive the PWM-VSI inverter through gate driver circuits.

8.2 Scope for Future Work

Some suggested new directions of research in the area of fuel cell based power system are summarized in this section.

- ➤ To improve the power quality of fuel cell power system by using dynamic voltage restorer (DVR).
- ➤ To meet the higher power requirements, a modular and multilevel inverter can be used.
- ➤ New control scheme for power electronic interface of FCPS system using soft computing technique can be developed by utility interactive operation.
- ➤ A complete FPGA based controller for fuel cell power system can be developed that would add flexibility for controller design. This would significantly reduce hardware requirement and it can further be extended to ASIC development.

References

[1]   "International Energy Outlook," US Department of Energy, 2009.

[2]   "World energy needs and nuclear power, http://www.worldnuclear.org/inf/inf16.html, 2009.".

[3]   "http://www.mnre.gov.in," 2013. [Online]. [Accessed November 2013].

[4]   Gerald Halpert, Harvey Frank, and Subbarao Surampudi, "Batteries and Fuel Cells in Space," *The Electrochemical Society Interface,* pp. 25-30, 1999.

[5]   Uzunoglu M, Alam MS, "Modeling and analysis of an FC/UC hybrid vehicular power system using a novel wavelet based load sharing algorithm.," *IEEE Transactions on Energy Conversion,* vol. 23, no. 1, pp. 263-272, 2008.

[6]   M.C. Kisacikoglu, M. Uzunoglu, M.S. Alam, "Load sharing using fuzzy logic control in a fuel cell/ultracapacitor hybrid vehicle," *International Journal of Hydrogen Energy,* vol. 34, pp. 1497-1507, 2009.

[7]   M. Uzunoglu, M.S. Alam, "Dynamic modeling, design and simulation of a PEM fuel cell/ultra-capacitor hybrid system for vehicular applications," *Energy Conversion and Management,* vol. 48, pp. 1544-1553, 2007.

[8]   Sadik Kakaç, Anchasa Pramuanjaroenkij, Xiang Yang Zhou, "A review of numerical modeling of solid oxide fuel cells," *International Journal of Hydrogen Energy,* vol. 32, pp. 761-786, 2007.

[9]   Roberto Bove,Stefano Ubertini, "Modeling solid oxide fuel cell operation: Approaches,techniques and results," *Journal of Power Sources,* vol. 159, pp. 543-559, 2006.

[10]   Abraham Gebregergis, Pragasen Pillay, Debangsu Bhattacharyya, and Raghunathan Rengaswemy, "Solid Oxide Fuel Cell Modeling," *IEEE Transactions*

on Industrial Electronics, vol. 56, no. 1, pp. 139-148, Jan 2009.

[11] Caisheng Wang, M. Hashem Nehrir and Steven R. Shaw, "Dynamic Models and Model Validation for PEM Fuel Cells Using Electrical Circuits," *IEEE Transactions on Energy Conversion,* vol. 20, no. 2, pp. 442-451, June 2005.

[12] Sahu B, Rincon-Mora G., "A high-efficiency,dual-mode, dynamic, buck-boost power supply IC for portable applications," in *International conference on embedded system design (VLSID '05)*, 2005.

[13] Canales F, Barbosa P, Aguilar C and Lee F L, "A High-Power-Density DC/DC Converter for High-Power Distributed Power Systems," in *IEEE Power Electronics Specialist Conference*, 2003.

[14] Franco L C, Pfitscher L L, and Gules R, "A New Static Gain Non-isolated DC-DC Converter," in *IEEE Power Electronics Specialist Conference*, 2003.

[15] Chen R Y, Lin R L,Liang T J, Chen J F and Tseng K C, "Current-fed full-Bridge Boost Converter with Zero Current Switching for high voltage Applications," in *IEEE Industry Applications Conference*, 2005.

[16] Haiping Xu, Li Kong, and Xuhui Wen, "Fuel Cell Power System and High Power DC-DC converter," *IEEE Transactions on Power Electronics,* vol. 19, no. 5, pp. 1250-1255, 2004.

[17] J.M. Andujar, F. Segura, M.J. Vasallo, "A suitable model plant for control of the set fuel cell-DC/DC converter," *Journal of Renewable Energy,* vol. 33, pp. 813-826, 2008.

[18] Xin Zhao, Dawei Gao, Jiajia Wu, Qingchun Lu, "The Digital Control of Auxiliary DC-DC Converter on Fuel Cell Vehicle," in *IEEE Vehicle Power and Propulsion Conference (VPPC)*, Harbin,China, 2008.

[19] V. Chandrasekar, Renji V. Chacko, Z.V. Lakaparampil, "Design and implementation of an energy efficient power conditioner for fuel cell generation system," *International Journal of Hydrogen Energy,* vol. 36, pp. 15009-15017,

2011.

[20] Adam PENCZEK, Robert STALA, Łukasz STAWIARSKI, Miłosz SZAREK, "Hardware-in-the-Loop FPGA-basedSimulations of Switch mode Converters for Research and Educational Purposes," *PRZEGLĄD ELEKTROTECHNICZNY (Electrical Review),* vol. 87, pp. 194-200, Nov 2011.

[21] Miro Milanovica, Mitja Truntic, Primoz Slibar, Drago Dolinar, "Reconfigurable digital controller for a buck converter based on FPGA," *Microelectronics Reliability,* vol. 47, pp. 150-154, 2007.

[22] Hajizadeh A., Golkar M.A. and Feliachi A., "Power Management Strategy of a Hybrid Distributed Generation System," *International Journal of Distributed Energy Resources,* vol. 3, no. 2, 2007.

[23] Bor-Ren Lin, "A single-phase three-level pulse width modulation ac/dc converter with the function of power factor corrector and active power filter," *Electric Power Systems Research,* vol. 58, no. 3, pp. 157-167, 2001.

[24] Andersen G K, Klumpner C, Kjaer and Blaabjerg F, "A New Green Power Inverter for Fuel Cells," in *IEEE Power Electronics Specialist Conference*, 2002.

[25] Andersen G K, Klumpner C, Kjaer and Blaabjerg, "A New Power Converter for Fuel Cells with High System Efficiency," *International Journal of Electronics,* vol. 90, no. 11-12, pp. 737-750, 2003.

[26] Gopinath R, Kim S, Hahn J-H, Webster M, Burghardt, Campell S, Becker D, Enjeti P, Yeary M and Howze J, "Development of a low cost Fuel Cell Inverter System with DSP Control," in *IEEE Power Electronics Specialist Conference*, 2002.

[27] Rajesh Gopinath,Sangsun Kim,Jae-Hong Hahn,Prasad N. Enjeti,Mark B. Yeary,Jo W. Howze, "Development of a Low Cost Fuel Cell Inverter System With DSP Control," *IEEE Transactions on Power Electronics,* vol. 19, no. 5, pp. 1256-1262, 2004.

[28] Kourosh Sedghisigarchi, and Ali Feliachi, "Dynamic and Transient Analysis of Power Distribution Systems With Fuel Cells-Part I: Fuel-Cell dynamic Model," *IEEE Transactions on Energy Conversion,* vol. 19, no. 2, pp. 423-428, 2004.

[29] Kourosh sedghisigarchi, and Ali Feliachi, "Dynamic and Transient Analysis of Power Distribution Systems With Fuel Cells- Part II: Control and Stability Enhancement," *IEEE Transactions on Energy Conversion,* vol. 19, no. 2, pp. 429-434, 2004.

[30] Jinhee Lee, Jinsang Jo, Sewan Choi,and Soo-Bin Han, "A 10-kW SOFC Low-Voltage Battery Hybrid Power Conditioning System for Residential Use," *IEEE Transactions on Energy Conversion,* vol. 21, no. 2, pp. 575-585, 2006.

[31] Wai R-J and Duan R-G, "High-Efficiency Power Conversion for Low Power Fuel Cell Generation System," *IEEE Transactions on Power Electronics,* vol. 20, no. 4, pp. 847-856, 2005.

[32] Guillaume Fontes, Christophe Turpin, Stéphan Astier, and Thierry A. Meynard, "Interactions Between Fuel Cells and Power Converters: Influence of Current Harmonics on a Fuel Cell Stack," *IEEE Transactions on Power Electronics,* vol. 22, no. 2, pp. 670-678, 2007.

[33] M. Y. EI-Sharkh, A. Rahman, M.S. Alam, P.C. Byrne, A.A. Sakla and T. Thomas, "A dynamic model for a stand-alone PEM fuel cell power plant for residential applications," *Journal of Power Sources,* vol. 138, no. 1-2, pp. 199-204, 2004.

[34] J. Padulles, G.W. Ault, and J. R. McDonald, "An integrated SOFC plant dynamic model for power systems simulation," *Journal of Power Sources,* vol. 86, pp. 495-500, 2000.

[35] Abhishek R. Sakhare, Asad Davari and Ali Feliachi, "Control of Stand Alone Solid Oxide Fuel Cell using Fuzzy Logic," in *IEEE Proceedings of the Thirty-Sixth Southeastern Symposium on System Theory*, 2004.

[36] Jin-Woo Jung, Ali Keyhani, "Modeling and Control of Fuel Cell Based Distributed

Generation Systems in a Standalone AC Power Supply," *Journal of Iranian Association of Electrical and Electronics Engineers,* vol. 2, no. 1, pp. 10-23, 2005.

[37] Tae-Won Lee, Sung-Ho Kim, Yong-Ho Yoon, Su-Jin Jang, and Chung-Yuen Won, "A 3 kW Fuel cell Generation System using the Fuel Cell Simulator," in *Proceedings of IEEE Conference*, 2004.

[38] J.J. Brey, C.R. Bordallo, J.M. Carrasco, E. Galvan, A. Jimenez, E. Moreno, "Power conditioning of fuel cell systems in portable applications," *International Journal of Hydrogen Energy,* vol. 32, pp. 1559-1566, 2007.

[39] Federico Zenith, Sigurd Skogestad, "Control of fuel cell power output," *Journal of Process Control,* vol. 17, pp. 333-347, 2007.

[40] Dae-Kyu Choi, Byoung-Kuk Lee, Se-Wan Choi, Chung-Yuen Won, "A novel power conversion circuit for cost-effective battery-fuel cell hybrid system," *Journal of Power Sources,* vol. 152, pp. 245-255, 2005.

[41] Jeferson M. Correa, Fleix A. Farret, Luciane N. Canha, ang Macelo G. Simoes, "An Electrochemical-Based Fuel-Cell Model Suitable for Electrical Enginneering Automation Approach," *IEEE Transactions on Industrial Electronics,* vol. 51, no. 5, pp. 1103-1112, 2004.

[42] Khaled Mammar,Abdelkader Chaker, "Modeling and Fuzzy Logic Control of PEM Fuel Cell System Power Generation for Residential Application," *Journal of Electrical and Electronics Engineering,* vol. 9, no. 2, pp. 1073-1081, 2009.

[43] Dachuan Yu, S. Yuvarajan, "Electronic circuit model for proton exchange membrane fuel cells," *Journal of Power Sources,* vol. 142, pp. 238-242, 2005.

[44] Woonki Na, Bei Gou, "The efficient and economic design of PEM fuel cell systems by multi-objective optimization," *Journal of Power Sources,* vol. 166, pp. 411-418, 2007.

[45] Jenn-Kun Kuo, Chi-Fa Wang, "An integrated simulation model for PEM fuel cell power systems with a buck DC-DC converter," *International Journal of Hydrogen*

Energy, vol. 36, pp. 11846-11855, 2011.

[46] Amin Hajizadeh, Samson G. Tesfahunegn, and Tore M. Undeland, "Intelligent control of hybrid photo voltaic/fuel cell/energy storage power generation system," *Journal of Renewable and Sustainable Energy,* vol. 3, 2011.

[47] N.Bizon, "Nonlinear control of fuel cell hybrid power sources: Part I-Voltage control," *Applied Energy,* vol. 88, pp. 2559-2573, 2011.

[48] C.J. Hatziadoniu, A.A. Lobo, F. Pourboghrat, and M. Daneshdoost, "A Simplified Dynamic Model of Grid-Connected Fuel-Cell Generators," *IEEE Transactions on Power Delivery,* vol. 17, no. 2, pp. 467-473, 2002.

[49] Matina Lakka, Eftichios Koutroulis, and Apostolos Dollas, "Development of an FPGA-Based SPWM Generator for High Switching Frequency DC/AC Inverters," *IEEE Transactions on Power Electronics,* vol. 29, no. 1, pp. 356-365, January 2014.

[50] Rickard Ekström and Mats Leijon, "FPGA Control Implementation of a Grid-Connected Current-Controlled Voltage-Source Inverter," *Journal of Control Science and Engineering,* vol. 2013, pp. 1-10, 2013.

[51] Gitanjali Mehta, S P Singh, R D Patidar, "Non-linear load compensation in Fuel Cell grid interfaced system using active power filter," in *IEEE PEDS*, Singapore, 2011.

[52] Mohamed Adel, Sherif Zaid, Osama Mahgoub, "Improved Active Power Filter Performance Based on an Indirect Current Control Technique," *Journal of Power Electronics,* vol. 11, no. 6, pp. 931-937, Nov 2011.

[53] Ambrish Chandra, Bhim Singh, B. N. Singh and Kamal Al-Haddad, "An Improved Control Algorithm of Shunt Active Filter for Voltage Regulation, Harmonic Elimination, Power-Factor Correction, and Balancing of Nonlinear Loads," *IEEE Transactions on Power Electronics,* vol. 15, no. 3, pp. 495-507, May 2000.

[54] Foulkes., A.J. Appleby and F.R., Fuel Cell Handbook, New York: Van Nostrand Reinhold, 1989.

[55] Swider-Lyons KE, Karlin RT, Rosenfeld RL, Nowak RJ, "Technical issue and opportunities for fuel cell development for autonomous underwater vehicles," in *Proceeedings of the 2002 workshop on autonomous underwater vehicle*, 2002.

[56] M. Laughton, "Fuel cells," *Power Engineering Journal,* vol. 16, no. 1, pp. 37-47, 2002.

[57] M. Julian, "A distributed power generation communication system," in *IEEE Canadian Conference on Electronic Computer Engineering*, 2003.

[58] Zhong Z.D., Zhu X.J., Cao G.Y., and Shi J.H., "A hybrid multi-variable experimental model for a PEMFC," *Journal of Power Sources,* vol. 164, no. 2, pp. 746-751, 2007.

[59] Ellis MW, Von Spakovsky MR, Nelson DJ., "Fuel cell systems: efficient flexible energy conversion for the 21st century," in *IEEE Proceedings*, 2001.

[60] R.F. Mann, J. C. Amphelett, M.A. I. Hooper, H.M. Jensen, B.A. Peppley, and P.R. Roberge, "Development and application of a generalized steady-state electrochemical model for a PEM fuel cell," *Journal of Power Sources,* vol. 86, pp. 173-180, 2000.

[61] Y. Zhu and K. Tomsovic, "Development of models for analysing the load following performance of micro-turbines and fuel cells," *Journal of Electric Power Systems Research,* vol. 62, no. 1, pp. 1-11, 2002.

[62] J. Larminie and A. Dicks,, Fuel cell systems explained, John Wiley & Sons, 2003.

[63] C. Boccaletti, G. Duni, G. Fabbri and E. Santini, "Simulation models of fuel cell systems," in *Proceedings of ICEM,Electrical Machines*, China,Greece, 2006.

[64] Pasricha S, Keppler M, Shaw SR, Hashem NM, "Comparision and identification of static electrical terminal fuel cell models," *IEEE Transactions on Energy*

Conversion, vol. 22, pp. 746-754, 2007.

[65] Cheng KWE, Sutanto D, Ho YL, Law KK, "Exploring the power conditioning system for fuel cell," in *Proceedings of the 32nd IEEE Annual Power Electronics Specialists Conference*, 2001.

[66] F. Blaabjerg, Z. Chen, and S.B. Kjaer, "Power Electronics as Efficient Interface In Dispersed Power Generation Systems," *IEEE Transactions on Power Electronics,* vol. 19, no. 5, 2004.

[67] Zhenhua Jiang, and Roger A. Dougal, "A Compact Digitally Controlled Fuel Cell/ Battery Hybrid Power Source," *IEEE Transactins on Industrial Electronics,* vol. 53, no. 4, pp. 1094-1104, 2006.

[68] Geoffrey R. Walker, and paul C. Sernia, "Cascaded DC-DC Converter Connection of Photovoltaic Modules," *IEEE Transactions on Power Electronics,* vol. 19, no. 4, pp. 1130-1139, 2004.

[69] D.W. Hart, Introduction to power electronics, Prentice-Hall International,INC.

[70] N. Mohan, T. Underland and W. Robbins, Power electronics: Converters application and design, New York: J. Wiley and sons, 2003.

[71] J.W. Jung and A. Keyhani, "Modeling and control of fuel cell based distributed generation systems in a standalone AC power supply," *Journal of Iranian Association of Electrical and Electronics Engineers,* vol. 2, no. 1, pp. 10-23, 2005.

[72] A. Bendre, G. Venkataramanan, and D. Divan, "Dynamic analysis of loss-limited switching full-bridge DC-DC converter with multimodal control," *IEEE Transactions on Industry Applications,* vol. 39, pp. 854-863, 2003.

[73] M. T. Aydemir, A. Bendre, and G. Venkataramanan, "A critical evaluation of high power hard and soft switched isolated DC-DC converters," in *IEEE IAS'02*, 2002.

[74] Eun-Soo Kim, Kee-Yeon Joe, Moon-Ho Kye, Yoon-Ho Kim, and Byung-Do Yoon, "An improved ZVZCS PWM FB DC/DC converter using energy recovery

snubber," in *IEEE APEC'97*, 1997.

[75] Dong-Yun Lee, Byoung-Kuk Lee, Sang-Bong Yoo, and Dong-Seok Hyun, "An improved full-bridge zero-voltage-transition PWM DC/DC converter with zero voltage/zero-current switching of the auxiliary switches," *IEEE Transactions on Industry Applications,* vol. 36, pp. 558-566, 2000.

[76] P. K. Jain, Wen Kang, H. Soin, and Youhao Xi, "Analysis and design considerations of a load and line independent zero voltage switching full bridge DC/DC converter topology," *IEEE Transactions on Power Electronics,* vol. 17, pp. 649-657, 2002.

[77] M. Brunoro and J.L.F. Vieira, "A high-performance ZVS full-bridge DC-DC 0-50-V/0-10-A power supply with phase-shift control," *IEEE Transactions on Power Electronics,* vol. 14, pp. 495-505, 1999.

[78] Seong-Jeub Jeon and Gyu-Hyeong Cho, "A zero-voltage and zero-current switching full bridge DC-DC converter with transformer isolation," *IEEE Transactions on Power Electronics,* vol. 16, pp. 573-580, 2001.

[79] Jung-Goo Cho, Chang-Yong Jeong, and F.C.Y. Lee, "Zero-voltage and zero current-witching full-bridge PWM converter using secondary active clamp," *IEEE Transactions on Power Electronics,* vol. 13, pp. 601-607, 1998.

[80] F.Z. Peng, Hui Li,Gui-Jia Su, and J.S. Lawler, "Zero-voltage and zerocurrent-witching full-bridge PWM converter using secondary active clamp," *IEEE Transactions on Power Electronics,* vol. 19, pp. 54-65, 2004.

[81] Z. Jiang, and R.A. Dougal, "Control design and testing of a novel fuel-cell-powered battery-charging," in *IEEE APEC'03*, 2003.

[82] M. Santhi, R. Rajaram and I. G. C. Raj, "A ZVCS LC – resonant push – pull power converter circuit for battery fuel cell hybrid systems," in *Proceedings of IEEE Conference on Electric and Hybrid Vehicles (ICEHV'06)*, 2006.

[83] Mohan N, Undeland TM, Robbins WP., Power Electronics converters, applications and design, Wiley & Sons, 2004.

[84] Choe, S.Y., Lee, J.G.,Ahn, J.W., and Baek, S.H., "Integrated modeling and control of a PEM fuel cell power system with PWM DC/DC converter," *Journal of Power Sources,* vol. 164, pp. 614-623, 2007.

[85] B. Hasaneen and A.A.E. Mohammed, "Design and simulation of DC-DC boost converter.," in *Proceedings of 12th International Middle East IEEE Conference on Power System (MEPCON)*, 2008.

[86] Muhammad H. Rashid, Power Electronics Handbook, US: Academic Press.

[87] Xu H, Kong L, Wen X., "Fuel cell power system and high power dc/dc converter," *IEEE Transactions on Power Electronics,* vol. 19, no. 5, pp. 1250-1255, 2004.

[88] Wang C, Nehrir MH, Gao H., "Control of PEM fuel cell distributed generation systems.," *IEEE Transactions on Energy Conversion,* vol. 21, pp. 586-595, 2006.

[89] Lopez, M., L.G. Vicuna, M. Castilla, O. Lopez, and J. Matas. , "Sliding mode control strategy applied to parallel connected converters.," in *European Power Electronics Conference (EPE'99)*, 1999.

[90] Sira-Ramirez, H. and Ilic, M., "A geometric approach to the feedback control of switch mode dc-dc power supplies," *IEEE Transactions on Circuits and Systems,* vol. 35, no. 10, pp. 1291-1298, 1998.

[91] Tan, SC, Lai, Y.M. Tse, C.K., "A unified approach to the design of PWM-based sliding-mode voltage controllers for basic DC-DC converters in continuous conduction mode," *IEEE Transactions on Circuits and Systems,* vol. 53, no. 8, pp. 1816-1827, 2006.

[92] Huang X, Zhang Z, Jiang J., "Fuel cell technology for distributed generation:an overview," in *IEEE Symposium on Industrial Electron*, 2006.

[93]   Hung J. Y., W. Gao, and J.C Hung, "Variable structure control: A survey," *IEEE Transactions on Industrial Electronics,* vol. 40, pp. 2-21, 1993.

[94]   I L. Song, Kim, "Sliding mode controller for the single-phase grid connected photovoltaic system," *Applied Energy,* vol. 83, pp. 1101-1115, 2006.

[95]   Slotine, J.J. and T.S. Liu, Applied Nonlinear Control, Prentice Hall, 1991.

[96]   Yuan Fong Chan, M. Moallan and Wei Wang, "Design and implementation of Modular FPGA Based PID Controller," *IEEE Transactions on Industrial Electronics,* vol. 54, no. 4, 2007.

[97]   S. Sirisukprasert, T. Seangsuwan, "Power Electronics based Fuel cell Emulator," in *Proceedings ECTI International Conference*, 2007.

[98]   T. W. Lee, S. H. Kim, Y. H. Yoon, S. J. Jang, C. Y. Won, "A 3 kW fuel cell generation system using the fuel cell simulator," in *Proceedings IEEE International Symposium on Industrial Electronics*, 2004.

[99]   "Xilinx Inc., Spartan IIE Data Sheet. (2007, Jun.). [Online]. Available: http://www.xilinx.com/bvdocs/publications/ds077.pdf".

[100] Haitao Y, Yulan Z, Zechang S, Gang W., "Model-based power control strategy development of a fuel cell hybrid vehicle.," *Journal of Power Sources,* vol. 180, pp. 821-829, 2008.

[101] Zbigniew Leonowicz, Andrzej Lempart, "Assessing the benefits and risks of application of inverter drives in industry," in *11th International Conference on Environment and Electrical Engineering (EEEIC)*, 2012.

[102] J. Hamelin,K Agbossou, A Laperriere,F Laurencelle, and T.K Bose, "Dynamic behaviour of a PEM fuel cell stack for stationary applications," *International Journal Hydrogen Energy,* vol. 26, no. 6, pp. 625-629, 2001.

[103] W. Shireen and M.S. Arefeen, "An utility interactive power electronics interface for alternate/renewablw energy systems," *IEEE Transactions on Energy*

Conversion, vol. 11, no. 3, pp. 643-649.

[104] J. Bauer, "Single Phase Voltage Source Inverter Photovoltaic Application," *Acta Polytechnica,* vol. 50, no. 4, pp. 7-11, 2010.

[105] S. Stevandic and J. Jiang, "Standalone, reduced-order model and control of a grid-connected fuel cell power plant," in *IEEE Power Engineering Society General Meeting*, 2003.

[106] Abdelmadjid Chaoui, Jean-Paul Gaubert, Fateh Krim and Laurent Rambault, "On the Design of Shunt-Active Filter for Improving Power Quality," in *IEEE International Symposium on Industrial Electronics*, 2008.

[107] Firuz Zare and Gerard Ledwich, "A Hysteresis Current Control for Single-Phase Multilevel Voltage Source Inverters: PLD Implementation," *IEEE Transactions on Power Electronics,* vol. 17, no. 5, pp. 731-738, 2002.

[108] Brod D.M, Novotny D.M, "Current control of VSI-PWM Inverters," *IEEE Transactions on Industry Applications,* vol. 21, no. 3, pp. 562-570, 1985.

[109] Akira Nabae, Satoshi Ogasawara, and Hirofumi Akagi, "A Novel Control Scheme for Current-Controlled PWM Inverters," *IEEE Transactions on Industry Applications,* vol. 22, no. 4, pp. 562-570, 1986.

[110] Jiang Zeng, Chang Yu, Qingru Qi, Zheng Yan, Yixin Ni, B.L. Zhang, Shousun Chen and Felix F. Wu, "A novel hysteresis current control for active power filter with constant frequency," *Electric Power Systems Research,* vol. 68, no. 1, pp. 75-78, 2004.

[111] G.H. Bode and D.G. Holmes, "Implementation of Three Level Hysteresis Current Control for a Single Phase Voltage Source Inverter," in *IEEE Proceedings on Power Electronics Specialists Conference*, 2000.

[112] Karuppanan P, Saswat Kumar Ram and Kamala Kanta Mahapatra, "Three level hysteresis current controller based active power filter for harmonic compensation," in *IEEE Emerging Trends in Electrical and Computer Technology (ICETECT)*,

2011.

[113] Murat Kale and Engin Ozdemir, "An adaptive hysteresis band current controller for shunt active power filter," *Electric Power Systems Research,* vol. 73, no. 2, pp. 113-119, 2005.

[114] Bimal Bose, "An adaptive hysteresis-band current control technique of a voltage-fed pwm inverter for machine drive system," *IEEE Transactions on Industrial Electronics,* vol. 37, no. 5, pp. 402-408, 1990.

[115] B. Mazari and F. Mekri , "Fuzzy Hysteresis Control and Parameter Optimization of a Shunt Active Power Filter," *Journal of Information Science and Engineering,* vol. 21, pp. 1139-1156, 2005.

[116] N. Gupta, S. P. Singh, S. P. Dubey , "DSP based adaptive hysteresis-band current controlled active filter for power quality conditioning under non-sinusoidal supply voltages," *International Journal of Engineering, Science and Technology,* vol. 3, no. 4, pp. 236-252, 2011.

[117] P. Rathika and Dr. D. Devaraj , "Fuzzy Logic-Based Approach for Adaptive Hysteresis Band and DC Voltage Control in Shunt Active Filter," *International Journal of Computer and Electrical Engineering,* vol. 2, no. 3, pp. 404-412, 2010.

[118] Brod D.M, Novotny D.M, "Current control of VSI-PWM Inverter," *IEEE Transactions on Industry Applications,* vol. 21, no. 3, pp. 562-570, 1985.

[119] J.Dixon, S.Tepper and L.Moran, "Practical Evaluationof Different Modulation Techniques for Current-Controlled Voltage Source Inverters," in *IEE Proceedings in Electric Power Application*, 1996.

[120] Chiara Boccaletti, Gianluca Fabbri, Ezio Santini, "A reformer model for fuel cell power systems," in *International Conference on Power Engineering, Energy and Electrical Drives (POWERENG 2007)*, 2007.

[121] S. K. Jain, P. Agrawal, H.O. Gupta, "Fuzzy logic controlled shunt active power filter for power quality improvement," *IEE Proceedings Electric Power*

Applications, vol. 149, no. 5, pp. 317-328, 2002.

[122] M Gopal, Digital Control and State Variable Methods, New Delhi: Tata McGraw-Hill Publishing Company Limited, 2010.

[123] Karuppanan P and Kamala Kanta Mahapatra , "PI with Fuzzy Logic Controller based Active Power Line Conditioners," *Asian Power Electronics Journal,* vol. 5, no. 1, pp. 13-18, 2011.

[124] Srinivas Ponnaluri and Axel Brickwedde, "Generalised System Design of Active filters," in *IEEE Conference on PESC*, 2001.

[125] Louis Cheng and Richard Cheung, "New Rotating Transformation for Efficient DSP Control of Active Power-Line Conditioners," *IEEE Transactions on Power Systems,* vol. 15, no. 1, pp. 382-387, 2000.

[126] N. Gupta, S. P. Singh, S. P. Dubey, "DSP based adaptive hysteresis-band current controlled active filter for power quality conditioning under non-sinusoidal supply voltages," *International Journal of Engineering, Science and Technology,* vol. 3, no. 4, pp. 236-252, 2011.

[127] Abdelmadjid Chaouia, Jean Paul Gaubertb, Fateh Krima and Gérard Champenois, "PI Controlled Three-phase Shunt Active Power Filter for Power Quality Improvement," *Electric Power Components and Systems ,* vol. 35, no. 12, pp. 1331-1344, 2007.

[128] Hocine Benalla and Hind Djeghloud, "Shunt Active Filter Controlled by Fuzzy Logic," *Journal of King Saud University,* vol. 18, no. 2, pp. 231-247, 2005.

[129] Bhim Singh, Kamal Al-Haddad and Ambrish Chandra, "A Review of Active Filters for Power Quality Improvements," *IEEE Transactions on Industrial Electronics,* vol. 46, no. 5, pp. 960-970, 1999.

[130] L.Gyugyi, E.C.Strycula, "Active AC Power Filters," in *Proceedings of IEEE/IAS Annual Meeting*, 1976.

[131] B. Singh, K. Al-Haddad and A. Chandra, "A new control approach to three-phase active filter for harmonics and reactive power compensation," *IEEE Transactions on Power System,* vol. 13, no. 1, pp. 133-138, 1998.

[132] M. Dai, M. N. Marwali, J.W. Jungand A. Keyhani, "Power Flow Control of a Single Distributed Generation Unit," *IEEE Transactions on Power Electronics,* vol. 23, no. 1, pp. 343-352, 2008.

[133] George J. Wakileh, Power System Harmonics: Fundamentals, Analysis and Filter Design, Springer, 2007.

[134] S. K. Jain, P. Agrawal, H.O. Gupta, "Fuzzy logic controlled shunt active power filter for power quality improvement," *IEE Proceedings Electric Power Applications,* vol. 149, no. 5, pp. 317-328, 2002.

[135] Alberto Pigazo, Victor M. Moreno and Emilio J. Estebanez, "A Recursive Park Transformation to Improve the Performance of Synchronous Reference Frame Controllers in Shunt Active Power Filters," *IEEE Transactions on Power Electronics,* vol. 24, no. 9, pp. 2065-2075, 2009.

[136] Subhashish Bhattacharya, and Deepak Divan, "Synchronous reference frame based controller for a hybrid series active filter system," in *Industry application Conference, IAS-Annual meetings*, 1995.

[137] Karuppanan P and Kamala kanta Mahapatra , "A Novel SRF Based Cascaded Multilevel Active Filter for Power Line Conditioners," in *IEEE-INDICON*, 2010.

[138] Subhash Joshi T.G., Aby Joseph and Gautam Poddar, "Active Power Factor Correction For Highly Fluctuating Industrial Load," in *National Power Electronics Conference (NEPC)*, 2003.

[139] P.J.H. Wingelaar,J.L. Duarte, and M.A.M. Hendrix, "Dynamic and static simulation tool for PEM fuel cells," in *IEEE ISIE*, 2006.

[140] S. Pasricha, and S.R. Shaw, "A Dynamic PEM Fuel Cell Mode," *IEEE*

Transactions on Energy Conversion, vol. 21, no. 2, 2006.

[141] M K Mishra, and K Karthikeyan, "A study on design and dynamics of voltage source inverter in current control mode to compensate unbalanced and non-linear loads," in *Conference Proceedings of IEEE Power Electronics, Drives and Energy Systems* , New Delhi, 2006.

[142] "LEM Datasheet: LV 25-P," LEM, Japan, 1996.

[143] "LEM Datasheet: LA 55-P," LEM, Japan, 1996.

[144] P K Linash, and M K Mishra, "Operation of single phase active power filter under weak ac source," in *Conference Proceedings of IET Power Electronics,Machines and Drives* , Dublin, 2006.

[145] Mahesh K. Mishra, K. Karthikeyan, Vincent G. and S. Sasitharan, "A DSP-based Integrated Hardware Set-up for a DSTATCOM: Design, Development, and Implementation Issues," *IETE Journal of Research,* vol. 56, no. 1, pp. 11-21, 2010.

[146] Michael Barr., "Embedded Systems Glossary," Netrino Technical Library.

[147] *NI CompactRIO concepts manual.*

[148] *NI 9201 Operating Instructions manual.*

[149] *NI 9263 Operating Instructions manual.*

Thesis Dissemination

International Journals

[1]. **Kanhu Charan Bhuyan**, Kamalakanta Mahapatra, "Control Strategies for Solid oxide Fuel cell voltage" *International Journal on Electrical and Power Engineering, vol.02, no.3, pp.50-55, Nov 2011.*

[2]. **Kanhu Charan Bhuyan**, Kamalakanta Mahapatra, "An FPGA Based Controller for SOFC DC-DC Power Systems," *International Journal of Advance in Power Electronics, vol. 2013 (2013), Article ID: 345646, Hindawi Publishing Corporation.*

[3]. **Kanhu Charan Bhuyan,** Rajesh Patjoshi, Subhransu Padhee, Kamalakanta Mahapatra, "Solid oxide fuel cell with DC-DC converter system control and grid interfacing," *WSEAS Transactions on Systems and Control, vol. 9, pp 247-254, 2014 .*

[4]. **Kanhu Charan Bhuyan**, Rajesh Patjoshi, Subhransu Padhee and Kamalakanta Mahapatra, "Development of FPGA based controllers for single phase fuel cell power system in standalone applications", *Electrical Energy and Power Systems, (Communicated).*

International Conferences

[1]. **Kanhu Charan Bhuyan**, Kamalakanta Mahapatra, "An Intelligent Control of Solid Oxide Fuel cell voltage", *IEEE International Conference on Power and Energy Systems (ICPS)*, 2011.

[2]. **Kanhu Charan Bhuyan**, Sumit Kumar Sao and Kamalakanta Mahapatra, "Fuel Cell connected to Grid through Inverter", *IEEE Student's Conference Engineering and Systems (SCES)*, 2012.

National Conferences

[1]. Karuppanan P, Kamalakanta Mahapatra, **Kanhu Charan Bhuyan** and Rajesh Kumar Patjoshi "Cascaded Voltage Source Inverter based Active Power Line Conditioners" *National Systems Conference (NSC)* 2011

[2]. **Kanhu Charan Bhuyan**, Kamalakanta Mahapatra, "An Active and Reactive Power Analysis of Solid Oxide Fuel Cell," *National Systems Conference (NSC)* 2011.

APPENDIX-A

System Parameters

Table A.1 List of parameters used in experimentation for single phase fuel cell power system

Parameters	Experimental Values
Supply voltage/ frequency	154 V / 50 Hz
Resistor (R_L) and Inductor (L_L)	15 W CFL Bulb
Interface inductor (R_c, L_c)	5 mH
DC-link capacitance (C_{dc})	6800 μF
Reference voltage (V_{dcref})	13 V
Voltage source inverter	SKM75GB063D IGBT module, TLP-250 for Gate driver circuit, Amplifier circuit, Separate Power supply for driver circuit.
Sensors	LEM make LV25-P for phase voltage, LA55-P for current transducer.

APPENDIX-B

NI cRIO-9014

Table B.1 Processor Datasheet

Network	
Network Interface	10 Base T and 100 Base TX Ethernet
Compatibility	IEEE 802.3
Communication Rates	10 Mbps, 100 Mbps, auto-negotiated
Maximum Cabling Distance	100 m/segment
SMB Connector	
Output Characteristics	
Logic High	3.3 V
Logic Low	0 V
Driver Type	CMOS
Sink/Source Current	± 50 mA
3-state output leakage current	± 5 µA
Input Characteristics	
Maximum Input level	-500 mV
Maximum input low level	990 mV
Minimum input high level	2.31 V
Maximum input level	5.5 V
Input capacitance	2.5 pF
Resistive strapping	1 kΩ to 3.3 V
USB Port	
Maximum data rate	12 Mb/s
Maximum current	500 mA
Memory	
cRIO-9014	2 GB
DRAM	
cRIO-9014	128 MB
Internal Real-Time Clock	
Recommended power supply	48 W secondary, 18 V DC to 24 V DC
Power Consumption	
Controller only	6 W
Controller supplying power to eight CompactRIO modules	20 W
Power Supply	
On Power	9 to 35 W

After power up	6 to 35 V
Safety Voltages	
V-to-C	35 V max

Table B.2 Input Modules NI 9201
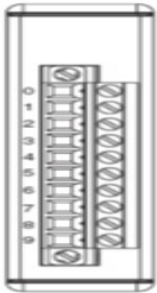
Module	Terminal	Signal
	0	AI0
	1	AI1
	2	AI2
	3	AI3
	4	AI4
	5	AI5
	6	AI6
	7	AI7
	8	NO CONNECTION
	9	COM

Table B.3 Output Module NI 9263

Module	Terminal	Signal
	0	AO0
	1	COM
	2	AO1
	3	COM
	4	AO2
	5	COM
	6	AO3
	7	COM
	8	NO CONNECTION
	9	COM